Développement de surfaces de PDMS antibactériennes par différentes approches

Yuzhen Lou

Normandie Université

THESE

Pour obtenir le diplôme de doctorat

Spécialité CHIMIE ET PHYSICO-CHIMIE DES POLYMERES

Préparée au sein de L'Institut National des Sciences Appliquées Rouen Normandie

Développement de surfaces de PDMS antibactériennes par différentes approches

Présentée et soutenue par
Yuzhen LOU

Thèse soutenue publiquement le 08 juillet 2021 devant le jury composé de			
Mme	Karine VALLEE REHEL	Professeur, Université Bretagne Sud	Rapporteur
Mme	Lydie PLOUX	DR CNRS à INSERM/Unistra U1121, Strasbourg	Rapporteur
M	Guy LOUARN	Professeur, Polytech Nantes	Examinateur
M	Pascal THEBAULT	Maître de Conférences (HDR), Université de Rouen Normandie, PBS	Co-Directeur de thèse
M	Nasreddine KEBIR	Maître de Conférences (HDR), INSA Rouen Normandie, PBS	Directeur de thèse

Thèse dirigée par Nasreddine KEBIR et Pascal THEBAULT, Laboratoire Polymères, Biopolymères, Surface UMR6270

INSA INSTITUT NATIONAL DES SCIENCES APPLIQUÉES ROUEN

UNIVERSITÉ DE ROUEN NORMANDIE

ED 508 NC Normande de Chimie

PBS Polymères Biopolymères Surfaces UMR 6270

CHINA SCHOLARSHIP COUNCIL

Remerciements

Ces travaux ont été réalisés au sein des équipes MM et BRICS du laboratoire Polymères, Biopolymères, Surfaces (PBS, UMR CNRS 6270). Je tiens à remercier Fabrice BUREL et Emmanuelle DE de m'avoir permis de réaliser mes travaux de thèse au sein de leurs laboratoires.

J'adresse mes sincères et respectueux remerciments aux membres du Jury : à M^{me} Karine VALLEE REHEL et M^{me} Lydie PLOUX pour avoir accepté d'être rapporteurs et à M. Guy LOUARN pour avoir accepté d'être examinateur à la soutenance de ma thèse.

Je tiens à remercier le 'China Scholarship Council' (CSC), pour le soutien financier de ma thèse.

Je voudrais remercier toutes les personnes ayant été présentes à mes côtés au cours des trois dernières années et demie. Grâce à vous, les travaux de cette thèse ont pu aboutir. Pour commencer, je remercie chaleureusement mon directeur de thèse, Nasreddine KEBIR pour ses précieux conseils, sa gentillesse et sa bonne humeur tout le long de ces années et pour ses jeux de mots toujours intéressants. Je te remercie de m'avoir aidé et guidé depuis le tout début de mes travaux de recherche, de l'apprentissage de la préparation du PDMS jusqu'à la rédaction du rapport de thèse, merci de m'avoir acccompagné tout au long de ma thèse. Je remercie tout autant mon co-directeur de thèse, Pascal THEBAULT pour sa patience, sa gentillesse et ses remarques toujours avisées. Je te remercie pour la patience et l'attention dont tu as fait preuve en m'apprenant à faire les expériences de bactériologie, mais aussi pour ton soutien lors de mes périodes de découragement.

J'aimerais remercier Stéphane ALEXANDRE de l'équipe BRICS qui m'a fait découvrir le domaine de l'AFM et Damien SCHAPMAN du laboratoire PRIMACEN qui m'a fait découvrir le domaine de la microscopie à fluorescence. Cela a été très agréable de discuter avec vous de sujets scientifiques et non-scientifiques. Je remercie également Dimitri Mercier pour la caractérisation de mes surfaces par XPS.

J'aimerais aussi remercier l'ensemble des équipes, collègues et amis que j'ai pu rencontrer durant ma thèse et avec qui j'ai apprécié de travailler et/ou d'échanger :

- J'adresse un grand merci à tout les chercheurs, ingénieurs et techiniciens du MM et BRICS. Merci en particulier à Julie HARDOUIN qui est toujours dynamique et folâtre.

- L’équipe BRICS est plus joyeuse et vivante avec toi. Merci à Catherine LEGRAND et Jérémy DESHAIS de l’équipe MM pour leurs gentillesses et leurs disponibilités pour répondre à toutes mes questions techniques au laboratoire.

- Merci à tous les stagiaires, doctorants et post-doctorants, que j’ai eu le plaisir de rencontrer : Charlotte 1 et Charlotte 2, Estelle, Brandon, Hung, Sébastien, Salomé, Xuelian, Bo, Di, Vincent, Gonnot, Cyrille, Ghislain, Alice, Pierre, Jaja, Klara, Ugo, Alejandra, Fufu et Roman. J’ai vécu avec vous trois années de bonne humeur, dans une excellente ambiance de travail. Merci à Hung pour m’avoir formé sur l’utilisation de l’appareil de mesure du potentiel zeta pour mes bactéries. Merci à Charlotte 1, Charlotte 2, Sébastien, Bo, Ghislain, Alice et Cyrille, pour tous ces moments passés à discuter de nos thèses respectives et pour leurs précieuses aides au laboratoire. Merci à Xuelian avec qui j’ai occupé le même bureau pendant ma thèse. Merci pour les échanges scientifiques (et culturels) et aussi de m’avoir soutenu lors des périodes de découragement. Merci Alice pour tes précieux conseills et les moments passés ensemble au Château de Versailles. Merci à Vincent pour tous ces moments passés ensemble à discuter des sujets scientifiques et culturels, de m’avoir appris le français (des mots ou expressions vraiment très utiles et couramment utilisées), et de m’avoir fait découvrir la guitare. Merci à Jaja de m’avoir inviter et de m’avoir acompagner pour courir. Merci à Gonnot pour tous les moments passés ensemble au laboratoire et de m’avoir aidé aussi à apprendre le français. Merci à toutes et à tous pour tous ces moments passés ensemble au cours de ces trois dernières années et demie (les escape games, les gâteaux, les pique-nique, l’escalade….).

- Merci à tous mes amies chinois que j’ai rencontré : Shan, Jin, Xiao jia, Jun dong, Jie, Jin, Hong bo, Hao, Rui pin, Xue fei, Lin lin et Qiu shi. Merci à vous de m’avoir acompagné, encouragé et aidé tout le long de ma thèse.

Enfin, un immense merci à mes parents et ma petite soeur pour leur aide, leur écoute, leur soutien inébranlable et leurs encouragements.

Résumé & Abstract

Développement de surfaces de PDMS antibactériennes par différentes approches

Résumé **:** Les silicones sont largement utilisés dans le domaine médical mais sont, cependant, sujets à la contamination bactérienne en raison de leur caractère hydrophobe. Dans cette thèse, trois méthodes ont été utilisées pour développer de nouvelles surfaces de PDMS antibactériennes. Dans la première, un champ électrique a été appliqué entre deux électrode métalliques revêtues de PDMS. Un effet répulsif cathodique spécifique aux staphylocoques a été obtenu. Dans la seconde, une surface de PDMS bactéricide porteuse d'un dérivé de la claramine a été préparée par l'addition click de Huisgen. Dans la troisième, des surfaces cationiques bactéricides ont été préparées par photo-greffage de polymères cationiques sur des surfaces de PDMS via des procédés de 'grafting to' et de 'grafting from'. Les surfaces développées dans cette thèse pourraient être utilisées dans des dispositifs qui ne sont pas en contact avec le sang, comme les surfaces externes des cathéters et les équipements extracorporels.

Development of antibacterial PDMS surfaces by different approaches

Abstract : Silicones are widely used in the medical field but are, however, prone to bacterial contamination due to their hydrophobic nature. In this thesis, three methods were used to develop new antibacterial PDMS surfaces. In the first one, an electric field was applied between two PDMS-coated metallic electrodes. A cathodic repulsive effect specific to staphylococci was obtained. In the second, a bactericidal PDMS surface carrying a claramine derivative was prepared by the Huisgen click addition. In the third, bactericidal cationic surfaces were prepared by photo-grafting of cationic polymers onto PDMS surfaces via 'grafting to' and 'grafting from' processes. The surfaces developed in this thesis could be used in devices that are not in contact with blood, such as the external surfaces of catheter chambers and extracorporeal equipment.

Productions Scientifiques

Liste des publicaitons

Articles publiées:

Y. Lou, P. Thebault, F. Burel, N. Kébir, "Antibacterial properties of metal and PDMS surfaces under weak electric fields," *Surf. Coatings Technol.*, vol. 394, p. 125912, 2020.

Y. Lou, D. Schapman, D. Mercier, S. Alexandre, F. Burel, P. Thebault, N. Kébir, "Self-disinfecting PDMS surfaces with high quaternary ammonium functionality by direct surface photoinitiated polymerization of vinylbenzyl dimethylbutylammonium chloride," *Eur. Polym. J.*, vol. 152, p. 110473, 2021.

Y. Lou, D. Schapman, D. Mercier, S. Alexandre, F. Burel, P. Thebault, N. Kébir, "Preparation of bactericidal surfaces with high quaternary ammonium content through photo-initiated polymerization of *N*-[2-(acryloyloxy)ethyl]-*N*,*N*-dimethyl-N-butylammonium iodide from native and thiolated PDMS surfaces," *Reactive and Functional Polymers*., Vol. 165, p. 104941, 2021.

Publications en cours:

Y. Lou, D. Schapman, D. Mercier, S. Alexandre, E. Dé, J.M. Brunel, N. Kébir, P. Thebault, "Antibacterial PDMS surfaces based on a claramine-derivative through click-chemistry grafting". (*Soumis dans Materials Chemistry and Physics*).

Y. Lou, D. Schapman, D. Mercier, N.C. Süer, T. Eren, P. Thebault, N. Kébir, "Preparation of bactericidal PDMS surfaces by benzophenone photo-initiated grafting of polynorbornenes functionalized with quaternary phosphonium or pyridinium groups". (*Accepté dans European Polymer Journal*).

Communications scientifiques :

Journée de l'école doctorale normande de chimie : « Elaboration of antibacterial surfaces using different methods» Yuzhen LOU, Nasreddine KEBIR, Pascal THEBAULT, (Affiche)

40èmes journées de la section grand ouest du GFP, Université d'Orléans : « Elaboration of bacteria repellent surfaces using an electric field » Yuzhen LOU, Nasreddine KEBIR, Pascal THEBAULT, (Affiche)

Sommaire

Introduction générale

La contamination microbienne des surfaces peut conduire à la formation d'un biofilm, entraînant de graves problèmes pour la santé humaine (comme par exemple, les infections liées aux biomatériaux implantables) ainsi que dans les secteurs industriels (par exemple, la corrosion des surfaces métalliques, la contamination des aliments, la détérioration des canalisations...), avec un important impact socio-économique négatif [1,2].

Par ailleurs, il est à noter que les bactéries en mode biofilm nécessitent des concentrations d'antibiotiques 100 à 1000 fois supérieures à celles des bactéries planctoniques pour obtenir une éradication efficace [3]. Par conséquent, le développement de matériaux capables d'empêcher l'adhésion des bactéries et/ou la formation de biofilms à leur surface est un élément clé dans la lutte contre la contamination bactérienne.

Trois catégories de surfaces antibactériennes sont décrites dans la littérature : les surfaces anti-adhésives, les surfaces à libération d'agents biocides et les surfaces bactéricides par contact [4]. Les surfaces anti-adhésives sont conçues pour repousser les bactéries en optimisant leurs propriétés physico-chimiques telles que la charge de surface (charges négatives), la mouillabilité ou la topographie (surfaces à micro/nano-motifs) [5,7]. Cependant, elles ne peuvent pas affecter la viabilité des agents pathogènes qui peuvent être libérés pour contaminer d'autres surfaces. En outre, l'utilisation de modifications physiques de la surface (en particulier la topographie de la surface) comme méthodes non spécifiques pour empêcher l'adhésion bactérienne est un procédé relativement complexe [8]. Les surfaces à libération sont

[1] A. I. Doulkeraki et al., Methicillin-resistant food-related Staphylococcus aureus : a review of current knowledge and biofilm formation for future studies and applications, Res. Microbiol., vol. 168 (2017), pp. 1-15.

[2] D. Romero, Bacterial determinants of the social behavior of Bacillus subtilis, Res. Microbiol., vol. 164 (2013), pp. 788-798.

[3] M. Salwiczek *et al.*, Emerging rules for effective antimicrobial coatings, Trends Biotechnol., vol. 32 (2014), no. 2, pp. 82–90.

[4] M. Cloutier, D. Mantovani, and F. Rosei, Antibacterial Coatings: Challenges, Perspectives, and Opportunities, Trends Biotechnol., vol. 33, no. 11 (2015), pp. 637–652.

[5] D. Alves and M. Olívia Pereira, Mini-review: Antimicrobial peptides and enzymes as promising candidates to functionalize biomaterial surfaces, Biofouling, vol. 30 (2014), no. 4, pp. 483–499.

[6] L. Liu, B. Ercan, L. Sun, K. S. Ziemer, and T. J. Webster, Understanding the Role of Polymer Surface Nanoscale Topography on Inhibiting Bacteria Adhesion and Growth, ACS Biomater. *Sci. Eng.*, vol. 2, no. 1 (2016), pp. 122–130.

[7] C. Satriano, G. M. L. Messina, S. Carnazza, S. Guglielmino, and G. Marletta, Bacterial adhesion onto nanopatterned polymer surfaces, Mater. Sci. Eng. *C*, vol. 26, no. 5–7 (2006), pp. 942–946.

[8] Y. Ammar, D. Swailes, Ben Bridgens, J. Chen, Influence of surface roughness on the initial formation of biofilm, Surface and Coatings Technology, vol. 284 (2015), pp. 410-416.

conçues pour libérer des agents antibactériens qui tuent non seulement les bactéries adhérentes mais aussi les bactéries planctoniques [9-10]. L'inconvénient de ce type de surface est son activité limitée dans le temps en raison de la quantité limitée de composés antibactériens chargés. De plus, l'utilisation excessive d'antibiotiques peut entraîner un phénomène de résistance bactérienne [11]. Enfin, les surfaces bactéricides par contact, qui sont généralement basées sur des agents biocides cationiques liés de manière covalente aux surfaces du substrat, attirent les bactéries chargées négativement et les tuent en perturbant leur membrane [12-14]. Cependant, ces surfaces peuvent devenir inactives après avoir été ensevelies sous une couche de bactéries mortes ou du matériel cellulaire des bactéries mortes.

Grâce à leur grande flexibilité, leur hydrophobie, leur stabilité chimique et thermique et leur biocompatibilité, les matériaux en silicone (à base de poly(diméthylsiloxane) : PDMS) sont largement utilisés dans le domaine médical, notamment dans les applications orthopédiques (par exemple : les implants articulaires de la main et du pied), les cathéters, les équipements extracorporels (par exemple : l'oxygénateur sanguin, les machines de pontage thermique et la dialyse rénale) et les implants esthétiques (par exemple : l'implant mammaire en silicone) [15-17]. Néanmoins, l'hydrophobie du PDMS l'expose facilement à l'adsorption de protéines, à la contamination bactérienne et à la formation de biofilms, ce qui peut limiter son utilisation en raison de graves implications sanitaires et économiques [18-19].

[9] H. Kao *et al*., Metal ion-dependent tailored antibacterial activity and biological properties of polydopamine-coated titanium implants, Surface and Coatings Technology, vol 378 (2019), pp. 124998.

[10] D. Campoccia, L. Montanaro, and C. R. Arciola, A review of the biomaterials technologies for infection-resistant surfaces, Biomaterials, vol. 34, no. 34 (2013), pp. 8533–8554.

[11] A. C. Riosa, C. G. Moutinho, F. C. Pinto, F. S. Del Fiol, A. Jozala, M. V. Chaud, M. M.D.C. Vila, J. A. Teixeira, V. M. Balcão. Alternatives to overcoming bacterial resistances: State-of-the-art. Microbiological Research, vol. 191 (2016), pp. 51–80.

[12] J. Foksowicz-Flaczyk *et al.*, Multifunctional durable properties of textile materials modified by biocidal agents in the sol-gel process, Surface and Coatings Technology, vol 304 (2016), pp. 160-166.

[13] K. Lewis and A. M. Klibanov, Surpassing nature: Rational design of sterile-surface materials, Trends Biotechnol., vol. 23, no. 7 (2005), pp. 343–348.

[14] R. Kaur and S. Liu, Antibacterial surface design – Contact kill, Prog. Surf. Sci., vol. 91, no. 3 (2016), pp. 136–153.

[15] A. B. Swanson, "Silicone Rubber Implants for Replacement of Arthritic or Destroyed Joints in the Hand," Surg. Clin. North Am., vol. 48, no. 5, pp. 1113–1127, 1968.

[16] A. U. Daniels, "Silicone breast implant materials," *Swiss Med. Wkly.*, vol. 142, no. JULY, 2012.

[17] A. Colas and J. Curtis, "Silicone biomaterials: history and chemistry," *Biomater. Sci. an Introd. to Mater. Med.*, vol. 2, pp. 80–85, 2004.

[18] J. Winiecka-Krusnell and E. Linder, "Bacterial infections of free-living amoebae," Res. Microbiol., vol. 152, no. 7, pp. 613–619, 2001.

[19] A. I. Doulgeraki, P. Di Ciccio, A. Ianieri, and G. J. E. Nychas, "Methicillin-resistant food-related Staphylococcus aureus: a review of current knowledge and biofilm formation for future studies and applications," *Res. Microbiol.*, vol. 168, no. 1, pp. 1–15, 2017.

Dans le cadre de cette thèse, l'objectif est de développer de nouvelles surfaces de PDMS antibactériennes permettant de limiter le phénomène d'infection bactérienne dans le milieu médical et d'augmenter la longévité des dispositifs médicaux à base de ce matériau.

Le présent manuscrit de thèse est divisé en quatre chapitres. Le premier chapitre est une synthèse de l'état de l'art concernant les méthodes physico-chimiques de modification de surface de PDMS, développées jusqu'alors, en vue d'améliorer sa biocompatibilité et/ou de lui prodiguer des propriétés antibactériennes.

Le deuxième chapitre porte sur le développent d'une nouvelle stratégie antibactérienne consistant à utiliser un champ électrique pour polariser la surface du PDMS, déposé sur deux électrodes métalliques, et d'étudier son impact sur l'adhésion bactérienne et la viabilité des bactéries en suspension.

Le troisième chapitre porte sur le greffage par une réaction de cyclo-addition de Huisgen d'un dérivé de la claramine porteur d'une fonction azoture sur une surface de PDMS préalablement modifié pour introduire une fonction alcyne. Les propriétés physicochimiques et antibactérienne des surfaces obtenues seront présentées.

Le quatrième et dernier chapitre portera sur l'élaboration de surfaces cationiques par des procédés de 'grafting from' et 'grafting to' photo-amorcés en présence de la benzophénone. Dans un premier temps, nous décriront la photopolymérisation de deux monomères, un styrénique et un autre acrylique, porteurs de groupements ammonium quaternaire, à partir de surfaces de PDMS natives et thiolées. Dans un second temps, des polymères cationiques synthétisés par polymérisation par ouverture de cycle par métathèse (ROMP) et porteurs de doubles liaisons carbone-carbone seront greffés par 'grafting to' sur des surfaces de PDMS thiolées. Les propriétés physicochimiques et bactéricides de toutes les surfaces cationiques obtenues seront présentées et discutées par rapports aux données de la littérature.

Chapitre I : État de l’art

Introduction

De nos jours, la résistance microbienne vis-à-vis des antibiotiques accroît fortement la menace générée par les infections bactériennes, en particulier lorsqu'elles s'accompagnent de la formation d'un biofilm. La présence de ce dernier est à l'origine de nombreux échecs thérapeutiques et augmente ainsi le coût des soins de santé et surtout la mortalité [1,2].

La résistance microbienne est un terme qui désigne la capacité des micro-organismes (par exemple, les bactéries, les virus, les champignons et les protozoaires) à résister aux médicaments antimicrobiens. Le premier antibiotique, qui est la pénicilline, a été découvert par Alexander Fleming en 1928 dont sa première utilisation pour soigner des malades à grande échelle a eu lieu durant la Seconde Guerre mondiale [3]. Par la suite, une série d'antimicrobiens naturels, semi-synthétiques et synthétiques ont été découverts et appliqués en thérapie, transformant la médecine moderne et sauvant des millions de vies durant l'âge d'or entre les années 1930 et 1960 [4–7]. Néanmoins, l'utilisation inappropriée et excessive des antibiotiques a favorisé l'émergence de la résistance bactérienne aux antibiotiques. Depuis, le développement de nouveaux médicaments a fortement diminué. Face à la "crise mondiale de la résistance aux antibiotiques", nous sommes désormais dans "l'ère post-antibiotique" comme l'a baptisé l'Organisation Mondiale de la Santé (OMS) [8]. Les dépenses de santé directes annuelles liées au traitement des maladies infectieuses aux États-Unis sont estimées à plus de 120 milliards de dollars, et les coûts dus à des infections causées par des agents pathogènes résistants atteignent 5 milliards de dollars par an [1]. Le Centre américain de contrôle et de prévention des maladies (CDC) a estimé que plus de deux millions d'infections provenant de bactéries résistantes se produisent chaque année, entraînant au moins 23000 décès aux États-Unis [9].

Concernant les biofilms, ceux sont des structures spatiales complexes de cellules bactériennes intégrées dans une matrice autoproduite composée d'exo-polysaccharides, de protéines, d'ADN et de lipides, qui renforcent la protection des micro-organismes contre les facteurs défavorables (comme les médicaments, les contraintes environnementales ou le système immunitaire de l'organisme hôte) [10–12]. On estime qu'environ 65 % des infections bactériennes sont associés à ces communautés de micro-organismes [13]. Les bactéries en mode biofilm sont plus résistantes que les bactéries planctoniques en raison, entre autres, de la faible pénétration des antibiotiques à travers la matrice et de l'hétérogénéité de leurs microenvironnements. En effet, Il serait nécessaire d'utiliser des concentrations d'antibiotiques 100 à 1000 fois supérieures pour éradiquer des bactéries sous forme de biofilm par rapport à

des bactéries planctoniques [14, 15]. Ainsi, les infections liées aux biofilms touchent des millions de personnes et entraînent jusqu'à 550 000 décès aux États-Unis chaque année [16–18]. En outre, plus de 60 % des infections nosocomiales sont dues à des contaminations bactériennes sur des implants, des cathéters et des dispositifs cardiaques [19–25]. L'OMS estime qu'environ 1,7 million de patients seraient touchés par les infections associées aux soins, avec 37000 décès par an aux États-Unis [26]. Par conséquent, la résistance aux antibiotiques et la structure particulière des biofilms conduisent à des échecs thérapeutiques [2]. Il est donc impératif de trouver de nouvelles solutions pour lutter contre les biofilms en milieu hospitalier, et tout particulièrement dans le cas des dispositifs médicaux et des implants, bien entendu, sans effets secondaires ou dommages pour l'Homme.

Dans ce chapitre, nous allons introduire les stratégies générales de lutte contre la contamination bactérienne de surface. Nous nous concentrerons ensuite sur le PDMS, qui est très utilisé dans l'élaboration de biomatériaux, en présentant ses propriétés et ses applications, et en développant tout particulièrement les principales méthodes physiques et tout particulièrement chimiques de modification de sa surface.

I.1 Les principales stratégies de lutte contre la contamination bactérienne de surface

I.1.1 Les méthodes physiques

À ce jour, plusieurs approches physiques comme le plasma, les ultrasons basse fréquence (UBF) ou encore les méthodes électriques ont fait l'objet d'une attention croissante dans le domaine biomédicale (mais aussi agroalimentaire), et sont considérées comme prometteuses [27–33]. De plus, il a été démontré que ces approches peuvent améliorer l'efficacité des antibiotiques par un effet synergique [34–37]. Nous allons brièvement décrire ces trois approches.

I.1.1.1 Le traitement par plasma

Le plasma est un mélange gazeux globalement neutre mais composé d'ions, de molécules neutres et d'électrons, il est considéré comme le quatrième état de la matière [26,38]. Il a été démontré que le plasma a des propriétés antibactériennes grâce à la génération d'un mélange d'espèces réactives oxygénées et azotées [39], de particules chargées [40,41], de particules électriquement neutres mais chimiquement réactives et d'un rayonnement ultraviolet (UV) [42,43]. Le plasma thermique (PT) et le plasma non thermique (PNT) sont deux types de plasma en fonction des niveaux d'énergie relatifs des électrons et des particules lourdes [44,45]. Dans le plasma thermique (quasi-équilibré), qui est généré à une pression et une puissance élevée, les électrons et les particules lourdes sont à la même température élevée. En revanche, le PNT, également appelé plasma froid à pression atmosphérique (non équilibré), est généré à faible pression et puissance et ne contient que des particules lourdes à température ambiante, impliquant une température d'application inférieur ou égal à 40°C [45,46]. Par rapport au plasma thermique, le PNT a la même efficacité pour l'élimination des tissus, la stérilisation et la cautérisation [47] mais avec de plus faibles dommages pour les tissus et autres surfaces [48]. Le PNT est décrit comme un procédé prometteur pour les traitements biomédicaux systémiques tels que les applications en dermatologie [49,50], la guérison des blessures [51–54], la coagulation sanguine in vitro [55,56], la décontamination des instruments et des consommables chirurgicaux [57,58], le traitement des maladies buccales [59,60] et cela en raison de sa faible température d'application, des faibles dommages thermiques engendrés sur les tissus et de ses propriétés antimicrobiennes. De plus, le traitement par plasma peut également être appliqué dans le domaine de la

modification de surfaces, comme la fonctionnalisation chimique et le dépôt de couches minces [61–63].

I.1.1.2 Le traitement par ultrasons

On appelle ultrasons une onde sonore dont la fréquence est égale ou supérieure à 20 kHz. Si l'onde sonore a une fréquence comprise entre 20 et 100 kHz, on parle d'ultrasons de basse fréquence (UBF) (qui sont également appelés ultrasons de haute puissance) [64]. Il semblerait que le phénomène de cavitation acoustique soit le mécanisme élémentaire de l'effet bactéricide des ultrasons. La cavitation acoustique est un processus physique qui consiste en la formation, la croissance et l'effondrement de microbulles dans des milieux liquides qui peuvent générer des forces mécaniques localisées telles que des ondes de choc, des forces de cisaillement et des micro-jets pour endommager les micro-organismes [33,65]. D'après les données de la littérature (à la fois *in vitro* et *in vivo*), on constate que l'UBF peut renforcer, par le processus décrit précédemment, l'action des antibiotiques sur les bactéries planctoniques [66–68] et celles en mode biofilms [69–71]. De plus, dans le cas des implants incorporant des antibiotiques, l'UBF peut favoriser par cavitation la libération des actifs afin d'obtenir une efficacité optimale contre les bactéries qu'elles soient sous forme planctoniques ou biofilms [72–77]. Cependant, les effets de l'UBF, entre autres, sur les propriétés physiques des biomatériaux, ou encore sur d'autres espèces bactériennes que celles déjà étudiées restent à explorer avant une application potentielle de cette technique en synergie ou non avec d'autres traitements dont les antibiotiques.

I.1.1.3 Les traitements de type électrique

L'efficacité de traitements électriques tels que les courants électriques directs et alternatifs [78,79], les ondes acoustiques (par des actionneurs piézo-électriques) [31] et les champs électriques [80,81] contre l'adhésion et la croissance bactérienne a été démontré par des expériences *in vitro* et *in vivo*. Pour le courant électrique, le mécanisme de son activité antibactérienne reste encore à éclaircir. Cependant, deux hypothèses majeures ont été avancées : la perturbation de l'intégrité de la membrane bactérienne ou la toxicité des substances produites à la suite de l'électrolyse telles que les molécules de chlore ou de peroxyde d'hydrogène (H_2O_2). A part le courant électrique, les autres sont censés affecter la somme des forces d'attraction et de répulsion entre les bactéries et la surface afin d'interférer sur l'adhésion bactérienne. Hazan *et al.* [31] ont supposé que l'énergie vibratoire des ondes acoustiques de surface pouvait amener les bactéries à vibrer à la même fréquence que la surface concernée, par l'intermédiaire du milieu

environnant. Ensuite, en ajustant les amplitudes des vibrations bactériennes générées par les ondes acoustiques de surface, une force nette globale pourrait être attractive ou répulsive, provoquant la promotion ou la prévention de l'adhésion bactérienne. Quant au champ électrique, il provoque la polarisation de la surface du substrat qui peut être chargée négativement ou positivement. Les forces répulsives générées entre la surface et les bactéries chargées du même signe peuvent contribuer à empêcher l'adhésion des bactéries.

De plus, il a été constaté que le courant électrique [35,82–85] et les champs électriques [86,87] augmentent l'efficacité des agents antibiofilm dans une action synergique appelée "effet bioélectrique", qui peut permettre une diminution importante de la concentration des composés antibiofilm à utiliser. Cependant, le mécanisme d'un tel effet bioélectrique n'est pas totalement élucidé. Plusieurs mécanismes ont été proposés sous forme d'hypothèses [35] :

- Une réduction de la capacité du biofilm à fixer l'agent antimicrobien en perturbant les charges de la matrice par un courant électrique.

- La perméabilisation accrue de la membrane par électroporation facilitant la pénétration des agents antimicrobiens.

- L'augmentation, au sein du biofilm, de la quantité d'oxygène généré par l'électrolyse augmentant la sensibilité des bactéries aux antibiotiques.

I.1.2 Les méthodes chimiques

Dans l'environnement, les bactéries préfèrent se développer sur toutes les surfaces biotiques et abiotiques disponibles pour former un biofilm plutôt qu'en suspension sous forme planctonique qui est fréquemment exposée à de nombreux facteurs défavorables tels que les antibiotiques, les fluctuations de température ou de pH [11,88–90]. La formation d'un biofilm sur une surface est un processus dynamique complexe qui comporte généralement cinq étapes (T I-1): 1) fixation initiale réversible des cellules bactériennes planctoniques sur une surface, 2) fixation irréversible à la surface et production de substances polymères extracellulaires (EPS), 3) prolifération des cellules bactériennes et augmentation de la matrice d'EPS au sein du biofilm, 4) maturation du biofilm, 5) dispersion de certaines bactéries du biofilm vers le milieu environnant [91–93]. Comme évoqué dans l'introduction, les bactéries planctoniques ou celles en contact avec la surface lors de l'étape 1 sont plus sensibles aux facteurs environnementaux que les bactéries au sein du biofilm [14, 15]. Par conséquent, le développement de matériaux capables

de prévenir l'adhésion des bactéries et/ou la formation de biofilms à leur surface est un élément clé pour lutter contre la contamination bactérienne.

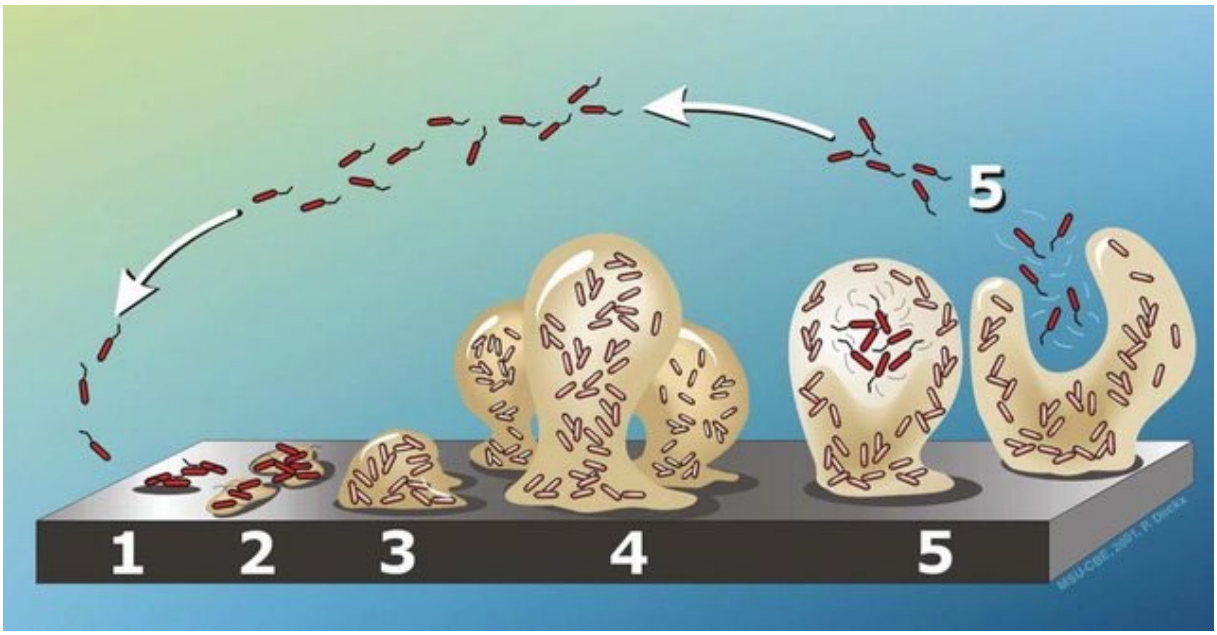

Figure I-1. Les différentes étapes de la formation du biofilm : 1) fixation initiale réversible des bactéries, 2) fixation irréversible des bactéries, 3) prolifération bactérienne et formation de la matrice, 4) maturation du biofilm, 5) dispersion de certaines bactéries. Reproduit de la réf. [92].

Trois principaux types de surfaces antibactériennes sont décrits dans la littérature : les surfaces antiadhésives, les surfaces à libération d'agents antibactériens et les surfaces « contact-killing » [94] (Figure I-2).

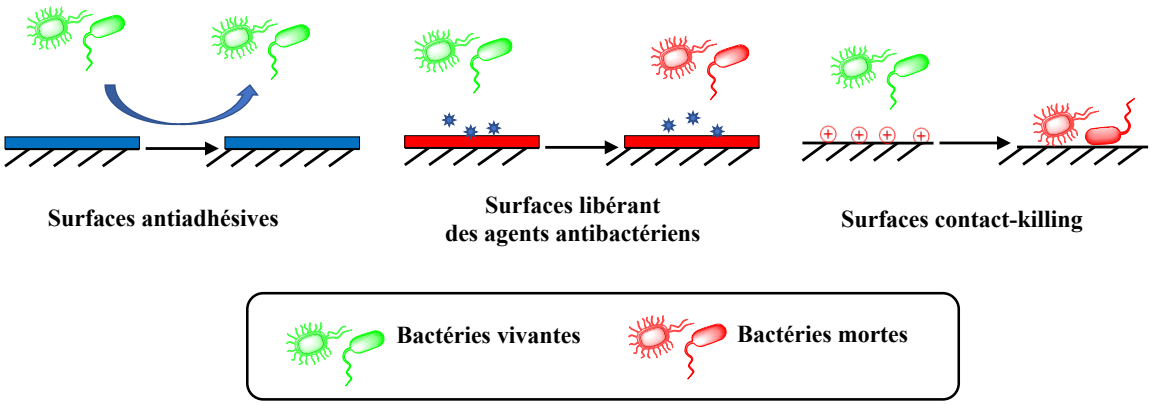

Figure I-2. Illustration des trois principaux types de surfaces antibactériennes.

I.1.2.1 Les surfaces antiadhésives

Les surfaces antiadhésives repoussent les bactéries en raison de certaines propriétés physico-chimiques telles que la charge de surface (charges négatives), la mouillabilité ou la topographie (surfaces micro/nano-structurées) [95–98]. Le greffage d'un revêtement polymère antiadhésif sur la surface du substrat est l'une des stratégies les plus utilisées. Par exemple des polymères très hydrophiles [99], tel que le poly(éthylène glycol) (PEG), peuvent être utilisé en raison de la couche d'humidité formée à la surface du substrat [100]. Des polymères de type zwitterionique peuvent aussi être utilisés [99]. Dans ce cas, en plus d'interagir avec les molécules d'eau *via* des liaisons hydrogènes comme le PEG, ces polymères peuvent former des coquilles d'hydratation plus solides par une interaction ion-dipôle entraînant une adsorption plus dense et plus serrée de l'eau ce qui empêche l'adhésion bactérienne et aussi l'adsorption non spécifique de protéines [101]. D'autres polymères tels que les polysaccharides [102], les polyhydroxy-polymères comme le poly(alcool vinylique) [103,104] peuvent également être utilisés comme revêtement antiadhésif. Comme le mode d'action des surfaces antiadhésives n'est pas de tuer les bactéries, ce type de surface n'est pas impacté par la résistance bactérienne. Cependant, ces surfaces n'affectant pas la viabilité des agents pathogènes, ces derniers, une fois repoussés, peuvent contaminer d'autres surfaces. De plus, l'approche antiadhésive peut rapidement être limitée par les facteurs physico-chimiques et environnementaux qui gouvernent le phénomène d'adhésion bactérienne. C'est pour cela qu'il est nécessaire d'avoir plusieurs stratégies antibactériennes en fonction des applications visées [105].

I.1.2.2 Les surfaces à libération d'agents antibactériens

Les surfaces libérant des agents antibactériens sont élaborées pour permettre la diffusion de ces dernier et ainsi avoir une action en solution (à distance de la surface) mais aussi au niveau de la surface (par les molécules non libérées) [106–108]. Une méthode de modification couramment utilisée pour permettre l'immobilisation non covalente sur une surface d'agents antibactériens tels que des antibiotiques [108], des peptides antimicrobiens [109,110], des éléments métalliques [111,112], des enzymes [113] ou des composés cationiques [114], est la création de multicouches de polyélectrolytes, formées par dépôt couche par couche (Layer by Layer (LBL)) d'un polycation et d'un polyanion, en raison de leur simplicité, de leur polyvalence et de leur faible coût. Par rapport aux méthodes traditionnelles d'administration d'agents antimicrobiens, cette technique permet de libérer localement une forte concentration de composés actifs, et donc d'exercer une activité antibactérienne uniquement là où elle est nécessaire. Cependant, la libération continue excessive d'antibiotiques peut également conduire au phénomène de résistance bactérienne [115].

De plus, l'activité de ce type de surface est finalement temporaire en fonction de la cinétique de libération des composés antibactériens.

I.1.2.3 Les surfaces « contact-killing »

Les surfaces « contact-killing » sont généralement basées sur des agents biocides cationiques tels que les composés d'ammoniums quaternaires, les phosphoniums quaternaires, les polymères à base de guanidine [116] ou les peptides antimicrobiens cationiques qui sont liés de manière covalente aux surfaces du substrat. Ces composés attirent les bactéries chargées négativement et peuvent entrainer la mort cellulaire des bactéries par perturbation (voire perméabilisation) de leur membrane [117–119]. Comme les composés antimicrobiens sont fixés de manière covalente à la surface et ne sont pas libérés dans le milieu, les surfaces « contact-killing » peuvent éviter le problème de l'épuisement temporaire des agents actifs, évoqué précédemment dans le cas des surfaces libérant des agents antibactériens. Bien que le mécanisme d'action exacte de ces types d'agents, une fois immobilisés, ne soit pas totalement élucidé, il semblerait qu'ils agissent par la pénétration de leur partie hydrophobe dans la membrane bactérienne [118,120–123] et/ou encore par un échange d'ions avec les bactéries [124]. Ainsi, les surfaces bactéricides par contact pourraient éviter le problème de la résistance bactérienne mais peuvent, cependant, devenir inactives par la formation d'une couche de bio-passivation constitué du matériel cellulaire des bactéries mortes [124].

I.2 Généralités sur le poly(diméthylsiloxane) (PDMS)

Les silicones sont une catégorie de polymères synthétiques qui n'existent pas dans la nature contrairement à de nombreux autres composés ou matériaux contenant du silicium, tels que l'acide orthosilicique et le minéral de quartz. Ils ont été synthétisés pour la première fois par Kipping en 1904 et ont reçu le nom de "silicones" en raison de leur similitude avec les cétones [125]. Les silicones sont des polymères mixtes inorganiques-organiques de formule chimique $(R_2SiO)n$ dont le squelette est constitué de liaisons répétées entre le silicium et l'oxygène, appelé "siloxane". En plus de se lier à l'oxygène pour former la chaîne polymère, les atomes de silicium sont également attachés à des groupes latéraux organiques tels que les groupements méthyles, phényles, vinyles et trifluoropropyles. Lorsque les groupes organiques sont des groupements méthyles et que les silicones sont terminés par des groupes triméthylsilyloxy, on parle de "polydiméthylsiloxane", abrégé en PDMS, qui est le plus courant des silicones, avec sa structure représentée sur la Figure I-3 [126].

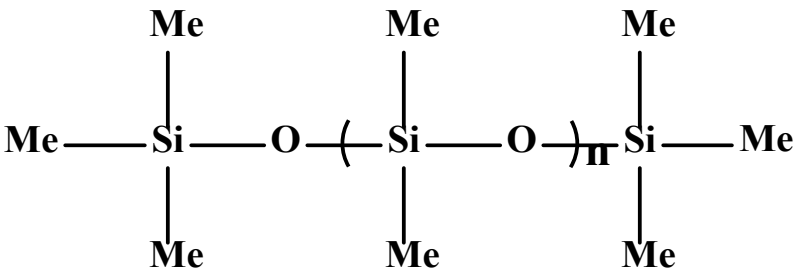

Figure I-3. Structure chimique du PDMS.

La présence simultanée de groupes "organiques" attachés à un squelette "inorganique" donne aux silicones une combinaison de propriétés uniques [127], ce qui permet leur utilisation dans de nombreuses applications et dans divers domaines tels que les matériaux isolants, les revêtements et l'encapsulation [128,129].

I.2.1 Les propriétés du PDMS

Le PDMS que nous avons utilisé dans notre étude est le Sylgard 184® de DOW Corning qui est largement cité dans la littérature scientifique [130–138]. Il est composé de deux parties (A et B) : la base, majoritairement constitué d'oligomères de diméthylsiloxane avec des groupes terminaux vinyliques (>60%), et le réticulant, majoritairement constitué de méthylhydrosiloxane, (entre 40–70%)[139]. La réaction de réticulation du Sylgard 184® est réalisée par hydrosilylation entre la double liaison carbone-carbone de la base et la fonction hydrosiloxane (Si-H) de l'agent réticulant (Figure I-4).

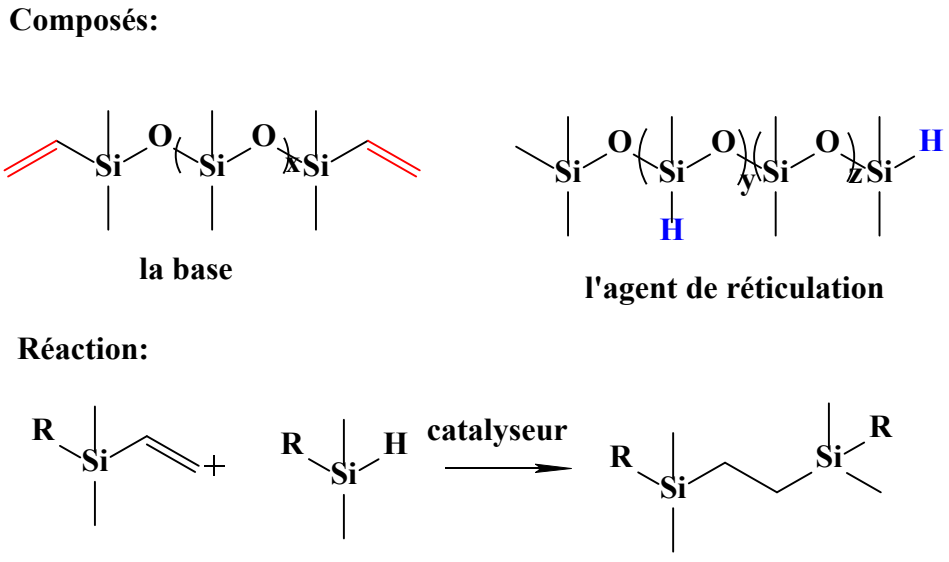

Figure I-4. Réaction de réticulation du polydiméthylsiloxane (PDMS).

Les principales caractéristiques physico-chimiques du PDMS sont regroupés dans le Tableau I-1. Le PDMS allie des propriétés exceptionnelles, il est optiquement transparent (240-1100 nm) [140–142], biocompatible, flexible avec une valeur de module d'élasticité de Young environ 1-3 MPa [143,144], résistant à la chaleur avec une valeur de conductivité thermique égale à 0,27 $W \cdot m^{-1}K^{-1}$, isolant thermique et électrique avec une grande valeur de résistivité électrique de $2{,}9 \times 10^{14}$ $\Omega \cdot cm$ [139], [145]. Il possède également une grande perméabilité aux gaz tel que l'oxygène ou le dioxyde de carbone[146–148], une faible constante diélectrique (2,72 à 100 kHz) et présentent des valeurs de tension superficielle très faibles environ 20 mN/m [149].

Tableau I-1. Quelques caractéristiques physico-chimiques importantes du PDMS (Sylgard 184).

Caractéristiques	Valeurs	Références
Transparence optique	240-1100 nm	140–142
Angle de contact à l'eau	100-112°	150
Module d'élasticité de Young E	~1-3 MPa	143,144
Conductivité thermique	0,27 $W \cdot m^{-1}K^{-1}$	145
Résistivité volumique électrique	$2{,}9 \times 10^{14}$ $\Omega \cdot cm$	139
Constante diélectrique à 100 Hz	2,68-2,72	145
Tension de surface	21-22 mN/m	149
Coefficient de diffusion de la vapeur d'eau	~1000-6000 $\mu m^2 s^{-1}$	147
Coefficient de diffusion de l'oxygène	~2000-4000 $\mu m^2 s^{-1}$	146
Coefficient de diffusion du CO_2	~1000 $\mu m^2 s^{-1}$	148

I.2.2 Les applications et problématique du PDMS dans le domaine médical

En raison de sa grande souplesse, son hydrophobicité, sa stabilité chimique et thermique et sa biocompatibilité [126,151], le PDMS est largement utilisé dans le domaine médical. En particulier dans les applications orthopédiques comme par exemple les implants articulaires de la main et du pied [152], les cathéters [153], les équipements extracorporels [127] et les implants esthétiques [154,155]. Néanmoins, son hydrophobicité engendrent l'absorption des petites molécules hydrophobes dans la masse du matériau et l'adsorption des grosses molécules telles que les protéines à la surface [156], ce qui peut entraîner une contamination bactérienne et la formation d'un biofilm à sa surface. Ceci posent de graves problèmes pour la santé humaine, pouvant ainsi limiter son utilisation [157–159]. Selon la dernière enquête nationale de prévalence commandée en 2017 par le ministère de la santé, le nombre d'infections nosocomiales est en augmentation [160]. Parmi ces infections, les infections urinaires, causées couramment par la contamination bactérienne de cathéters, sont les plus fréquentes avec une prévalence de 28,47%. Pour résoudre ces problèmes, un certain nombre d'efforts ont été faits pour modifier ou fonctionnaliser les surfaces de PDMS afin d'empêcher l'adsorption non spécifique de protéines ou la contamination bactérienne, tout en conservant les avantages de ses propriétés, en particulier sa transparence optique et sa grande flexibilité.

Dans les paragraphes suivants, nous présenterons quelques traitements physiques majeures telles que le traitement par plasma d'oxygène, le traitement par UV/Ozone, ainsi que des méthodes chimiques telles que le dépôt couche par couche (LBL), la silanisation, l'hydrosilylation, le chimie click ou le photogreffage.

I.3 Traitements physiques de surfaces de PDMS

I.3.1 Le traitement par plasma d'oxygène

Le traitement par plasma d'oxygène est de loin la méthode la plus couramment utilisée pour modifier la surface du PDMS, ce qui permet non seulement d'augmenter sa mouillabilité à l'eau mais aussi de créer des groupes fonctionnels chimiques tels que les groupes hydroxyles [161–163]. En effet, comme représenté sur la Figure I-5, la forte densité d'espèces réactives ionisées générées par le plasma d'oxygène attaque le squelette siloxane et peut ainsi former, entre autre, des groupes silanols (Si-OH), rendant la surface du PDMS hydrophile [163,164]. Cependant, ce traitement n'est pas stable dans le temps et l'hydrophobie d'origine du PDMS se rétablit après

quelques minutes à plusieurs heures, provenant de la dynamique élevée des chaînes macromoléculaires du PDMS entrainant la diffusion des groupes hydroxyles dans la masse [165].

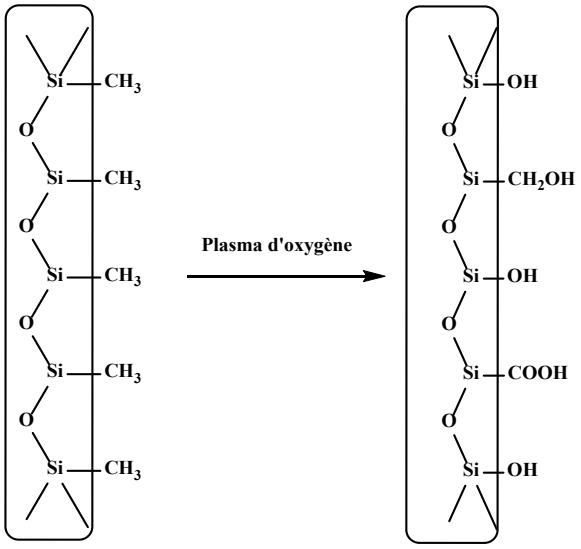

Figure I-5. Schéma du processus de réaction de modification par plasma d'oxygène [163].

De nombreux paramètres influencent la stabilité du traitement par plasma d'oxygène. Il semblerait que les conditions de réticulation du PDMS telles que la température, le temps de réticulation, et le rapport massique entre la base et le réticulant influencent la stabilité du traitement plasma dans le temps. En effet, une réticulation incomplète permet aux espèces libres de migrer plus facilement à travers le réseau du PDMS [166]. Par exemple, Kim *et al.* [156] ont étudié l'influence du traitement par plasma d'oxygène à pression atmosphérique sur des surfaces de PDMS préparées avec deux différents rapports entre la base et le réticulant (5 :1 (PDMS-5) et 20 :1 (PDMS-20)). Ils ont caractérisé les surfaces par des mesures de l'angle de contact avec l'eau (ACE), par microscopie électronique à balayage (MEB) et par spectroscopie infrarouge à transformée de Fourier (IRTF). Ils ont constaté que la valeur de l'ACE des deux types de PDMS avait fortement diminué après le traitement plasma, passant d'environ 100° à environ 10° (mesuré 2 heures plus tard), rendant le PDMS très hydrophile. Cependant, ce caractère hydrophile a diminué avec le temps avec des valeurs d'ACE de 74,3° et 63,6° après 120 h pour le PDMS-5 et le PDMS-20 respectivement. De plus, on peut noter que l'ACE du PDMS-20 était toujours inférieure à celui du PDMS-5 avant ou après le traitement plasma, ce qui indique que l'ACE des échantillons augmente avec le réticulant. En plus des conditions de préparation du PDMS, les conditions du traitement plasma (telles que la puissance et la durée) [167,168] et les conditions de stockage post-traitement [168–171] peuvent également influencer la stabilité du

traitement par plasma. En effet, par exemple, un stockage dans l'eau permet de conserver l'hydrophilie de ces surfaces.

I.3.2 Le traitement par UV/Ozone (UVO)

L'exposition aux UV/Ozone (UVO) est une autre technique couramment utilisée pour modifier la surface du PDMS. Berdichevsky *et al* [172] ont découvert que les échantillons de PDMS modifiés par un traitement aux UVO pendant 30 minutes ne provoquent pas de fissures, contrairement au traitement au plasma d'oxygène qui engendre des fissures dès 1 minute de traitement. De plus, le traitement UVO semble plus stable que le traitement plasma. En effet, l'hydrophobie d'origine du PDMS se rétablit plus lentement que le traitement plasma (environ 3 jours contre quelques heures respectivement). Si l'on suppose que le mécanisme de récupération de l'hydrophobie est le même cela suggère que les échantillons traités aux UVO ont probablement une couche modifiée plus épaisse que les échantillons traités au plasma d'oxygène avec un changement chimique de surface similaires. Cependant, pour des raisons probablement cinétiques, le traitement UVO nécessite une durée de traitement plus longue que le plasma pour avoir une bonne fonctionnalisation de la surface [172,173]. Le mécanisme de modification de la surface du PDMS par les UVO, représenté sur la figure I-6, est un processus photochimique. Lorsque la lumière UV (longueur d'onde 185 nm ou 254 nm) est mise en contact avec la surface du polymère dans une atmosphère d'oxygène une réaction d'oxydation se produit [172,174].

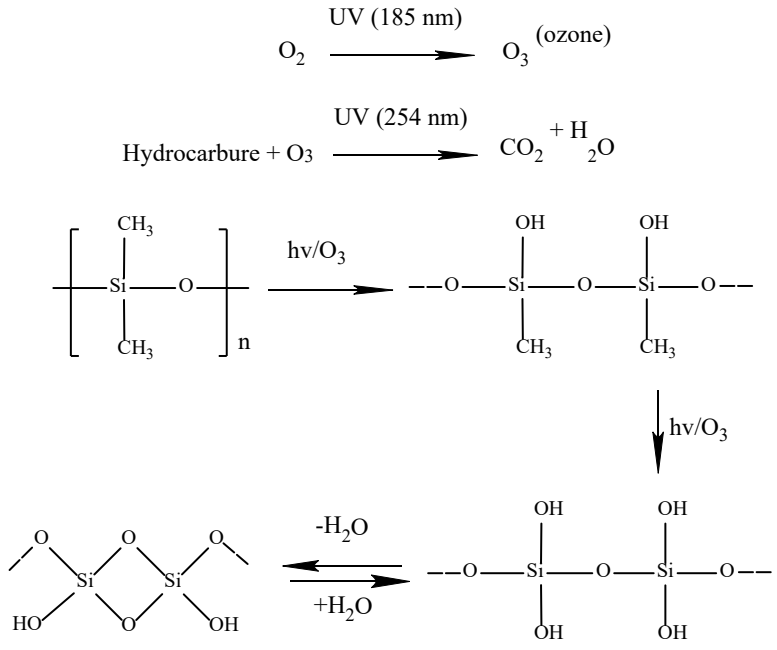

Figure I-6. Mécanisme du traitement UV/Ozone d'une surface en PDMS [172,174].

Comme pour le traitement par plasma, l'effet du traitement par UVO n'est pas stable dans le temps et est influencé par les mêmes paramètres [165,172,173,175]. Par exemple, Olah *et al.* [165] ont démontré par XPS qu'après un traitement UVO de 60 minutes, une couche de silice hydrophile (SiO_χ) s'est formée. De plus, les valeurs d'angles de contact à l'avancée (θ_{adv}) et au retrait (θ_{rec}) diminuent de 100° pour le PDMS natif jusqu'en dessous de 40° pour un temps de traitement de 60 minutes ou plus, correspondant à une surface de PDMS hydrophile. Cependant, le caractère hydrophile diminue au fur et à mesure du temps post-traitement [176].

I.4 Modifications chimiques de surfaces de PDMS

I.4.1 Modification non covalente par dépôt couche par couche (layer-by-layer (LBL))

Le dépôt de film LBL est une stratégie de modification de surface qui permet de former un film mince par adsorption alternée de polyanions et de polycations sur pratiquement tous types de substrats afin de produire des multicouches de polyélectrolytes (PEMs) [177]. Cette technique est simple, efficace, facile à mettre en place et un contrôle de l'épaisseur à l'échelle nanométrique est possible. Cependant, l'inconvénient, pour une application de cette approche, est la stabilité du revêtement dans les temps. Le processus de formation des LBLs est illustré sur la Figure I-7.

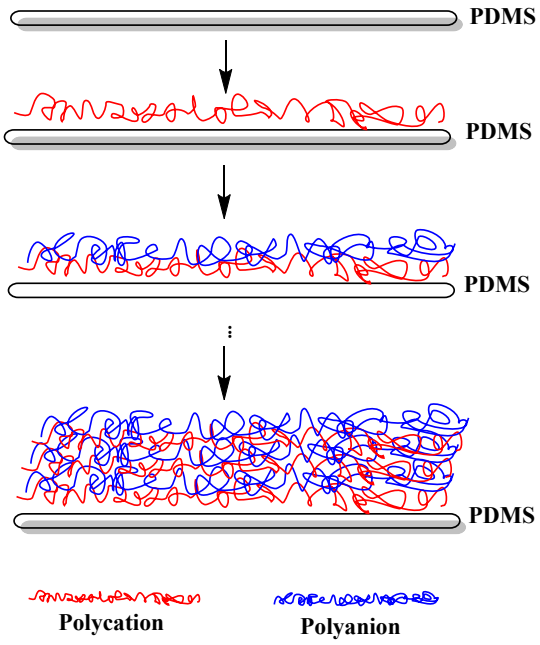

Figure I-7. Schéma du dépôt couche par couche.

Tian *et al.* [163] ont utilisé cette technique pour modifier des surfaces de PDMS à partir du poly(chlorure de diméthyldiallyl ammonium) (PDDA, 20 % en poids dans l'eau) et du poly (4-styrène sulfonate de sodium) (PSS, 30 % en poids dans l'eau) en réalisant des films à 5, 10 et 15 couches à différentes concentrations en polymères de 0,01 %, 0,02 % et 0,03 % (V/V). Ils ont constaté qu'à partir d'une concentration de 0,02 % la valeur de l'ACE ne varie quasiment plus. De plus, les résultats des tests de vieillissement des échantillons modifiés à une concentration de 0,02% ont montré qu'il existe toujours des phénomènes de récupération après un stockage de longue durée. Cependant, plus le nombre de couches augmente plus le retour à l'état initial du PDMS est lent. En effet, quel que soit le temps de stockage, la surface de PDMS recouverte de 10 couches permet d'obtenir le caractère le plus hydrophile avec, par exemple, un ACE égal à 61° après 15 jours de stockage.

L'architecture poreuse et supramoléculaire des films PEMs [178] permet l'incorporation d'une large gamme de molécules bioactives, en général, par interactions électrostatiques [179–181]. La force ionique, le type de solvant, la température, la concentration de la solution et le pH de la solution (pour les polyélectrolytes faibles) peuvent affecter la stabilité et la fonctionnalité de surface des films PEMs [182]. Par exemple, Wang *et al.* [183] ont préparé des films en utilisant du poly(acide acrylique) modifié avec de la dopamine (PAA-dopa) ou non et de la poly(éthylèneimine) (PEI) et ils ont étudié l'effet du pH sur l'incorporation du sulfate de gentamicine (SG), qui est un antibiotique. Ils ont constaté que la valeur du pH influençait l'incorporation de la SG et que pour des pH acides, la déprotonation des fonctions carboxyles du PAA permettaient d'augmenter l'incorporation du SG par interaction électrostatique. De plus, ils ont étudié l'effet de la réticulation des films sur le taux de libération du SG afin de contrôler la diffusion de la molécule active qui est un paramètre important pour une activité à long terme. Pour cela, ils ont comparé la vitesse de diffusion du GS dans des films avec du PAA non réticulé et des films avec du PAA réticulé par la dopamine. Ils ont observé que 99 % de la SG était libérée après 8 heures pour le film avec du PAA non réticulé, contre seulement 46 % après 8 heures et 88 % après 168 heures pour le film avec du PAA réticulé. Ceci montre la possibilité de contrôler la diffusion des composés actifs incorporés dans des films LBLs. Parallèlement, ils ont montré que les films PEMs chargés de SG présentaient une activité bactéricide contre *Staphylococcus aureus* (*S. aureus*) et aucune cytotoxicité envers les cellules épithéliales du cristallin humain (HLEC pour anglais human lens epithelial cells). En outre, ils ont réalisé une expérience *in vivo* qui a démontré que le PDMS modifié peut favoriser la

cicatrisation des plaies et avoir un effet anti-inflammatoire. Le Tableau I-2 regroupe certains travaux publiés sur la modification de la surface du PDMS par dépôt LBL.

Tableau I-2. Résumé des travaux publiés sur la modification de la surface du PDMS pour une application biomédicale en utilisant le dépôt LBL.

Matériau	**Principales propriétés de la surface modifiée**	**Application potentielle**	**REF**	**Type d'action antibactérienne**
$(PAA\text{-}dopa/PEI)_n$ films multicouches chargés de SG	Libération prolongée de SG : ≈95% de réduction de *S. aureus ;* Non cytotoxique pour les HLEC ; Propriétés de cicatrisation des plaies et d'anti-inflammation.	Surfaces thérapeutiques (applications biomédicales)	183	Libération d'agents antibactériens
$(dopa\text{-}PAA/PEI\text{-}AgNPs)_n$[a] films multicouches	Libération prolongée de Ag^+ ; Bactéricide contre *S. aureus* et *E. coli* ; Faible cytotoxicité envers HLECs ; Propriétés de cicatrisation des plaies et d'anti-inflammation.	Modification des implants et autres dispositifs biomédicaux	184	Libération d'agents antibactériens
$(PAA/(PVP/CHI))_n$[b] films multicouches chargés de SG	ACE : 50,4±3,4° (n=10) ; Propriétés bactéricides contre trois types de Gram+, trois types de Gram- et un type de champignon.	Applications biomédicales	185	Libération d'agents antibactériens
(Poly (acide acrylique) /poly (chlorhydrate d'allylamine))$_n$ $(PAA/PAH)_n$ films multicouches chargés de AgNPs	Activité antibactérienne contre *S. epidermidis* et *P. aeruginosa* (99,99% de destruction bactérienne en 12 h lorsque [Ag] = 1,0±0,12 µg/cm^2)	Fonctionnalisation des surfaces des tissus biologiques/des dispositifs médicaux	138	Libération d'agents antibactériens

Tableau I-2 (Suite).

Matériau	Principales propriétés de la surface modifiée	Application potentielle	REF	Type d'action antibactérienne
$(PAH/PAA)_n$ films multicouches chargés de chlorhexidine	Activité antibactérienne contre *S. aureus* (3 log ou 4 log de réduction avec "n" égal à 40 ou 80 respectivement)	Fonctionnalisation des surfaces des tissus biologiques/des dispositifs implantables	186	Libération d'agents antibactériens
$(Urushiol/BPEI)_n$[c] films multicouches	ACE : 130,96 ±4,76° (n=50) ; Effets inhibiteurs contre *S. aureus* et *P. aeruginosa*	Applications biomédicales	187	Surfaces Antiadhésives
(PSS/PTMAEMA-*co*-dérivées de PSPE /CDH)$_n$[d] films multicouches	ACE : 22° ; Propriétés antiadhésives et bactéricides contre *S. aureus*	Sondes urinaires antimicrobiennes	188	Antiadhésive/ Contact-killing

[a] AgNPs : Nanoparticules d'Ag

[b] PVP : polyvinylpyrrolidone ; CHI : chitosan

[c] BPEI : polyéthylèneimine ramifiée

[d] PSS : poly (sulfonate de styrène); PTMAEMA-*co*-dérivées de PSPE : polymères multifonctionnels comprenant des zwitterions et des groupes d'ammonium quaternaire; CDH : cellobiose déshydrogénase.

La modification de surface de PDMS par des méthodes physiques ou par LBL est expérimentalement simple et rapide, mais n'est cependant pas stable à long terme. Afin de pallier ce problème, une autre approche est de modifier chimiquement la surface du PDMS via une liaison covalente entre un groupe fonctionnel de la surface et un groupe fonctionnel d'une (macro)molécule bioactive.

I.4.2 Modification covalente de surfaces de PDMS

Le greffage covalent de (macro)molécules actives sur des surfaces de PDMS peut être réalisé par différentes méthodes [189–197]. Cependant, dans la majorité des cas, la modification directe de la surface native est difficile à réaliser en raison de l'inertie et de la stabilité chimique de ce matériau. Il est donc souvent nécessaire d'effectuer un traitement préalable afin de générer des sites d'ancrage fonctionnels tels que des fonctions hydroxyles par exemple [198]. Ces groupes

hydroxyles peuvent être introduits à la surface du PDMS par oxydation dans une solution H_2SO_4/H_2O_2 [102,199], par traitement plasma d'oxygène ou par traitement UVO [172,174,176]. Par contre, le couplage post-traitement doit être réalisé rapidement (de l'ordre de quelques minutes) en raison du phénomène de retour à l'hydrophobie, expliqué précédemment.

Dans le paragraphe suivant, nous présentons quelques méthodes de modifications chimiques covalentes de surface du PDMS, décrites lors des deux dernières décennies, à savoir la silanisation, l'hydrosilylation, la chimie click et le photo-greffage.

I.4.2.1 La silanisation

La silanisation est l'une des stratégies de modification covalente les plus utilisées, basée sur la réaction entre un groupement alcoxysilane porté par la (macro)molécule à greffer et un groupement hydroxyle de la surface, donnant lieu à des liaisons siloxanes (Figure I-8).

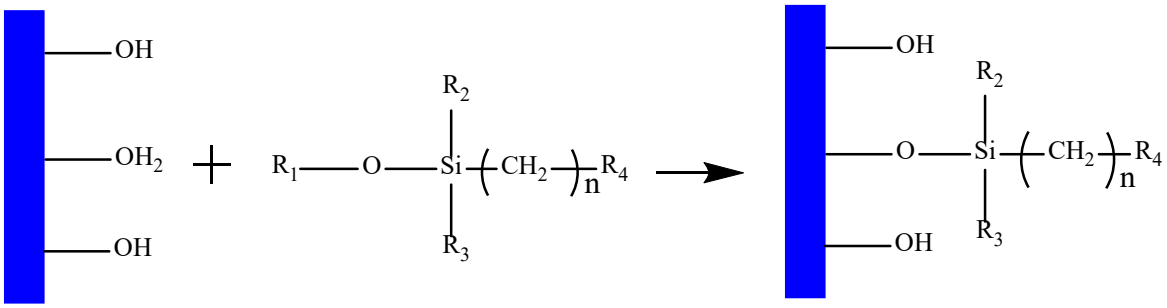

Figure I-8. Réaction de condensation d'alcoxysilanes avec des fonctions hydroxyle sur des surfaces.

La silanisation présente de nombreux avantages tels que son faible coût, son efficacité, sa simplicité ainsi qu'un large éventail de composés alcoxysilane commerciaux, ce qui explique son importante utilisation dans la littérature pour modifier la surface du PDMS [133,137,200–206]. De plus, la liaison entre les alcoxysilanes et les fonctions hydroxyles de la surface peut se faire par l'intermédiaire d'un à trois groupes alcoxyles, ce qui permet une bonne orientation du greffon et une modification stable.

Il est donc possible d'élaborer des surfaces antibactériennes directement par modification du PDMS par des (macro)molécules actives ayant des groupes alcoxysilanes. Par exemple, Yeh *et al.* [207] ont modifié la surface du PDMS préalablement traité par plasma d'oxygène par un silane sulfobétaïne (SBSi) pour développer une interface zwitterionique superhydrophile (ACE = 6,8±1,7°) stable (PDMS-SBSi). Le PDMS-SBSi préparé a montré une excellente résistance à l'adhésion bactérienne à l'égard de *S. epidermidis* et *P. aeruginosa* avec des taux d'inhibition de 99,78% et 99,86%, respectivement, par rapport à l'adhésion sur la

surface de PDMS non modifiée. De plus, la surface modifiée a présenté également une excellente résistance à l'adsorption de bio(macro)molécules, avec des taux d'inhibition de 98 % et 97 % contre l'albumine de sérum bovine (BSA) et la mucine, respectivement. De plus, la modification est stable dans le temps avec une conservation de sa biointégrité après 30 jours de stockage dans des conditions ambiantes.

Cependant, cette méthode de modification est plutôt utilisée comme un deuxième prétraitement pour apporter une fonction chimique d'ancrage, autre que des fonctions hydroxyles, pouvant permettre par la suite l'immobilisation de (macro)molécules actives. A cet effet, le (3-aminopropyl) triéthoxysilane (APTES) a été largement utilisé comme agent de couplage pour introduire un groupement amino permettant l'immobilisation covalente de (macro)molécules ayant par exemple des fonctions acides carboxyliques ou aldéhydes[133].

Tang *et al.* [208] ont développé des surfaces de PDMS antiadhésives par polymérisation radicalaire contrôlée par transfert de chaîne réversible par addition-fragmentation de molécules antimicrobiennes, initiée à partir de la surface du PDMS (SI-RAFT) (Figure I-9). Ils ont immobilisé l'agent RAFT (l'acide 4-cyano-4-(phénylcarbonothioylthio)pentanoïque (CPCTTPA)) par immersion du PDMS traité à l'APTES dans une solution contenant cet agent et des molécules permettant la réaction de couplage. Ensuite, la surface PDMS-PEG a été obtenue en polymérisant le méthacrylate de polyéthylène glycol (PEGMA) à partir de la surface du PDMS (grafting from), en présence d'amorceurs appropriés préalablement immobilisés sur la surface. La surface modifiée a présenté une grande hydrophilie avec un ACE de 50,6° et 8,0° après que la goutte d'eau ait été en contact avec la surface pendant 30s et 11 minutes, respectivement. En outre, la surface PDMS-PEG a montré d'excellentes propriétés antisalissures contre les protéines (réduction de l'adhésion de 60 % par rapport à la surface vierge), les cellules épithéliales du cristallin (LEC : lens epithelial cell) et *S. aureus*.

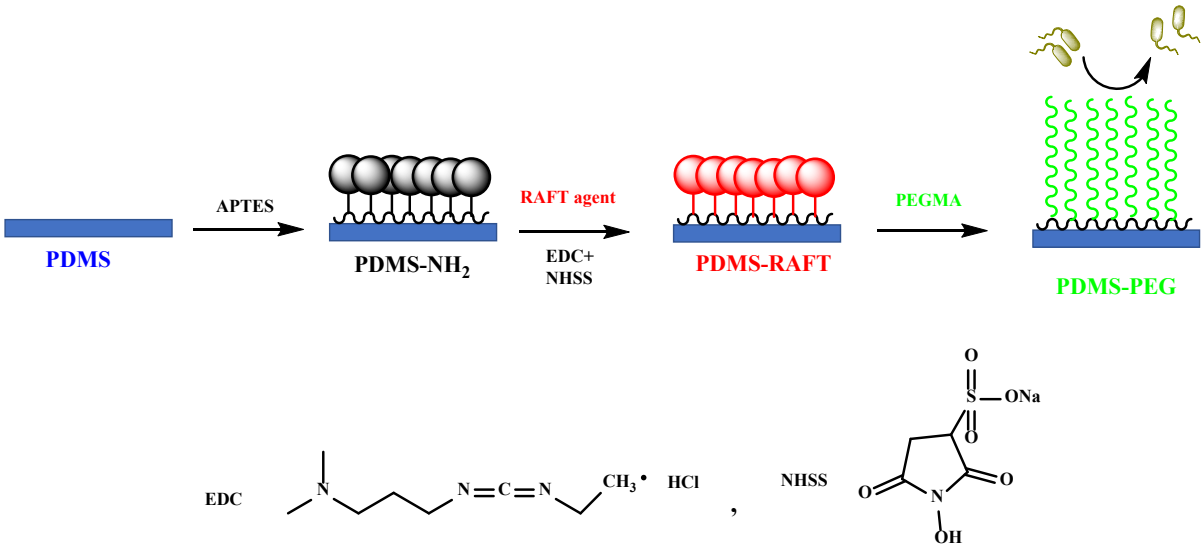

Figure I-9. Illustration schématique d'exemples de modification de la surface du PDMS par la combinaison de la silanisation et du " grafting from ".

Fernandes *et al.* [200] ont introduit le groupe époxy sur la surface du PDMS via l'immobilisation du (3-glycidyloxypropyl) triéthoxysilane (GOPTS). Ensuite, des nanosphères d'aminocellulose antibactériennes (ACNS) ont été immobilisées sur le PDMS par la technique du "grafting to" [209] via une réaction époxy-amine (Figure I-10). La surface PDMS modifiée par les ACNS a montré une inhibition efficace de la formation de biofilms de *E. coli* en réduisant la masse totale de bactéries sessiles jusqu'à 80% par rapport au PDMS prétraité par le silane.

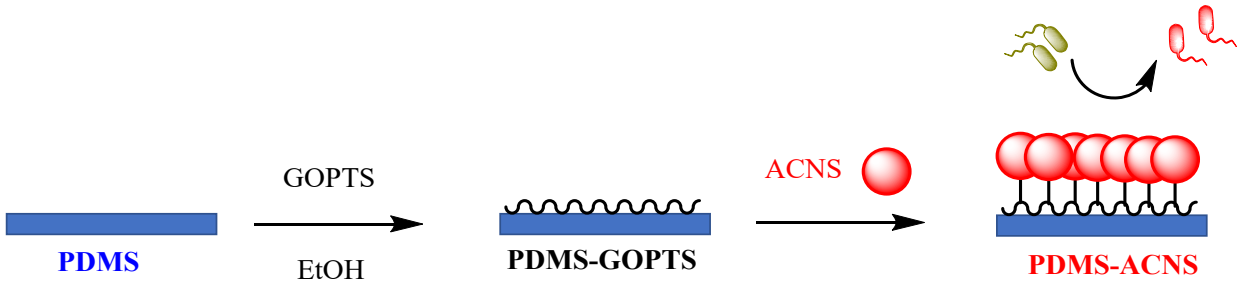

Figure I-10. Illustration schématique d'exemples de modification de la surface du PDMS par la combinaison de la silanisation et du " grafting to ".

Certains travaux publiés sur la modification de surface du PDMS par silanisation sont représentés dans le Tableau I-3.

Tableau I-3. Résumé des travaux publiés sur la modification de la surface du PDMS pour des applications biomédicales en utilisant le PDMS prétraité par silanisation.

Type de surface	Principales propriétés de la surface modifiée	Application potentielle	REF	Type d'action antibactérienne
PDMS-SBSi	ACE : 6,8±1,7° ; Réduction de plus de 99% de l'adhésion de *S. epidermidis* et *P. aeruginosa*, Antifouling	Dispositifs implantables	207	Antiadhésive
PDMS-PEG (grafting from)	ACE : 50,6° (30s) et 8,0° (11min) ; Résistance à l'adhésion des protéines, des LEC et de *S.aureus*	Biomatériaux implantables	208	Antiadhésive
PDMS-p (MA POSS-co-DMAEMA^{+})[a] (grafting from)	ACE : 101,6±3,1°, 92,1±1,3° et 86,4±2,8° avec une teneur en DMAEMA^{+} de 0,05, 0,10 et 0,20, respectivement, Propriétés antiadhésives et bactéricides contre *S. aureus*	Réduction de l'occurrence de l'opacification de la capsule postérieure après une chirurgie de la cataracte	133	Antiadhésive / Contact-killing
PDMS-GO-DMA[c]	ACE : 54,2°, Propriétés antibactériennes contre *S. aureus* et *E. coli*	Applicabilité sur les micro-dispositifs biomédicaux	204	
PDMS-MPA-N^{+} [d]	ACE : 78,6±1,3°, Propriétés antimicrobiennes et antibiofilm contre *S. aureus*, *E. coli* et *P. aeruginosa*, Hémocompatibilité et non cytotoxicité	Implants biomédicaux à court terme (11 jours)	210	Contact-killing

Tableau I-3 (Suite).

Type de surface	Principales propriétés de la surface modifiée	Application potentielle	REF	Type d'action antibactérienne
PDMS conjuguée IA[b] ou PIA	ACE : 34,6±1,8° et 42,3±0,4° du PDMS conjugué IA ou PIA, respectivement ; Antifouling et non cytotoxicité	Applications biomédicales	137	Antiadhésive
PDMS-APTES chargé de SA[e]	Propriété antimicrobienne contre *E. coli*, *S. aureus* et *S. epidermidis*	Applicabilité aux dispositifs médicaux	202	Libération d'agents antibactériens
PDMS-ACNSs (grafting to)	Propriété antibiofilm contre *E. coli* (réduction de 80% de la masse totale des bactéries sessiles)	Réduction des infections associées aux cathéters causées par *E. coli*	200	Contact-killing
PDMS-HB-PEI$^+$ [f] (grafting to)	Efficacité élevée contre toutes les souches de bactéries Gram+ testées, mais pas contre toutes les souches Gram- testées	Implants et dispositifs temporaires en PDMS (cathéters et prothèses vocales, etc.)	205	Contact-killing

[a] p (MA POSS-co-DMAEMA$^+$: poly (méthacrylisobutyl-silsesquioxane oligomère polyédrique-co-2-(diméthylamino)-méthacrylate d'éthyle) quaternisées.

[b] IA : l'acide itaconique.

[c] GO : l' oxyde de graphene; DMA : un dérivé de catéchol-monomère de méthacrylamide de dopamine.

[d] MPA-N$^+$: le cation ammonium quaternaire de l'acide maléopimarique.

[e] SA : l' acide salicylique.

[f] HB : hyberbranché; PEI$^+$: polyéthylèneimine (PEI) quaternisées avec du bromohexane et de l'iodométhane.

I.4.2.2 L'hydrosilylation

Des groupes Si-H peuvent être introduits à la surface du PDMS réticulé par insertion catalysée par un acide de polyméthylhydroxysiloxane [193,194] qui peuvent être mis à profit pour greffer des (macro)molécules bioactifs contenant des doubles liaisons carbone-carbone via une

réaction de couplage par hydrosilylation (Figure I-11), qui est l'une des stratégies les plus utilisées pour fonctionnaliser les surfaces du PDMS.

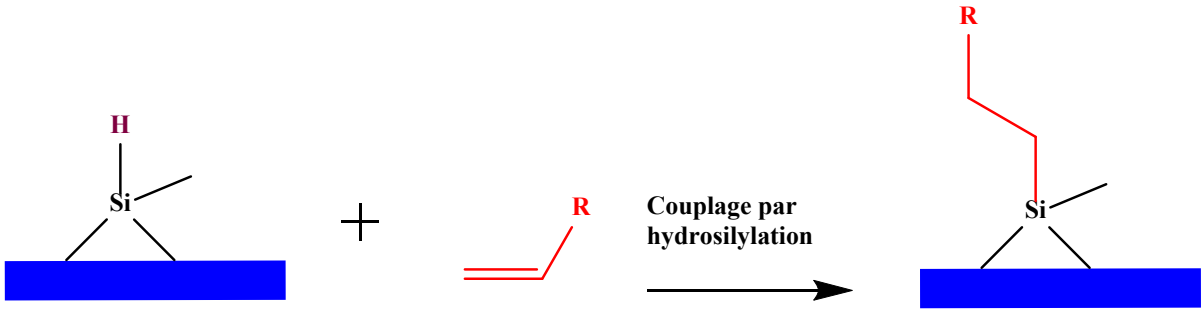

Figure I-11. Illustration de la réaction de couplage par hydrosilylation.

Chen *et al.* [194] ont incorporé du Si-H à la surface du PDMS en utilisant du $(MeHSiO)_n$ dans des conditions acides. Ensuite, des mono- et di-vinyl PEG de différentes masses molaires (de 350 à 2000 g/mol) ont été greffés sur du PDMS via une réaction d'hydrosilylation entre le Si-H surfacique et les groupes vinyles du PEG. Les surfaces obtenues se sont révélées plus hydrophiles que le PDMS natif avec un θ_{adv} allant de 65° à 110° et un θ_{rec} inférieure à 56° contre environ 120° et 110° pour le PDMS natif, respectivement. De plus, les auteurs ont étudié la propriété d'antisalissure des surfaces en utilisant du fibrinogène radiomarqué et les résultats ont montré que toutes les surfaces modifiées pouvaient réduire de manière significative (plus de 90%) l'adsorption des protéines, à l'exception de l'échantillon fonctionnalisé avec du PEG 2000 difonctionnel présentant une densité de fibrinogène adsorbé en surface de 220 ng/cm^2 contre 250 ng/cm^2 sur le PDMS vierge. Dans une autre étude, Chen *et al.* [193] ont immobilisé l'héparine sur la surface du PDMS grâce à un espaceur PEG hétérobifonctionnel (porteur d'un groupement vinyle et d'un groupement carbonate de succinimidyle) qui a été greffé sur le substrat de PDMS par hydrosilylation entre les groupes vinyles du PEG et les groupes Si-H introduits sur la surface du PDMS en utilisant la méthode précédente [194]. La surface finale obtenue (PDMS-PEG-Héparine) a présenté des valeurs de θ_{adv} et θ_{rec} de 48° et 31° contre 85° et ≈56° pour le PDMS-PEG, respectivement. De plus, les deux surfaces (PDMS-PEG et PDMS-PEG-Héparine) ont montré une réduction significative de l'adsorption des protéines avec seulement 5 et 6 ng/cm^2 respectivement par rapport à la surface témoin (46 ng/cm^2). Alors que pour l'adsorption de l'antithrombine (AT), des niveaux élevés d'AT ont adhérés sur la surface PDMS-PEG-Héparine avec 660 ng/cm^2 mais seulement 50 et 7 ng/cm^2 sur la surface témoin et la surface PDMS-PEG. D'autres tests de prévention de la formation de thrombus sur la surface PDMS-PEG-Héparine ont été effectués et le résultat a montré que la surface PDMS-PEG-Héparine était significativement moins thrombogène que les autres surfaces testées, ce qui

suggère que cette surface peut être utilisée pour améliorer les propriétés thrombogènes des biomatériaux en contact avec le sang.

D'autres travaux ont utilisé les groupes Si-H résiduels à la surface du PDMS après sa réticulation pour directement modifier la surface de PDMS par hydrosilylation. Par exemple, Mussard *et al.* [190]ont développé un nanofilm antiadhésif de type glycocalyx sur du PDMS par hydrosilylation entre les groupes Si-H surfaciques et des groupes vinyles d'un dérivé de méthylcellulose (Figure I-12-***1***). La réaction a été conduite dans l'eau en une étape sans ajout de catalyseur au platine. La surface de PDMS modifiée a montré un caractère plus hydrophile que le PDMS natif avec un $\theta_{adv} \approx 90°$ et un $\theta_{rec} \approx 35°$ contre $\theta_{adv} \approx 110°$ et $\theta_{rec} \approx 75°$ respectivement. En outre, cette surface de PDMS biomimétique modifiée a présenté non seulement une propriété d'adsorption non spécifique des protéines (telles que la BSA et le fibrinogène), mais aussi une propriété antiadhésive à l'égard des bactéries et des cellules de mammifères, ce qui peut permettre une potentielle utilisation de cette surface dans le domaine de la microtechnique et de la biomédecine.

Afin d'augmenter la densité de greffage de polymères par la technique d'hydrosilylation, Zhang *et al.* [211] et Kebir *et al.* [131] ont préparé des surfaces du PDMS avec plus de groupes Si-H résiduels en ajustant les rapports massiques entre le précurseur et son agent réticulant. (Figure I-12).

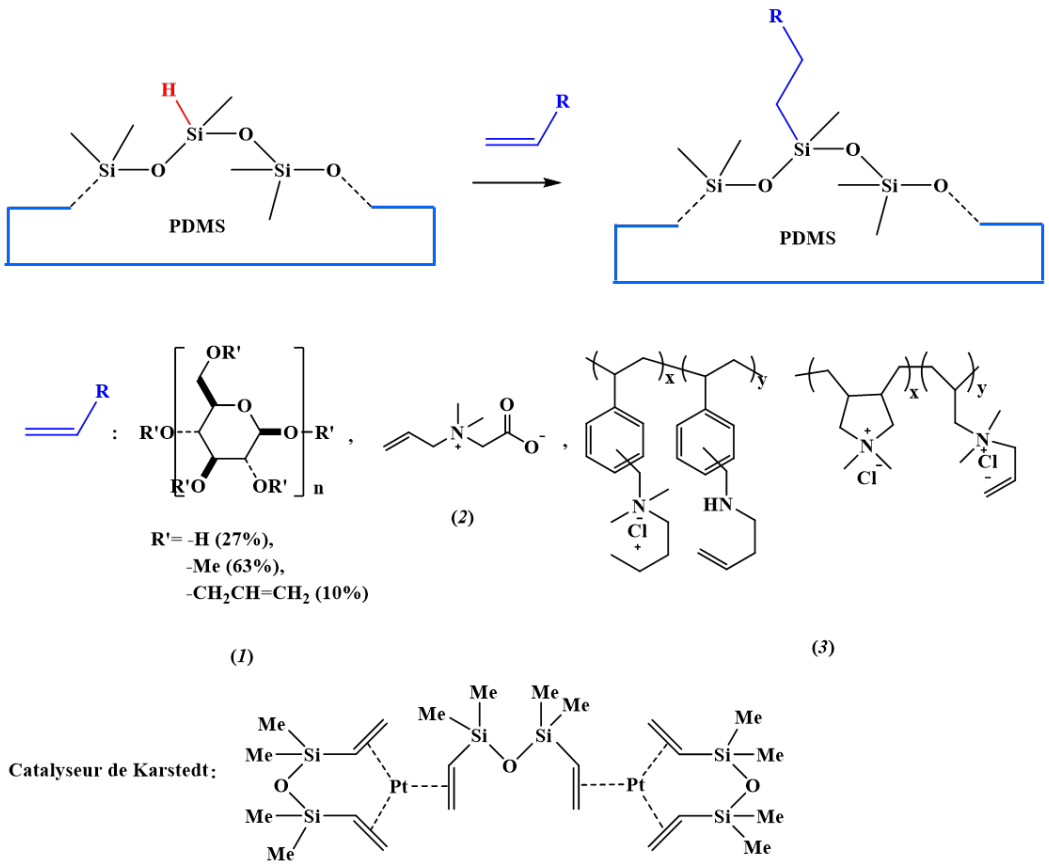

Figure I-12. Illustration schématique de quelques exemples de modification de surface de PDMS par réaction d'hydrosilylation.

Zhang *et al.* ont synthétisé une nouvelle molécule zwitterionique (allyl carboxybetaine (CB), (Figure I-12-***2***)) par la réaction de quaternisation de la *N,N*-diméthylallylamine avec le chloroacétate de sodium et ont ensuite greffé de manière covalente cette molécule sur une surface de PDMS par hydrosilylation en présence d'un catalyseur organométallique à base de platine, connu sous le nom de catalyseur de Karstedt. Ils ont choisi un rapport massique de 1:1 entre la base et le réticulant pour préparer un PDMS de haute densité en Si-H surfacique. L'hydrophilie du PDMS modifié (PDMS-CB) a été significativement améliorée avec une valeur d'ACE de ≈ 46° contre 103° pour le PDMS non modifié, avec une stabilité à long terme testée sur une période de 3 mois. Les auteurs ont également étudié la biocompatibilité et la propriété d'antisalissure de la surface de PDMS-CB contre les protéines et les bactéries. Les résultats ont montré que le PDMS-CB n'était pas toxique pour les cellules L929 et présentait une amélioration significative de la biocompatibilité du sang. De plus, la surface PDMS-CB a montré des propriétés d'antisalissure à travers sa résistance à l'adsorption non spécifique de protéines (BSA), avec une réduction de plus de 75 % par rapport au PDMS vierge, mais aussi sa résistance à l'adhésion bactérienne de *S. aureus* et *E. coli.*

Kebir *et al.* ont eux développé une surface de PDMS contact-killing en greffant deux polymères cationiques contenant des groupes vinyle et ammonium quaternaire (Figure I-12-***3***) sur le PDMS *via* la réaction d'hydrosilylation dans l'eau sans utiliser de catalyseur exogène. Ils ont montré que la concentration des groupes Si-H résiduels sur le PDMS après le durcissement n'est pas seulement influencée par le rapport (en poids) des composants du PDMS comme Guo *et al.* [191] ou Zhang *et al* [211] l'ont rapporté mais peut également être influencée par le temps de réticulation (augmentation des groupes Si-H en diminuant le temps de réticulation). Parallèlement, les auteurs ont également étudié l'influence du temps de réaction, de la nature du solvant et de la concentration de la solution de polymère cationique sur l'efficacité du greffage. Toutes les surfaces de PDMS greffées en polymères cationiques ont présenté des densités de charge de surface variant de $1{,}8 \times 10^{14}$ à $2{,}8 \times 10^{15}$ N^{+} cm^{-2} avec une valeur d'ACE variant entre 78 et 99° et ont montré d'excellentes propriétés bactéricides contre *E. coli* et *S. epidermidis* avec presque 100% d'éradication bactérienne après 1 heure de contact. Cependant, les fortes interactions entre les protéines plasmatiques (BSA et fibrinogène), macromolécules chargées électriquement, et les polymères cationiques greffés en surface du PDMS conduisent à la passivation des surfaces de PDMS cationique et à l'affaiblissement de leurs propriétés bactéricides, limitant ainsi leurs applications en contact avec le sang.

Certains travaux publiés sur la modification de la surface du PDMS par la méthode d'hydrosilylation sont regroupés dans le Tableau I-4.

Tableau I-4. Résumé des travaux publiés sur la modification de la surface du PDMS pour des applications biomédicales par la méthode d'hydrosilylation.

Type de surface	Principales propriétés de la surface modifiée	Application potentielle	REF	Type d'action antibactérienne
PDMS revêtu d'un film de type glycocalyx	$\theta_{adv} \approx 90°$ and $\theta_{rec} \approx 35°$, Propriétés antiadhésives contre les protéines (BSA et fibrinogène) et les bactéries (*S. aureus*, *S. epidermidis*, *E. coli* et *P. aeruginosa*) et des cellules de mammifères (cellules rénales canines Madin Darby)	Microtechnique (microfluidique, micropatterning)/ Biomatériaux et matériel biomédical	[190]	Antiadhésive

Tableau I-4 (Suite).

Type de surface	Principales propriétés de la surface modifiée	Application potentielle	REF	Type d'action antibactérienne
PDMS revêtu de PEG	ACE : 27°, 34° et 29° pour trois types de PEG différentes respectivement en présence du catalyseur de Karstedt, Résistance aux protéines non spécifiques (BSA et lysozyme).	Biomatériaux et matériel biomédical	[191]	Antiadhésive
PDMS greffée de Carboxybetaine	ACE : ≈ 46°, Propriété antisalissure contre BSA, *S. aureus* et *E. coli.*	Biomatériaux et matériel biomédical	[211]	Antiadhésive
Surface de PDMS greffée de polymère cationique	ACE : 78-99°, Densité de charge de surface : 1.8×10^{14} à 2.8×10^{15} N^+ cm^{-2}, Propriété bactéricide contre *E. coli* et *S. epidermidis*.	Surfaces externes de biomatériaux (ex : chambre cathéters) et matériel biomédical	[131]	Contact-killing
PDMS revêtue de PEG	ACE : θ_{adv} =65-110° et θ_{rec} <56°, Propriété antisalissure contre les protéines	Biomatériaux et matériel biomédical	[194]	Antiadhésive
PDMS modifié par l'héparine	ACE : θ_{adv} =48° et θ_{rec} =31°, Résistance à l'adsorption non spécifique des protéines, Amélioration de la propriété anti-thrombogène	Biomatériaux implantables	[193]	Antiadhésive

I.4.2.3 La chimie click

La "chimie click" est un ensemble de réactions qui sont sélectives, efficaces, à haut rendement et sans produits secondaires dans des conditions de réaction simples. Son concept a été introduit pour la première fois par Sharpless *et al* [212] en 2001 pour fournir une technique de choix pour la préparation de médicaments [213]. Cependant, son concept et sa méthodologie ont été largement acceptés et peuvent être appliqués dans presque tous les domaines de la recherche et de la technologie, y compris la modification de surfaces qui nécessite généralement la modification préalable de la surface et/ou du composé actif [214–219]. Le paragraphe suivant présente deux grands types de chimie click : la chimie click thiol-ène et la cycloaddition azide-alkyne catalysée par le cuivre.

La réaction des thiols avec les doubles liaisons carbone-carbone peut se dérouler dans des conditions radicalaires (appelée réaction click thiol-ène) ou anioniques (appelée addition de Michael thiol) (Figure I-13). Les radicaux thiol sont faciles à générer (thermiquement ou photo-chimiquement) et à manipuler. La réaction thiol-ène est simple, flexible et efficace, ce qui en fait une stratégie prometteuse pour la modification des surfaces [220,221].

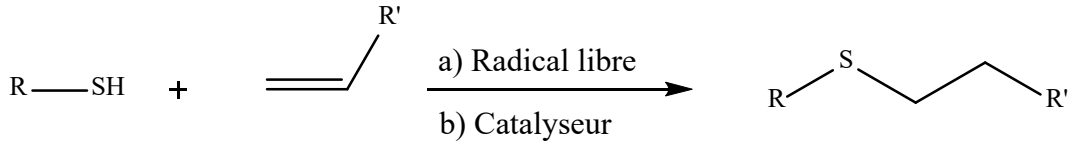

Figure I-13. Illustration de la chimie click thiol-ène qui peut être soit : a) radicalaires, soit b) anioniques. Reproduit de la réf. [220].

Magennis *et al.* [199] ont présilanisé la surface du PDMS avec du (3-mercaptopropyl) triméthoxy silane afin d'introduire sur la surface la fonction thiol. Ensuite, l'acrylate d'éther dicyclopentényle d'éthylène glycol (EGdPEA), le méthacrylate d'éther méthylique de di-(éthylène glycol) (DEGMA) ou un copolymère de ces deux monomères ont été greffés sur la surface du PDMS , *via* des procédés de « grafting from » ou de « grafting to », en utilisant une réaction thiol-ène (Figure I-14). Les auteurs ont remarqué que l'introduction du silane thiolé sur le PDMS permettait déjà d'améliorer ses propriétés antiadhésives à l'égard des bactéries et que la surface modifiée finale (PDMS-EGdPEA-DEGMA) réduisait de 99% l'adhésion de *P. aeruginosa* et de *Proteus mirabilis*.

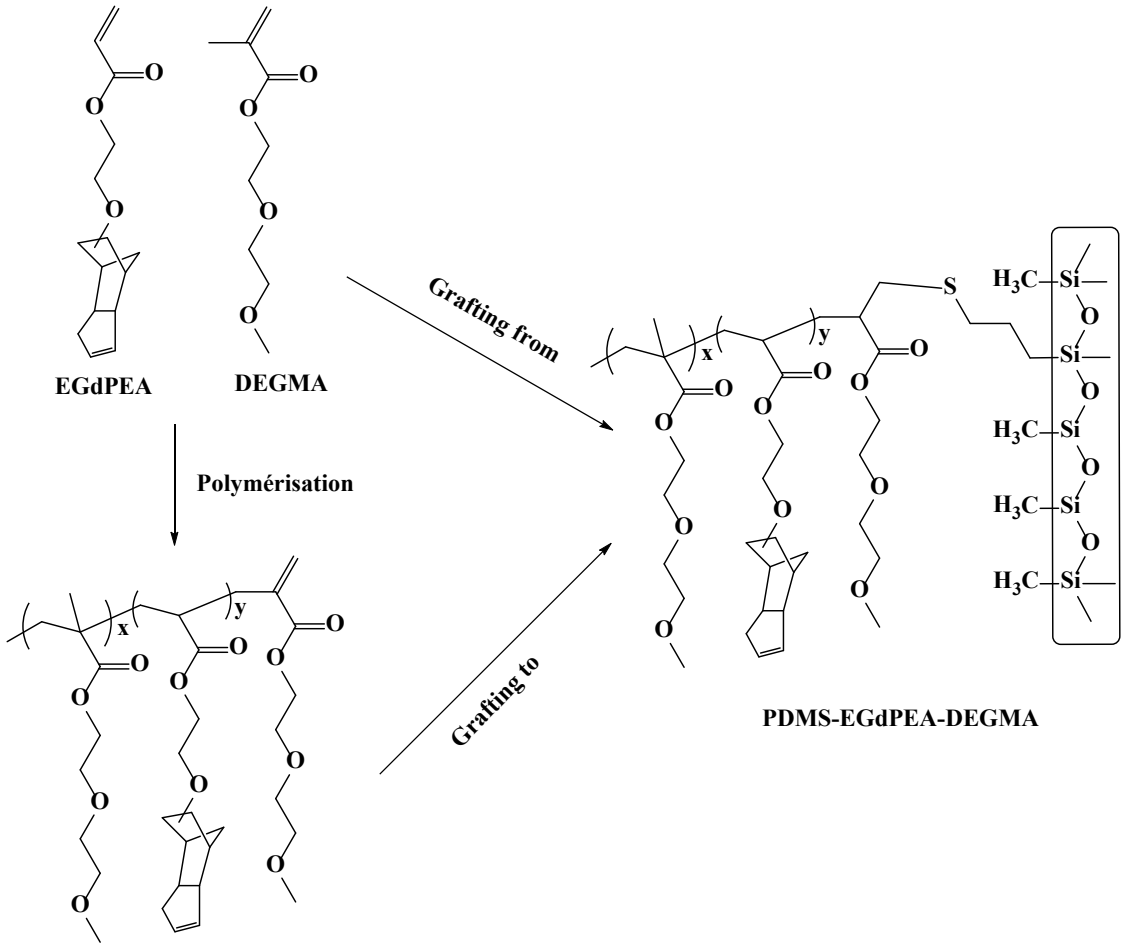

Figure I-14. Illustration schématique de la préparation de revêtements antimicrobiens sur PDMS par la chimie click thiol-ène en utilisant EGdPEA et DEGMA *via* des procédés « grafting from » ou « grafting to ». Reproduit de la réf. [199].

La cycloaddition azoture-alcyne catalysée par le cuivre (CuAAC) est la plus courante parmi les réactions de chimie click. La réaction CuAAC permet la formation du cycle 1,4-disubstitué-1,2,3-triazole provenant de la cycloaddition d'un groupement azoture et d'une fonction alcyne en présence d'un catalyseur au cuivre (Figure I-15).

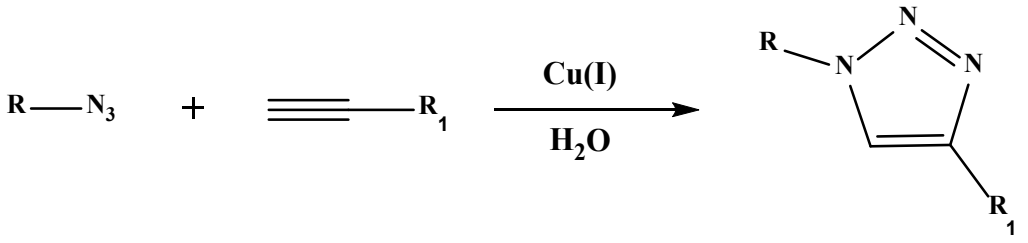

Figure I-15. Illustration de la cycloaddition azoture-alcyne catalysée par le cuivre (CuAAC).

Zhang *et al.* [222] ont d'abord introduit des atomes de chlore sur le PDMS via une réaction de silanisation entre le 3-chloropropyltrichlorosilane et la surface du PDMS prétraitée par plasma d'oxygène. Ils ont ensuite introduit des groupements azotures par réaction entre les

atomes de chlore de la surface et de l'azoture de sodium (PDMS-N_3). Pour finir, ils ont greffé de façon covalente un PEG ayant une fonction alcyne sur la surface du PDMS-N_3 *via* la réaction de CuAAC (Figure I-16). Le PDMS-PEG obtenu a montré un caractère hydrophile avec une diminution de l'ACE par rapport au PDMS-N_3 et au PDMS natif, avec des valeurs de 64°, 87° et 115° respectivement. De plus, cette valeur de 64° a été maintenue pendant environ 30 jours montrant la stabilité du lien formé. Les auteurs ont également mis en évidence les propriétés antiadhésives du PDMS modifié contre différentes protéines telles que la BSA et l'albumine d'œuf, même après 30 jours.

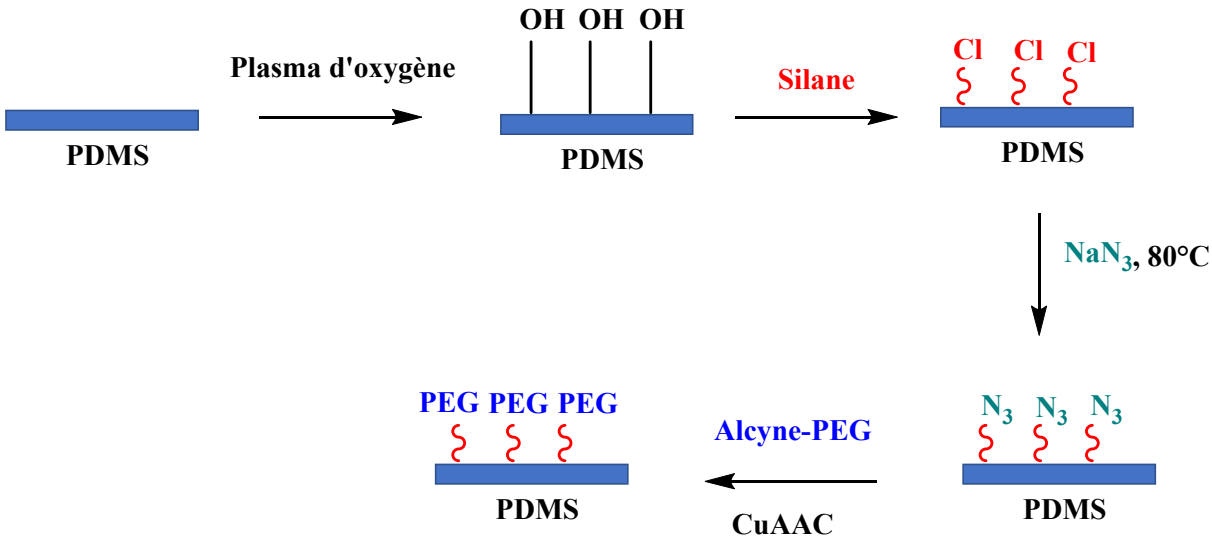

Figure I-16. Illustration schématique de la préparation de revêtements antimicrobiens sur PDMS par la réaction CuAAC en utilisant du PEG fonctionnalisé par une fonction alcyne. Reproduit de la réf. [222].

Le Tableau I-5 regroupent certains travaux publiés sur la modification de la surface du PDMS par une réaction de chimie click.

Tableau I-5. Résumé des travaux publiés sur la modification de la surface du PDMS pour des applications biomédicales par la chimie click.

Modification de surface	Type de surface	Principales propriétés de la surface modifiée	Application potentielle	REF	Type d'action antibactérienne
Silanisation / réaction thiol-ène	PDMS modifié au PEG	ACE : 73° de l'échantillon fraîchement préparé, 92° de l'échantillon stocké à l'air pendant 6 mois et 82° de ce dernier échantillon trempé dans l'eau pendant 3 jours	Microtechnique (microfluidique)/ Biomatériaux	221	Non mentionné

Tableau I-5 (Suite).

Modification de surface	Type de surface	Principales propriétés de la surface modifiée	Application potentielle	REF	Type d'action antibactérienne
Silanisation / réaction thiol-ène	PDMS-BODIPY-Br[a]	Propriétés bactéricides contre *E. coli*	Applicabilité aux dispositifs médicaux	[203]	Libération d'agents antibactériens
Silanisation / réaction thiol-ène	PDMS-EGdPEA-DEGMA	Propriétés antiadhésives contre *P. aeruginosa* et *Proteus mirabilis* avec une réduction de 99 % de leur adhésion en surface	Applicabilité aux dispositifs médicaux	[199]	Antiadhésive
Silanisation / CuAAC	PDMS-PEG	ACE : 64°, Propriété antisalissure contre les protéines telles que la BSA, etc.	Application pour la séparation biomédicale	[222]	Antiadhésive

[a] BODIPY : le bore-dipyrrométhène.

I.4.2.4 Photogreffage

La modification chimique directe des surfaces de PDMS peut également être réalisée par des processus photo-induits impliquant la formation de radicaux sur la surface qui permettront le greffage de (macro)molécules actives. Normalement, ces processus ont besoin d'un ou plusieurs photoamorceurs qui sont susceptibles d'absorber les radiations ultraviolettes afin de créer des espèces réactives par photolyse. En fonction de la façon de générer les radicaux amorceurs, les photoamorceurs peuvent être divisées en deux grandes familles : les type I qui sont des photoamorceurs générant des espèces réactives par scission homolytique de la liaison carbone-carbonyle et les type II qui le font par arrachement d'un atome d'hydrogène ou par transfert d'électrons ou de protons.

Par exemple, la micro-structuration covalente de la surface du PDMS a été réalisée par photo-greffage, à travers un masque, d'acide acrylique [195,223], de monoacrylate de polyéthylène glycol et de diacrylate de polyéthylène glycol, en utilisant la benzophénone comme photo-amorceur [196]. La benzophénone (BP) est le photo-amorceur Norrish de type II le plus utilisé pour générer des radicaux à la surface d'un substrat, car son état triplet produit photo-

chimiquement peut extraire des atomes d'hydrogène de presque tous les polymères [224] (Figure I-17). Keskin *et al.* [225] ont étudié l'influence du type de monomère, de la concentration de monomère et du temps d'irradiation UV sur les propriétés du PDMS modifié en surface par polymérisation radicalaire amorcée par UV/benzophénone. Ils ont constaté que lorsque la concentration en monomère et le temps d'irradiation UV augmentaient, des surfaces plus hydrophiles et rugueuses avec des épaisseurs importantes se formaient. En outre, leurs résultats ont montré que les conditions de réaction affectaient non seulement la surface mais aussi les propriétés du matériau final.

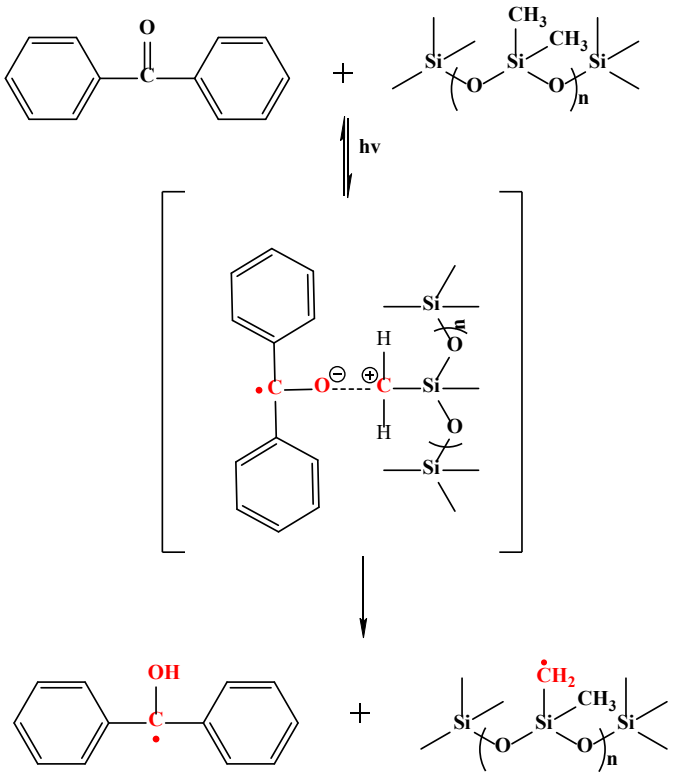

Figure I-17. Schéma du mécanisme d'action de la benzophénone sur le substrat PDMS sous UV.

Récemment, Leigh *et al.* [197] ont développé un processus simultané de photogreffage/photo réticulation pour préparer des substrats de PDMS antisalissures en recouvrant la surface du PDMS avec deux polymères zwitterioniques : le poly (méthacrylate de sulfobétaïne) (pSBMA) et le poly (méthacrylate de carboxybétaïne) (pCBMA), en présence de diacrylate de poly (éthylène glycol) comme réticulant. Les auteurs ont étudié les propriétés d'antisalissure de la surface de PDMS modifiée contre les protéines (fibrinogène) et les cellules (fibroblastes). Le test d'adsorption des protéines a indiqué que les surfaces revêtues de pSBMA et de pCBMA présentaient une réduction significative de l'adsorption des protéines par rapport au PDMS natif. De même, l'adhésion des cellules sur les surfaces revêtues de pSBMA et de

pCBMA a été significativement réduite, avec respectivement environ 5% et 3% de la densité cellulaire du PDMS vierge. En outre, le PDMS modifié a pu maintenir la résistance à l'adhésion des fibroblastes même après une exposition aux milieux de culture pendant 14 jours *in vitro*. Sur la base de leurs résultats, Shen *et al.* [226] ont continué à travailler sur des surfaces de PDMS revêtues de pSBMA / pCBMA préparées par la même technique de photo-greffage pour tester les propriétés antiadhésives à l'égard de bactéries. Une réduction statistiquement significative de quasiment 100% de *S. aureus* ($p<0,05$) et environ 95% de *S. epidermidis* ($p<0,05$) sur la surface pCBMA par rapport au PDMS natif a été obtenue (la valeur p signifie le niveau de signification statistique, $p \leqslant 0,05$ signifie statistiquement significatif). Cependant, pour le pSBMA, l'adhésion de *S. aureus* a été réduite de manière statistiquement significative (environ 90% de réduction, $p<0,05$) mais pas pour *S. epidermidis* (environ 45% de réduction, $p>0,05$). De plus, le PDMS revêtu de pCBMA a été utilisé comme matériau implantable et a révélé une grande efficacité en matière de résistance à l'adhésion et à la croissance bactérienne contre *S. aureus in vivo* par exemple avec une réduction d'environ 90% après 21 jours d'inoculation bactérienne.

Kuliasha *et al.* [227] ont greffé de l'acide acrylique (AAc), de l'acrylamide (AAm) et du méthacrylate de 2-hydroxyéthyle (HEMA) sur un substrat de PDMS par une technique RAFT conjointe avec un photo-greffage amorcé par le BP. Les surfaces modifiées, P(AAm)-g-PDMS, P(AAm-co-AAc)-g-PDMS et P(AAm-co-AAc-co-HEMA)-g-PDMS ont amélioré l'hydrophilie du PDMS avec des ACE de 41 ± 7°, 62 ± 3° et 66 ± 4°, respectivement. En outre, ils ont utilisé cette technique pour greffer un réseau nanotopographiques chimiques anisotropes à base de poly(AAm) sur le PDMS afin d'étudier l'efficacité antisalissure de ces nanotopographies qui utilisent des géométries latérales inspirées de la microtopographie physique antisalissure Sharklet (SK) et des canaux parallèles analogues (CH). Les surfaces obtenues ont montré une diminution modeste d'environ 4 à 11° par rapport au PDMS natif présentant un ACE de 110°. De plus, ils ont étudié la propriété antisalissure contre *Ulva. linza*, une algue verte salissante marine commune. Les expériences d'antisalissure ont montré que, par rapport au PDMS non greffé, les surfaces de poly(AAm) sans motif pouvaient réduire de manière significative l'adhésion de la salissure de 59 %, tandis que les surfaces à motifs avaient un impact minimal [228]. Des efforts supplémentaires dans l'amélioration des modèles et la recherche de produits chimiques plus efficaces sont donc nécessaires.

Gao *et al.* [158] ont synthétisé des copolymères séquencés (MA-PEGn-*b*-AMP) par réaction des polyéthylènes glycols (MA-PEG_n, n=10/45/90) de différente longueur porteur d'un

groupe tosyle et d'un groupe méthacrylate avec un polypeptide antimicrobien cationique (AMP : Lys(NH_3^+)$_{12.5}$-*ran*-Phe$_{12.5}$). La partie PEG doit apporter un effet antiadhésif et la partie AMP un effet bactéricide par contact. Les copolymères ont ensuite été greffés sur du PDMS activé par plasma d'argon par un procédé en une étape sous rayonnement UV selon la technique du "grafting from" sans utiliser de photo-amorceur exogène (Figure I-18). Des valeurs d'ACE pour la surface PDMS-*g*-PEGn-*b*-AMP de 37°, 35° et 30° ont été obtenus lorsque n (nombre de motifs de PEG) était égal à 10, 45 et 90 respectivement. Les surfaces PDMS revêtues ont montré une activité antimicrobienne très efficace contre *S. aureus*, *P. aeruginosa* et *E. coli* avec 100%, >99% et 92-95% d'éradication bactérienne pour n=10, 45 et 90 respectivement, à travers un test antimicrobien dans une suspension bactérienne pendant 1 heure. Ils ont également effectué un essai de viabilité des bactéries par microscopie à fluorescence (test LIVE/DEAD) pour étudier l'activité antibiofilm contre *S. aureus* et *E. coli* de la surface modifiée, après trois jours de culture. Les résultats ont montré 15% d'adhésion bactérienne sur la surface de PDMS-*g*-PEG$_{10}$ par rapport au PDMS natif et que la plupart des bactéries adhérées étaient vivantes. La surface PDMS-g-PEG$_{45}$-*b*-AMP a, quant-à-elle, présenté la plus faible adhésion bactérienne mais aussi avec des cellules vivantes. De plus, le nombre de bactéries adhérées sur la surface PDMS-g-PEG$_{90}$-b-AMP s'est avéré le plus élevée avec encore une fois une majorité de cellules vivantes. Comme pour les résultats des tests antibactériennes précédentes, la surface PDMS-PEG$_{10}$-*b*-AMP présentait l'activité biocide la plus puissante. Quelques bactéries adhérées mais aucune vivante a été observées. En outre, les surfaces de PDMS modifiés ont présenté une excellente résistance à l'adsorption de protéines (BSA, fibrinogène et lysozyme) et ont montré leur non-toxicité vis-à-vis des cellules de mammifères (cellules de fibroblastes murins) *via* des tests de cytotoxicité *in vitro*. Le revêtement *g*-PEG$_{45}$-*b*-AMP a également montré un excellent effet antimicrobien, antibiofilm et antisalissure dans l'organisme, comme en témoigne l'activité anti-infectieuse *in vivo* contre *E. coli*, offrant ainsi une méthode simple et efficace pour lutter contre les infections associées aux dispositifs biomédicaux.

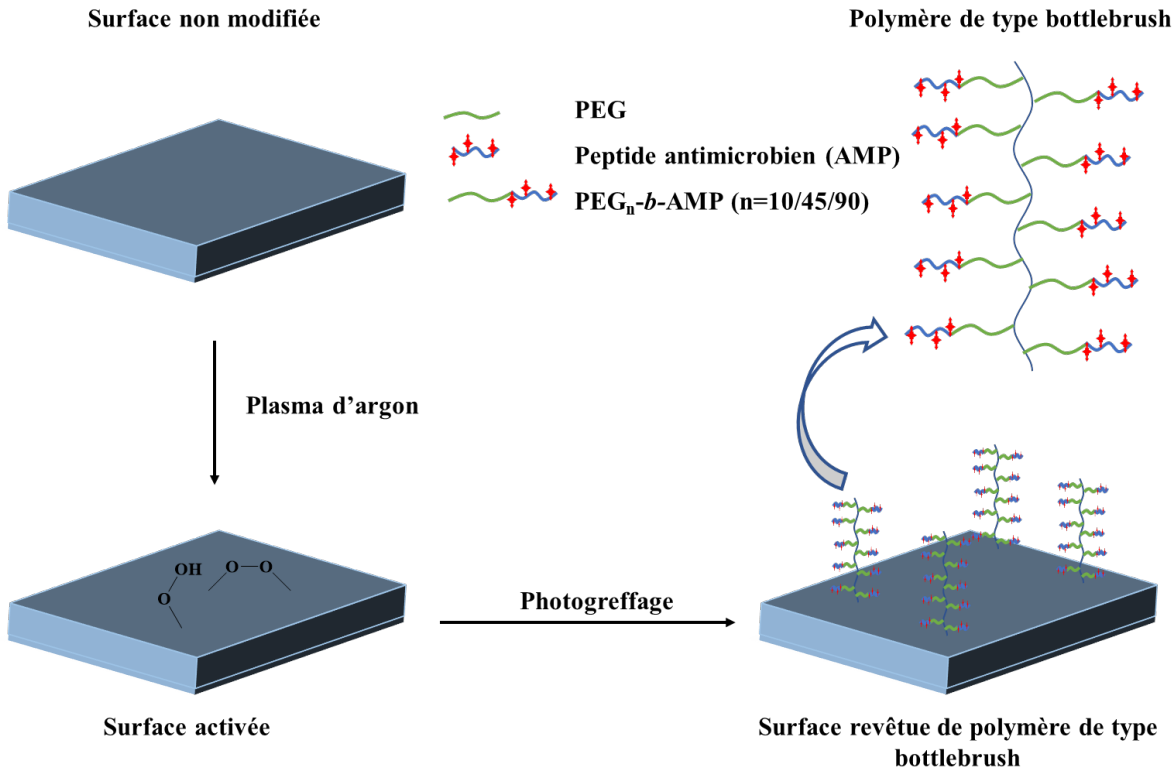

Figure I-18. Illustration schématique de la préparation de revêtements antimicrobiens de type bottlebrush sur la surface de PDMS par polymérisation de surface induite par plasma/UV. Reproduit de la réf. [158].

Certains travaux publiés sur la modification de la surface du PDMS par la méthode de photo-greffage sont représentés dans le Tableau I-6.

Tableau I-6. Résumé des travaux publiés sur la modification de la surface du PDMS par la méthode de photografting.

Modification de la surface	**Type de surface**	**Principales propriétés de la surface modifiée**	**Application potentielle**	**REF**	**Type d'action antibactérienne**
Photogreffage / grafting from	PDMS revêtu de pSBMA/pCBMA	Propriétés antisalissures contre les protéines et les cellules	Propriétés antisalissures contre les protéines et les cellules	197	Antiadhésive
Photogreffage / grafting from	PDMS revêtu de pSBMA/pCBMA	Propriété antiadhésive bactérienne contre *S. aureus* et *S. epidermidis.*	Applicabilité aux dispositifs médicaux	226	Antiadhésive

Tableau I-6 (Suite).

Modification de la surface	Type de surface	Principales propriétés de la surface modifiée	Application potentielle	REF	Type d'action antibactérienne
Photogreffage / grafting from	PDMS revêtu de P(AAm)	ACE : 41 ± 7°, Propriété antisalissure contre *Ulva linza.*	Application pour le biofouling contre les organismes marins	[227], [228]	Antiadhésive
Photogreffage / grafting to	PDMS revêtu de g-PEG$_n$-b-AMP	ACE : 37°, 35° et 30° avec n = 10, 45 et 90 respectivement, Propriété antimicrobienne, anti-biofilm et antisalissure, Non toxicité pour les cellules de mammifères	Application pour les dispositifs médicaux	[158]	Contact-killing/ Antiadhésive

Conclusion

Le PDMS est un matériau couramment utilisé en tant que biomatériau grâce à ses propriétés physicochimiques exceptionnelles : optiquement transparent, biocompatible, flexible, non toxique... Par contre, son hydrophobicité le rend sujet à la bioadhésion et à la contamination bactérienne limitant son utilisation. Il est donc plus que nécessaire de développer des approches variées d'action antibactérienne pour couvrir un large spectre de bactéries et un maximum d'applications biomédicales.

Les approches physiques tels que le plasma, l'UBF et les méthodes électriques (courant direct ou indirect et champs électrique) sont couramment utilisés dans la domaine biomédicale et agroalimentaire contre la contamination bactérienne. En outre, il a été constaté que ces approches peuvent augmenter l'efficacité des antibiotiques dans une action synergique. Cependant, il reste encore beaucoup de travail à faire avant d'utiliser ces approches en application clinique avec ou sans les autres traitements tels que les antibiotiques.

Le traitement physique de la surface par des traitements au plasma d'oxygène et aux UVO est généralement utilisée pour l'activation des surfaces de PDMS, générant des groupes hydroxyles pour rendre la surface hydrophile. En outre, les groupes hydroxyles peuvent également être générés par un traitement chimique tel que l'immersion de la surface dans une solution de piranha. Ces méthodes sont faciles à mettre en œuvre, avec un temps de traitement court et efficace. Cependant, les surfaces de PDMS modifiées par ces méthodes ne sont pas stables à long terme [165]. Les surfaces modifiées par la méthode LBL (non covalente), qui repose essentiellement sur des interactions hydrophobes ou électrostatiques et qui permet d'incorporer des agents antibiotiques, montre une meilleure stabilité que les traitements par plasma d'oxygène ou par UVO. Par ailleurs, les modifications chimiques covalentes telles que la silanisation, l'hydrosilylation, la chimie click ou le photo-greffage permettent d'élaborer des surfaces antibactériennes stables grâce à la liaison covalente crée entre les (macro)molécules actives et la surface du PDMS.

Les avantages et les inconvénients des différentes méthodes de modification chimiques sont regroupés dans le Tableau I-7.

Tableau I-7. Résumé des avantages et les inconvénients des différentes méthodes de modification chimiques de PDMS.

Méthode de modification	Avantages	Inconvénients	REF
LBL	-Facile à mettre en œuvre, avec un temps de traitement court et efficace. -Contrôle de l'épaisseur fine des multicouches à l'échelle nanométrique. -Peut tuer les bactéries à la fois en planctonique et en biofilm.	-Le revêtement n'est pas stable à long terme. - Nécessite un contrôle de la diffusion de la (macro)molécule active	138,183–187
Silanisation	-Procédé facile à mettre en œuvre, peu coûteux et efficace.	-Il n'est pas stable à long terme si les molécules greffées sont de petites tailles (Effet de retour de l'hydrophobie). -Méthode indirecte pour apporter des propriétés antibactériennes.	200,201,205,229
Hydrosilylation	-Procédé facile à mettre en œuvre, peu coûteux et efficace. -Méthode directe (une étape) pour immobiliser des (macro)molécules actives.	(Macro)molécules actives doivent avoir un groupe vinyle.	131,190,191,193,194,211

Tableau I-7 (Suite).

Méthode de modification	Avantages	Inconvénients	REF
Chimie click	Haute sélectivité, efficaces, haut rendement et sans produits secondaires sous des conditions de réaction simples.	-Toxicité potentielle du cuivre dans la réaction click catalysée par Cu(I). - La cycloaddition 1,3-dipolaire de Huisgen, a une vitesse de réaction très faible en raison d'une énergie d'activation élevée.	199,221,222,230
Photogreffage	-Méthode directe (une étape) et très rapide pour apporter des propriétés antibactériennes. -Possibilité de faire des modifications micro/nano structurées.	-Il faut trouver le photo-amorceur approprié. -Il faut bien ajuster les conditions de réaction telle que l'intensité de lumière ou temps de réaction pour ne pas brûler l'échantillon.	158,197,225,226,228

Dans le cadre de cette thèse, l'objectif est de développer de nouvelles approches permettant de diminuer voire d'empêcher l'adhésion bactérienne sur la surface du PDMS soit par un moyen physique soit par l'élaboration de nouvelles surfaces de PDMS antibactériennes. Pour cela, différentes méthodes de modifications de surface et différentes (macro)molécules seront testées. Dans le chapitre II, l'objectif est d'étudier l'adhésion et la viabilité de différentes espèces bactériennes sur des surfaces de PDMS sous l'effet d'un champ électrique comme stimulus physique entre deux lames métalliques. Le chapitre III fera l'objet de l'étude de l'activité antibactérienne de surface de PDMS modifiée de façon covalente par un dérivé de la claramine *via* une réaction de chimie-click. Pour finir, le chapitre IV portera sur l'élaboration de nouvelles surfaces de PDMS cationique bactéricides *via* des procédés de 'grafting from' et de 'grafting to' photo-amorcés.

Références bibliographiques

1. Karaman, D. Ş., Manner, S., Fallarero, A. & Rosenholm, J. M. Current approaches for exploration of nanoparticles as antibacterial agents. *Antibact. Agents* 61 (2017).
2. Şen Karaman, D., Ercan, U. K., Bakay, E., Topaloğlu, N. & Rosenholm, J. M. Evolving Technologies and Strategies for Combating Antibacterial Resistance in the Advent of the Postantibiotic Era. *Adv. Funct. Mater.* **30**, 1908783 (2020).
3. Ligon, B. L. Penicillin: its discovery and early development. in *Seminars in pediatric infectious diseases* **15**, 52–57 (Elsevier, 2004).
4. Golkar, Z., Bagasra, O. & Pace, D. G. Bacteriophage therapy: a potential solution for the antibiotic resistance crisis. *J. Infect. Dev. Ctries.* **8**, 129–136 (2014).
5. Aslam, B. *et al.* Antibiotic resistance: a rundown of a global crisis. *Infect. Drug Resist.* **11**, 1645 (2018).
6. Nathan, C. & Cars, O. Antibiotic resistance—problems, progress, and prospects. *N. Engl. J. Med.* **371**, 1761–1763 (2014).
7. Gould, I. M. & Bal, A. M. New antibiotic agents in the pipeline and how they can help overcome microbial resistance. *Virulence* **4**, 185–191 (2013).
8. Organization, W. H. *Thirteenth general programme of work, 2019–2023: promote health, keep the world safe, serve the vulnerable*. (World Health Organization, 2019).
9. Prestinaci, F., Pezzotti, P. & Pantosti, A. Antimicrobial resistance: a global multifaceted phenomenon. *Pathog. Glob. Health* **109**, 309–318 (2015).
10. Santos, A. L. S. dos *et al.* What are the advantages of living in a community? A microbial biofilm perspective! *Mem. Inst. Oswaldo Cruz* **113**, (2018).
11. Elbourne, A. *et al.* Antibacterial Liquid Metals: Biofilm Treatment via Magnetic Activation. *ACS Nano* **14**, 802–817 (2020).
12. Xu, Y., Dhaouadi, Y., Stoodley, P. & Ren, D. Sensing the unreachable: challenges and opportunities in biofilm detection. *Curr. Opin. Biotechnol.* **64**, 79–84 (2020).
13. Jamal, M. *et al.* Bacterial biofilm and associated infections. *J. Chinese Med. Assoc.* **81**, 7–11 (2018).
14. Gu, H., Lee, S. W., Carnicelli, J., Zhang, T. & Ren, D. Magnetically driven active topography for long-term biofilm control. *Nat. Commun.* **11**, 1–11 (2020).
15. Salwiczek, M. *et al.* Emerging rules for effective antimicrobial coatings. *Trends Biotechnol.* **32**, 82–90 (2014).
16. Worthington, R. J., Richards, J. J. & Melander, C. Small molecule control of bacterial biofilms. *Org. Biomol. Chem.* **10**, 7457–7474 (2012).
17. Davies, D. Understanding biofilm resistance to antibacterial agents. *Nat. Rev. Drug Discov.* **2**, 114–122 (2003).
18. Bjarnsholt, T. The role of bacterial biofilms in chronic infections. *Apmis* **121**, 1–58 (2013).
19. Santos, A. P. A., Watanabe, E. & Andrade, D. de. Biofilm on artificial pacemaker: fiction or reality? *Arq. Bras. Cardiol.* **97**, e113–e120 (2011).
20. Abreu, A. C., Tavares, R. R., Borges, A., Mergulhão, F. & Simões, M. Current and emergent strategies for disinfection of hospital environments. *J. Antimicrob. Chemother.* **68**, 2718–2732 (2013).
21. Khardori, N. & Yassien, M. Biofilms in device-related infections. *J. Ind. Microbiol.* **15**, 141–147 (1995).

22. Donlan, R. M. Biofilms and device-associated infections. *Emerg. Infect. Dis.* **7**, 277 (2001).

23. Murakami, M., Nishi, Y., Seto, K., Kamashita, Y. & Nagaoka, E. Dry mouth and denture plaque microflora in complete denture and palatal obturator prosthesis wearers. *Gerodontology* **32**, 188–194 (2015).

24. Song, Z. *et al.* Prosthesis infections after orthopedic joint replacement: the possible role of bacterial biofilms. *Orthop. Rev. (Pavia).* **5**, (2013).

25. Tran, P. L. *et al.* An organoselenium compound inhibits Staphylococcus aureus biofilms on hemodialysis catheters in vivo. *Antimicrob. Agents Chemother.* **56**, 972–978 (2012).

26. Gupta, T. T. & Ayan, H. Application of non-thermal plasma on biofilm: a review. *Appl. Sci.* **9**, 3548 (2019).

27. Neuber, J. U., Song, S., Malik, M. A., Heller, L. & Jiang, C. Nanosecond pulsed plasma brush for bacterial inactivation on laminate. *IEEE Trans. Radiat. Plasma Med. Sci.* **1**, 368–375 (2017).

28. Shimizu, T., Lachner, V. & Zimmermann, J. L. Surface microdischarge plasma for disinfection. *Plasma Med.* **7**, (2017).

29. Kawamura, K. *et al.* Evaluation of bactericidal effects of low-temperature nitrogen gas plasma towards application to short-time sterilization. *Microbiol. Immunol.* **56**, 431–440 (2012).

30. Freebairn, D. *et al.* Electrical methods of controlling bacterial adhesion and biofilm on device surfaces. *Expert Rev. Med. Devices* **10**, 85–103 (2013).

31. Hazan, Z. *et al.* Effective prevention of microbial biofilm formation on medical devices by low-energy surface acoustic waves. *Antimicrob. Agents Chemother.* **50**, 4144–4152 (2006).

32. Yu, H. *et al.* Ultrasound-involved emerging strategies for controlling foodborne microbial biofilms. *Trends Food Sci. Technol.* **96**, 91–101 (2020).

33. Chen, Z. Microbial inactivation in foods by ultrasound. *J Food Microbiol Saf Hyg* **2**, E102 (2017).

34. Yang, Y. *et al.* A novel cold atmospheric pressure air plasma jet for peri-implantitis treatment: An in vitro study. *Dent. Mater. J.* **37**, 157–166 (2018).

35. Del Pozo, J. L., Rouse, M. S. & Patel, R. Bioelectric effect and bacterial biofilms. A systematic review. *Int. J. Artif. Organs* **31**, 786–795 (2008).

36. Johnson, L. L., Vaughn Peterson, R. & Pitt, W. G. Treatment of bacterial biofilms on polymeric biomaterials using antibiotics and ultrasound. *J. Biomater. Sci. Polym. Ed.* **9**, 1177–1185 (1998).

37. Qian, Z., Sagers, R. D. & Pitt, W. G. The effect of ultrasonic frequency upon enhanced killing of P. aeruginosa biofilms. *Ann. Biomed. Eng.* **25**, 69–76 (1997).

38. Liao, X. *et al.* Inactivation mechanisms of non-thermal plasma on microbes: A review. *Food Control* **75**, 83–91 (2017).

39. Jha, N., Ryu, J. J., Choi, E. H. & Kaushik, N. K. Generation and role of reactive oxygen and nitrogen species induced by plasma, lasers, chemical agents, and other systems in dentistry. *Oxid. Med. Cell. Longev.* **2017**, (2017).

40. Gaunt, L. F., Beggs, C. B. & Georghiou, G. E. Bactericidal action of the reactive species produced by gas-discharge nonthermal plasma at atmospheric pressure: a review. *IEEE Trans. Plasma Sci.* **34**, 1257–1269 (2006).

41. Graves, D. B. The emerging role of reactive oxygen and nitrogen species in redox biology and some implications for plasma applications to medicine and biology. *J. Phys. D. Appl. Phys.* **45**, 263001 (2012).

42. Mai-Prochnow, A., Bradbury, M., Ostrikov, K. & Murphy, A. B. Pseudomonas aeruginosa biofilm response and resistance to cold atmospheric pressure plasma is linked to the redox-active molecule phenazine. *PLoS One* **10**, e0130373 (2015).

43. Duske, K. *et al.* Atmospheric plasma enhances wettability and cell spreading on dental implant metals. *J. Clin. Periodontol.* **39**, 400–407 (2012).

44. Sakudo, A., Yagyu, Y. & Onodera, T. Disinfection and sterilization using plasma technology: fundamentals and future perspectives for biological applications. *Int. J. Mol. Sci.* **20**, 5216 (2019).

45. Moreau, M., Orange, N. & Feuilloley, M. G. J. Non-thermal plasma technologies: new tools for bio-decontamination. *Biotechnol. Adv.* **26**, 610–617 (2008).

46. Hoffmann, C., Berganza, C. & Zhang, J. Cold Atmospheric Plasma: methods of production and application in dentistry and oncology. *Med. Gas Res.* **3**, 21 (2013).

47. Fridman, G. *et al.* Applied plasma medicine. *Plasma Process. Polym.* **5**, 503–533 (2008).

48. Keidar, M. *et al.* Cold atmospheric plasma in cancer therapy. *Phys. Plasmas* **20**, 57101 (2013).

49. Bernhardt, T. *et al.* Plasma medicine: Applications of cold atmospheric pressure plasma in dermatology. *Oxid. Med. Cell. Longev.* **2019**, (2019).

50. Daeschlein, G. *et al.* Cold plasma is well-tolerated and does not disturb skin barrier or reduce skin moisture. *JDDG J. der Dtsch. Dermatologischen Gesellschaft* **10**, 509–515 (2012).

51. Isbary, G. *et al.* Cold atmospheric argon plasma treatment may accelerate wound healing in chronic wounds: Results of an open retrospective randomized controlled study in vivo. *Clin. Plasma Med.* **1**, 25–30 (2013).

52. Schmidt, A., Bekeschus, S., Wende, K., Vollmar, B. & von Woedtke, T. A cold plasma jet accelerates wound healing in a murine model of full-thickness skin wounds. *Exp. Dermatol.* **26**, 156–162 (2017).

53. Isbary, G. *et al.* Successful and safe use of 2 min cold atmospheric argon plasma in chronic wounds: results of a randomized controlled trial. *Br. J. Dermatol.* **167**, 404–410 (2012).

54. Chuangsuwanich, A., Assadamongkol, T. & Boonyawan, D. The healing effect of low-temperature atmospheric-pressure plasma in pressure ulcer: a randomized controlled trial. *Int. J. Low. Extrem. Wounds* **15**, 313–319 (2016).

55. Nomura, Y. *et al.* Investigation of blood coagulation effect of nonthermal multigas plasma jet in vitro and in vivo. *J. Surg. Res.* **219**, 302–309 (2017).

56. Fridman, G. *et al.* Blood coagulation and living tissue sterilization by floating-electrode dielectric barrier discharge in air. *Plasma Chem. plasma Process.* **26**, 425–442 (2006).

57. Gupta, T. T., Karki, S. B., Matson, J. S., Gehling, D. J. & Ayan, H. Sterilization of biofilm on a titanium surface using a combination of nonthermal plasma and chlorhexidine digluconate. *Biomed Res. Int.* **2017**, (2017).

58. Rupf, S. *et al.* Removing biofilms from microstructured titanium ex vivo: a novel approach using atmospheric plasma technology. *PLoS One* **6**, e25893 (2011).

59. Gherardi, M., Tonini, R. & Colombo, V. Plasma in dentistry: brief history and current status. *Trends Biotechnol.* **36**, 583–585 (2018).

60. Sladek, R. E. J., Stoffels, E., Walraven, R., Tielbeek, P. J. A. & Koolhoven, R. A. Plasma treatment of dental cavities: a feasibility study. *IEEE Trans. plasma Sci.* **32**, 1540–1543 (2004).

61. Bazaka, K., Jacob, M. V, Crawford, R. J. & Ivanova, E. P. Plasma-assisted surface modification of organic biopolymers to prevent bacterial attachment. *Acta Biomater.* **7**, 2015–2028 (2011).

62. Jacobs, T. *et al.* Plasma surface modification of polylactic acid to promote interaction with fibroblasts. *J. Mater. Sci. Mater. Med.* **24**, 469–478 (2013).

63. Bazaka, K. *et al.* Plasma-enhanced synthesis of bioactive polymeric coatings from monoterpene alcohols: a combined experimental and theoretical study. *Biomacromolecules* **11**, 2016–2026 (2010).

64. Gao, S., Lewis, G. D., Ashokkumar, M. & Hemar, Y. Inactivation of microorganisms by low-frequency high-power ultrasound: 1. Effect of growth phase and capsule properties of the bacteria. *Ultrason. Sonochem.* **21**, 446–453 (2014).

65. Ashokkumar, M. The characterization of acoustic cavitation bubbles–an overview. *Ultrason. Sonochem.* **18**, 864–872 (2011).

66. Pitt, W. G., McBride, M. O., Lunceford, J. K., Roper, R. J. & Sagers, R. D. Ultrasonic enhancement of antibiotic action on gram-negative bacteria. *Antimicrob. Agents Chemother.* **38**, 2577–2582 (1994).

67. Xie, S. *et al.* Bactericidal effects of high intensity focused ultrasound on Bacillus Calmette–Guerin in vivo and in vitro. *Int. J. Hyperth.* **36**, 885–895 (2019).

68. Liu, B. *et al.* The influence of ultrasound on the fluoroquinolones antibacterial activity. *Ultrason. Sonochem.* **18**, 1052–1056 (2011).

69. Rediske, A. M. *et al.* Pulsed Ultrasound Enhances the Killing of Escherichia coli Biofilms by Aminoglycoside Antibiotics In Vivo. *Antimicrob. Agents Chemother.* **44**, 771–772 (2000).

70. Liu, X., Wang, J., Weng, C., Wang, R. & Cai, Y. Low-Frequency Ultrasound Enhances Bactericidal Activity of Antimicrobial Agents against Klebsiella pneumoniae Biofilm. *Biomed Res. Int.* **2020**, (2020).

71. Liu, X., Yin, H., Weng, C.-X. & Cai, Y. Low-Frequency Ultrasound Enhances Antimicrobial Activity of Colistin–Vancomycin Combination against Pan-Resistant Biofilm of Acinetobacter baumannii. *Ultrasound Med. Biol.* **42**, 1968–1975 (2016).

72. Yan, S., Cai, X., Yan, W., Dai, X. & Wu, H. Continuous wave ultrasound enhances vancomycin release and antimicrobial efficacy of antibiotic-loaded acrylic bone cement in vitro and in vivo. *J. Biomed. Mater. Res. Part B Appl. Biomater.* **82**, 57–64 (2007).

73. Norris, P. *et al.* Ultrasonically controlled release of ciprofloxacin from self-assembled coatings on poly (2-hydroxyethyl methacrylate) hydrogels for Pseudomonas aeruginosa biofilm prevention. *Antimicrob. Agents Chemother.* **49**, 4272–4279 (2005).

74. Hendriks, J. G. E. *et al.* Increased release of gentamicin from acrylic bone cements under influence of low-frequency ultrasound. *J. Control. release* **92**, 369–374 (2003).

75. Ensing, G. T. *et al.* The influence of ultrasound on the release of gentamicin from antibiotic-loaded acrylic beads and bone cements. *J. Biomed. Mater. Res. Part B Appl. Biomater. An Off. J. Soc. Biomater. Japanese Soc. Biomater. Aust. Soc. Biomater. Korean Soc. Biomater.* **75**, 1–5 (2005).

76. Ensing, G. T. *et al.* Effect of pulsed ultrasound in combination with gentamicin on bacterial viability in biofilms on bone cements in vivo. *J. Appl. Microbiol.* **99**, 443–448 (2005).

77. Lin, T. *et al.* In vitro and in vivo evaluation of vancomycin-loaded PMMA cement in combination with ultrasound and microbubbles-mediated ultrasound. *Biomed Res. Int.* **2015**, (2015).

78. Del Pozo, J. L., Rouse, M. S., Mandrekar, J. N., Steckelberg, J. M. & Patel, R. The electricidal effect: reduction of Staphylococcus and Pseudomonas biofilms by prolonged exposure to low-intensity electrical current. *Antimicrob. Agents Chemother.* **53**, 41–45 (2009).

79. Del Pozo, J. L. *et al.* The electricidal effect is active in an experimental model of Staphylococcus epidermidis chronic foreign body osteomyelitis. *Antimicrob. Agents*

Chemother. **53**, 4064–4068 (2009).

80. Busalmen, J. P. & De Sanchez, S. R. Adhesion of Pseudomonas fluorescens (ATCC 17552) to nonpolarized and polarized thin films of gold. *Appl. Environ. Microbiol.* **67**, 3188–3194 (2001).

81. Busalmen, J. P. & de Sánchez, S. R. Electrochemical polarization-induced changes in the growth of individual cells and biofilms of Pseudomonas fluorescens (ATCC 17552). *Appl. Environ. Microbiol.* **71**, 6235–6240 (2005).

82. Costerton, J. W., Ellis, B., Lam, K., Johnson, F. & Khoury, A. E. Mechanism of electrical enhancement of efficacy of antibiotics in killing biofilm bacteria. *Antimicrob. Agents Chemother.* **38**, 2803–2809 (1994).

83. Del Pozo, J. L. *et al.* Effect of electrical current on the activities of antimicrobial agents against Pseudomonas aeruginosa, Staphylococcus aureus, and Staphylococcus epidermidis biofilms. *Antimicrob. Agents Chemother.* **53**, 35–40 (2009).

84. Jass, J. & Lappin-Scott, H. M. The efficacy of antibiotics enhanced by electrical currents against Pseudomonas aeruginosa biofilms. *J. Antimicrob. Chemother.* **38**, 987–1000 (1996).

85. Blenkinsopp, S. A., Khoury, A. E. & Costerton, J. W. Electrical enhancement of biocide efficacy against Pseudomonas aeruginosa biofilms. *Appl. Environ. Microbiol.* **58**, 3770–3773 (1992).

86. Stoodley, P., deBeer, D. & Lappin-Scott, H. M. Influence of electric fields and pH on biofilm structure as related to the bioelectric effect. *Antimicrob. Agents Chemother.* **41**, 1876–1879 (1997).

87. Kim, Y. W. *et al.* Effect of electrical energy on the efficacy of biofilm treatment using the bioelectric effect. *npj Biofilms Microbiomes* **1**, 1–8 (2015).

88. Paluch, E., Rewak-Soroczyńska, J., Jędrusik, I., Mazurkiewicz, E. & Jermakow, K. Prevention of biofilm formation by quorum quenching. *Appl. Microbiol. Biotechnol.* **104**, 1871–1881 (2020).

89. Carpentier, B. & Cerf, O. Biofilms and their consequences, with particular reference to hygiene in the food industry. *J. Appl. Bacteriol.* **75**, 499–511 (1993).

90. Michael Dunne Jr., W. Bacterial Adhesion : Seen Any Good Biofilms Lately ? *Clin. Microbiol. Rev.* **15**, 155–166 (2002).

91. Mahamuni-Badiger, P. P. *et al.* Biofilm formation to inhibition: Role of zinc oxide-based nanoparticles. *Mater. Sci. Eng. C* **108**, (2020).

92. Ahmed Mosselhy Abdelrehiem, D. Silica-drug delivery systems: From prolonged drug release to wound dressings and orthopedic applications. (2019).

93. Kurmoo, Y. *et al.* Real time monitoring of biofilm formation on coated medical devices for the reduction and interception of bacterial infections. *Biomater. Sci.* **8**, 1464–1477 (2020).

94. Cloutier, M., Mantovani, D. & Rosei, F. Antibacterial Coatings: Challenges, Perspectives, and Opportunities. *Trends Biotechnol.* **33**, 637–652 (2015).

95. Alves, D. & Olívia Pereira, M. Mini-review: Antimicrobial peptides and enzymes as promising candidates to functionalize biomaterial surfaces. *Biofouling* **30**, 483–499 (2014).

96. Liu, L., Ercan, B., Sun, L., Ziemer, K. S. & Webster, T. J. Understanding the Role of Polymer Surface Nanoscale Topography on Inhibiting Bacteria Adhesion and Growth. *ACS Biomater. Sci. Eng.* **2**, 122–130 (2016).

97. Satriano, C., Messina, G. M. L., Carnazza, S., Guglielmino, S. & Marletta, G. Bacterial adhesion onto nanopatterned polymer surfaces. *Mater. Sci. Eng. C* **26**, 942–946 (2006).

98. Hasan, J. & Chatterjee, K. Recent advances in engineering topography mediated antibacterial

surfaces. *Nanoscale* **7**, 15568–15575 (2015).

99. Zhang, H. & Chiao, M. Anti-fouling coatings of poly (dimethylsiloxane) devices for biological and biomedical applications. *J. Med. Biol. Eng.* **35**, 143–155 (2015).

100. Gillich, T. *et al.* PEG-stabilized core–shell nanoparticles: Impact of linear versus dendritic polymer shell architecture on colloidal properties and the reversibility of temperature-induced aggregation. *ACS Nano* **7**, 316–329 (2013).

101. Zhou, L.-Y. *et al.* Novel zwitterionic vectors: Multi-functional delivery systems for therapeutic genes and drugs. *Comput. Struct. Biotechnol. J.* (2020).

102. Yang, L. *et al.* Photocatalyzed surface modification of poly (dimethylsiloxane) with polysaccharides and assay of their protein adsorption and cytocompatibility. *Anal. Chem.* **82**, 6430–6439 (2010).

103. Zhao, C., Li, L., Wang, Q., Yu, Q. & Zheng, J. Effect of film thickness on the antifouling performance of poly (hydroxy-functional methacrylates) grafted surfaces. *Langmuir* **27**, 4906–4913 (2011).

104. Wu, D., Luo, Y., Zhou, X., Dai, Z. & Lin, B. Multilayer poly (vinyl alcohol)-adsorbed coating on poly (dimethylsiloxane) microfluidic chips for biopolymer separation. *Electrophoresis* **26**, 211–218 (2005).

105. Ammar, Y., Swailes, D., Bridgens, B. & Chen, J. Influence of surface roughness on the initial formation of biofilm. *Surf. Coatings Technol.* **284**, 410–416 (2015).

106. Procaccini, R. A., Studdert, C. A. & Pellice, S. A. Silver doped silica-methyl hybrid coatings. Structural evolution and antibacterial properties. *Surf. Coatings Technol.* **244**, 92–97 (2014).

107. Kao, H. *et al.* Metal ion-dependent tailored antibacterial activity and biological properties of polydopamine-coated titanium implants. *Surf. Coatings Technol.* **378**, 124998 (2019).

108. Campoccia, D., Montanaro, L. & Arciola, C. R. A review of the biomaterials technologies for infection-resistant surfaces. *Biomaterials* **34**, 8533–8554 (2013).

109. Kazemzadeh-Narbat, M. *et al.* Multilayered coating on titanium for controlled release of antimicrobial peptides for the prevention of implant-associated infections. *Biomaterials* **34**, 5969–5977 (2013).

110. Glinel, K., Thebault, P., Humblot, V., Pradier, C.-M. & Jouenne, T. Antibacterial surfaces developed from bio-inspired approaches. *Acta Biomater.* **8**, 1670–1684 (2012).

111. Lemire, J. A., Harrison, J. J. & Turner, R. J. Antimicrobial activity of metals: mechanisms, molecular targets and applications. *Nat. Rev. Microbiol.* **11**, 371–384 (2013).

112. Eckhardt, S. *et al.* Nanobio silver: its interactions with peptides and bacteria, and its uses in medicine. *Chem. Rev.* **113**, 4708–4754 (2013).

113. Zhou, B., Li, Y., Deng, H., Hu, Y. & Li, B. Antibacterial multilayer films fabricated by layer-by-layer immobilizing lysozyme and gold nanoparticles on nanofibers. *Colloids Surfaces B Biointerfaces* **116**, 432–438 (2014).

114. Carmona-Ribeiro, A. M. & de Melo Carrasco, L. D. Cationic antimicrobial polymers and their assemblies. *Int. J. Mol. Sci.* **14**, 9906–9946 (2013).

115. Rios, A. C. *et al.* Alternatives to overcoming bacterial resistances: state-of-the-art. *Microbiol. Res.* **191**, 51–80 (2016).

116. Peng, K. *et al.* Development of contact-killing non-leaching antimicrobial guanidyl-functionalized polymers via click chemistry. *RSC Adv.* **7**, 24903–24913 (2017).

117. Foksowicz-Flaczyk, J., Walentowska, J., Przybylak, M. & Maciejewski, H. Multifunctional durable properties of textile materials modified by biocidal agents in the sol-gel process. *Surf. Coatings Technol.* **304**, 160–166 (2016).

118. Lewis, K. & Klibanov, A. M. Surpassing nature: rational design of sterile-surface materials. *Trends Biotechnol.* **23**, 343–348 (2005).

119. Kaur, R. & Liu, S. Antibacterial surface design – Contact kill. *Prog. Surf. Sci.* **91**, 136–153 (2016).

120. Tiller, J. C., Liao, C.-J., Lewis, K. & Klibanov, A. M. Designing surfaces that kill bacteria on contact. *Proc. Natl. Acad. Sci.* **98**, 5981–5985 (2001).

121. Lin, J., Qiu, S., Lewis, K. & Klibanov, A. M. Mechanism of bactericidal and fungicidal activities of textiles covalently modified with alkylated polyethylenimine. *Biotechnol. Bioeng.* **83**, 168–172 (2003).

122. Friedrich, C. L., Moyles, D., Beveridge, T. J. & Hancock, R. E. W. Antibacterial action of structurally diverse cationic peptides on gram-positive bacteria. *Antimicrob. Agents Chemother.* **44**, 2086–2092 (2000).

123. Tiller, J. C. Antimicrobial surfaces. *Bioact. surfaces* 193–217 (2010).

124. Murata, H., Koepsel, R. R., Matyjaszewski, K. & Russell, A. J. Permanent, non-leaching antibacterial surfaces-2: How high density cationic surfaces kill bacterial cells. *Biomaterials* **28**, 4870–4879 (2007).

125. Kipping, F. S. Organic derivative of silicon. Preparation of alkylsilicon chlorides. in *Proc. Chem. Soc* **20**, 15 (1904).

126. Colas, A. Silicones: preparation, properties and performance. *Dow Corning, Life Sci.* (2005).

127. Colas, A. & Curtis, J. Silicone biomaterials: history and chemistry. *Biomater. Sci. an Introd. to Mater. Med.* **2**, 80–85 (2004).

128. Momen, G. & Farzaneh, M. Survey of micro/nano filler use to improve silicone rubber for outdoor insulators. *Rev. Adv. Mater. Sci* **27**, 1–13 (2011).

129. Morari, C., Balan, I., Pintea, J., Chitanu, E. & Iordache, I. Electrical conductivity and electromagnetic shielding effectiveness of silicone rubber filled with ferrite and graphite powders. *Prog. Electromagn. Res.* **21**, 93–104 (2011).

130. Wang, X., Zhu, S., Liu, L. & Li, L. Flexible antibacterial film based on conjugated polyelectrolyte/silver nanocomposites. *ACS Appl. Mater. Interfaces* **9**, 9051–9058 (2017).

131. Kebir, N., Kriegel, I., Estève, M. & Semetey, V. Preparation of bactericidal cationic PDMS surfaces using a facile and efficient approach. *Appl. Surf. Sci.* **360**, 866–874 (2016).

132. Wang, B. L. *et al.* Bio-inspired terpolymers containing dopamine, cations and MPC: a versatile platform to construct a recycle antibacterial and antifouling surface. *J. Mater. Chem. B* **3**, 5501–5510 (2015).

133. Wang, B. *et al.* Surface-initiated RAFT polymerization of p (MA POSS-co-DMAEMA+) brushes on PDMS for improving antiadhesive and antibacterial properties. *Int. J. Polym. Mater. Polym. Biomater.* **65**, 55–64 (2016).

134. Voo, Z. X. *et al.* Antimicrobial/antifouling polycarbonate coatings: Role of block copolymer architecture. *Macromolecules* **48**, 1055–1064 (2015).

135. Li, C., Ding, Y., Kuddannaya, S., Zhang, Y. & Yang, L. Anti-bacterial properties of collagen-coated glass and polydimethylsiloxane substrates. *J. Mater. Sci.* **52**, 9963–9978 (2017).

136. Wu, M. *et al.* Development of functional biointerfaces by surface modification of polydimethylsiloxane with bioactive chlorogenic acid. *Colloids Surfaces B Biointerfaces* **116**, 700–706 (2014).

137. Birajdar, M. S., Cho, H., Seo, Y., Choi, J. & Park, H. Surface conjugation of poly (dimethyl siloxane) with itaconic acid-based materials for antibacterial effects. *Appl. Surf. Sci.* **437**, 245–256 (2018).

138. Agarwal, A. *et al.* Polymeric multilayers that contain silver nanoparticles can be stamped onto biological tissues to provide antibacterial activity. *Adv. Funct. Mater.* **21**, 1863–1873 (2011).

139. Wolf, M. P., Salieb-Beugelaar, G. B. & Hunziker, P. PDMS with designer functionalities—Properties, modifications strategies, and applications. *Prog. Polym. Sci.* **83**, 97–134 (2018).

140. Cai, D. K., Neyer, A., Kuckuk, R. & Heise, H. M. Optical absorption in transparent PDMS materials applied for multimode waveguides fabrication. *Opt. Mater. (Amst).* **30**, 1157–1161 (2008).

141. Stankova, N. E. *et al.* Optical properties of polydimethylsiloxane (PDMS) during nanosecond laser processing. *Appl. Surf. Sci.* **374**, 96–103 (2016).

142. McDonald, J. C. & Whitesides, G. M. Poly (dimethylsiloxane) as a material for fabricating microfluidic devices. *Acc. Chem. Res.* **35**, 491–499 (2002).

143. Berthier, E., Young, E. W. K. & Beebe, D. Engineers are from PDMS-land, Biologists are from Polystyrenia. *Lab Chip* **12**, 1224–1237 (2012).

144. Johnston, I. D., McCluskey, D. K., Tan, C. K. L. & Tracey, M. C. Mechanical characterization of bulk Sylgard 184 for microfluidics and microengineering. *J. Micromechanics Microengineering* **24**, 35017 (2014).

145. Dow Corning. Product Information: Sylgard® 184 Silicone Elastomer. *Dow Corning* 1–4 (2014).

146. Shiku, H. *et al.* Oxygen permeability of surface-modified poly (dimethylsiloxane) characterized by scanning electrochemical microscopy. *Chem. Lett.* **35**, 234–235 (2006).

147. Heo, Y. S. *et al.* Characterization and resolution of evaporation-mediated osmolality shifts that constrain microfluidic cell culture in poly (dimethylsiloxane) devices. *Anal. Chem.* **79**, 1126–1134 (2007).

148. Mäki, A.-J., Peltokangas, M., Kreutzer, J., Auvinen, S. & Kallio, P. Modeling carbon dioxide transport in PDMS-based microfluidic cell culture devices. *Chem. Eng. Sci.* **137**, 515–524 (2015).

149. Noll, W. *Chemistry and technology of silicones*. (Elsevier, 2012).

150. Bodas, D. & Khan-Malek, C. Formation of more stable hydrophilic surfaces of PDMS by plasma and chemical treatments. *Microelectron. Eng.* **83**, 1277–1279 (2006).

151. Henstock, J. R., Canham, L. T. & Anderson, S. I. Silicon: the evolution of its use in biomaterials. *Acta Biomater.* **11**, 17–26 (2015).

152. Swanson, A. B. Silicone Rubber Implants for Replacement of Arthritic or Destroyed Joints in the Hand. *Surg. Clin. North Am.* **48**, 1113–1127 (1968).

153. Todd, D. A. Silicone catheter. (1976).

154. Daniels, A. U. Silicone breast implant materials. *Swiss Med. Wkly.* **142**, (2012).

155. Dunn, K. W., Hall, P. N. & Khoo, C. T. K. Breast implant materials: sense and safety. *Br. J. Plast. Surg.* **45**, 315–321 (1992).

156. Kim, H. T. & Jeong, O. C. PDMS surface modification using atmospheric pressure plasma. *Microelectron. Eng.* **88**, 2281–2285 (2011).

157. Winiecka-Krusnell, J. & Linder, E. Bacterial infections of free-living amoebae. *Res. Microbiol.* **152**, 613–619 (2001).

158. Gao, Q. *et al.* Rationally designed dual functional block copolymers for bottlebrush-like coatings: In vitro and in vivo antimicrobial, antibiofilm, and antifouling properties. *Acta Biomater.* **51**, 112–124 (2017).

159. Doulgeraki, A. I., Di Ciccio, P., Ianieri, A. & Nychas, G. J. E. Methicillin-resistant food-related

Staphylococcus aureus: a review of current knowledge and biofilm formation for future studies and applications. *Res. Microbiol.* **168**, 1–15 (2017).

160. Enquête Nationale De Prévalence Des Infections Nosocomiales Et Des Traitements Anti-Infectieux En Établissements De Santé, Mai-Juin 2017. *Saint-Maurice: Santé publique* 270 (2019).

161. Eduok, U., Faye, O. & Szpunar, J. Recent developments and applications of protective silicone coatings: A review of PDMS functional materials. *Prog. Org. Coatings* **111**, 124–163 (2017).

162. Tu, Q. *et al.* Surface modification of poly(dimethylsiloxane) and its applications in microfluidics-based biological analysis. *Rev. Anal. Chem.* **31**, 177–192 (2012).

163. Tian, L., Wu, L., Wang, W. & Liu, Xi. Research on the PDMS surface modification technique. *Key Eng. Mater.* **562**–**565**, 131–135 (2013).

164. Gokaltun, A., Yarmush, M. L., Asatekin, A. & Usta, O. B. Recent advances in nonbiofouling PDMS surface modification strategies applicable to microfluidic technology. *Technology* **5**, 1–12 (2017).

165. Oláh, A., Hillborg, H. & Vancso, G. J. Hydrophobic recovery of UV/ozone treated poly (dimethylsiloxane): adhesion studies by contact mechanics and mechanism of surface modification. *Appl. Surf. Sci.* **239**, 410–423 (2005).

166. Almutairi, Z., Ren, C. L. & Simon, L. Evaluation of polydimethylsiloxane (PDMS) surface modification approaches for microfluidic applications. *Colloids Surfaces A Physicochem. Eng. Asp.* **415**, 406–412 (2012).

167. Fritz, J. L. & Owen, M. J. Hydrophobic recovery of plasma-treated polydimethylsiloxane. *J. Adhes.* **54**, 33–45 (1995).

168. Tan, S. H., Nguyen, N.-T., Chua, Y. C. & Kang, T. G. Oxygen plasma treatment for reducing hydrophobicity of a sealed polydimethylsiloxane microchannel. *Biomicrofluidics* **4**, 32204 (2010).

169. Bausch, G. G., Stasser, J. L., Tonge, J. S. & Owen, M. J. Behavior of plasma-treated elastomeric polydimethylsiloxane coatings in aqueous environment. *Plasmas Polym.* **3**, 23–34 (1998).

170. Morra, M. *et al.* On the aging of oxygen plasma-treated polydimethylsiloxane surfaces. *J. Colloid Interface Sci.* **137**, 11–24 (1990).

171. Zhao, L. H., Lee, J. & Sen, P. N. Long-term retention of hydrophilic behavior of plasma treated polydimethylsiloxane (PDMS) surfaces stored under water and Luria-Bertani broth. *Sensors Actuators A Phys.* **181**, 33–42 (2012).

172. Berdichevsky, Y., Khandurina, J., Guttman, A. & Lo, Y.-H. UV/ozone modification of poly (dimethylsiloxane) microfluidic channels. *Sensors Actuators B Chem.* **97**, 402–408 (2004).

173. Efimenko, K., Wallace, W. E. & Genzer, J. Surface modification of Sylgard-184 poly (dimethyl siloxane) networks by ultraviolet and ultraviolet/ozone treatment. *J. Colloid Interface Sci.* **254**, 306–315 (2002).

174. Fu, Y.-J. *et al.* Effect of UV-ozone treatment on poly (dimethylsiloxane) membranes: surface characterization and gas separation performance. *Langmuir* **26**, 4392–4399 (2010).

175. Ma, K., Rivera, J., Hirasaki, G. J. & Biswal, S. L. Wettability control and patterning of PDMS using UV–ozone and water immersion. *J. Colloid Interface Sci.* **363**, 371–378 (2011).

176. Hillborg, H., Tomczak, N., Olàh, A., Schönherr, H. & Vancso, G. J. Nanoscale hydrophobic recovery: A chemical force microscopy study of UV/ozone-treated cross-linked poly (dimethylsiloxane). *Langmuir* **20**, 785–794 (2004).

177. Makamba, H., Hsieh, Y.-Y., Sung, W.-C. & Chen, S.-H. Stable permanently hydrophilic

protein-resistant thin-film coatings on poly (dimethylsiloxane) substrates by electrostatic self-assembly and chemical cross-linking. *Anal. Chem.* **77**, 3971–3978 (2005).

178. Decher, G. Fuzzy nanoassemblies: toward layered polymeric multicomposites. *Science (80-.).* **277**, 1232–1237 (1997).

179. Smith, R. C., Riollano, M., Leung, A. & Hammond, P. T. Layer-by-layer platform technology for small-molecule delivery. *Angew. Chemie* **121**, 9136–9139 (2009).

180. Boudou, T., Crouzier, T., Ren, K., Blin, G. & Picart, C. Multiple functionalities of polyelectrolyte multilayer films: new biomedical applications. *Adv. Mater.* **22**, 441–467 (2010).

181. Su, X., Kim, B.-S., Kim, S. R., Hammond, P. T. & Irvine, D. J. Layer-by-layer-assembled multilayer films for transcutaneous drug and vaccine delivery. *ACS Nano* **3**, 3719–3729 (2009).

182. Mehta, G. *et al.* Polyelectrolyte-clay-protein layer films on microfluidic PDMS bioreactor surfaces for primary murine bone marrow culture. *Adv. Funct. Mater.* **17**, 2701–2709 (2007).

183. Wang, B. *et al.* Loading of antibiotics into polyelectrolyte multilayers after self-assembly and tunable release by catechol reaction. *J. Phys. Chem. C* **120**, 6145–6155 (2016).

184. Wang, B. *et al.* In situ construction of Ag NPs in bio-inspired multilayer films for long-term bactericidal and biofilm inhibition properties. *Polym. Test.* **62**, 162–170 (2017).

185. Xu, Q. *et al.* Antimicrobial efficiency of PAA/(PVP/CHI) erodible polysaccharide multilayer through loading and controlled release of antibiotics. *Carbohydr. Polym.* **161**, 53–62 (2017).

186. Agarwal, A. *et al.* Polymeric multilayers that localize the release of chlorhexidine from biologic wound dressings. *Biomaterials* **33**, 6783–6792 (2012).

187. Jeong, H. *et al.* Intrinsic hydrophobic Cairnlike multilayer films for antibacterial effect with enhanced durability. *ACS Appl. Mater. Interfaces* **7**, 26117–26123 (2015).

188. Vaterrodt, A. *et al.* Antifouling and antibacterial multifunctional polyzwitterion/enzyme coating on silicone catheter material prepared by electrostatic layer-by-layer assembly. *Langmuir* **32**, 1347–1359 (2016).

189. Kébir, N., Kriegel, I., Estève, M. & Semetey, V. Preparation of bactericidal cationic PDMS surfaces using a facile and efficient approach. *Appl. Surf. Sci.* **360**, 866–874 (2016).

190. Mussard, W., Kebir, N., Kriegel, I., Estève, M. & Semetey, V. Facile and efficient control of bioadhesion on poly (dimethylsiloxane) by using a biomimetic approach. *Angew. Chemie* **123**, 11063–11066 (2011).

191. Guo, D.-J., Han, H.-M., Xiao, S.-J. & Dai, Z.-D. Surface-hydrophilic and protein-resistant silicone elastomers prepared by hydrosilylation of vinyl poly (ethylene glycol) on hydrosilanes-poly (dimethylsiloxane) surfaces. *Colloids Surfaces A Physicochem. Eng. Asp.* **308**, 129–135 (2007).

192. Wu, Y., Huang, Y. & Ma, H. A facile method for permanent and functional surface modification of poly (dimethylsiloxane). *J. Am. Chem. Soc.* **129**, 7226–7227 (2007).

193. Chen, H., Chen, Y., Sheardown, H. & Brook, M. A. Immobilization of heparin on a silicone surface through a heterobifunctional PEG spacer. *Biomaterials* **26**, 7418–7424 (2005).

194. Chen, H., Zhang, Z., Chen, Y., Brook, M. A. & Sheardown, H. Protein repellant silicone surfaces by covalent immobilization of poly (ethylene oxide). *Biomaterials* **26**, 2391–2399 (2005).

195. Wang, Y. *et al.* Covalent micropatterning of poly (dimethylsiloxane) by photografting through a mask. *Anal. Chem.* **77**, 7539–7546 (2005).

196. Sugiura, S., Edahiro, J., Sumaru, K. & Kanamori, T. Surface modification of polydimethylsiloxane with photo-grafted poly (ethylene glycol) for micropatterned protein adsorption and cell adhesion. *Colloids Surfaces B Biointerfaces* **63**, 301–305 (2008).

197. Leigh, B. L. *et al.* Antifouling photograftable zwitterionic coatings on PDMS substrates. *Langmuir* **35**, 1100–1110 (2018).

198. Donzel, C. *et al.* Hydrophilic poly (dimethylsiloxane) stamps for microcontact printing. *Adv. Mater.* **13**, 1164–1167 (2001).

199. Magennis, E. P., Hook, A. L., Williams, P. & Alexander, M. R. Making silicone rubber highly resistant to bacterial attachment using thiol-ene grafting. *ACS Appl. Mater. Interfaces* **8**, 30780–30787 (2016).

200. Fernandes, M. M., Ivanova, K., Francesko, A., Mendoza, E. & Tzanov, T. Immobilization of antimicrobial core-shell nanospheres onto silicone for prevention of Escherichia coli biofilm formation. *Process Biochem.* **59**, 116–122 (2017).

201. Groza, A. *et al.* The Effect of the Ionizing Radiation on Hydroxyapatite–Polydimethylsiloxane Layers. *Polym. Eng. Sci.* **59**, 2406–2412 (2019).

202. Sorzabal-Bellido, I. *et al.* Exploiting Covalent, H-Bonding, and π–π Interactions to Design Antibacterial PDMS Interfaces That Load and Release Salicylic Acid. *ACS Appl. Bio Mater.* **2**, 4801–4811 (2019).

203. Peveler, W. J. *et al.* Covalently attached antimicrobial surfaces using BODIPY: improving efficiency and effectiveness. *ACS Appl. Mater. Interfaces* **10**, 98–104 (2018).

204. Tu, Q. *et al.* Antibacterial properties of poly (dimethylsiloxane) surfaces modified with graphene oxide-catechol composite. *Prog. Org. Coatings* **129**, 247–253 (2019).

205. Dong, J. J. *et al.* Contact Killing of Gram-Positive and Gram-Negative Bacteria on PDMS Provided with Immobilized Hyperbranched Antibacterial Coatings. *Langmuir* **35**, 14108–14116 (2019).

206. Ye, Q. *et al.* Grafting robust thick zwitterionic polymer brushes via subsurface-initiated ring-opening metathesis polymerization for antimicrobial and anti-biofouling. *ACS Appl. Mater. Interfaces* **11**, 39171–39178 (2019).

207. Yeh, S.-B., Chen, C.-S., Chen, W.-Y. & Huang, C.-J. Modification of silicone elastomer with zwitterionic silane for durable antifouling properties. *Langmuir* **30**, 11386–11393 (2014).

208. Tang, J., Han, Y., Chen, H. & Lin, Q. Bottom-up fabrication of PEG brush on poly (dimethylsiloxane) for antifouling surface construction. *Int. J. Polym. Sci.* **2016**, (2016).

209. Zhou, T. *et al.* Surface functionalization of biomaterials by radical polymerization. *Prog. Mater. Sci.* **83**, 191–235 (2016).

210. Li, Z. *et al.* Surface modification of silicone elastomer with rosin acid-based quaternary ammonium salt for antimicrobial and biocompatible properties. *Mater. Des.* **189**, 108493 (2020).

211. Zhang, A., Cheng, L., Hong, S., Yang, C. & Lin, Y. Preparation of anti-fouling silicone elastomers by covalent immobilization of carboxybetaine. *RSC Adv.* **5**, 88456–88463 (2015).

212. Kolb, H. C., Finn, M. G. & Sharpless, K. B. Click chemistry: diverse chemical function from a few good reactions. *Angew. Chemie Int. Ed.* **40**, 2004–2021 (2001).

213. Ramapanicker, R. & Chauhan, P. Click Chemistry: Mechanistic and Synthetic Perspectives. *Click Reactions in Organic Synthesis* 1–24 (2016).

214. Ostaci, R.-V. *et al.* Polymer brushes grafted to "passivated" silicon substrates using click chemistry. *Langmuir* **24**, 2732–2739 (2008).

215. Ostaci, R.-V., Damiron, D., Al Akhrass, S., Grohens, Y. & Drockenmuller, E. Poly (ethylene glycol) brushes grafted to silicon substrates by click chemistry: influence of PEG chain length, concentration in the grafting solution and reaction time. *Polym. Chem.* **2**, 348–354 (2011).

216. Flavel, B. S. *et al.* Grafting of poly (ethylene glycol) on click chemistry modified Si (100)

surfaces. *Langmuir* **29**, 8355–8362 (2013).

217. Lafarge, J., Kebir, N., Schapman, D. & Burel, F. Design of self-disinfecting PVC surfaces using the click chemistry. *React. Funct. Polym.* **73**, 1464–1472 (2013).

218. Britcher, L., Barnes, T. J., Griesser, H. J. & Prestidge, C. A. PEGylation of porous silicon using click chemistry. *Langmuir* **24**, 7625–7627 (2008).

219. He, J. *et al.* Immobilization of an antimicrobial peptide on silicon surface with stable activity by click chemistry. *J. Mater. Chem. B* **6**, 68–74 (2018).

220. Hoyle, C. E. & Bowman, C. N. Thiol–ene click chemistry. *Angew. Chemie Int. Ed.* **49**, 1540–1573 (2010).

221. Zhang, J., Chen, Y. & Brook, M. A. Facile functionalization of PDMS elastomer surfaces using thiol–ene click chemistry. *Langmuir* **29**, 12432–12442 (2013).

222. Zhang, Z., Feng, X., Xu, F., Liu, X. & Liu, B. "Click" chemistry-based surface modification of poly (dimethylsiloxane) for protein separation in a microfluidic chip. *Electrophoresis* **31**, 3129–3136 (2010).

223. Lee, J. S. *et al.* Modulation of Foreign Body Reaction against PDMS Implant by Grafting Topographically Different Poly (acrylic acid) Micropatterns. *Macromol. Biosci.* **19**, 1900206 (2019).

224. Sangermano, M. & Razza, N. Light induced grafting-from strategies as powerful tool for surface modification. *Express Polym. Lett.* **13**, 135 (2019).

225. Keskin, D., Mokabbar, T., Pei, Y. & Van Rijn, P. The relationship between bulk silicone and benzophenone-initiated hydrogel coating properties. *Polymers (Basel).* **10**, 534 (2018).

226. Shen, N. *et al.* Photograftable Zwitterionic Coatings Prevent Staphylococcus aureus and Staphylococcus epidermidis Adhesion to PDMS Surfaces. *ACS Appl. Bio Mater.* (2021).

227. Kuliasha, C. A., Fedderwitz, R. L., Calvo, P. R., Sumerlin, B. S. & Brennan, A. B. Engineering the surface properties of poly (dimethylsiloxane) utilizing aqueous RAFT photografting of acrylate/methacrylate monomers. *Macromolecules* **51**, 306–317 (2018).

228. Kuliasha, C. A. *et al.* Engineered Chemical Nanotopographies: Reversible Addition–Fragmentation Chain-Transfer Mediated Grafting of Anisotropic Poly (acrylamide) Patterns on Poly (dimethylsiloxane) To Modulate Marine Biofouling. *Langmuir* **36**, 379–387 (2019).

229. Tu, Q. *et al.* Antifouling properties of poly (dimethylsiloxane) surfaces modified with quaternized poly (dimethylaminoethyl methacrylate). *Colloids Surfaces B Biointerfaces* **102**, 361–370 (2013).

230. Eissa, A. M., Khosravi, E. & Cimecioglu, A. L. A versatile method for functionalization and grafting of 2-hydroxyethyl cellulose (HEC) via click chemistry. *Carbohydr. Polym.* **90**, 859–869 (2012).

Chapitre II : Surfaces de PDMS antibactériennes par effet de champ électrique

Introduction

Ce chapitre est consacré à l'étude de l'adhésion de différentes espèces bactériennes (Gram positif et Gram négatif) sur des surfaces métalliques et des surfaces métalliques recouvertes de PDMS sous l'effet d'un champ électrique ainsi que la viabilité des bactéries en suspension.

Lorsque les bactéries s'approchent de la surface à une distance de 10-20 nm, les interactions de Van der Waals (force attractive) et les interactions électrostatiques jouent un rôle important dans l'adhésion bactérienne. Une fois que les bactéries s'approchent de la surface à une distance critique de 1 nm, la somme nette des forces attractives ou répulsives générées entre la surface des bactéries et celle du substrat, telles que les interactions de Van der Waals, les interactions électrostatiques ou les interactions hydrophobes déterminent finalement l'adhésion bactérienne.

Le but de cette étude est de diminuer ou de prévenir l'adhésion des bactéries par l'augmentation (ou la modulation) des interactions électrostatiques répulsives entre les bactéries et les surfaces cathodiques qui seront chargées négativement sous l'effet d'un champ électrique en mode statique (sans flux). Le champ électrique a été généré entre deux électrodes parallèles qui ont été connectées au potensiostat (Velleman®) comme dans un condensateur. Le potensiostat peut être contrôlé pour fournir une tension entre 0 et 30 V sans aucun courant (pour éviter toute réaction d'électrolyse) en fonction des électrodes utilisées dans la suspension bactérienne.

Pour l'étude, des électrodes en cuivre, en zinc et en aluminium ont été utilisés car ceux sont des métaux assez classiques et cela nous permettra aussi de vérifier s'il y a un impact de la nature de l'électrode sur l'adhésion bactérienne. Ensuite, les électrodes de cuivre ont été revêtu de PDMS pour étudier l'adhésion bactérienne, sous champ électrique, sur ce polymère qui, comme décrit dans le chapitre I, est un polymère couramment utilisé dans le domaine des biomatériaux. De plus cette étude a été réalisée avec trois types de bactéries à Gram-positif (*S. aureus*, *S. epidermidis* et *E. faecalis*) et deux types de bactéries à Gram-négatif (*E. coli* et *P. aeruginosa*), qui sont parmi les espèces les plus représentatives de la contamination bactérienne.

Les résultats de ce chapitre seront présentés sous forme d'un article publié sous la référence « Y. Lou, P. Thebault, F. Burel, N. Kebir, "Antibacterial properties of metal and

PDMS surfaces under weak electric fields," *Surf. Coatings Technol.*, vol. 394, p. 125912, 2020 ».

De plus, des expériences non décrites dans l'article sont présentées et discutées dans le paragraphe II.2, intitulé « informations supplémentaires ».

II.1 Article 1: Antibacterial properties of metal and PDMS surfaces under weak electric fields

Yuzhen LOU[1], Pascal THEBAULT[2], Fabrice BUREL[1], Nasreddine KEBIR[1]

[1]Normandie Université, INSA Rouen Normandie, Laboratoire PBS, UMR CNRS 6270 & FR 3038, Avenue de l'Université, 76801 Saint Etienne du Rouvray, France

[2]Normandie Université, UNIROUEN, Laboratoire PBS, UMR CNRS 6270 & FR 3038, 76821 Mont-Saint-Aigan, France

Correspondence to:

Nasreddine KEBIR (E-mail: *nasreddine.kebir@insa-rouen.fr*)

Pascal THEBAULT (E-mail: *pascal.thebault@univ-rouen.fr*)

Abstract

The adhesion of several species of bacteria on two parallel rectangular electrodes under weak electric fields was studied. The electrodes were based on native metal or PDMS coated Cu. After 2 hours of contact at a voltage of 0.2 to 1V without any current, the Zn cathode showed a bacterial repellent effect with a difference in bacterial adhesion of about 1.5 to 2 log CFU/cm^2 on the anode. Al electrodes were inactive due to their passivation by the alumina layer. At 1V, both Zn and Al exhibited more than 80% mortality of suspended bacteria. The Cu electrodes showed a very high bactericidal effect even at 0V, and the bacterial adhesion on its surface was too weak to see a difference between the two electrodes. A similar study carried out on PDMS surfaces, covering Cu electrodes, revealed that a difference of 1 log CFU/cm^2 of bacterial adhesion between the cathode and anode surfaces can be obtained by applying a voltage ranging from 10 to 30V. This cathodic repellent effect was specific to staphylococcus species, suggesting that in the presence of a PDMS coating, the electrostatic forces on the surface are too low to be the main factor governing bacterial adhesion.

Keywords: Electrical field; Bacterial adhesion; PDMS; Metallic surface; Bactericidal effect.

Introduction

Microbial contamination of surfaces often leads to the formation of a biofilm, resulting in serious problems for human health (e.g. device-related infections, healthcare-related infections) as well as for industrial sectors (e.g. corrosion of metal surfaces, food contamination, deterioration of pipes...), leading to a negative socio-economic impact [1-3].

However, it should be noted that bacteria in their biofilms require antibiotic concentrations 100 to 1000 times higher than those of planktonic bacteria to achieve effective eradication [4]. Therefore, the development of materials capable of preventing the adhesion of bacteria and/or the formation of biofilms on their surface is a key element to avoid contamination. Gottenbos *et al*. have reported that the initial attachment of bacteria depends on the result of non-specific interactions such as Van der Waals, electrostatic, acid-base interactions and Brownian motion forces [5]. Dunne *et al* also repoted that once the bacteria approache surfaces at a critical distance (usually less than 1 nm), adhesion is determined by the net sum of attractive or repulsive forces, including electrostatic and hydrophobic interactions, steric hindrance, van der Waals forces etc [6].

Three types of antibacterial surfaces are described in the literature: anti-adhesive surfaces, contact-killing surfaces and release-based surfaces [7].

Anti-adhesive surfaces are designed to repel bacteria by optimizing their physico-chemical properties such as the surface charge (negative charges), the wettability or the topography (micro/nano-patterned surfaces) [8-11]. However, they cannot affect the viability of pathogen that can be released to contaminate others. Furthermore, the use of physical surface modifications (particularly surface topography) as non-specific methods to prevent the bacterial adhesion is much more complex than we can imagine [12].

Contact-killing surfaces which are generally based on cationic biocidal agents covalently bonded to substrate surfaces that attract negatively charged bacteria and kill them by disrupting their cell membrane [13-15]. However, these surfaces quickly become inactive after being buried under a layer of dead bacteria.

Released-based surfaces are designed to leach antibacterial agents that kill not only adhered bacteria but also planktonic bacteria [16-18]. The disadvantage of this kind of surfaces is its limited activity owing to the limited amount of the loaded antibacterial compounds. However, excessive use of antibiotics may lead to the phenomenon of bacterial resistance [19].

It is noteworthy that the use of an electrical method to prevent infection of medical devices, without traumatising the patient by removal of the device, is of great interest In addition, over time, bacteria should not adapt as well with electrical treatment as with antibiotics [20]. Direct and alternating currents [21, 22] as well as acoustic (by piezo-electric actuators) [23] and radio frequency wave [24] treatments have already proven to be effective techniques to prevent initial bacterial adhesion and growth, through *in vitro* and *in vivo* experiments. On the other hand, the electrical current has been found to increase the efficacy of antibiofilm agents in a synergistic action called 'the bioelectric effect' [25-29], which can lead to a dramatic decrease in the concentration of the antibiofilm compounds used. Thus, the development of electrically stimulated surfaces that prevent bacterial adhesion and biofilm formation is an emergent and attractive pathway.

Busalmen *et al*. [30] have studied, using an optical microscope, the influence of an electrical field on the adhesion of *Pseudomonas fluorescens* onto the surface of gold electrodes, under flow conditions at two different ionic strengths (0.01 and 0.1 M NaCl; pH 7). By applying negative electric potentials (-0.5 and -0.2V relative to a reference electrode [Ag/AgCl-KCl saturated solution]), they have evidenced a decrease in bacterial adhesion of one Log (CFU/mm^2) after 15 min of contact, compared to adhesion at a potential of 0.2V. In another work [31], using the same system, they demonstrated the impact of this electrical field on the growth of planktonic cells and biofilms of *Pseudomonas fluorescens* (cell morphology, size at cell division, time to division, and biofilm structure). Gall *et al*. [32] have studied, using Quartz Crystal Microbalance with Dissipation analysis (QCM-D), the effect of applying an electrical field, perpendicular to the flow of a *Pseudomonas fluorescens* suspension, on the adhesion of bacterial cells to the gold electrode. Surprisingly, they demonstrated that the tested bacteria were rigidly attached to the negatively charged surface, unlike to the positively charged one, suggesting that the applied electric potential could influence the conformation of the bacterial cell surface, allowing the cells to overcome the electrostatic energy barrier.

In this study, we investigated the adhesion of different bacterial species, in a static mode (without flow), on metallic and PDMS surfaces under an electrical field (without any current), generated by two parallel metal electrodes (as in a capacitor) immersed in an aqueous suspension of bacteria. The impact of the applied electrical field on bacterial survival has also been studied.

Materials and methods

Materials

Sylgard® 184 was purchased from DOW chemical company (USA) and was used as the coating material. Copper, zinc and aluminum blades (10×100×1.5 mm^3, Jeulin, France) were used as electrodes. *Staphylococcus aureus* (ATCC 29213), *Staphylococcus epidermidis* (ATCC 35984), *Enterococcus faecalis* (ATCC 29212), *Pseudomonas aeruginosa* (PA14) and *Escherichia coli* (K12 MG1655) strains were stored as frozen aliquots in brain heart infusion broth (BHI, Bacto, France) and 30% of glycerol at -20°C. Ultrapure water, obtained from a Milli-Q system (Siemens, France), was used in all cases.

Preparation of PDMS-coated copper or zinc electrodes

15 g of the two parts of Sylgard® 184, i.e. silicone elastomer base and curing agent, in a ratio of 10:1 (w/w) were mixed and casted into a low-density polyethylene petri dish square (120×120×17 mm^3). Then, the mixture was degassed under vacuum, until all air bubbles were removed, and cured at 70 °C for 3 h to form a first PDMS layer. Six blades were then put on top of this layer and covered with a second layer of PDMS (20 g) using the same process. The resulting PDMS-coated electrodes (12×3.5×40 mm^3) were cut out by using a scalpel. The thickness of the coating was around 1 mm.

Preparation of Bacterial suspensions

For each experiment, all bacterial species were pre-cultured in BHI at 37°C under shaking at 140 rpm for approximately16 h. Then, bacteria were harvested by centrifugation (Sigma® 3-16KL, rotor 19776, Germany) under 1600 g for 15 minutes at 20°C and resuspended at a concentration of 10^7 ~10^8 CFU/ml in Milli-Q water to avoid the influence of charged particles in BHI or Phosphate Buffered Saline (PBS, Gibco, UK).

Zeta potential measurements

Zeta potentials of bacteria were measured with a Zetasizer Nano-ZS system (Malvern Panalytical, Ltd., UK) at 25 °C in Milli-Q water solution at 10^7 ~10^8 CFU/ml. Three measurements were carried out for each bacterial suspension.

Assessment of bacteria attachment onto PDMS and metallic blade surfaces under an electric field

The process used to evaluate the attachment of bacteria to the surface of metallic or PDMS-coated electrodes is shown in Figure 1. The PDMS-coated electrodes were sterilized in 70% ethanol overnight and washed twice with Milli-Q water before use. Uncoated electrodes were sterilized in 70% ethanol for 20 min, followed by sonication for 30 min, and washed twice with Milli-Q water before use.

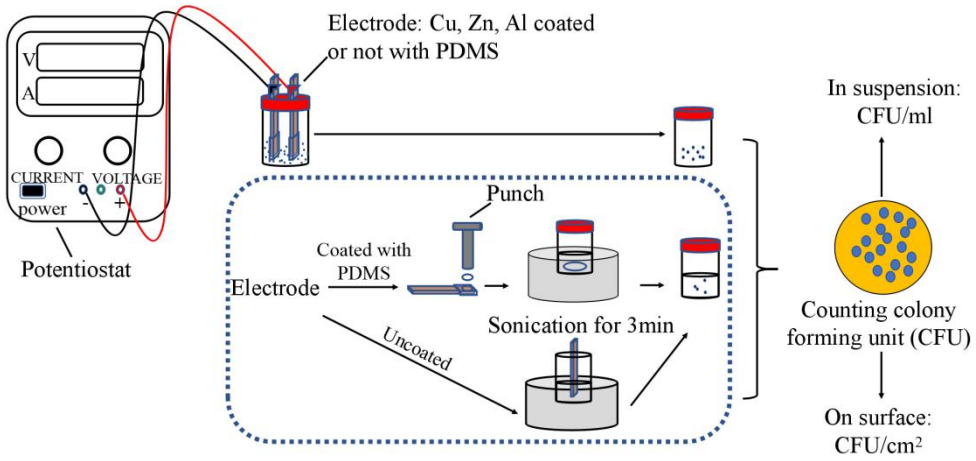

Figure 1. Process used to evaluate the adhesion of bacteria to the surface of metallic or PDMS-coated electrodes.

The bacterial adhesion was studied in a system of parallel plates with a distance of 1 cm between the two electrodes connected to the potensiostat (0-30 V, Velleman®). The electrodes were immersed (1 cm) in 7 ml of the previous prepared bacterial suspension during 2 h. Then, to remove unattached bacteria, these electrodes were washed in 15 ml of sterile Milli-Q water under slight shaking while the potentiostat was still on. They were then detached from the potentiostat. To recover the bacteria fixed to the surface, metallic electrodes were directly immersed in 7 mL of PBS solution, under sonication for 3 min. For PDMS-coated electrodes, a sample of PDMS was taken with a circular punch (Ø=1 cm) and was immersed in 3 ml of PBS solution under sonication for 3 min. Decimal dilutions of the resulting bacterial suspensions, containing bacteria detached from the surface, as well as those where the experiments were conducted, containing unattached surviving bacteria, were spread (20 µl or 100 µl) on BHI agar plates and incubated at 37°C for 24 h before colony counting. All experiments were performed in at least triplicate.

Results and discussion

Bacterial adhesion onto a surface is often explained by the Derjaguin, Landau, Verwey and Overbeek (DLVO) theory of colloidal stability. It describes initially repulsive electrical double layer interactions (electrostatic repulsion) between bacteria and similarly charged surfaces. At the same time, bacteria are attracted by van der Waals forces and approach surface contact as soon as they cross the electrostatic energy barrier by decreasing the interfacial distance. [5,6]

Thus, we have used two parallel electrodes, as in a capacitor, immersed in an aqueous suspension of bacteria (Figure 2). Cu, Al and Zn were used as models for metallic electrodes; PDMS was used as representative electrodes for plastic-based biomaterials.

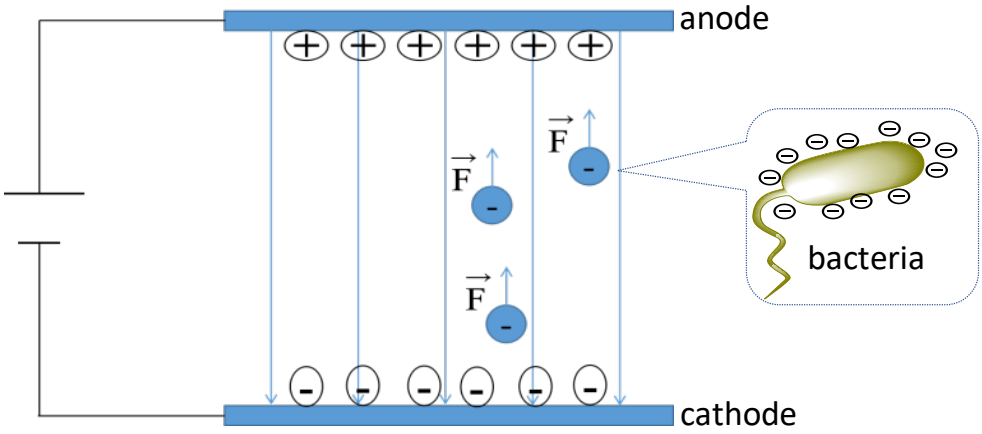

Figure 2. Schematic principle of antibacterial action of cathode.

Bacterial adhesion to metal electrodes

The results of the enumeration of live *S. aureus* adhering to electrodes of Cu, Zn and Al, after immersion in bacterial suspensions for 2 hours at an electrical voltage of 0 to 1 V, are shown in Figure 3 (A1). Above 1 V, the presence of current and electrolysis reactions can be observed, making it unnecessary to study electrostatic interactions. The survival of suspended bacteria was also monitored before and after immersion of the electrodes (Figure 3 (A2)).

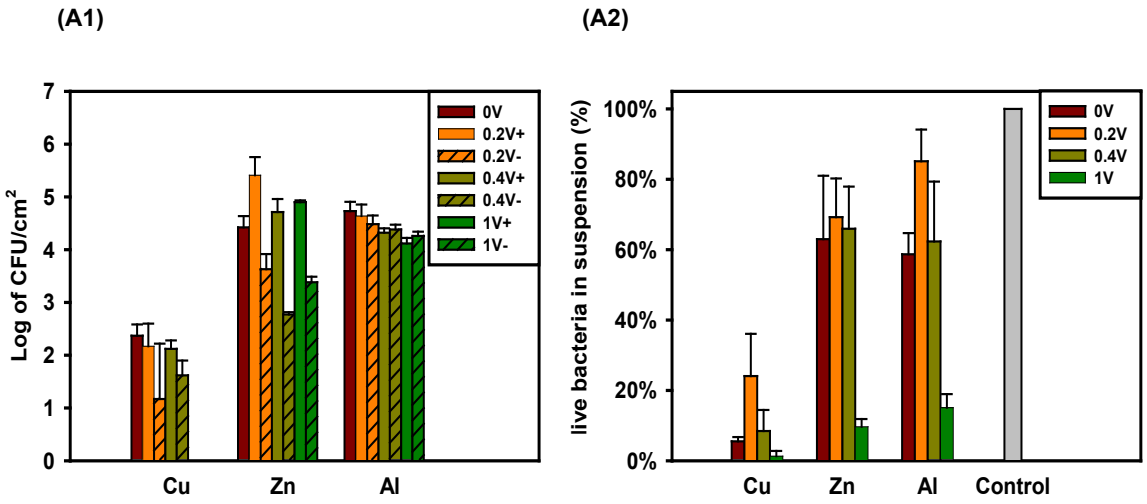

Figure 3. Adhesion of *S. aureus* onto the surface of Cu, Zn and Al after 2h of contact under 0, 0.2, 0.4 and 1V: (A1) live bacteria adhered to the surface; (A2) live bacteria in suspension; control: live bacteria in suspension without any electrode.

For copper electrodes at 0 V, the concentration of adhered *S. aureus* was only about 2 log of CFU/cm^2 (Figure 3 (A1)). This low adhesion can be explained by the well-known bactericidal properties of copper [33-35], which is confirmed by the percentage of bacterial surviving in solution (Figure 3 (A2)). Indeed, less than 20 % of bacteria in solution are still alive (or cultivable) after 2 h. However, a slight difference in bacterial adhesion between anode (positively charged) and cathode (negatively charged) at 0.2 and 0.4 V was observed. Furthermore, the increase of voltage to 1 V, suppressed the adhesion *of S. aureus* onto the surface and increased the suspended bacterial mortality to more than 95 %. These results suggest that the bactericidal effect of copper could be enhanced by the application of an electric field and are consistent with the "bioelectric effect" [25-29].

For the two other electrodes, a bacterial adhesion of approximately 4.5 log of CFU/cm^2 was achieved at 0 V. In the case of Al, no difference in bacterial adhesion between cathode and anode was observed regardless of the applied voltage. This could be explained by the well-known passivation of the aluminum surface by oxidation leading to the formation of a thin layer of alumina, which is an ionic salt (Al_2O_3). The electrical properties of this layer are very different from those of its pure metal, and its electrochemical static polarization is more difficult to achieve. For Zn electrodes, at all applied voltages, there was a decrease in the adhesion of *S. aureus* on the cathode compared to bacterial adhesion at 0V. At the same time, a slight increase on the anode was observed inducing a difference of more or less 2 log of CFU/cm^2 between these two electrodes. This result suggests that electrostatic interactions are, in this case, quite predominant. Therefore, this result also indicates that bacterial adhesion could be modulated on the Zn electrodes by the use of an electric field. Moreover, for a voltage ranging

from 0 to 0.4V, an insignificant decrease, of about 10 to 40%, of live bacteria in suspension was observed for both Al and Zn electrodes. However, at 1 V, a decrease in the live bacteria population in solution of about 80 % was observed for both electrodes. Soumya *et al.* [36] reported that potentials at about 0.9 V would affect the redox potential across the cell membrane and disrupt redox homeostasis, thereby accelerating the production of endogenous reactive oxygen species (ROS) and inhibiting bacterial growth. In summary, these results show that the nature of the electrode and the voltage values have an impact on the adhesion of *S. aureus* to the surface as well as on suspended bacterial mortality.

On the other hand, in order to determine whether the structure of the external membrane of bacteria cells has any influence on these results, we studied the adhesion of *E. coli,* as a model of Gram-negative bacteria, to zinc electrodes under voltage values ranging from 0 to 1 V.

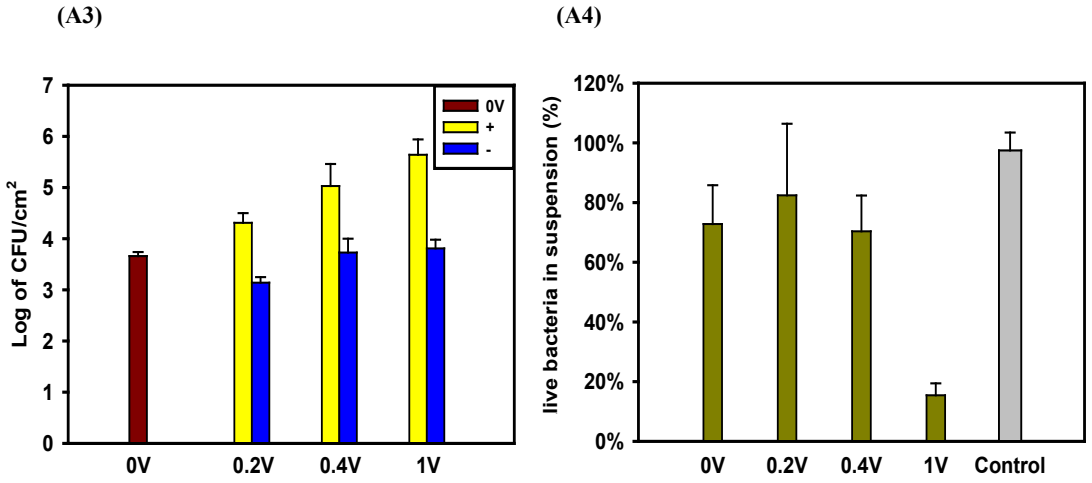

Figure 4. Adhesion *of E. coli* to the surface of zinc electrodes after 2h of contact at voltage values between 0 and 1 V: (A3) live bacteria adhered to the surface; (A4) live bacteria in suspension; control: live bacteria in suspension without any electrode.

Figure 4 shows that *E. coli* behaves almost similarly to *S. aureus* in terms of adhesion to the Zn electrodes after 2 h of contact. Indeed, a difference in *E. coli* adhesion of about 1.5 to 2 log of CFU/cm^2 between the anode and cathode was observed. In addition, the percentage of killing of E. coli in suspension was also quite similar to that of *S. aureus*, i.e. low for a voltage of 0, 0.2 or 0.4 V, and higher than 80% at 1 V.

Experiments were then carried out with different types of bacteria to verify whether these results are universal or not on zinc electrodes. The bacteria chosen are the most representative species involved in the phenomenon of contamination in the hospital environment. *S. epidermidis* and *E. faecalis* are Gram-positive bacteria and mainly cause skin

and endocardial infections, respectively [37, 38]. Gram-negative bacteria such as *P. aeruginosa* and *E. coli* account for more than 30 % of nosocomial infections [37]. *P. aeruginosa* causes several infections in human organs such as the urinary, blood, respiratory and gastrointestinal systems [40]. *E. coli* can also cause urinary or bloodstream infections for example [41]. These experiments were performed only at 0 and 0.2 V.

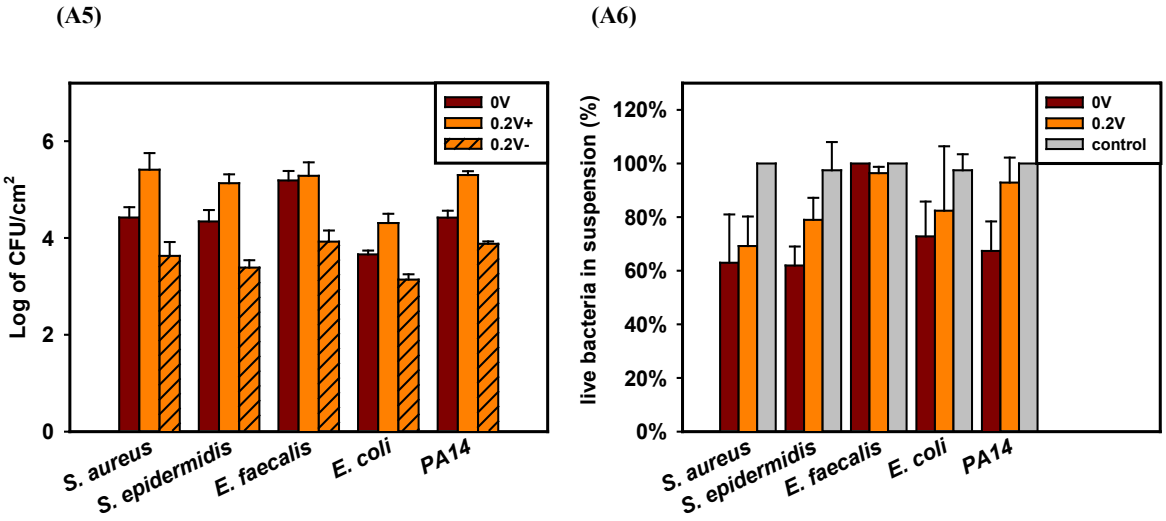

Figure 5. Adhesion of different bacterial species to the surface of zinc after 2h of contact at voltage values of 0 and 0.2 V: (A5) live bacteria adhered to the surface; (A6) live bacteria in suspension, control: live bacteria in suspension without any electrode.

As shown in Figure 5, at 0.2 V, a difference of bacterial adhesion was obtained between the cathode and the anode for each strain, with a lower adhesion on the cathode. These results suggest that bacterial adhesion could be controlled under an electric field whatever the bacterial species. Furthermore, no significant decrease of bacterial concentration in solution was observed for all tested species.

Bacterial adhesion to the surface of PDMS under an electrical field

In a second part, we studied the bacterial adhesion, under the effect of an electric field, on the surface of PDMS, which is a material widely used as biomaterial. Previous copper electrodes were coated with a PDMS layer of a thickness around 1 mm and used as electrodes. The applied voltage ranged from 0 to 30 V, which is the maximum voltage provided by the potentiostat. The copper electrodes were chosen because they can easily reveal whether the metal surface was completely covered by the PDMS or not due to the disappearance of the bactericidal activity of the Cu in suspension.

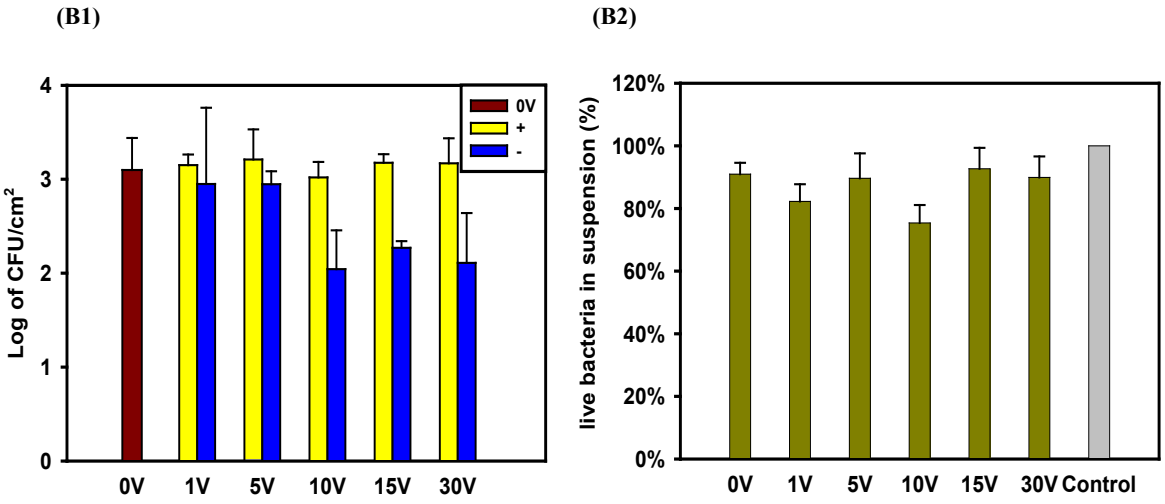

Figure 6. Adhesion of S. aureus to the PDMS-coated copper surface (1mm) after 2 hours of contact at voltage values between 0 and 30 V: (B1) live bacteria adhering to the surface; (B2) live bacteria in suspension; control: live bacteria in suspension without electrode.

The results of the adhesion of S. aureus to the surface of the PDMS under an electric field are shown in Figure 6. It can be seen that without an electrical voltage, the bacterial adhesion was about 3 log CFU/cm^2, which is higher than its value on the surface of the uncoated copper (Figure 3). The difference in bacterial adhesion between cathode and anode at 1 and 5 V was not significant. On the other hand, at higher applied voltages (10 to 30 V), a lower bacterial adhesion on the cathode, around 2 log CFU/cm^2, was observed, probably due to the electrostatic repulsion between the negative charges on the surface of the PDMS and the negatively charged bacterial cells. In addition, the percentage of live bacteria in suspension was approximately 90% regardless of the applied voltage, which is quite consistent with the percentage observed in milli-Q water. These results show that the PDMS coating on the copper electrodes leads to (i) the disappearance of the bactericidal effect of copper in the bacterial suspension, meaning that the electrodes were fully coated, and (ii) no significant bacterial stress at applied high voltage, probably due to the chemical and electrical insulating properties of PDMS. Consequently, the applied voltage must be increased above 30 V to achieve a greater anti-adhesion effect.

The study of adhesion of different bacterial species onto PDMS surfaces was also carried out at 30 V (Figure 7). No copper bactericidal activity was detected for all species. However, *S. epidermidis* appears to be quite sensitive to the applied electric field and showed a reduction of about 50% in the concentration of live bacteria in suspension. For surface adhesion, only *S. epidermidis* showed the same behavior as *S. aureus* with a difference of about 1 log CFU/cm^2 between cathode and anode. This result is in contradiction with the previous

result on the zinc electrodes at 0.2V. To understand this specificity of the Staphylococcus genus, measurements of the zeta potential of the bacterial membrane were performed (Table 1).

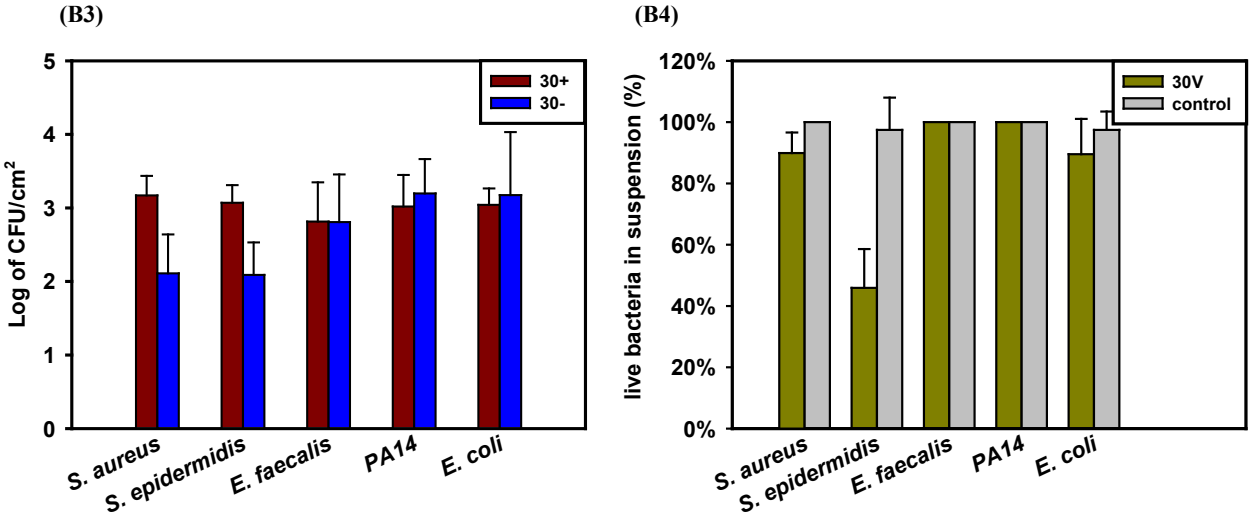

Figure 7. Adhesion of different bacterial species to the surface of PDMS coated copper (1mm) after 2 hours of contact at 30 V: (B3) live bacteria adhering to the surface; (B4) live bacteria in suspension; control: live bacteria in suspension without any electrode.

Table 1. Zeta potential of bacteria in sterile milli-Q water at a concentration of 10^7-10^8 CFU / ml.

Bacteria	Zeta potential (mV)	Percentage
S. aureus **(ATCC 29213)**	-39.3± 0.9	100%
S. epidermidis **(ATCC 35984)**	-38.5±1.7	51.80%±0.02
	-26.8±1.2	48.20%±0.02
E. faecalis **(ATCC 29212)**	-35.8±1.0	100%
E. coli **(K12 MG1655)**	-50.6±1.0	100%
P. aeruginosa **(PA 14)**	-41.6±0.9	100%

As expected, all bacterial membranes are negatively charged, but *E. coli* and *P. aeruginosa* bacteria have the lowest zeta potential and therefore the highest overall negative charge. Theoretically, with a higher negative charge, *E. coli* and *P. aeruginosa* should undertake stronger repulsive electrostatic interactions with the PDMS surface, resulting in lower adhesion

to the anode surface, which is in contradiction with our experimental results (Figure 7). Therefore, these observations suggest that, in the presence of a PDMS coating, the electrostatic interactions are too weak to be the predominant factor governing bacterial adhesion. There are two possible reasons why Staphylococcus species are more sensitive to the low surface polarization of PDMS: (1) they are Gram+ bacteria, which have only one external phospholipidic membrane, unlike Gram- bacteria, which have two; (2) they are spherical in shape with a lower contact surface, while the other bacteria are bacillus-shaped.

Conclusion

In this work, we have studied the bacterial adhesion of Gram positive (*S. aureus, S. epidermidis and E. faecalis*) and Gram negative (*E. coli* and *P. aeruginosa*) bacteria to metal and PDMS electrode surfaces under an electric field. After 2h of contact with each of these bacteria, the Zn electrodes showed a difference of 1.5-2 log of UFC/cm^2 between cathode and anode at voltages of 0.2 and 0.4 V, without significant killing of bacteria in suspension. Under the same conditions, the Al electrodes were found to be inactive in limiting and directing bacterial adhesion, probably because of surface oxidation causing its passivation. However, at 1V, the Zn and Al electrodes became bactericidal by killing bacteria in suspension. On the other hand, the bactericidal effect of Cu electrodes was very high at 0 V and seems to be reinforced by the electrical filed. Nevertheless, the bacterial adhesion on its surface was too weak to see a difference between the cathode and the anode. Once coated with PDMS, the bactericidal effect of Cu disappeared and a difference of 1 log of UFC/cm^2, specific to staphylococcus species, was observed between the two electrodes above 10 V. Finally, this study demonstrates that the electrostatic force is the predominant factor governing the bacterial adhesion to Zn surfaces but not to those of Al and PDMS. For future works, high voltage should be used in order to increase the electrostatic bacterial repellent effect onto PDMS surfaces. Furthermore, metal electrodes could be used as physical disinfecting agents at 1V without current.

Acknowledgments

This work was funded by China Scholarship Council (CSC).

References

[1] A. I. Doulkeraki et al., Methicillin-resistant food-related Staphylococcus aureus: a review of current knowledge and biofilm formation for future studies and applications, Res. Microbiol., vol. 168 (2017）, pp. 1 – 15.

[2] D. Romero, Bacterial determinants of the social behavior of Bacillus subtilis, Res. Microbiol., vol. 164 (2013), pp. 788-798.

[3] J. Winiecka-Krusnell and E. Linder, Bacterial infections of free-living amoebae, Res. Microbiol., vol. 152 (2001), pp. 613–619.

[4] M. Salwiczek et al., Emerging rules for effective antimicrobial coatings, Trends Biotechnol., vol. 32 (2014), no. 2, pp. 82–90.

[5] B. Gottenbos, H. J. Busscher, H. C. Van Der Mei, and P. Nieuwenhuis, Pathogenesis and prevention of biomaterial centered infections, Mater. Sci. Mater. Med., vol. 13 (2002), no. 8, pp. 717–722.

[6] W. M. Jr. Dunne, Bacterial Adhesion: Seen Any Good Biofilms Lately?, Clin. Microbiol. Rev., vol. 15, no. 2 (2002), pp. 155–166.

[7] M. Cloutier, D. Mantovani, and F. Rosei, Antibacterial Coatings: Challenges, Perspectives, and Opportunities, Trends Biotechnol., vol. 33, no. 11 (2015), pp. 637–652.

[8] D. Alves and M. Olívia Pereira, Mini-review: Antimicrobial peptides and enzymes as promising candidates to functionalize biomaterial surfaces, Biofouling, vol. 30 (2014), no. 4, pp. 483–499.

[9] L. Liu, B. Ercan, L. Sun, K. S. Ziemer, and T. J. Webster, Understanding the Role of Polymer Surface Nanoscale Topography on Inhibiting Bacteria Adhesion and Growth, ACS Biomater. Sci. Eng., vol. 2, no. 1 (2016), pp. 122–130.

[10] C. Satriano, G. M. L. Messina, S. Carnazza, S. Guglielmino, and G. Marletta, Bacterial adhesion onto nanopatterned polymer surfaces, Mater. Sci. Eng. C, vol. 26, no. 5–7 (2006), pp. 942–946.

[11] J. Hasan and K. Chatterjee, Recent advances in engineering topography mediated antibacterial surfaces, Nanoscale, vol. 7, no. 38 (2015), pp. 15568–15575.

[12] Y. Ammar, D. Swailes, Ben Bridgens, J. Chen, Influence of surface roughness on the initial formation of biofilm, Surface and Coatings Technology, vol 284 (2015), pp. 410-416.

[13] J. Foksowicz-Flaczyk et al., Multifunctional durable properties of textile materials modified by biocidal agents in the sol-gel process, Surface and Coatings Technology, vol 304 (2016), pp. 160-166.

[14] K. Lewis and A. M. Klibanov, Surpassing nature: Rational design of sterile-surface materials, Trends Biotechnol., vol. 23, no. 7 (2005), pp. 343–348.

[15] R. Kaur and S. Liu, Antibacterial surface design – Contact kill, Prog. Surf. Sci., vol. 91, no. 3 (2016), pp. 136–153.

[16] R. A. Procaccini, C. A. Studdert and S. A. Pellice, Silver doped silica-methyl hybrid coatings. Structural evolution and antibacterial properties, Surface and Coatings Technology, vol. 244 (2014), pp. 92-97.

[17] H. Kao et al., Metal ion-dependent tailored antibacterial activity and biological properties of polydopamine-coated titanium implants, Surface and Coatings Technology, vol 378 (2019), pp. 124998.

[18] D. Campoccia, L. Montanaro, and C. R. Arciola, A review of the biomaterials technologies for infection-resistant surfaces, Biomaterials, vol. 34, no. 34 (2013), pp. 8533–8554.

[19] A. C. Riosa, C. G. Moutinho, F. C. Pinto, F. S. Del Fiol, A. Jozala, M. V. Chaud, M. M.D.C. Vila, J. A. Teixeira, V. M. Balcão. Alternatives to overcoming bacterial resistances: State-of-the-art. Microbiological Research, vol. 191 (2016), pp. 51–80.

[20] D. Freebairn, D. Linton, E. Harkin-Jones, D. S. Jones, B. F. Gilmore, and S. P. Gorman, Electrical methods of controlling bacterial adhesion and biofilm on device surfaces, Expert Rev. Med. Devices, vol. 10, no. 1 (2013), pp. 85–103.

[21] J. L. Del Pozo, M. S. Rouse, J. N. Mandrekar, J. M. Steckelberg, and R. Patel, The electricidal effect: reduction of Staphylococcus and Pseudomonas biofilms by prolonged exposure to low-intensity electrical current, Antimicrob. Agents Chemother., vol. 53, no. 1 (2009), pp. 41–45.

[22] J. L. Del Pozo et al., The electricidal effect is active in an experimental model of Staphylococcus epidermidis chronic foreign body osteomyelitis, Antimicrob. Agents Chemother., vol. 53, no. 10 (2009), pp. 4064–4068.

[23] Z. Hazan et al., Effective prevention of microbial biofilm formation on medical devices by low-energy surface acoustic waves, Antimicrob. Agents Chemother., vol. 50, no. 12 (2006), pp. 4144–4152.

[24] R. Caubet et al., A radio frequency electric current enhances antibiotic efficacy against bacterial biofilms, Antimicrob. Agents Chemother., vol. 48, no. 12 (2004), pp. 4662–4664.

[25] J. L. Del Pozo, M. S. Rouse, and R. Patel, Bioelectric effect and bacterial biofilms. A systematic review, Int. J. Artif. Organs, vol. 31, no. 9 (2008), pp. 786–795.

[26] J. W. Costerton, B. Ellis, K. Lam, F. Johnson, and A. E. Khoury, Mechanism of electrical enhancement of efficacy of antibiotics in killing biofilm bacteria., Antimicrob. Agents Chemother., vol. 38, no. 12 (1994), pp. 2803–2809.

[27] J. L. Del Pozo, M. S. Rouse, J. N. Mandrekar, M. F. Sampedro, J. M. Steckelberg, and R. Patel, Effect of electrical current on the activities of antimicrobial agents against Pseudomonas aeruginosa, Staphylococcus aureus, and Staphylococcus epidermidis biofilms, Antimicrob. Agents Chemother., vol. 53, no. 1 (2009), pp. 35–40.

[28] S. A. Blenkinsopp, A. E. Khoury, and J. W. Costerton, Electrical enhancement of biocide efficacy against Pseudomonas aeruginosa biofilms., Appl. Environ. Microbiol., vol. 58, no. 11 (1992), pp. 3770–3773.

[29] J. Jass and H. M. Lappin-Scott, The efficacy of antibiotics enhanced by electrical currents against Pseudomonas aeruginosa biofilms, Antimicrob. Chemother., vol. 38, no. 6 (1996), pp. 987–1000.

[30] J. P. Busalmen and S. R. De Sanchez, Adhesion of Pseudomonas fluorescens (ATCC 17552) to nonpolarized and polarized thin films of gold, Appl. Environ. Microbiol., vol. 67, no. 7 (2001), pp. 3188–3194.

[31] J. P. Busalmen and S. R. de Sánchez, Electrochemical polarization-induced changes in the growth of individual cells and biofilms of Pseudomonas fluorescens (ATCC 17552), Appl. Environ. Microbiol., vol. 71, no. 10 (2005), pp. 6235–6240.

[32] I. Gall, M. Herzberg, and Y. Oren, The effect of electric fields on bacterial attachment to conductive surfaces, Soft Matter, vol. 9, no. 8 (2013), pp. 2443–2452.

[33] G. Grass, C. Rensing, and M. Solioz, Metallic copper as an antimicrobial surface, Appl. Environ. Microbiol., vol. 77, no. 5 (2011), pp. 1541–1547.

[34] M. Vincent, R. E. Duval, P. Hartemann, and M. Engels-Deutsch, Contact killing and antimicrobial properties of copper, Appl. Microbiol., vol. 124, no. 5 (2018), pp. 1032–1046.

[35] F.S.da Silva et al., Corrosion resistance and antibacterial properties of copper coating deposited by cold gas spray, Surface and Coatings Technology, vol. 361 (2019), pp. 292-301.

[36] S. Pandit, S. Shanbhag, M. Mauter, Y. Oren, and M. Herzberg, Influence of Electric Fields on Biofouling of Carbonaceous Electrodes, Environ. Sci. Technol., vol. 51, no. 17 (2017), pp. 10022–10030.

[37] J. Y. H. Lee et al., Global spread of three multidrug-resistant lineages of Staphylococcus epidermidis, Nat. Microbiol., vol. 3, no. 10 (2018), pp. 1175–1185.

[38] V. D. Wells, E. S. Wong, B. E. Murray, P. E. Coudron, D. S. Williams, and S. M. Markowitz, Infections due to beta-lactamase-producing, high-level gentamicin- resistant Enterococcus faecalis, Ann. Intern. Med., vol. 116, no. 4 (1992), pp. 285–292.

[39] A. Y. Peleg and D. C. Hooper, Hospital-Acquired Infections Due to Gram-Negative Bacteria, new Engl. J. Med. Rev., vol. 362, no. 19 (2010), pp. 1804–1813.

[40] S. Mamoudou, D. Lassina, and K. Fla, Les infections à pseudomonas aeruginosa au service des maladies infectieuses du CHU YO, Burkina Faso : À propos de deux cas, Pan Afr. Med. J., vol. 21 (2015), pp. 183–186.

[41] R. A. Welch, E. P. Dellinger, B. Minshew, and S. Falkow, Haemolysin contributes to virulence of extra-intestinal E. coli infections, Nature, vol. 294, no. 5842 (1981). pp. 665–667.

II.2 Informations supplémentaires

Avant les expériences sous champ électrique, nous avons voulu valider certains points du protocole. Tout d'abord, nous avons réalisé la courbe de croissance bactérienne dans les conditions de préculture utilisé par la suite (i.e., incubation à 37°C dans du milieu BHI sous agitation à 140 rpm) afin de connaître l'état dans laquelle se situe les bactéries lors des expériences (après 16h de préculture). Les résultats sont regroupés sur la Figure II-1. On a remarqué que les espèces bactériennes avaient le même profil de croissance et qu'elles étaient en phase stationnaire à 16 h de préculture.

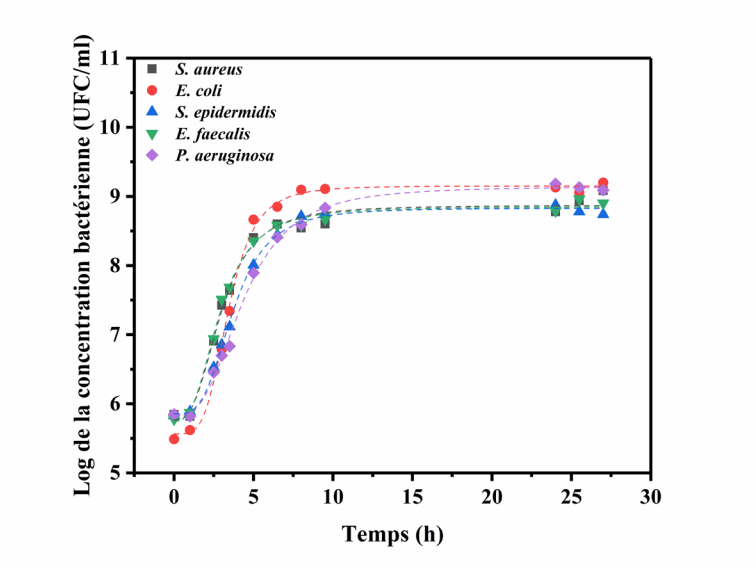

Figure II-1. Courbe de croissance de *S. aureus*, *E. coli*, *S. epidermidis*, *E. faecalis* et *P. aeruginosa*.

Ensuite, nous avons étudié la viabilité des bactéries dans l'eau, qui est le milieu utilisé pour les expériences sous champ électrique (Figure II-2). Nous avons choisi de réaliser les expériences sous champ électrique dans l'eau car la présence de composés chargées dans un milieu de culture ou une solution tampon, telles que les protéines peuvent influencer le résultat de l'expérience. En effet, ces espèces chargées peuvent aussi adhérer à la surface des électrodes et les passiver. De plus, la présence de sels en solution peut entrainer l'écrantage des charges des bactéries et de la surface et donc annuler les interactions électrostatiques. Les résultats ont montré aucune diminution de la concentration bactérienne de ces cinq types de bactéries dans le temps étudié.

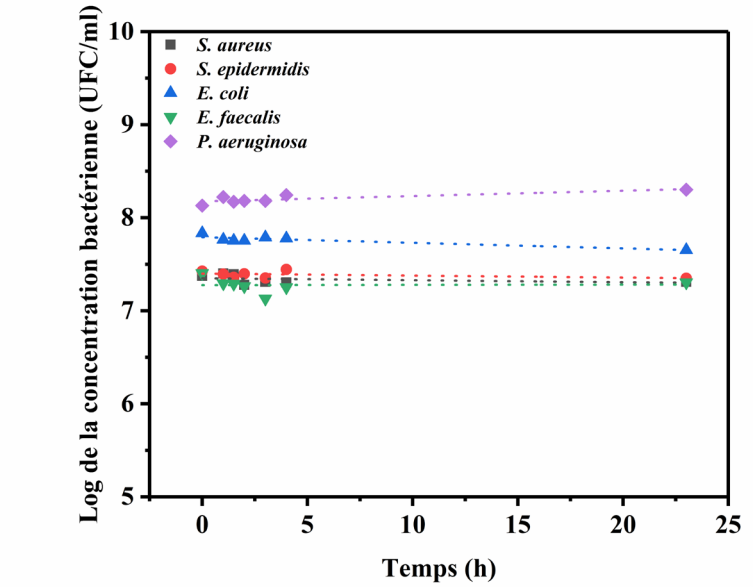

Figure II-2. Test de viabilité de *S. aureus*, *S. epidermidis*, *E. coli*, *E. faecalis* et *P. aeruginosa* dans une solution d'eau milli-Q stérile en fonction du temps.

Ensuite, l'adhésion d'une suspension bactérienne sur la surface du PDMS native (1×1 cm^2) en fonction du temps a été étudié pour déterminer la durée de contact entre les bactéries et les électrodes lors de l'expérience sous l'effet du champ électrique. En effet, il est nécessaire d'avoir une concentration bactérienne adhérée sur le PDMS suffisante pour pouvoir discriminer l'effet du champ électrique sur l'adhésion bactérienne en fonction de l'électrode. Pour cela, *S. aureus* a été utilisé comme modèle avec une concentration dans l'eau d'environ 10^7 UFC/ml. D'après la Figure II-3, on remarque que l'adhésion bactérienne a augmenté avec le temps de contact. De plus, après 2 h de contact, environ 5,6 log d'UFC/cm^2 de *S. aureus* ont déjà adhérés à la surface du PDMS, ce qui est suffisant pour l'expérience sous champ électrique. De plus, cette durée, nous permet d'étudier l'adhésion initial des bactéries sur les électrodes sans avoir d'effet sur la viabilité bactérienne dû à la solution aqueuse.

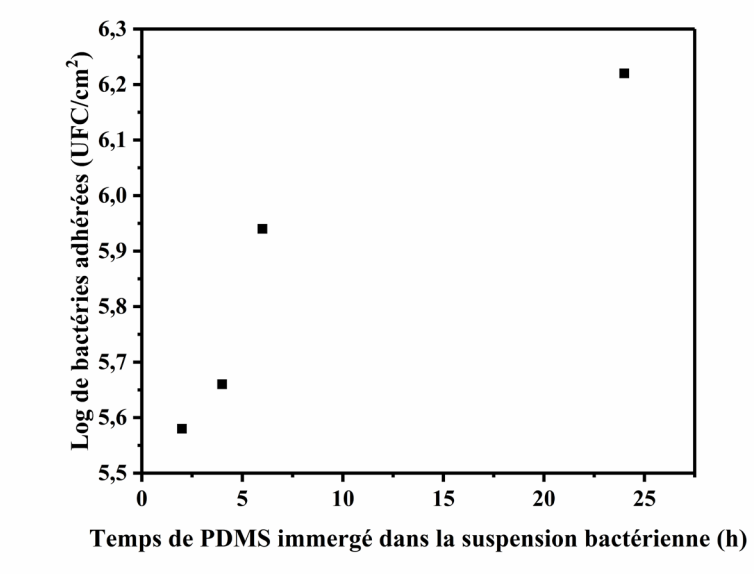

Figure II-3. Test de l'adhésion d'une suspension de *S. aureus* à 10^7 UFC/ml dans l'eau sur une surface de PDMS surface en fonction du temps.

Par la suite, nous avons aussi voulu vérifier si le PDMS était toxique pour les bactéries en utilisant, encore une fois, *S. aureus* comme modèle. Pour cela, une suspension bactérienne à environ 3×10^8 UFC/ml a été mise en contact, pendant 2 et 4h, avec des surfaces de PDMS de 1 cm^2 non stérilisées et, stérilisées par une solution d'éthanol à 70%. Les résultats ont été comparés avec des solutions n'ayant pas été en contact avec des surfaces de PDMS (Figure II-4). Aucune différence n'a été observée pour le même temps de contact, ce qui indique que le PDMS n'a aucun effet sur la population bactérienne et donc qu'il est non toxique.

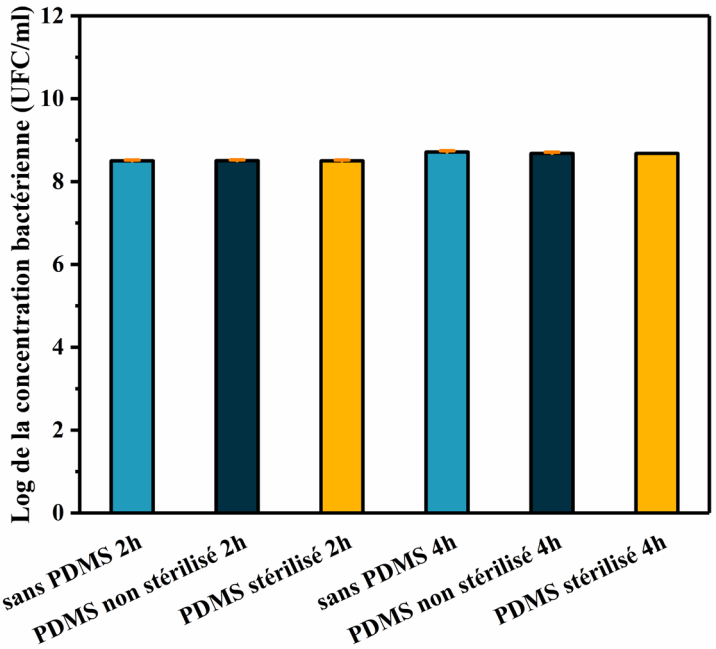

Figure II-4. Test de la toxicité du PDMS sur une suspension de *S. aureus*.

Le PDMS étant un matériau électriquement isolant et demandant un champ électrique plus important en vue de subir une polarisation, nous avons voulu vérifier si le protocole utilisé pour l'étude de l'adhésion bactérienne sur les surfaces métalliques non revêtues était applicable pour les surfaces métalliques une fois revêtues par le PDMS. Pour cela, une surface de cuivre recouverte de PDMS d'épaisseur d'environ 1 mm (Figure II-5) a été utilisée, et une tension de 30 V qui est la tension maximale que le potentiostat peut fournir a été appliqué en utilisant le même protocole que celui décrit dans l'article pour les surfaces métalliques non revêtues.

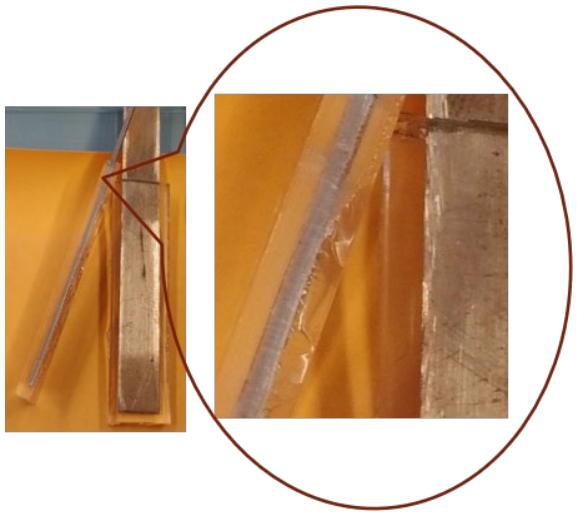

Figure II-5. Illustration d'électrode de cuivre revêtu de PDMS avec une épaisseur d'environ 1 mm.

Cependant, aucune différence d'adhésion bactérienne entre la cathode et l'anode a été constaté comme le montre la Figure II-6.

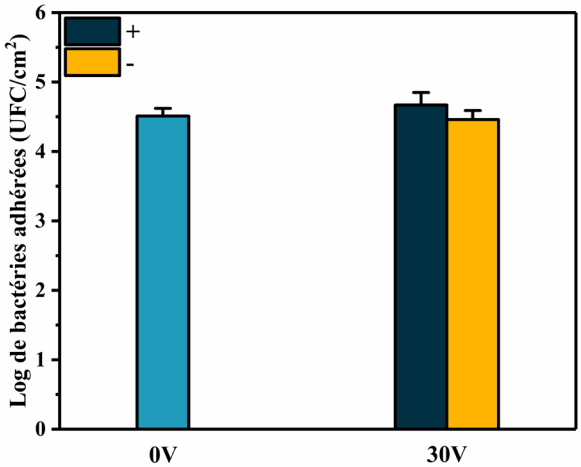

Figure II-6. Adhésion de *S. aureus* à la surface de cuivre revêtue de PDMS (1 mm) après 2 heures de contact à des valeurs de tension de 0 V et 30 V.

Plusieurs hypothèses étaient possibles : (i) le revêtement PDMS était peut-être trop épais pour subir une polarisation significative à 30V, (ii), le champ électrique n'était pas homogène sur l'ensemble du revêtement (en particulier sur les côtés des électrodes), et/ou (iii) que la rugosité, visible à l'œil nu, du revêtement PDMS se trouvant sur les côtés et au bout des électrodes favorisait l'adhésion des bactéries et donc masquait l'influence du champ électrique sur l'adhésion bactérienne.

Pour vérifier la première hypothèse, des électrodes revêtues de PDMS d'une épaisseur plus faible de l'ordre de 0,05 mm et aussi intégralement lisses ont été préparées (Figure II-7). Cependant, les revêtements minces étant fragiles et cassants, une diminution de la tension appliquée durant l'expérience a été observée. En effet, la tension a chuté de 30 V au début de l'expérience à 2 V pour maintenir le courant à 0 A, laissant supposer que le revêtement s'était dégradé et n'était donc plus homogène.

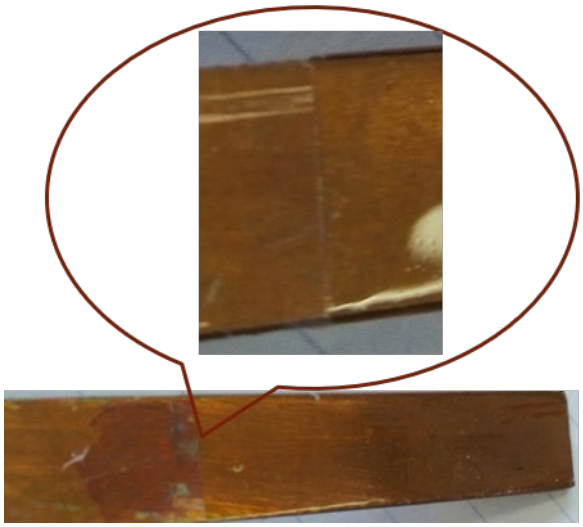

Figure II-7 Illustration d'électrode de cuivre revêtu de PDMS avec une épaisseur d'environ 0,05 mm.

Afin de s'affranchir des endroits rugueux du revêtement PDMS, nous avons décidé d'utiliser un emporte-pièce circulaire (Ø=1 cm) pour détacher des parties du revêtement PDMS des électrodes se trouvant face à face suite au 2h de contact avec la suspension bactérienne et après avoir retiré les électrodes du potensiostat. Ensuite, les échantillons de PDMS ont été immergés dans 3 ml d'une solution de PBS afin de compter les bactéries adhérées à la surface des différents revêtements de PDMS. Une différence d'adhésion bactérienne entre l'anode et la cathode a été observée. Suite à ces résultats, nous avons décidé d'utiliser ce protocole pour réaliser l'ensemble des expériences sur les surfaces métalliques revêtues de PDMS (cf. article résultats article II.1).

Chapitre III : Surfaces de PDMS antibactériennes par chimie Click

Introduction

Ce chapitre porte sur l'élaboration d'une surface de PDMS modifiée par un dérivé de la claramine via une réaction de chimie click. La cycloaddition 1,3-dipolaire de Huisgen azide-alkyne catalysée par le cuivre(I) (CuAAC) est l'une des réactions de chimie click les plus populaires en raison de ses nombreux avantages tels que la simplicité, l'efficacité et la chimio-sélectivité. Elle a été largement appliquée à la modification des surfaces pour immobiliser de façon covalente des composés conférant aux surfaces des propriétés antibactériennes. Mais à notre connaissance, la modification de la surface du PDMS par cette réaction pour concevoir une surface « Contact-Killing », qui est l'un des trois principaux types de surface antibactérienne décrits dans le chapitre I, n'a jamais été exploitée auparavant. Ici, nous avons donc utiliser cette méthode pour concevoir une surface de PDMS antibactérienne.

Comme nous l'avons présenté dans le chapitre I, le développement de nouveaux composés antibactériens est l'un des challenges les plus importants dans la lutte contre la contamination bactérienne due à la résistance bactérienne aux antibiotiques. Les composés polyaminostérols tels que les dérivés de la squalamine ou de la claramine ont suscité de plus en plus d'intérêt en raison de leurs activités antibactériennes à large spectre et à leurs procédés de synthèse plus simple à partir de matières premières moins coûteuses que les peptides antimicrobiens par exemple. Ainsi, dans ce chapitre, un dérivé de la claramine permettant de la réaliser une réaction de chimie click a été utilisé comme molécule active. Celle-ci a été synthétisée par le Dr Jean-Michel Brunel de l'UMR_MD1 "Membranes et Cibles Thérapeutiques" dans le cadre d'une collaboration.

Le dérivé de la claramine a ensuite été immobilisé par la réaction CuAAC sur la surface de PDMS préalablement modifiée par silanisation afin d'incorporer une fonction alcyne. La surface a été caractérisée par des mesures d'angle de contact avec l'eau en mode statique et en mode dynamique, par microscopie à force atomique (AFM) et par spectroscopie photoélectronique par rayons X (XPS). Enfin, l'activité antibactérienne de la surface de PDMS modifiée a été évaluée par le test Live/Dead contre deux bactéries pathogènes : *S. epidermidis* et *E. coli*.

Les résultats de ce chapitre seront présentés sous forme d'un article soumis à « colloids and surface B » (le 27/04/2021) sous le titre « Antibacterial PDMS surfaces based on a claramine-derivative through click-chemistry grafting ».

De plus, des expériences non décrites dans l'article sont présentées et discutées dans le paragraphe III.2, intitulé « informations supplémentaires ».

III.1 Article 2: Antibacterial PDMS surfaces based on a claramine-derivative through click-chemistry grafting

Yuzhen Lou[1], Damien Schapman[2], Dimitri Mercier[3], Stéphane Alexandre[4], Emmanuelle Dé[4], Jean-Michel Brunel[5], Nasreddine Kébir[1], Pascal Thébault[4]

[1] Normandie Université, INSA Rouen Normandie, Laboratoire PBS, UMR CNRS 6270 & FR 3038, Avenue de l'Université, 76801 Saint Etienne du Rouvray, France

[2] Normandie univ, UNIROUEN, INSERM, PRIMACEN, 76000 Rouen, France

[3] PSL Research University, Chimie ParisTech – CNRS, Institut de Recherche de Chimie Paris, 11 rue Pierre et Marie Curie, 75005 Paris, France

[4] Normandie Université, UNIROUEN, laboratoire PBS, UMR CNRS 6270 & FR 3038, 76821 Mont-Saint-Aigan, France

[5] UMR_MD1, U-1261, Aix Marseille Univ, INSERM, SSA, MCT, 13385 Marseille, France

Correspondence to:

Nasreddine KEBIR (E-mail: *nasreddine.kebir@insa-rouen.fr*)

Pascal THEBAULT (E-mail: *pascal.thebault@univ-rouen.fr*)

Abstract

PDMS is one of the most widely used materials in the biomedical field, but due to its hydrophobic character it is subject to bacterial adhesion and biofilm formation. Prevention of bacterial adhesion by contact-killing surface is one of the promising strategies even if the bacterial resistance toward classical active molecules complicates the antibacterial fight. A PDMS surface with alkyne groups was covalently modified with an azidated claramine-derivative, through the simple and orthogonal CuI-catalyzed Huisgen 1,3-dipolar click cycloaddition. The azidated claramine derivative was prepared in a four-step synthesis from deoxycholic acid and the alkyne groups were introduced onto the PDMS surface via a silanization reaction. XPS analysis has demonstrated the covalent immobilization of claramine with a total conversion of the azide group into a triazole ring. Fluorescent microscopy has showed an antibacterial activity of the modified surface against both Gram – (*Escherichia coli*) and Gram + (*Staphyloccocus epidermidis*) bacteria, which could be derived from electrostatic attraction leading to destabilization of the bacterial membrane. These results confirmed the importance of using a chemioselective reaction to control the orientation of covalently immobilized antibacterial molecules in order to keep their activity. PDMS surfaces based on claramine-derivative can be potentially useful for the elaboration of biomaterials preventing biofilm formation and addressing the issue of antibacterial resistance.

Keywords: PDMS; claramine; antibacterial surfaces; click-addition.

Introduction

PDMS, or silicone, is a well-known biocompatible material currently used in medical devices such implants[1], catheters[2] or contact lenses[3]. But due to its hydrophobic nature, PDMS is likely to be colonized by bacteria and also by proteins or biomolecules[4]. Bacterial adhesion could lead to biofilm formation which corresponds to an adhered microbial population grouped in community with other cells, embedded in a biopolymer matrix[5]. Bacteria in biofilm mode are protected against any treatments and lead to unsolved infections causing devices failure, removed of biomaterials and even death[6]. Prevention of biofilm formation seems clearly preferable to any treatment.

One strategy to prevent bacterial contamination and biofilm formation is the covalent immobilization of (macro)molecules on the surface of biomaterials in order to bring them an antiadhesive property to repel bacteria or a bactericidal property to kill adhered bacteria[7,8]. The majority of the studies are based on antiadhesive (or antifouling) PDMS through hydrophilic polymers (e.g., polyethylene glycol) or zwitterionic polymers (e.g., polysulfobetaine)[4,9]. But the complex process of bacterial adhesion, involving many parameters, makes it very complicated to develop a "universal" antiadhesive strategy able to completely inhibiting bacterial adhesion. Some works deal with the elaboration of bactericidal/bacteriostatic PDMS by grafting cationic polymers[9] or antimicrobial peptides[11], which act directly on the bacterial integrity[12].

The greatest challenge in order to not decrease or lose the activity of the active compound after its covalent immobilization is (i) not to use reactive functions involved in the antibacterial activity (ii) to have a suitable orientation of the molecule once immobilized. It is therefore important to use an orthogonal and chemoselective reaction. The click chemistry reaction possesses these advantages and also the creation of a long-term stable bound[13]. This reaction can occur thanks to the copper(I)-catalyzed azide-alkyne Huisgen 1,3-dipolar cycloaddition (CuAAC)[14]. It has been used to design killing-contact surfaces through the formation of a stable triazole group between active molecules and different surfaces such as glass[15], silicon[16] or graphene[17] but never on PDMS.

Since the last decades, multi-drug resistant (MDR) bacteria have emerged and have been declared as a global health threat[18,19]. Indeed, due to the overuse and misuse of antibiotics and others biocides, bacterial adaptation leading to resistance phenomenon has been accelerated. Moreover, discovery of new antibiotics has declined over the past 20 years[20]. To overcome this

problem, the development of new active compounds is one of the major issues in the field of antibacterial fighting (in solution or on surface)[21]. For this purpose, more attention is being given to molecules of natural origin[22,23]. The most important class of such molecules are the antimicrobial peptides (AMPs) but none of them has been approved due to their proteolytic degradation, high cost, low availability and recent bacterial resistant appearance[24]. Besides AMPs, polyaminosterol compounds such as squalamine **1** and claramine A1 **2** recently appeared as a promising family of antibacterial compounds[25,26] (Figure 1).

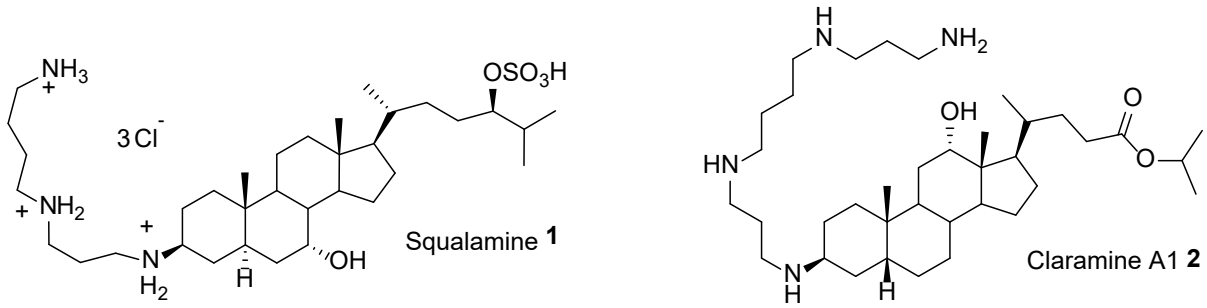

Figure 1. Structure of squalamine **1** and claramine A1 **2.**

Herein, we report the design of an antibacterial PDMS surface based on the versatile CuAAC click addition to covalently immobilized a claramine derivative. Prior to surface modification, azidated claramine derivative was synthesized and characterized by ^{1}H and ^{13}C NMR and ESI mass spectrometry. Then, selective CuAAC reaction was performed with alkyne groups incorporated onto a PDMS surface via a silanization reaction. Surface modifications were characterized by contact angle measurements, Atomic Force Microscopy (AFM) and X-ray Photoelectron Spectroscopy (XPS) analyses. The final antibacterial activity of the claramine-based surface against two common pathogenic bacteria, i.e. *Staphylococcus epidermidis* and *Escherichia coli*, was evaluated through the Live and Dead fluorescent microscopy test.

Materials and methods

Materials

All solvents were purified according to reported procedures, and reagents were used as commercially received.

Sylgard® 184 was purchased from DOW chemical company (USA). [3-(2-propynylcarbamate)propyl]triethoxysilane (PPTEOS, 90%) was purchased from Gelest. Methanol, ethyl acetate, dichloromethane, ammonia and petroleum ether (35-60 °C) were

purchased from Merck and used without further purification. Column chromatography was performed on Macherey-Nagel silica gel (70-230 mesh). Ethanol (99,8%) was analytical grade and was purchased form Fisher. Copper (II) sulfate pentahydrate (ca. 100%) was purchased from VWR and sodium ascorbate (99%) was purchased from Acros. Ultrapure water purified with the Milli-Q system (Siemens, France) was used in all cases.

S. epidermidis (ATCC 35984) and *E. coli* (K12 MG1655) strains were stored as frozen aliquots in brain heart infusion (BHI, Bacto, France) broth and 30 % of glycerol at -20 °C. The LIVE/DEAD Bacterial Viability Kit, L7007 (SYTO®9 dye, 1.67 mM / Propidium iodide, 18.3 mM) was purchased form Thermo Fisher Scientific. Phosphate buffered saline (PBS) prepared from the PBS tablets (Gibro, Swiss) and ultrapure water, obtained from a Milli-Q system (Siemens, France) ware autoclaved before use.

Synthesis

Synthesis of bromopropyl deoxycholate 4

In a 50 mL two necked round flask were introduced 3.5 mL of bromopropanol (37 mmol), 20 mL of dichloromethane, 3.3 g of deoxycholic acid (8.44 mmol) and 1 g of para-toluene sulfonic acid (6 mmol). The mixture was heated at reflux under vigorous stirring for 8 hours. The reaction was subsequently concentrated under vacuum and 50 mL of dichloromethane was added. The organic phase was washed 3 times with 25 mL of $NaHCO_3$ (10%) solution. The aqueous phases were extracted twice with dichloromethane and the combined organic phases were dried over Na_2SO_4, filtered, and concentrated in vacuo. The residue was purified by flash chromatography on silica gel (ethylacetate/ petroleum ether (1/1)) to afford the expected product as a viscous oil in 92% yield. NMR ^{1}H (400 MHz, $CDCl_3$): δ (ppm) = 4.58-4.62 (m, 2H), 4.46-4.48 (m, 1H), 4.20-4.22 (m, 1H), 3.98-4.12 (m, 4H), 3.79 (s, 1H), 3.39-3.53 (m, 4H, 1.92-2.12 (m, 4H), 1.44-1.66 (m, 18H), 0.81- 1.29 (m, 7H), 0.59 (s, 3H). NMR ^{13}C (100 MHz, $CDCl_3$): δ (ppm) = 173.30, 71.04, 70.01, 59.80, 58.45, 47.48, 46.14, 46.03, 41.66, 36.31, 35.68, 35.52, 35.19, 34.98, 33.84, 32.94, 32.04, 31.31, 30.96, 30.69, 27.24, 27.03, 26.15, 23.55, 20.78, 16.85, 12.42. MS (ESI^+): m/z 513.2501 ($[M+H]^+$)

Synthesis of 3-oxo bromopropyl deoxycholate 5

In a 50 mL two necked round flask were introduced 30 mL of toluene, 15 mL of acetone and 3 g of bromopropyl deoxycholate **4** (5.85 mmol). 3g of aluminum *tert*-butoxide (12 mmol) were subsequently added and stirring was maintained under reflux for 12 hours. 20 mL of H_2SO_4 solution (2N) was added, and the mixture was stirred for an additional 1 hour. The

organic phase was washed 3 times with 20 mL of H_2SO_4 solution and 25 mL of water. The combined organic phases were dried over Na_2SO_4, filtered, and concentrated in vacuo to afford a crude product, which was purified by flash chromatography on silica gel (ethylacetate/ petroleum ether (1/1)). The expected 3-oxo bromopropyl deoxycholate **5** was successfully obtained as a clear oil in 56% yield. NMR ^1H (400 MHz, $CDCl_3$): δ (ppm) = 3.90-4.10 (m, 3H), 3.58-3.62 (m, 2H), 3.41-3.45 (m, 5H), 2.41-2.46 (m, 1H), 1.60-1.95 (m, 8H), 0.99-1.46 (m, 15H), 0.72-0.81 (m, 6H), 0.50 (s, 3H). NMR ^{13}C (100 MHz, $CDCl_3$): δ (ppm) = 208.29, 174.20, 73.12, 61.95, 60.28, 52.82, 48.30, 47.12, 46.48, 35.60, 35.08, 33.76, 32.90, 31.68, 31.15, 30.86, 30.46, 29.52, 29.11, 27.42, 25.73, 23.70, 22.12, 21.08, 17.30, 14.21, 12.80. MS (ESI^+): m/z 512.2324 ($[M+H]^+$).

Synthesis of 3-oxo azidopropyl deoxycholate 6

In a 50 mL two necked round flask was introduced in 10 mL of DMSO 1.25g of 3-oxo bromopropyl deoxycholate **5** (2.45 mmol). 175 mg of sodium azide (2.69 mmol) were subsequently added (diluted in DMSO as a 0.5M solution) and stirring was maintained at room temperature for 12 hours. Then, 20 mL of water was added and the mixture was stirred for an additional 1 hour and after, 30 mL of ethylacetate were added. The organic phase was washed with NaCl solution. The combined organic phases were dried over Na_2SO_4, filtered, and concentrated in vacuo to afford a crude product, which was purified by flash chromatography on silica gel (ethylacetate/ petroleum ether (1/1)). The expected 3-oxo azidopropyl deoxycholate **6** was obtained as a clear oil in 82% yield. NMR ^1H (400 MHz, $CDCl_3$): δ (ppm) = 4.06-4.11 (m, 3H), 3.38-3.40 (m, 1H), 2.21-2.38 (m, 5H), 1.57-2.11 (m, 16H), 1.02-1.34 (m, 12H), 0.88-0.91 (m, 3H), 0.68 (s, 3H). NMR ^{13}C (100 MHz, $CDCl_3$) : δ (ppm) = 211.60, 173.94, 71.01, 63.57, 48.62, 47.16, 46.32, 45.84, 45.71, 43.91, 42.34, 37.91, 37.49, 35.92, 35.87, 35.03, 31.40, 30.91, 29.95, 29.27, 28.91, 27.85, 26.81, 23.55, 18.01, 16.83, 12.53. MS (ESI^+): m/z 474.3287 ($[M+H]^+$).

Synthesis of 3-spermino azidopropyl deoxycholate 7

In a 25 mL two necked round flask were introduced 10 mL of methanol and a mixture of 3-oxo azidopropyl deoxycholate **6** (852 mg, 1.8 mmol), titanium(IV) isopropoxide (1.6 g, 7.2 mmol) and spermine (1 g, 5.4 mmol). This mixture was stirred under argon at room temperature for 24 hours. After cooling the flask at -78°C, sodium borohydride (136 mg, 3.6 mmol) was then added, and the resulting mixture was stirred for additional 12 hours. The reaction was then quenched by adding water (4 mL). Stirring was continued at room temperature for 1 hour. Then, the reaction mixture was filtered over a pad of Celite, which was

subsequently rinsed with NH_4OH and methanol. The mixture was concentrated in vacuo to afford the expected crude compound, which was purified by flash chromatography on silica gel using CH_2Cl_2/MeOH/NH_4OH (7:3:1) as eluent. The expected 3-spermino azidopropyl deoxycholate **7** was obtained as a viscous yellow oil in 34% yield. NMR ^1H (250 MHz, CD_3OD): δ (ppm) = 4.06-4.11 (m, 3H), 3.11-3.27 (m, 2H), 2.89-2.95 (m, 6H), 2.13-2.77 (m, 10H), 1.08-2.09 (m, 37H), 0.86-1.04 (m, 8H), 0.68 (s, 3H). NMR ^{13}C (63 MHz, CD_3OD): δ (ppm) = 176.42, 74.00, 58.91, 50.52, 49.85, 49.17, 48.77, 48.23, 48.04, 47.60, 46.22, 45.64, 45.08, 43.91, 40.59, 37.43, 37.22, 36.95, 36.72, 35.75, 34.80, 34.32, 33.16, 32.22, 31.84, 30.17, 29.84, 28.66, 28.47, 28.20, 27.49, 24.89, 23.91, 23.03, 22.34, 17.55, 13.19. MS (ESI^+): m/z 660.5495 ($[M+H]^+$).

PDMS preparation

PDMS was prepared following the manufacturer's instructions. Briefly, silicone elastomer base and curing agent (Sylgard® 184) at a ratio of 10:1 (w/w) were mixed and poured into a flat petri dish. Then, the mixture was degassed under vacuum, until all the air bubbles formed during mixing were removed, and cured at 100°C for 40 min in an oven. The cured PDMS film at a thickness of around 1 mm was cut into 10×10 mm^2 pieces for further chemical modification and analysis.

Chemical modification of PDMS surface

The PDMS substrates were subjected to UV-Ozone treatment (Jelight Company, Inc.) for 45 min. A low-pressure mercury (Hg) vapor lamp with an average intensity from 28 to 32 mW/cm^2 at 253,7 nm at a distance of 2,5 cm is used in the UV-Ozone equipment. Immediately after, the PDMS substrates were immersed in an ethanol/water (21/9 mL) solution containing 511 µl (50 mM) of PPTEOS. After, the solution was slightly shaken at room temperature overnight to obtain PDMS-PPTEOS. Then, the PDMS-PPTEOS samples were rinsed with 70% ethanol and dried at least 3 h at room temperature under vacuum and were kept in a sealed container with argon at 4°C until next step or analysis.

The PDMS-PPTEOS substrates were immersed in 15 ml of methanol containing about 15 µmol of claramine derivative, 2 mol% of copper (II) sulphate and 10 mol% of sodium ascorbate with regards to claramine derivative content. Then, the system was slightly shaken at room temperature during 24 h. After, the obtained samples (PDMS-clar) were washed with methanol and dried 3 h at room temperature under vacuum and stored in a sealed container with argon at 4°C until analysis.

Characterization

^{1}H NMR and ^{13}C NMR spectra were recorded in $CDCl_3$ or CD_3OD on a Bruker AC 400 spectrometer working at 400 MHz and 100 MHz, respectively (the usual abbreviations are used: s: singlet, d: doublet, t: triplet, q: quadruplet, m: multiplet). Tetramethylsilane was used as internal standard. All chemical shifts are given in ppm. Mass spectroscopy analysis was performed using a QStar Elite (Applied Biosystems SCIEX) mass spectrometer equipped with an atmospheric pressure ionization source (API) at the Spectropole (Analytical Laboratory, Aix Marseille University).

Static and dynamic water contact angles measurements (3 µl) on modified an unmodified PDMS substrates were carried out by using a contact angle goniometer "digidrop" (United Kingdom) in air at room temperature on at least three independent samples, using at least three different zones by sample.

The topography of PDMS surfaces before and after modification were analyzed by using a Nanoscope 8 Multimode microscope (Bruker Nano Surfaces, Santa Barbara, CA, USA). Imaging was achieved in the air using the PeakForce®-QNM mode with a 100µm piezoelectric scanner. A silicon (RTESPA-300, Bruker) cantilever with a spring constant of about 40 N/m and a silicon tip was used. Images were obtained with a PeakForce tapping frequency of 1 kHz and the auto-amplitude on. The AFM imaging was performed in multiple locations on at least two independent samples at two scan sizes: 5 × 5 and 20 × 20 µm2. All images are presented in the height mode and are top view images.

The surface chemical characterization was performed using a Thermo ESCALAB 250 R-Ray photoelectron spectrometer with a monochromatic Al-Kα ray source (hν = 1486.6 eV) with a size spot of 500µm operating at a pressure around 2 10-9mbar. The analyzer pass energy was 50 eV for survey spectra and 20 eV for C1s and N1s high-resolution spectra. Charging effect was compensated during analysis and corrected using the aliphatic carbon of the C1s peak at 285.0 eV. Spectra were recorded and analyzed using Thermo Avantage software.

Antimicrobial activity assay (Live/Dead test)

A 130 µl droplet of *E. coli* or *S. epidermidis* suspension in distilled water (about 5.10^8 CFU/ml) were spread on the modified surfaces (1.8 ×1.8 cm^2) using a glass slide with the same surface size for 1 h. Then, the glass slide was taken away and the studied surface was washed by a distilled water flow to remove the non-attached bacteria. After, 130 µl of an 80-fold diluted

solution of fluorescent markers were deposited and spread on the surface for 15 min. Images (1024x1024 pixels) of surfaces were acquired using an upright fixed-stage Leica TCS SP8 CFS confocal microscope (Leica Microsystems, Nanterre, France) equipped with diodes laser (Coherent, Les Ulis, France) at 488 nm to excite the SYTO®9 and at 552 nm to excite Propidium Iodide and a conventionnal scanner at 400 Hz. Using a 63x (1.40, oil immersion) objective, fluorescence emission was sequentially detected through hybrid detector (Leica Microsystems, Nanterre, France) in photon counting mode with a specific band from 500 to 540 nm for SYTO®9 and 580 to 630 nm for Propidium Iodide. Z-Stack's images were acquired using an adapted step-size from Nyquist Criteria. ImageJ (Rasband W.S., U.S. National Institutes of Health, Bethesda, Maryland, USA, http://imagej.nih.gov/ij/, 1997-2020) was used to adjust brightness and contrast and to perform z projections of 3D images (xyz).

Results and discussion

Synthesis

Squalamine was first isolated from the dogfish shark and exhibited antimicrobial activity against a broad spectrum of bacteria and fungi[27]. However, obtention of a large amount of squalamine from natural sources is difficult. Thus, many researchers decided to synthesize squalamine mimics and investigated their antimicrobial properties[28-34]. More recently, Blanchet *et al.* reported the design and biological evaluation of claramine A1 **2**, which possesses excellent antimicrobial activities against a large panel of both Gram-positive and Gram-negative bacteria[26]. Based on our continued interest in squalamine biogical evaluation, we were interested in designing a concise and economical synthesis of a compound that could be grafted onto a surface. In this respect, a polyaminosterol parent compound, namely claramine A1 **7**, possessing a suitable azido group was prepared in a four-step synthesis (14% overall yield) from deoxycholic acid, using an efficient stereoselective titanium-mediated reductive amination that controlled the stereochemistry at the C-3 position (Figure 2).

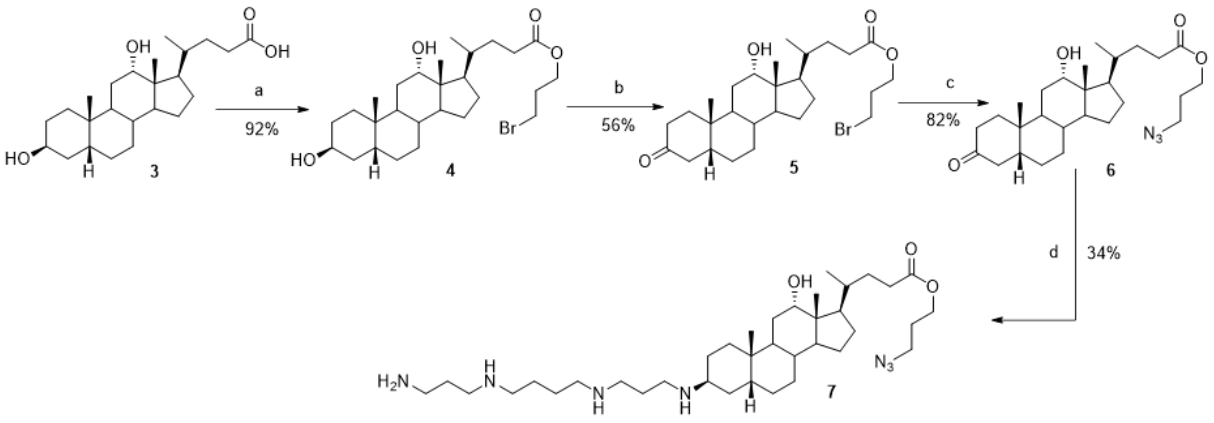

Conditions: a) PTSA, Bromopropanol (1equiv.), CH_2Cl_2, reflux, 8h. b) Al(O*t*-Bu)$_3$, acetone, toluene, reflux, 12 h. c) NaN_3, DMSO, 20°C, 12h. d) 1)Ti(O*i*-Pr)$_4$, spermine, MeOH, 20°C, 12h; 2) $NaBH_4$, -78°C, 2h.

Figure 2. Synthetic pathway for the preparation of azido-claramine A1 derivative 7.

Surface modification and characterization

The procedure of surface modification was illustrated in Figure 3. Briefly, hydroxyl groups were introduced on PDMS surface through an UV/Ozone treatment, immediately followed by immersion in PPTEOS solution under ambient conditions overnight to obtain alkyne-terminated PDMS. Then, the CuAAC coupling reaction between the alkyne-PDMS surface and the azido-claramine derivative was achieved in the presence of copper sulfate and sodium ascorbate.

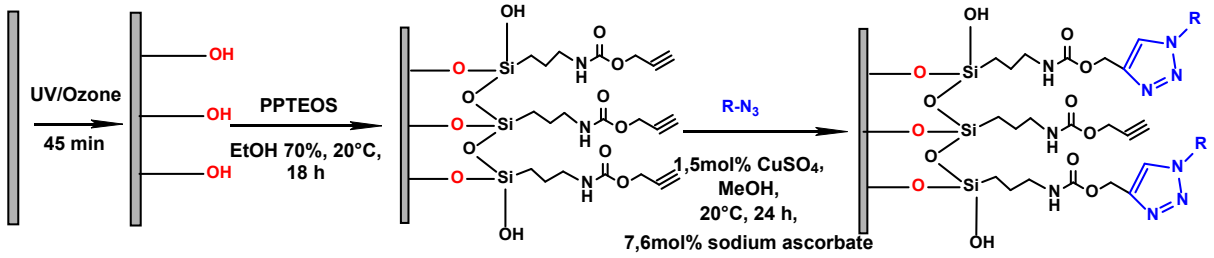

Figure 3. Chemical pathway of grafting antibacterial molecules bearing an azide group onto a PDMS surface (R=claramine derivative).

First, static water contact angle (WCA) measurements were realized. Pristine PDMS (control 1), PDMS treated with UV/Ozone for 45 minutes and then immersed immediately in EtOH/water (21/9 ml) solution without PPTEOS (control 2) or with PPTEOS (control 3) overnight were used as controls. Pristine PDMS was hydrophobic with an average WCA at approximately 108° while the fresh prepared PDMS-UV/O_3 and PDMS-PPTEOS after drying under vacuum for 3 hours exhibit a WCA of around 48 and 62°, respectively. The WCA value of PDMS-UV/O_3 and PDMS-PPTEOS were both increased after 3 days of storage in ambient

with around 65 and 83° respectively owing to the hydrophobic recovery behavior of PDMS[35,36]. However, the WCA values of PDMS-PPTEOS were always higher than that of PDMS-UV/O_3 suggesting the successful grafting of silane onto PDMS. In contrast, the difference before and after the introduction of claramine derivative via CuAAC was not significant with an average WCA of 83 and 77°, respectively.

Table 1. Data of water contact angles measurements and surface roughness on the optimal modified PDMS surface and its controls.

	Static mode	**Dynamic mode**			**Roughness by AFM[b] (nm)**	
Samples	**θ_{water} (°)[a]**	**AA (°)[a]**	**RA (°)[a]**	**Hyst (°)[a]**	**Ra**	**RMS**
PDMS (control 1)	108±2	116±3	58±4	57±2	1.6±0.3	2.3±0.0
PDMS-UV/O_3 (control 2)	65±6	74±1	47±6	27±5	/	/
PDMS-PPTEOS (control 3)	83±5	89±5	51±3	39±7	3.0±1.4	5.4±2.4
PDMS-clar	77±6	88±7	45±5	43±4	13.7±0.4	20.4±5.9

[a] **θ_{water}**: contact angle with water after 3 days of storage; **AA**: Advancing Angle; **RA**: Receding Angle; **Hyst**: Hysteresis.

[b] Ra: arithmetic roughness, RMS: Mean Square roughness.

The dynamic water contact angle measurements were also performed. The advancing angle of PDMS-PPTEOS increased significantly compared to PDMS-UV/O_3 from 74 to 89°. Moreover, the receding angle of PDMS-PPTEOS was also decreased with a difference of 4°, resulting in an increase in hysteresis from 27 to 39° compared to PDMS-UV/O_3, suggesting the successful modification of PDMS surface with PPTEOS. However, the advancing angle of silanized PDMS before and after claramine derivative grafting was almost the same, and only around 5° of difference for the receding angle value was observed, which was not significant neither.

The surface morphologies of pristine PDMS, silanized PDMS and claramine derivative grafted PDMS were observed by atomic force microscopy (AFM) at two different magnifications (5 × 5 µm^2 and 20 × 20 µm^2) as shown in Figure 4. It revealed that unmodified PDMS exhibited smooth and homogenous surface with an average roughness (R_a) and a root

mean square roughness (R_q) of 0.9 and 1.2 nm at 5 × 5 μm^2 and 1.4 and 2.4 nm at 20 × 20 μm^2, respectively. After silanization, samples became slightly rougher with a R_a and R_q of 0.9 and 2.2 nm at 5 × 5 μm^2, and 2.2 and 6.5 nm at 20 × 20 μm^2, respectively, due to the presence of some aggregates. Excepted that, the PPTEOS layer was homogenous and smooth. PDMS-clar exhibited higher values of R_a and R_q , i.e. 1.8 and 5.7 nm at 5 × 5 μm^2, and 13.4 and 16.3 nm at 20 × 20 μm^2, respectively. Much larger aggregates can be observed compared to PDMS-PPTEOS suggesting that claramine derivatives were successfully grafted.

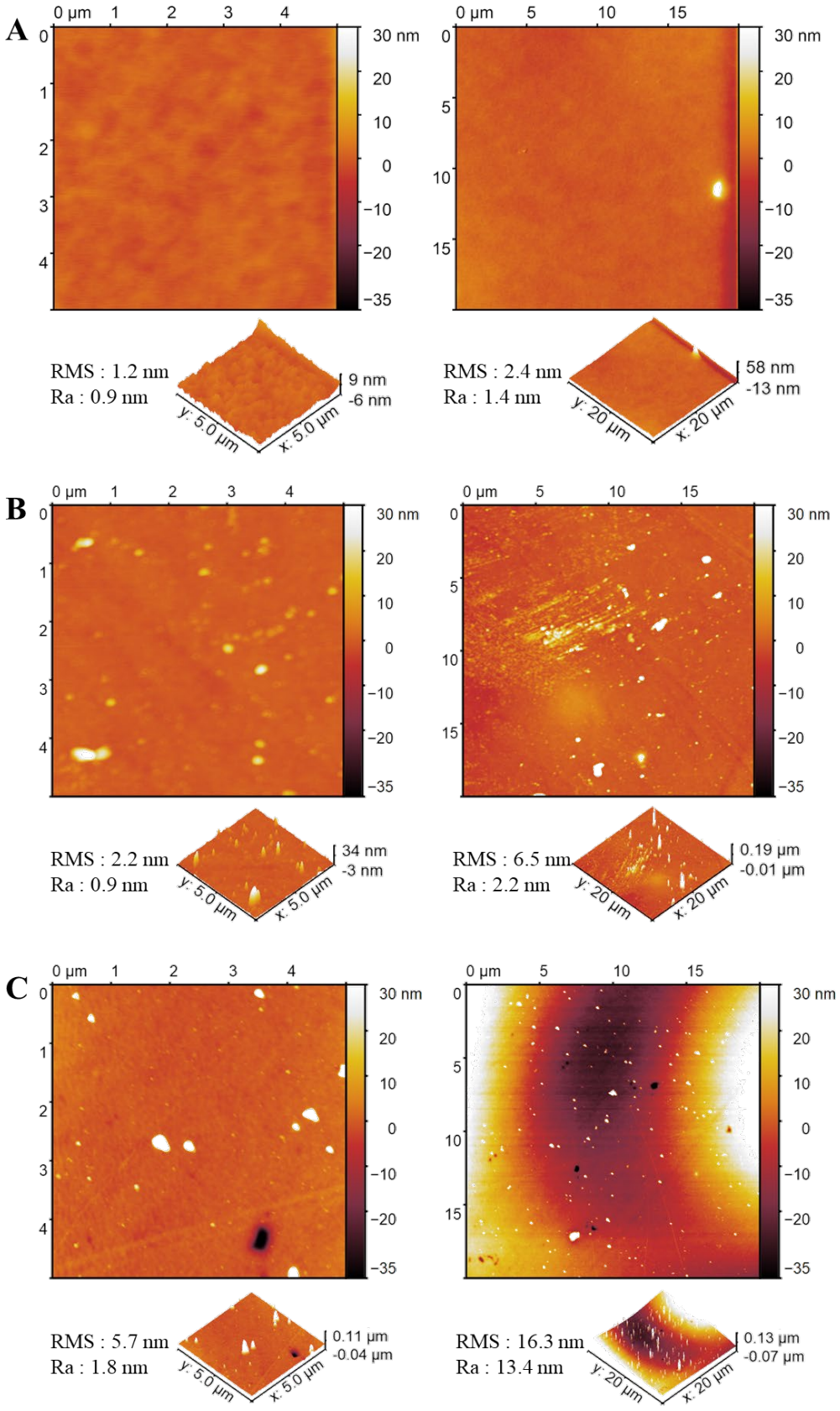

Figure 4. AFM images of (A) PDMS surface (control 1), (B) PDMS-PPTEOS surface (control 3) and (C) PDMS-clar surface.

To confirm the covalent click-chemistry reaction between the PDMS surface and the azido-claramine molecules, high resolution XPS spectrum of the N1s region for the PDMS-clar surface was realized (Figure 5). It has been deconvoluted using 3 components at 399.4, 399.9 and 401.9 eV. The first component can be attributed to the amino groups from the claramine derivate[38]. The second and third components are characteristic of nitrogen from the triazole ring (N-**N**=**N** and **N**-N=N respectively)[39]. The ratio obtained between each component (57/28/14) is in agreement with expected stoichiometry of nitrogen group (4/2/1) indicating that claramine derivative is grafted at the surface of the PDMS. Furthermore, no peak was observed around 405 eV corresponding to the electron deficient nitrogen atom of the azido group present in the claramine derivative. This result shows that the claramine is undoubtedly covalently bound to the surface. Furthermore, no residual copper was observed on the survey spectrum of the PDMS-clar surface (see Fig. S1 of the supporting information) which could have (i) an impact on the antibacterial activity and (ii) a problematic toxicity for later biological applications.

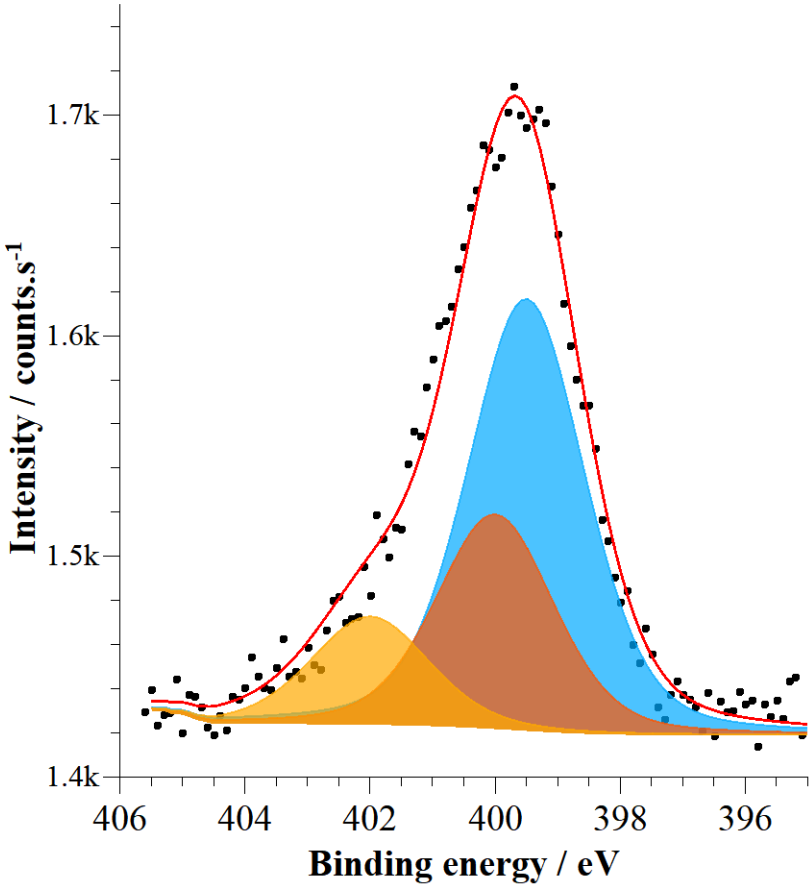

Figure 5. High resolution XPS spectrum of the N1s region for the PDMS-Clar surface.

Assessment of the antibacterial properties

E. coli and *S. epidermidis* were used to evaluate the antibacterial properties of modified PDMS via the LIVE/DEAD test by using confocal fluorescent microscopy (Figure 6 and S2, S3 et S4 in supporting information). A droplet of bacterial suspension was spread onto modified or untreated PDMS surface for 1 hour, then the adhered bacteria were stained and observed. The bacteria with intact membrane were stained in green whereas bacteria with damaged membrane were stained in red. As shown in Figure 6, no bacteria were observed for pristine PDMS and for PDMS-PPTEOS, expected some red *E. coli* for the silanized surface. These results were probably due to the short time of contact between bacteria and surface. On the other hand, a lot of adhered bacteria were observed for the PDMS-clar surface with a majority of red bacteria. Furthermore, a less affinity and attachment onto PDMS-clar of *S. epidermidis* compared to *E. coli* was noticed. But as for *E. coli*, the membrane integrity of adhered bacteria was perturbed. The presence of only red bacteria for the modified surface may suggested an antibacterial action of covalently immobilized claramine derivative by an electrostatic attraction of bacteria onto the surface via its amino cationic tail leading to a membrane destabilization.

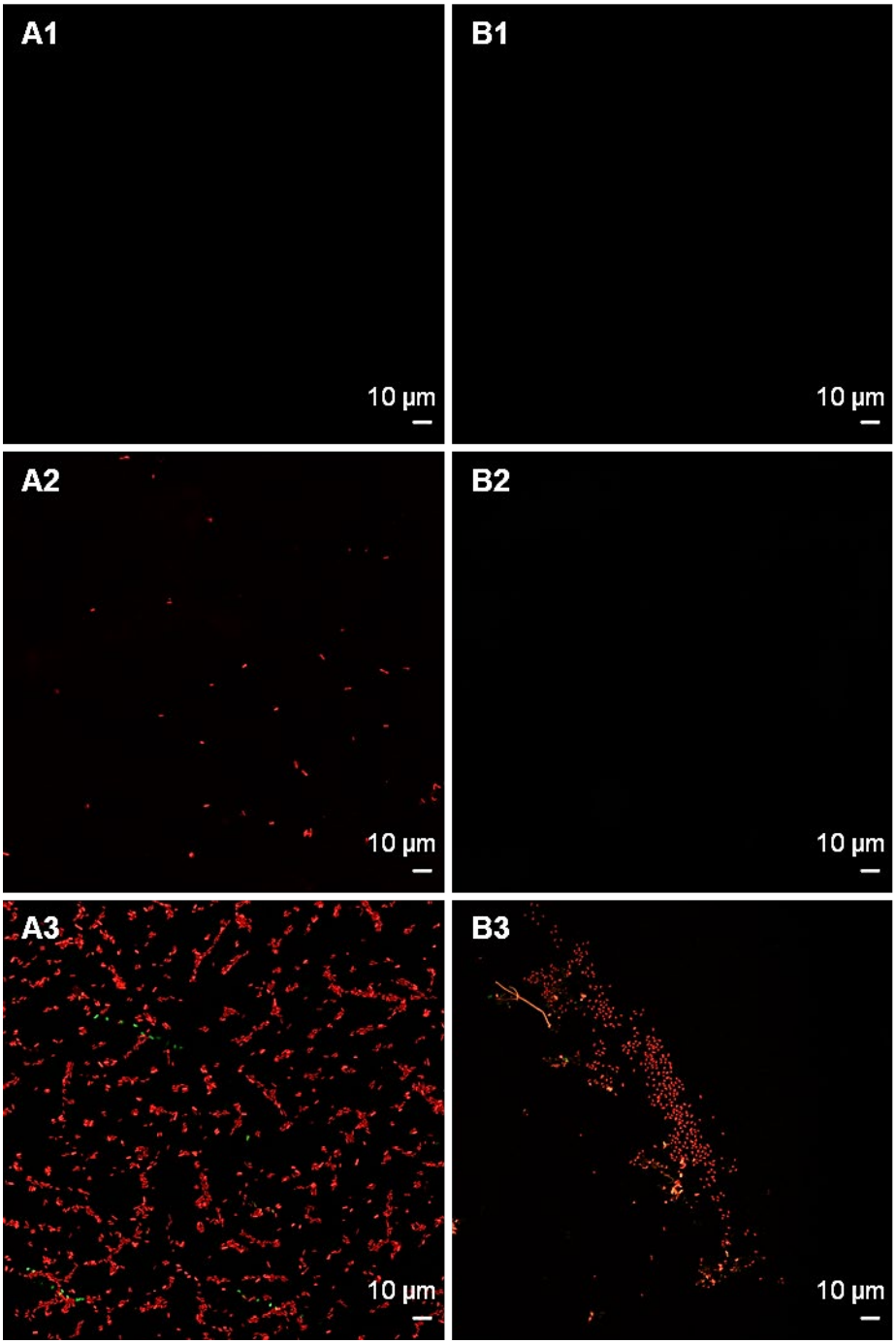

Figure 6. Fluorescence microscopy images of sessile bacteria cells stained with a marker of viability and deposited on surfaces of modified and unmodified PDMS surfaces: (A1) E. coli on pristine PDMS surface (control 1), (A2) E. coli on PDMS-PPTEOS (control 3) surface, (A3) E. coli on PDMS-clar, (B1) *S. epidermidis* on unmodified PDMS surface (control 1), (B2) *S. epidermidis* on PDMS-PPTEOS (control 3) surface, (B3) *S. epidermidis* on PDMS-clar surface.

Conclusion

In the present work, a new claramine derivative **7** was synthezied and successfully grafted onto PDMS surface by chemioselective CuAAC click chemistry. XPS analysis of the N1s region has confirmed covalent claramine derivative immobilization by the formation of triazole ring. The membrane integrity of *E. coli* and *S. epidermidis* was destabilized probably by a strong eltrostatic attraction via the cationic amino tail of immobilized claramine derivative. These results confirmed the importance of the orientation of active molecules once immobilized and the usefulness of the CuAAC reaction. PDMS grafted with a claramine derivative can be potentially applied in medical divices to prevent bacterial infections and overcome the bacterial resistance's problem. The biocomptibility and *in vivo* antibacterial properties need to be further investigated.

Acknowledgments

Authors thanks the INSA ROUEN NORMANDIE and China Scholarship Council (CSC) for the financial supports.

References

[1] F. Abbasi, H. Mirzadeh, M. Simjoo, Hydrophilic interpenetrating polymer networks of poly(dimethyl siloxane) (PDMS) as biomaterial for cochlear implants, J. Biomater. Sci. Polym. Ed. 17 (2006) 341–355.

[2] K. Stenzelius, L. Laszlo, M. Madeja, H. Pessah-Rasmusson, M. Grabe, Catheter- associated urinary tract infections and other infections in patients hospi- talized for acute stroke: A prospective cohort study of two different sili- cone catheters, Scand. J. Urol. 50 (2016) 483–488.

[3] J.-S. Chen, T.-Y. Liu, H.-M. Tsou, Y.-S. Ting, Y.-Q. Tseng, C.-H. Wang, Biopolymer brushes grown on PDMS contact lenses by in situ atmospheric plasma- induced polymerization, J. Polym. Res. 24 (2017) 69-77.

[4] M. Li, K.G. Neoh, L.Q. Xu, R. Wang, E.-T. Kang, T. Lau, D.P. Olszyna, E. Chiong, Surface modification of silicone for biomedical applications requiring long-term antibacterial, antifouling, and hemocompatible properties, Langmuir 28 (2012) 16408–16422.

[5] H.C. Flemming, J. Wingender, U. Szewzyk, P. Steinberg, S.A. Rice, S. Kjelleberg, Biofilms: An emergent form of bacterial life, Nat. Rev. Microbiol. 14 (2016) 563–575.

[6] D. Campoccia, L. Montanaro, C.R. Arciola, A review of the biomaterials technologies for infection-resistant surfaces, Biomaterials 34 (2013) 8533–8554.

[7] E.K. Riga, M. Vöhringer, V.T. Widyaya, K. Lienkamp, Polymer-based surfaces designed to reduce biofilm formation: from antimicrobial polymers to strategies for long-term applications, Macromol. Rapid Commun. 38 (2017) 1700216-1700233.

[8] J.-B. Paris, D. Seyer, T. Jouenne, P. Thébault, Elaboration of antibacterial plastic surfaces by a combination of antiadhesive and biocidal coatings of natural products, Colloids Surf. B 156 (2017) 186–193.

[9] H. Zhang, M. Chiao, Anti-fouling coatings of poly(dimethylsiloxane) devices for biological and biomedical applications, J. Med. Biol. Eng. 35 (2015) 143-155.

[10] X. Li, P. Li, R. Saravanan, A. Basu, B. Mishra, S.H. Lim, X. Su, P.A. Tambyah, S.S.J. Leong, Antimicrobial functionalization of silicone surfaces with engi- neered short peptides having broad spectrum antimicrobial and salt-resistant properties, Acta Biomater. 10 (2014) 258–266.

[11] B. Wang, T. Jin, Y. Han, C. Shen, Q. Li, J. Tang, H. Chen, Q. Lin, Surface-initiated RAFT polymerization of p (MAPOSS-co-DMAEMA+) brushes on PDMS for improving antiadhesive and antibacterial properties, Int. J. Polym. Mater. 65 (2016) 55–64.

[12] M. Lam, V. Migonney, C. Falentin-Daudre, Review of silicone surface modification techniques and coatings for antibacterial/antimicrobial applications to improve breast implant surfaces, Acta Biomater. 121 (2021) 68–88.

[13] G. T. Qin, C. Santos, W. Zhang, Y. Li, A. Kumar, U.J. Erasquin, K. Liu, P. Muradov, B.W. Trautner, C.Z. Cai, Biofunctionalization on alkylated silicon substrate surfaces via “click” chemistry. J. Am. Chem. Soc. 132 (2010) 16432−16441.

[14] B.S. Favel, M. Jasieniak, L. Velleman, S. Ciampi, E. Luais, J.R. Peterson, H.J. Griesser, J.G. Shapter, J.J. Gooding, Grafting of poly(ethylene glycol) on click chemistry modified Si(100) surfaces, Langmuir 29 (2013) 8355–8362.

[15] A. Hasan, K. Lee, K. Tewari, L. M. Pandey, P. B. Messersmith, K. Faulds, M. Maclean, K. H. A. Lau, Surface design for immobilization of an antimicrobial peptide mimic for efficient anti‐biofouling, Chem. Eur. J. 26 (2020) 5789‒5793.

[16] J. He, J. Chen, G. Hu, L. Wang, J. Zheng, J. Zhan, Y. Zhu, C. Zhong, X. Shi, S. Liu, Y. Wang, L. Ren, Immobilization of an antimicrobial peptide on silicon surface with stable activity by click chemistry, J. Mater. Chem. B 6 (2018) 68–74.

[17] J. Huang, Z. Yin, J. Wu, Covalent attachment of chitosan to graphene via click chemistry for superior antibacterial activity, Mater. Adv. 1 (2020) 579-583.

[18] P. Fernandes, Antibacterial discovery and development--the failure of success? Nat. Biotechnol. 24 (2006) 1497–1503.

[19] J. Clardy, M.A. Fischbach, C.T. Walsh, New antibiotics from bacte-rial natural products, Nat. Biotechnol. 24 (2006) 1541–1550.

[20] M.S. Butler, M.A.T. Blaskovich, M.A. Cooper, Antibiotics in the clinical pipeline at the end of 2015, J. Antibiot. 70 (2017) 3–24.

[21] Q. Kong, Y. Yang, Recent advances in antibacterial agents, Bioorg. Med. Chem. Lett. 35 (2021) 127799-127806.

[22] S.E. Rossiter, M.H. Fletcher, W.M. Wuest, Natural products as platforms to overcome antibiotic resistance, Chem. Rev. 117 (2017) 12415–12474.

[23] K. Glinel, P. Thebault, V. Humblot, C.M. Pradier, T. Jouenne, Antibacterial surfaces developed from bio-inspired approaches, Acta Biomater. 8 (2012) 1670–1684.

[24] Y. Niu, M.Wang, Y.Cao, A. Nimmagadda, J. Hu, Y. Wu, J. Cai, X.-S. Ye, Rational design of dimeric lysine N-alkylamides as potent and broad-spectrum antibacterial agents, J. Med. Chem. 61 (2018) 2865–2874.

[25] K. Alhanout, S. Malesinki, N. Vidal, V. Peyrot, J. M. Rolain, J. M. Brunel, New insights into the antibacterial mechanism of action of squalamine, J. Antimicrob. Chemother. 65 (2010) 1688-1693.

[26] M. Blanchet, D. Borselli, A. Rodallec, F. Peiretti, N. Vidal, J.M. Bolla, C. Digiorgio, K.R. Morrison, W.M. Wuest, J.M. Brunel, Claramines: a new class of broad-spectrum antimicrobial Agents with bimodal activity, Chem. Med. Chem. 13 (2018) 1018-1027.

[27] K.S. Moore, S. Wehrli, H. Roder, M. Rogers, J.N. Forrest, D. Mccrimmon, M. Zasloff, Squalamine: an aminosterol antibiotic from the shark, Proc. Natl. Acad. Sci. 90 (1993) 1354–1358.

[28] A. Sadownik, G. Deng, V. Janout, S.L. Regen, Rapid construction of a squalamine mimic, J. Am. Chem. Soc. 117 (1995) 6138–6139.

[29] K. Kikuchi, E.M. Bernard, A. Sadownik, S.L. Regen, D. Armstrong, Antimicrobial activities of squalamine mimics, Antimicrob. Agents Chemother. 41 (1997) 1433–1438.

[30] H.-S. Kim, B.-S. Choi, K.-C. Kwon, S.-O. Lee, H. J. Kwak, and C. H. Lee, Synthesis and antimicrobial activity of squalamine analogue, Bioorg. Med. Chem. 8 (2000) 2059–2065.

[31] Y. Shu, S.R. Jones, W.A. Kinney, B.S. Selinsky, The synthesis of spermine analogs of the shark aminosterol squalamine, Steroids 67(2002) 291–304.

[32] J.M. Brunel, Y. Letourneux, Recent advances in the synthesis of spermine and spermidine analogs of the shark aminosterol squalamine, European J. Org. Chem., vol. 2003 (2003) 3897–3907.

[33] C. Loncle, C. Salmi, Y. Letourneux, J.M. Brunel, Synthesis of new 7-aminosterol squalamine analogues with high antimicrobial activities through a stereoselective titanium reductive amination reaction, Tetrahedron 63 (2007) 12968–12974.

[34] L. Djouhri, N. Vidal, J.M. Rolain, J.M. Brunel, Synthesis of new 3,20 bispolyaminosteroid squalamine analogues and evaluation of their antimicrobial activities. J. Med. Chem. 54 (2011) 7417-7421.

[35] Y. Berdichevsky, J. Khandurina, A. Guttman, Y.-H. Lo, UV/ozone modification of poly (dimethylsiloxane) microfluidic channels, Sensors Actuators B Chem. 97 (2004) 402–408.

[36] A. Oláh, H. Hillborg, G.J. Vancso, Hydrophobic recovery of UV/ozone treated poly (dimethylsiloxane): adhesion studies by contact mechanics and mechanism of surface modification, Appl. Surf. Sci. 239 (2005) 410–423.

[37] V.N. Vasilets, K. Nakamura, Y. Uyama, S. Ogata, Y. Ikada, Improvement of the micro-wear resistance of silicone by vacuum ultraviolet irradiation, Polymer. 39 (1998) 2875–2881.

[38] V. Gadenne, L. Lebrun, T. Jouenne, P. Thebault, Antiadhesive activity of ulvan polysaccharides covalently immobilized onto titanium surface. Colloids Surf. B 112 (2013) 229–236.

[39] M. Scalabrini, J. Hamon, I. Linossier, V. Ferrieres, K. Rehel, Pseudomonas aeruginosa resistance of monosaccharide-functionalized glass surfaces, Colloids Surf. B 183 (2019) 110383-110391.

Supporting information

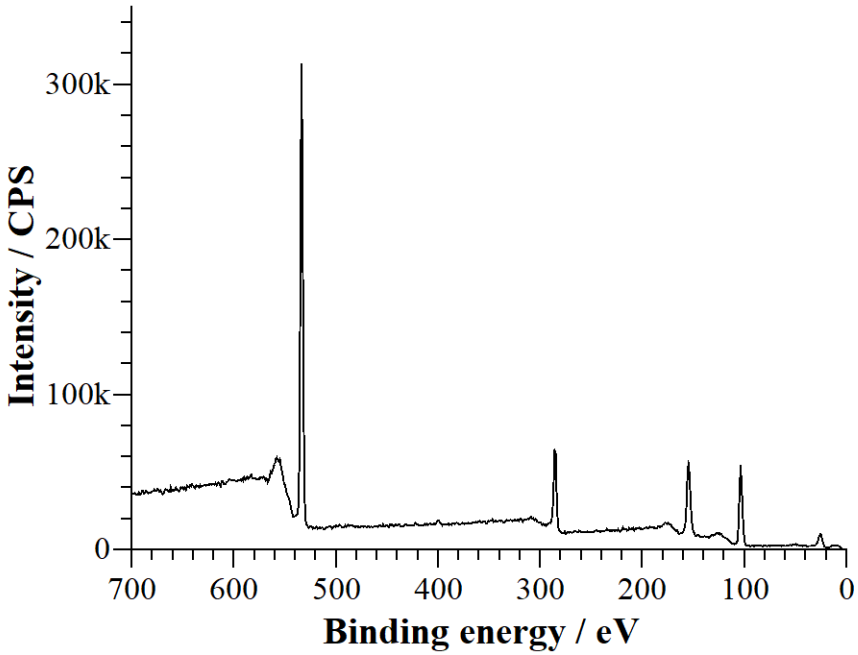

Figure S1. Survey XPS spectrum of PDMS-clar surface.

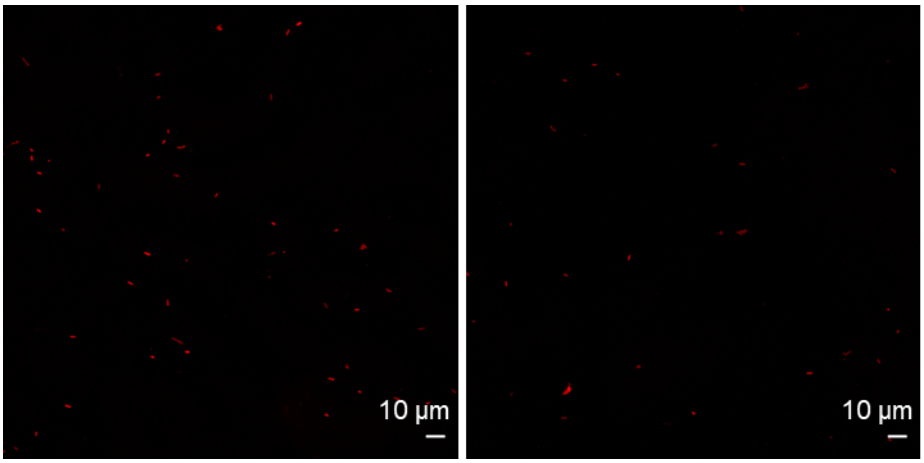

Figure S2. Supplemental fluorescence microscopy images of sessile *E. coli* cells stained with a marker of viability and deposited on PDMS-PPTEOS surface.

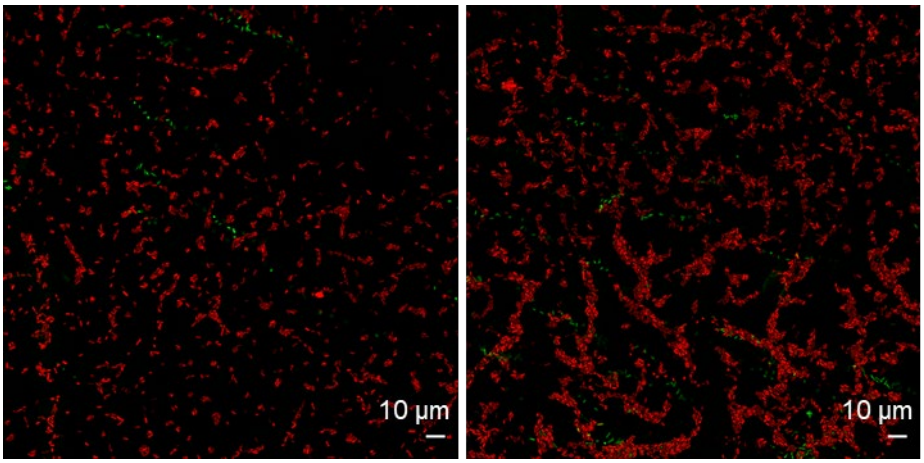

Figure S3. Supplemental fluorescence microscopy images of sessile *E. coli cells* stained with a marker of viability and deposited on PDMS-clar surfaces.

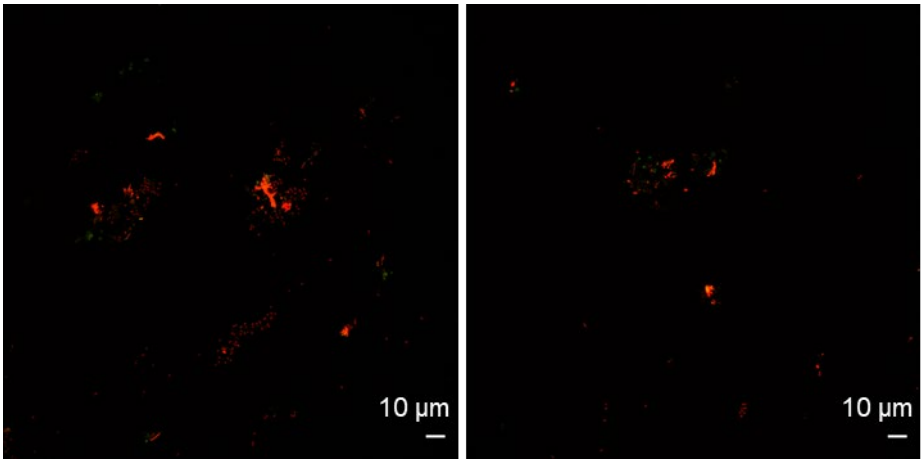

Figure S4. Supplemental fluorescence microscopy images of sessile *S. epidermidis* cells stained with a marker of viability and deposited on PDMS-clar surface.

III.2 Informations supplémentaires

Avant de réaliser les différentes étapes de modifications chimiques des surfaces de PDMS, les conditions d'activation de la surface du PDMS par traitement UV/Ozone, en termes de temps de réaction, ont été étudiées par la mesure de l'angle de contact avec l'eau en mode statique (Figure III-1) et par spectroscopie ATR-FTIR (Figure III-2). Le PDMS non traité a été utilisé comme contrôle. Les résultats de la mesure de l'angle de contact avec l'eau (ACE) en fonction du temps de traitement ont montré que les valeurs d'ACE diminuaient de manière linéaire au fur et à mesure que le temps d'exposition sous UV/Ozone augmentait. Après un traitement de 45 et 60 minutes, des valeurs de l'angle de contact avec l'eau d'environ 29 et 8° ont été respectivement obtenues contre une valeur initiale pour le PDMS natif de 108°, ce qui suggère une augmentation du caractère hydrophile du PDMS par le traitement UV/Ozone.

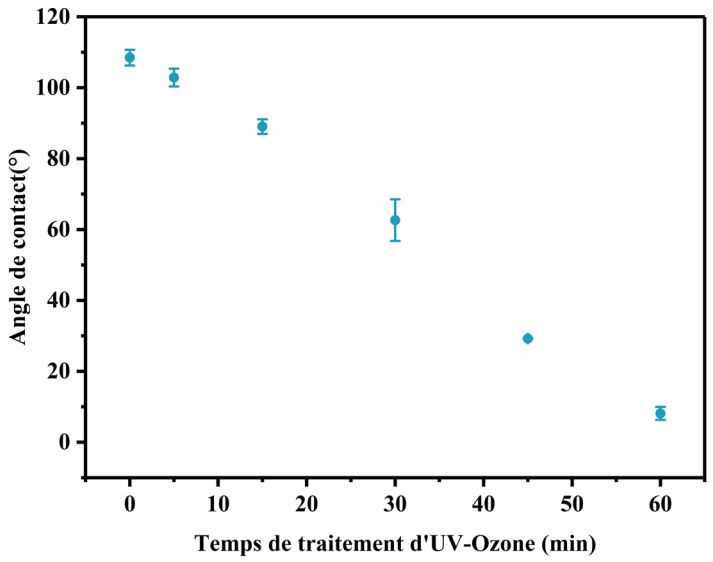

Figure III-1. Valeurs de l'angle de contact avec l'eau en mode statique des surfaces de PDMS exposées à un traitement UV/Ozone pendant différents temps.

Afin de connaitre, les modifications chimiques apportées par le traitement UV/Ozone, des analyses par ATR-FTIR ont donc été réalisées. D'après la Figure III-2, on remarque que la tendance observée lors des mesures d'angle de contact en fonction du temps de traitement correspond à l'augmentation de l'intensité de la large bande d'absorption entre 3600 et 3000 cm^{-1}, caractéristique des fonctions hydroxyles (-OH).

De plus, une diminution de l'intensité des différentes bandes des CH_3 (à 800, 1260 et 2965 cm^{-1} correspondant aux vibrations de déformation, d'élongation symétrique et

d'élongation asymétrique respectivement) a également été observée, suggérant la disparition progressive des groupements méthyles à la surface du PDMS, comme décrit par Berdichevsky *et al* [1]. De plus, la forme des bandes entre 1020 et 1100 cm^{-1}, correspondant aux vibrations d'élongation asymétrique de la liaison Si-O, a fortement changé lors de l'exposition au traitement UV/Ozone comme décrit dans la littérature pour ce type de traitement sur les surfaces de PDMS [1,2], indiquant la conversion des fragments CH_3-Si-O en réseau -O-Si-O-. En se basant sur les résultats d'angle de contact et de FTIR, et afin de s'assurer de la présence de fonctions hydroxyles sur la surface du PDMS sans former de fonctions carboxyles, un temps de traitement UV/Ozone de 45 min a été choisi pour la suite de l'étude.

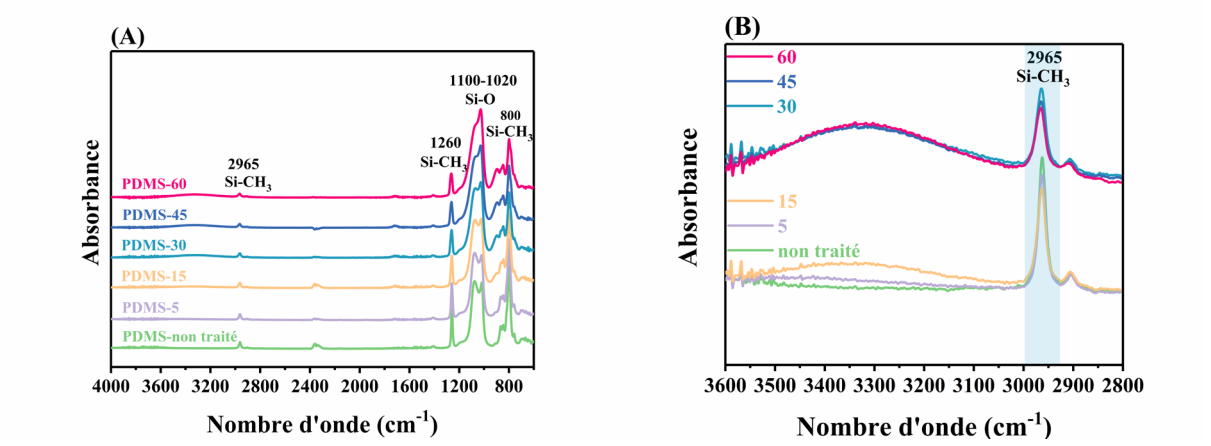

Figure III-2. Spectres ATR-FTIR des surfaces de PDMS exposées aux UV/Ozone avec des temps différents et leur contrôle : (A) 4000-800 cm^{-1} et (B) 3600-2800 cm^{-1}.

[1] Y. Berdichevsky, J. Khandurina, A. Guttman, Y.-H. Lo, UV/ozone modification of poly (dimethylsiloxane) microfluidic channels, Sensors Actuators B Chem., vol. 97, no. 2-3 (2004) 402–408.

[2] Y.-J. Fu, H. Qui, K.-S. Liao, S.J. Lue, C.-C. Hu, K.-R. Lee, J.-Y. Lai, Effect of UV-ozone treatment on poly (dimethylsiloxane) membranes: surface characterization and gas separation performance, Langmuir, vol. 26, no. 6 (2010) 4392–4399.

Ensuite, des molécules de PPTEOS ont été immobilisées sur les surfaces de PDMS par formation de lisons Si-O-Si au cours du processus d'auto-assemblage [4,5] permettant l'introduction sur les surfaces de PDMS des fonctions alcynes en position terminale. Pour déterminer les conditions optimales de cette étape de silanisation, les surfaces ont tout d'abord été analysées par AFM.

A l'aide de l'optique de l'AFM (Figure III-3), on observe que la concentration d'éthanol (EtOH), utilisé comme solvant lors de la réaction de silanisation, semble influencer la topographie de la surface du PDMS. En effet, des creux, d'environ une centaine de micromètres de long (valeur obtenue par comparaison avec les dimensions du micro-levier qui sont de 115×25 µm) se sont formés sur la surface même à des temps courts (dès 45 min). Il semble que l'apparition de ces creux proviendrait du phénomène d'évaporation de l'éthanol pendant le séchage (sous vide à température ambiante pendant au moins 3 h) [6]. Ensuite un mélange EtOH/eau (70/30 : v/v) a été testé et aucune modification visuelle de la surface de PDMS n'a été observée par rapport à la surface de PDMS native. Ce mélange a donc été choisi pour la suite des tests de l'étape de silanisation.

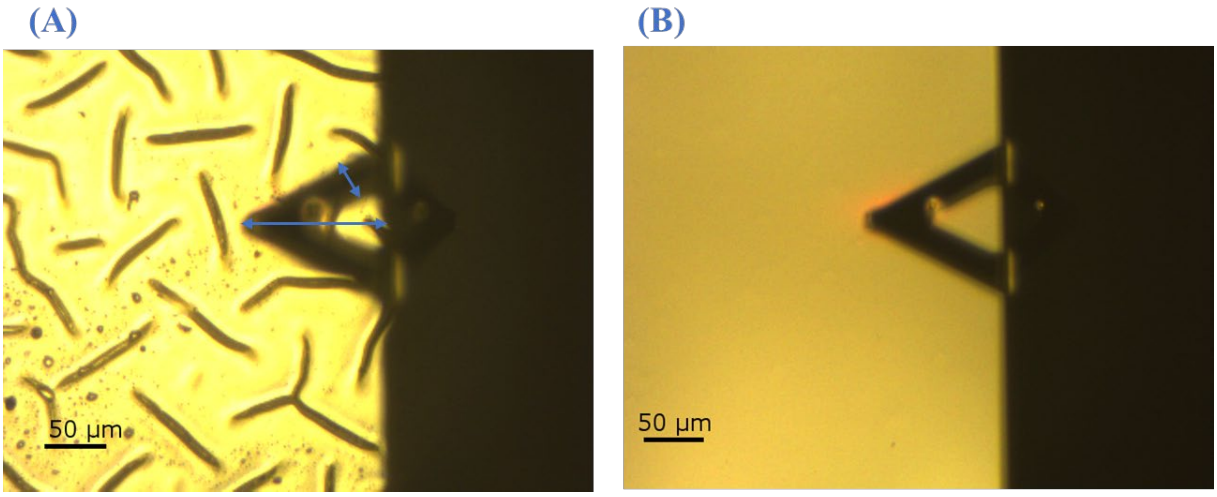

Figure III-3. Images obtenues à l'aide de l'optique de l'AFM de surfaces de PDMS après contact pendant la nuit avec différentes concentrations d'une solution d'EtOH : (A) 100% et (B) 70%.

[4] X. Meng, J. Hu, Z. Chao, Y. Liu, H. Ju, Q. Cheng, Thermoresponsive arrays patterned via photoclick chemistry: Smart MALDI plate for protein digest enrichment, desalting, and direct ms analysis, ACS Appl. Mater. Interfaces, vol. 10, no. 1 (2018), pp. 1324–1333.

[5] Q. Liu, Y. Sun, Z. Li, Terminal silanization of perfluoropolyether, polydimethylsiloxane, their block polymer and the self-assembled films on plasma-treated silicon surfaces, Chem. Pap., vol.73, no. 1 (2019), pp. 105–117.

[6] J. McQuade, L.T. Vuong, Solvent retention and crack evolution in dropcast PEDOT: PSS and dependence on surface wetting, ACS Omega., vol. 3, no. 4 (2018), pp. 3868–3873.

Ensuite, en se basant sur la littérature, différentes températures et différents temps de réaction de cette étape, regroupés dans le Tableau III-1, ont été testés, à partir d'une solution de PPTEOS à 50 mM (Tableau III-1).

Tableau III-1. Les différentes conditions opératoires testées lors de la réaction de silanisation.

N°	Température (°C)	Temps
(B)	Température ambiante	Toute la nuit (environ 18 h)
(C1)	40	45 min
(C2)	40	4 h
(C3)	40	6 h
(D)	60	4 h

L'ensemble des surfaces de PDMS modifiées sous les différentes conditions a été analysé par AFM (Figure III-4).

D'après les images AFM, on constate la présence d'agrégats sur l'ensemble des surfaces modifiées correspondant à la présence de PPTEOS sur les surfaces. Cependant, l'échantillon modifiée par les conditions B (température ambiante pendant 18 h) présente la surface la plus homogène et les plus petits agrégats avec un meilleur recouvrement de la surface. De ce fait, nous avons choisis, pour la suite, de travailler à température ambiante pendant la nuit avec une solution à 50 mM de PPTEOS dans un mélange EtOH/eau (70/30 : v/v).

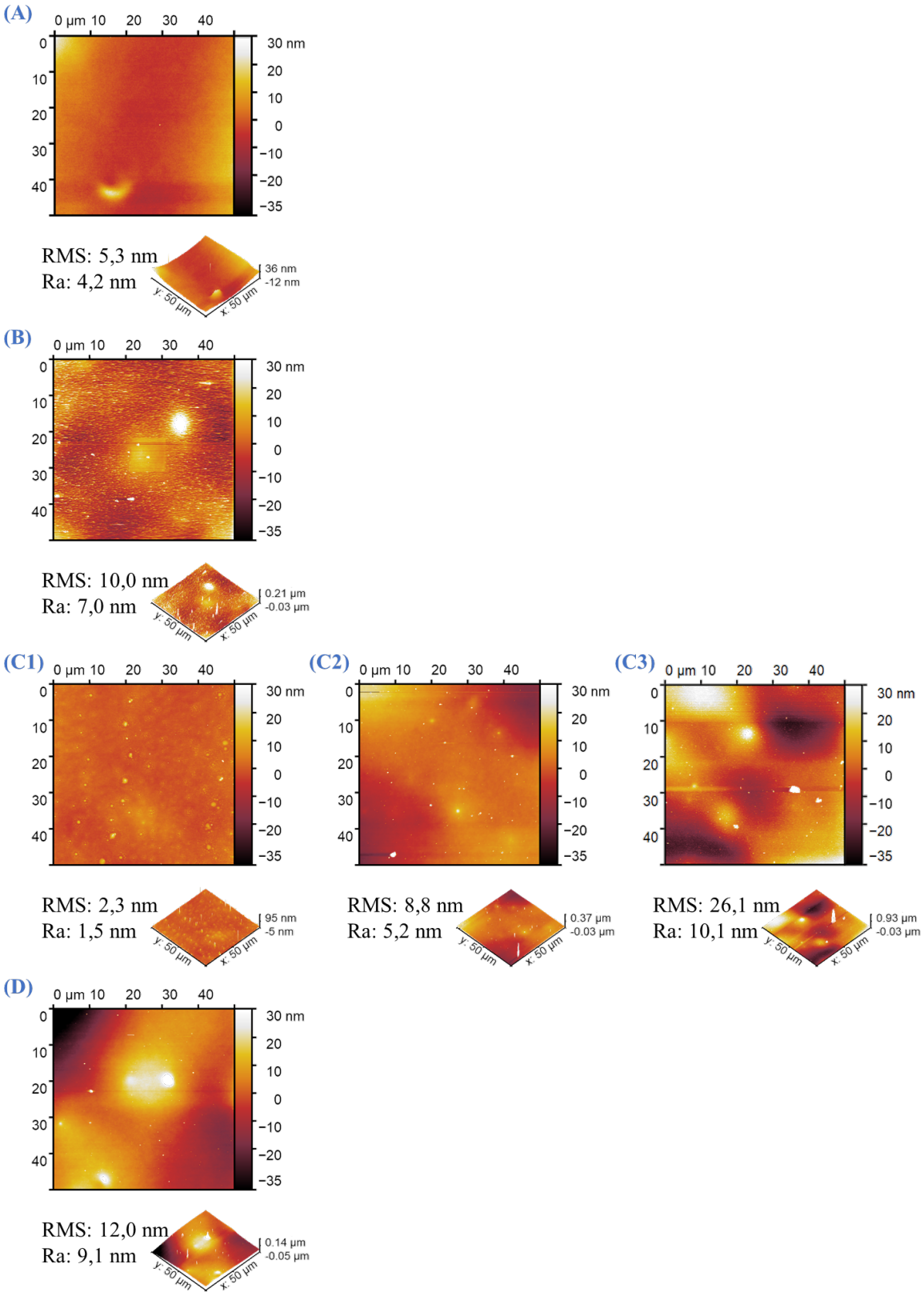

Figure III-4. Images AFM de surfaces de PDMS modifiées par le PPTEOS à différentes températures et à différents temps de réaction : (A) PDMS non modifié ; (B) 20 °C et 18 h ; (C1) 40 °C et 45 min ; (C2) 40 °C et 4 h ; (C3) 40 °C et 6 h et (D) 60 °C et 4 h.

Chapitre IV : Surfaces de PDMS antibactériennes par photo-greffage

Introduction

Ce chapitre est dédié à l'élaboration de surfaces de PDMS cationiques préparées par photo-greffage, amorcé par de la benzophénone, de polymères porteurs de groupements ammonium ou phosphonium quaternaire. Des procédés de 'grafting from' et 'grafting to' ont été testés. A notre connaissance, comme déjà décrit dans le chapitre I, il n'existe que deux voies chimiques pour la modification chimique directe de la surface du PDMS : le greffage par hydrosilylation et le greffage photo-induit. Dans ce chapitre, nous avons choisi cette dernière méthode pour modifier la surface du PDMS car il s'agit non seulement d'une méthode directe mais aussi d'un processus très rapide (en quelques minutes).

Les agents antibactériens à base de polymères présentent plus d'avantages que les agents antibactériens de faible poids moléculaire en raison de leur caractère non volatile, leur stabilité chimique et leur facilité d'utilisation. Les polymères polycationiques sont l'un des types de polymères antimicrobiens les plus importants présentant généralement une activité antibactérienne élevée à large spectre contre les bactéries à gram-positif et à gram-négatif, les champignons, les parasites et les virus lipophiles. Ainsi, deux monomères porteurs de groupements ammonium quaternaire et deux polymères porteurs de groupements ammonium ou phosphonium quaternaires ont été synthétisés et utilisés pour élaborer des surfaces de PDMS cationiques. Les deux polymères cationiques ont été synthétisées par le Dr Taril Eren de l'université de Yildiz Technique "Département de Chimie" dans le cadre d'une collaboration. Ce chapitre est divisé en trois parties.

La première partie porte sur la modification de la surface du PDMS par photopolymérisation d'un monomère de styrène ammonium *via* une approche 'grafting from' en présence de benzophénone préalablement immobilisée sur la surface. L'ensemble des modifications a été caractérisée par des mesures d'angle de contact avec l'eau en mode statique et en mode dynamique, par spectroscopie infrarouge à transformée de fourier (FTIR), par microscopie à force atomique (AFM) et par spectroscopie photoélectronique par rayons X (XPS). Enfin, l'activité antibactérienne du PDMS modifiée a été évaluée par microscopie à fluorescence à l'aide du kit live/dead contre *S. aureus*, *S. epidermidis* et *E. coli* et par dénombrement des bactéries en suspension contre *S. aureus* et *E. coli*. Les résultats de cette partie sont présentés sous forme d'un article publié sous la référence « Lou, Y., Schapman, D., Mercier, D., Alexandre, S., Burel, F., Thebault, P., & Kébir, N. "Self-disinfecting PDMS surfaces with high quaternary ammonium functionality by direct surface photoinitiated

polymerization of vinylbenzyl dimethylbutylammonium chloride," *Eur. Polym. J.*, vol. 152, p. 110473, 2021 ».

La deuxième partie concerne la modification de la surface du PDMS par photopolymérisation d'un monomère d'acrylate ammonium avec ou sans thiol comme espaceur *via* une approche 'grafting from'. La surface modifiée a été caractérisée par des mesures d'angle de contact avec l'eau, AFM, FTIR et XPS. Les propriétés antibactériennes ont été étudié par microscopie à fluorescence à l'aide du kit Live/Dead contre *S. epidermidis* et *E. coli*. Les résultats de cette partie sont présentés sous forme d'un article qui vient d'être accepté pour publication dans le journal « Reactive and Functional Polymers » sous le titre « Preparation of bactericidal surfaces through photo-initiated polymerization of *N*-[2-(acryloyloxy)ethyl]-*N,N*-dimethyl-*N*-butylammonium iodide from native and thiolated PDMS surfaces ».

La troisième et dernière partie porte sur la modification de la surface du PDMS par photogreffage de deux polymères cationiques, en utilisant un thiol comme espaceur, *via* une approche, cette fois ci, "grafting to" en présence encore une fois de benzophénone. Les surfaces modifiées ont été caractérisées avec les techniques mentionnées précédemment et l'activité antimicrobienne a été évalué de la même façon et contre les mêmes espèces bactériennes que la 2ème partie. Les résultats de cette partie sont présentés sous forme d'un article soumis au journal « European Polymer Journal » sous le titre « Preparation of bactericidal PDMS surfaces by benzophenone photo-initiated grafting of polynorbornenes functionalized with quaternary phosphonium or pyridinium groups ».

De plus, des expériences non décrites dans les articles sont présentées et discutées dans le paragraphe IV.4, intitulé « informations supplémentaires ».

IV.1 Article 3: Self-disinfecting PDMS surfaces with high quaternary ammonium functionality by direct surface photoinitiated polymerization of vinylbenzyl dimethylbutylammonium chloride

Yuzhen Lou[1], Damien Schapman[2], Dimitri Mercier[3], Stéphane Alexandre[4], Fabrice Burel[1], Pascal Thebault[4], Nasreddine Kébir[1]

[1] Normandie Université, INSA Rouen Normandie, Laboratoire PBS, UMR CNRS 6270 & FR 3038, Avenue de l'Université, 76801 Saint Etienne du Rouvray, France

[2] Normandie Université, UNIROUEN, IFR MP 23, PRIMACEN, 76821 Mont-Saint-Aignan, France

[3] PSL Research University, Chimie ParisTech – CNRS, Institut de Recherche de Chimie Paris, 11 rue Pierre et Marie Curie, 75005 Paris, France

[4] Normandie Université, UNIROUEN, laboratoire PBS, UMR CNRS 6270 & FR 3038, 76821 Mont-Saint-Aigan, France

Correspondence to:

Nasreddine KEBIR (E-mail: *nasreddine.kebir@insa-rouen.fr*)

Pascal THEBAULT (E-mail: *pascal.thebault@univ-rouen.fr*)

Abstract

Vinylbenzyl dimethylbutylammonium chloride was successfully grafted and photo-polymerized from a PDMS surface, in presence of benzophenone. The obtained surface exhibited quaternary ammonium density above 10^{17} charge/cm^2 and very high hydrophilicity compared to ungrafted surfaces. Bacterial enumeration and fluorescence microscopy revealed an efficient contact killing of this surface against *Escherichia coli*, *Staphylococcus* aureus and *Staphylococcus epidermidis*.

Keywords: Quaternary ammonium; photo; grafting from; PDMS; bactericidal, antibacterial.

Introduction

Planktonic bacteria or early attached cells are sensitive to environmental factors while bacteria in biofilms are more resistant. Indeed, it has been reported that antibiotic concentrations required to effectively eradicate biofilm bacteria are 100 to 1000 times higher than for planktonic bacteria. Therefore, it is suggested that preventing bacterial adhesion on material surfaces is a key property to avoid biofilm formation and microbial contamination [1-2].

There are three kinds of antibacterial surfaces: anti-adhesive or bacteriophobic surfaces that resist microbial adhesion [3-8]; release-based surfaces, which kill both adhered and planktonic bacteria by leaching antibacterial agents [9-11] and contact-killing surfaces bearing cationic groups that attract and kill bacteria by disrupting their cell membrane [12-13]. However, the antibacterial activity of release coatings is limited in time and overuse of antibiotics can lead to the phenomenon of bacterial resistance [14].

Polymer-based antibacterial agents called antibacterial polymers have more advantages over low molecular weight antibacterial agents, contributing not only to their non-volatile and chemically stable structure, but also to their ease of use [15]. Polycationic polymers especially quaternary ammonium (QA)-based polymers, are ones of the most efficient antibacterial polymers. Indeed, QA compounds exhibit extensive antimicrobial activity against bacteria, fungi, parasites and lipophilic viruses [16-18]. The hydrophilic-hydrophobic balance and molecular weight of the polymer, as well as the length of the alkyl chains attached to the nitrogen atom of the QA moieties, have been found to significantly affect their antimicrobial activity [19-22].

Thanks to their high flexibility, hydrophobicity, chemical and thermal stability and biocompatibility, silicone materials are widely used in medical field including orthopedic application (e.g., the hand and foot joint implants), catheters, extracorporeal equipment (e.g., blood oxygenator, thermal bypass machines and kidney dialysis) and aesthetic implants (e.g., silicone breast implant) etc. [23-29]. Nonetheless, its hydrophobicity easily exposes it to protein adsorption, bacterial contamination and biofilm formation, which limits its use due to serious health and economic implications [30-32].

Covalent grafting of antibacterial polymers onto silicone surfaces is one of the most important and promising strategies to avoid contamination and/or biofouling. Due to the chemical stability and inertness of PDMS, direct chemical modification is difficult to realize.

Often, plasma treatment is performed on PDMS surface to generate functional anchoring sites such as hydroxyl groups, which provide high hydrophilicity to the surface [33]. However, the post-chemical coupling must be achieved rapidly after a few minutes due to the recovery of hydrophobicity of plasma-treated PDMS surfaces, which results from the high dynamics of PDMS macromolecular chains and the diffusion of hydroxyl groups into the bulk [34].

In the last two last decades, some chemical routes have been developed to functionalize PDMS surfaces and to modify their properties [35-43]. One of the most used strategy is the coupling reaction by hydrosilylation between the surface Si-H groups and carbon-carbon double bonds from bioactive polymers or molecules [35-40]. Indeed, the Si-H groups present on the PDMS surface, before, during and after the hydrosilylation curing process, have been successfully used to graft bioactive copolymers onto PDMS surfaces [35-38]. Si-H groups can also be introduced to the surface by acid-catalyzed insertion of polymethylhydroxysiloxane [39-40].

Alternatively, direct chemical modification of PDMS surfaces can be also performed by photoinduced processes, using benzophenone as photo-initiator. For instance, covalent micropatterning of PDMS surface have been achieved by photo-grafting, through a mask, of acrylic acid, [41] polyethylene glycol monoacrylate and polyethylene glycol diacrylate [42]. Recently, Braden *et al*. developed a simultaneous photo-grafting/photo-crosslinking process to prepare antifouling PDMS substrates by coating the surface with two zwitterionic polymers: poly(sulfobetaine methacrylate) or poly(carboxybetaine methacrylate), in the presence of poly(ethylene) glycol diacrylate as crosslinker [43].

The “grafting to” and “grafting from” approaches are two major irreversible grafting methods to prepare antimicrobial surfaces by tethering functional polymers with QA functional groups [44]. In the “grafting to” approach, functionalized polymers are directly immobilized on a suitable surface under appropriate conditions. As a result, an already immobilized polymer film blocks other chains of that polymer from reaching the reactive sites on the surface, which limits the grafting density. In contrast, in the "grafting from" approach, suitable initiators are first immobilized on the surface, allowing the in situ polymerization of the monomers to form a homogeneous and dense polymer film on that surface [45].

Poly(trialkylvinylbenzyl ammonium chloride) polymers have been shown to be among the most bactericidal polymers [16-22]. Kebir *et al.* [35] prepared a Poly(*N*,*N*-dimethylbutyl vinylbenzyl ammonium chloride) random copolymer bearing carbon-carbon double bounds and

grafted it onto PDMS surfaces by hydrosilylation. The grafting density of the copolymer was modified by varying the Si-H content by changing the curing time or the ratio between the silicone components. The resulting cationic PDMS surfaces exhibited accessible ammonium charge densities ranging from 1.8×10^{14} to 2.8×10^{15} $N^{+}.cm^{-2}$ and contact angle with water varying between 102 and 88°, respectively. For Sylgard®184 PDMS films prepared with the conventional PartA/PartB = 1/10 ratio, grafting of the copolymer after curing led to the lowest surface coverage and wettability. Nevertheless, high killing efficiency (96-100%, respectively) against *E. coli* and *S. epidermidis* after 1h of contact was obtained in all cases.

In this work, we describe the design of highly QA-functionalized self-disinfecting PDMS surfaces by a straightforward process consisting of direct surface photoinitiated polymerization of vinylbenzyl dimethylbutylammonium chloride in the presence of benzophenone as photo-initiator. The physico-chemical and antimicrobial properties of the modified surfaces are investigated in comparison with literature data.

Experimental section

Materials

Sylgard® 184 was purchased from DOW chemical company (USA). *N,N*-dimethylbutylamine (99%) and vinylbenzyl chloride (>90%) were purchased from Sigma-Aldrich. Dry methanol (99.8%) and acetone were purchased from Acros Organics. Dry diethyl ether and glass coverslip (18×18 mm^2, Fisherbrand™) were purchased from Thermo Fisher Scientific. Benzophenone (BP) (≥99%) was purchased from Merck. Ultrapure water was obtained from a Milli-Q system (Siemens, France). All chemicals were used without further purification.

S. aureus (ATCC 29213), *S. epidermidis* (ATCC 35984) and *E. coli* (K12 MG1655) strains were stored as frozen aliquots in brain-heart infusion broth (BHI, Bacto, France) and 30 % glycerol at -20 °C. The LIVE/DEAD bacterial viability Kit, L7007 (SYTO®9 dye, 1.67 mM / Propidium iodide, 18.3 mM) was purchased form Thermo Fisher Scientific. Phosphate buffered saline (PBS), prepared from PBS tablets (Gibro, Swiss) and ultrapure water, was autoclaved before use.

Preparation of vinylbenzyl dimethylbutylammonium chloride (VBAC)

Vinylbenzyl dimethylbutylammonium chloride (VBAC) was synthesized according to a procedure described in the literature, [46-47] with some modifications. Briefly, vinylbenzyl

chloride (VBC) was added dropwise to a vigorously stirred solution of *N,N*-dimethylbutylamine (DMBA) in dry methanol (5.55 mol/L) at room temperature under an inert atmosphere. The final VBC/DMBA molar ratio was of 1/1.5 The mixture was left to react overnight under stirring. Then, the mixture was concentrated and added dropwise into a large excess of dry diethyl ether. The precipitated product was collected by filtration and dried under vacuum. ^{1}H NMR (MHz, DMSO-d_6): δ 7.57 (dd, 4H), 6.79 (dd, 1H), 5.96 (d, 1H), 5.39 (d, 1H), 4.61 (s, 2H), 3.29 (m, 2H), 2.99 (s, 6H), 1.76 (m, 2H), 1.30 (dt, 2H), 0.94 (t, 2H). FTIR-ATR (cm^{-1}): 3069 and 3031 (=C-H stretching vibration); 3000-2800 (C-H stretching vibration in CH, CH_2 and CH_3 groups); 1630, 1608, 1513 (C=C stretching vibration of the vinyl group and the benzene ring); 1498 (C-H bending vibration in N^+-CH_2-Ar); 1463 (C-H bending vibration in N^+-CH_2); 1440 (C-H bending vibration in N^+-CH_3); 1410 (=C-H bending vibration); 1300-1000 (C-H bending vibrations in plane of the benzene ring); 1062 (C-N stretching vibration); 950-700 (C-H bending vibrations out of plane of the benzene ring).

Preparation of PDMS film

15 g of a mixture of the two parts of Sylgard® 184, i.e. base and curing agent, in a ratio of 10:1 (w/w), were casted into a square low-density polyethylene Petri dish (120×120×17 mm^3). The mixture was then degassed under vacuum until the air bubbles were completely removed. The PDMS film formed after two days at room temperature and was cut into 18 × 18 mm^2 squares with a thickness less than 1 mm. The curing time can be considerably reduced by increasing the temperature (few hours at 70°C and about 1h at 120°C) [35].

Preparation of PDMS-PVBAC surfaces

The PDMS films were immersed in an acetone solution containing 20 wt% of BP for 30 min to absorb enough BP for the photografting and photopolymerization. The samples were quickly washed with methanol and then placed on a plate to dry in the dark. Then, 50 to 80 µl of a methanol solution containing VBAC was applied to the dry samples and covered with a glass slide so that the monomer solution was spread evenly over the surface of the PDMS by capillary force. The PDMS assembly was placed in a UV conveyor (UV Fusion Light Hammer 6), and irradiated with the UV light emitted from a small diameter electrodeless bulb combined with the elliptical reflector microwave-powered lamp (500 watts/inch) at a lamp-PDMS distance of 53 mm. Then, BP-initiated VBAC photopolymerization took place from the PDMS surface. After grafting, the samples were collected by immersion in water to detach from the glass slide and then washed in methanol three times. Samples were washed in methanol

overnight with gentle agitation and washed again with methanol the next day before being dried under vacuum to ensure that all unreacted monomer and ungrafted BP or VBAC compounds were removed. Untreated PDMS (control 1), PDMS treated with methanol and UV (control 2) as well as PDMS treated with a monomer solution (65wt%) without UV exposure (control 3) were prepared under the same conditions and they underwent the same washing procedure as the PDMS-PVBAC sample.

Measurements

^{1}H NMR spectra were recorded on a Bruker 300 MHz spectrometer. The ATR-FTIR spectra were recorded on a Nicolet IS-50 FTIR (Thermo, USA) spectrometer, using the VariGATR accessory (Harrick Scientific, Pleasantville, NY) and the DTGS detector, on three independent samples for each experimental condition, with a wave-number range between 600 and 4000 cm^{-1}. Data were obtained with a spectral resolution of 4 cm^{-1} per 250 scans.

Static and dynamic water contact angles measurements were performed using a contact angle goniometer “digidrop” (United Kingdom) in air at room temperature on at least three independent samples, using at least 3 droplets by sample.

X-Ray Photoelectron spectroscopy (XPS) analysis was performed using a Thermo Electron Escalab 250 spectrometer, with a monochromatic Al Ka X-ray source (hn = 1486.6eV) operating at a pressure around 10^{-9} mbar. The spectrometer was calibrated using Au4f7/2 at 84.1Ev. The take-off angle was 90° and the analyzed surface was a 500µm diameter disk. Survey spectra were recorded with a pass energy of 100eV and a step of 1eV. Spectra were recorded using the Thermo Avantage software and analyzed using CasaXPS software.

The topography of PDMS surfaces before and after modification were analyzed by using a Nanoscope 8 Multimode microscope (Bruker Nano Surfaces, Santa Barbara, CA, USA). Imaging was achieved in the air using the PeakForce®-QNM mode with a 100µm piezoelectric scanner. A silicon cantilever (RTESPA-300, Bruker) with a spring constant of approximately 40 N/m and a silicon tip was used. Images were obtained with a PeakForce tapping frequency of 1 kHz and the auto-amplitude on. AFM imaging was performed at multiple locations (at least 2) on at least two independent samples at two scan sizes: 5 x 5 and 20x20 μm^2. All images are presented in the height mode and are top view images. Flatten & three points levelling operations were usually done using the Gwyddion AFM software.

Determination of the surface accessible quaternary ammonium density

Surface quaternary ammonium densities were quantified according to a method described by Tiller *et al*. [48]. Modified and unmodified PDMS surfaces (1.8 × 1.8 cm^2) were immersed in a solution of fluorescein sodium salt (1% in distilled water) for 10 min. Afterwards, the unreacted fluorescein molecules were removed by washing the surface with distilled water. The samples were then placed in 3 mL of a 0.5% hexadecyltrimethyl ammonium bromide solution to exchange with the bounded fluorescein molecules under ultrasound for 15min. 0.45 mL of saturated $NaHCO_3$ solution was added after sonication. Then the absorbance of solution was recorded at 501 nm, using a 'Cary bio' UV-visible spectrophotometer (from Varian). The fluorescein concentration was then calculated using a calibration curve.

Antimicrobial activity assay of planktonic bacteria with CFU counting

The antimicrobial activity towards bacteria in suspension was performed by using a modified ASTM standard: *E2149-01 Standard Test Method for Determining the Anti-microbial Activity of Immobilized Antimicrobial Agents Under Dynamic Contact Conditions* [49]. Briefly, bacterial species were pre-cultured in 15 mL of BHI in a sterile 50 mL conical tube (Falcon) at 37 °C under shaking at 140 rpm overnight. Subsequently, the bacteria were harvested by centrifugation (Sigma® 3-16KI, rotor 19776, Germany) at 1600 rpm for 15 min at 20 °C and resuspended in PBS and diluted to the desired concentration. Modified and unmodified PDMS samples (control) were incubated with 10 ml of bacterial suspension in a 50 ml conical tube at 37 °C, 200 rpm for 1 h. The samples were then collected and rinsed with PBS (1 ml×3 times). Decimal dilutions of the resulting bacterial suspension were spread on BHI agar plates and incubated at 37 °C for 24 h before colony counting. All experiments were performed in triplicate and the experiments were repeated at least three times. The percentage of bacteria killed in suspension by the modified surface was calculated with regards to the number of suspended bacteria in the control (unmodified PDMS).

Antimicrobial activity assay (Live/Dead test)

A 130 µl droplet of *E. coli* or *S. aureus* suspension in distilled water (5.8×10^8 cell/ml) was spread on the modified surfaces (1.8 cm×1.8 cm) using a glass slide of the same surface size for 1 h. Then the glass slide was removed and the surface was washed with a stream of distilled water to remove unattached bacteria. After, a 130 µl mixture of two fluorescent markers: the SYTO® and the propidium iodide, was deposed and spread on the surface for 15 min. The mixture was diluted before use (20 µmol/l of SYTO®9). Images (1024x1024 pixels)

of the surfaces were acquired using a Leica TCS SP8 CFS confocal microscope with fixed stature (Leica Microsystems, Nanterre, France) equipped with diodes laser (Coherent, Les Ulis, France) at 488 nm to excite the SYTO®9 and at 552 nm to excite Propidium Iodide and a conventional scanner at 400 Hz. Fluorescence emission was detected sequentially by a hybrid detector (Leica Microsystems, Nanterre, France) in photon counting mode with a specific band from 500 to 540 nm for SYTO®9 and 580 to 630 nm for Propidium Iodide. Z-Stack images were acquired using an adapted step-size from Nyquist Criteria. ImageJ (Rasband W.S., U.S. National Institutes of Health, Bethesda, Maryland, USA, http://imagej.nih.gov/ij/, 1997-2020) was used to adjust brightness and contrast and to perform z projections of 3D images (xyz).

Results and discussion

Study of the photo-initiated polymerization of VBAC from the PDMS surface (preparation of PDMS-PVBAC)

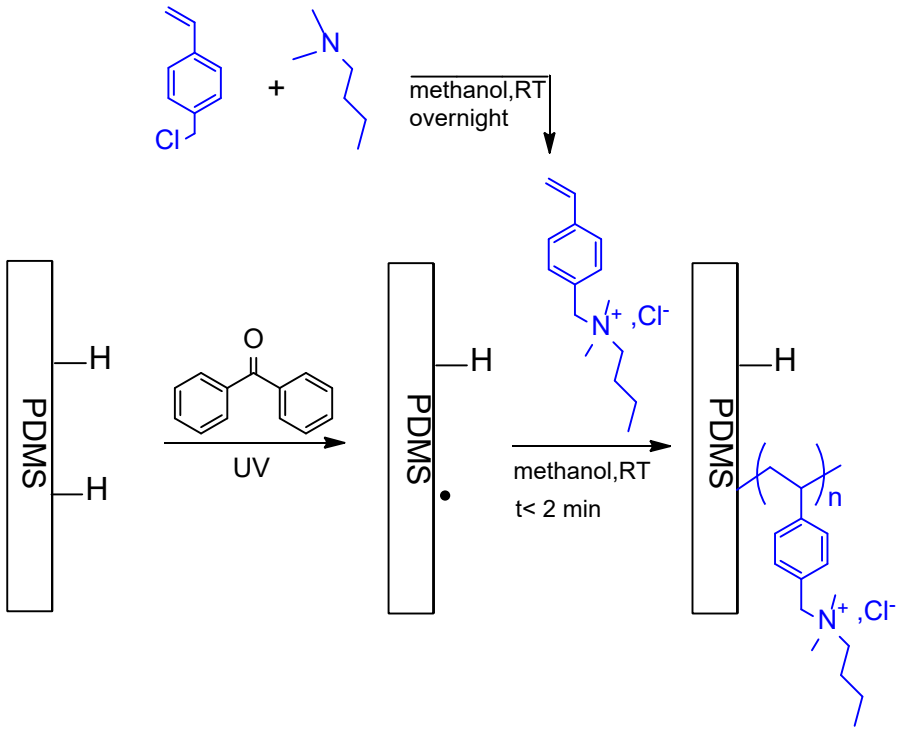

Scheme 1. Synthesis of *N*,*N*-dimethylbutyl vinylbenzyl ammonium chloride (VBAC) and its photo-polymerization from the PDMS surface.

In this work, we propose to prepare poly(*N*,*N*-dimethylbutyl vinylbenzyl ammonium chloride) grafted PDMS surfaces with high QA density and wettability, through a direct photo-initiated surface polymerization of the corresponding monomer. This 'grafting from' process will be compared to the previously described 'grafting to' process, where this polymer was grafted to the PDMS surface by hydrosilylation in water [35].

We have shown in previous works [35,55] that for poly(N,N-dimethylbutylvinylbenzylammonium chloride) (PVBAC) based homo- and co-polymers, prepared from a poly(vinylbenzyl chloride) (PVBC) of Mw=50000 g/mol, the butyl chain of the ammonium group was sufficiently long to provide an appropriate hydrophilic/hydrophobic balance to the polymer chain, making it water soluble and highly bactericidal. The minimum inhibitory concentration (MIC) of the polymer in water was estimated to be 12 g/ml against *E. coli* (Gram-) and 6 g/ml against *S. epidermidis* (Gram+). In contrast, for longer chain lengths (C8 and longer), the polymer partially or completely loses its solubility in water, so the "grafting on" process cannot be performed in pure water medium and MIC values cannot be determined under appropriate comparative conditions.

Ikeda *et al* [20] found that the activities of the synthesized polycations were highly dependent on their Mw and had a bell shape. The polymers were found to be much more active than their corresponding monomers. Effective antibacterial activity was obtained for optimal Mw values ranging from 50000 to 100000 g/mol. Thus, for Mw=24400 g/mol, poly(N,N-dimethylbutyl vinylbenzyl ammonium chloride) exhibited MIC values of 330-660 g/ml against *E. coli*, and 33-66 against *S. aureus* [47].

In this work, we anticipated that photopolymerization will lead to a grafted polymer with an appropriate molecular weight and/or charge density providing bactericidal properties on the PDMS surface.

The monomer *N*,*N*-dimethylbutyl vinylbenzyl ammonium chloride was prepared by reaction of benzyl chloride with *N*,*N*-dimethylbutyl amine in methanol overnight at room temperature. The pure monomer was recovered after crystallization and was soluble in water and alcohols, unlike its precursor, i.e. vinylbenzylchloride. ^{1}H NMR spectrum (supporting information) confirmed the chemical structure through the signals of protons of the carbon-carbon double bonds from 5.39 to 6.79 ppm and the protons of methylene of alkyl and benzyl groups in α position to the ammonium atoms from 2.99 to 4.61 ppm, respectively. FTIR analysis (supporting information) confirmed the complete conversion of the chloride group into an ammonium group, through the disappearance of the specific VBC vibration bands, especially the one at 1260 cm^{-1} related to C-H bending vibration in the CH_2Cl group. One can observe also three new bands at 1498, 1463 and 1440 cm^{-1}, corresponding to C-H bending vibration in CH_2 and CH_3 groups, respectively, in the alpha position to N^+.

The photopolymerization of the styrene ammonium monomer from the PDMS surface was initiated by benzophenone (Scheme 1) and was studied in several conditions in terms of reaction time (corresponding to the number of UV exposures) and monomer solution concentration. Fully cured Sylgard®184 PDMS films, prepared with the conventional PartA/PartB = 1/10 ratio, were used as model and control. A drop of monomer solution was deposed on the PDMS surface and spread using a thin glass plate. Then, the sample was placed in the UV conveyor with a passage speed of around 6.5 m/min, which corresponds to about 1.55 s of UV exposure per passage.

The polymer grafting densities on the silicone surfaces were monitored by contact angle measurements (Figures 1 and 2, Table 1). Untreated PDMS (control 1), PDMS treated with methanol and UV (control 2) as well as PDMS treated with a monomer solution (65wt%) without UV exposure (control 3) were used as controls. They exhibited water contact angle values around 108, 99 and 105°, respectively, consistent with the high hydrophobicity of PDMS. First, the effect of the number of UV exposures was studied for two monomers concentration (25 and 50wt%) (Figure 1). One can observe that for 25wt%, the value of the contact angle with water decreased slightly from 108° to around 100° regardless of the number of passages under UV, suggesting a small change in the surface, which kept its hydrophobic character. On the other hand, for a 50wt% monomer solution, the average value of the water contact angle decreased from 101° to 25° when the number of passages under UV increased from 10 to 60, suggesting an enhancement in surface coverage. Next, we monitored the impact of monomer concentration on surface modification for 50 UV exposures (Figure 2). The results showed that between 25 and 40wt% monomer concentration, the contact angle values were between 100 and 80°, which are close to the values obtained with similar surfaces prepared by the ‘grafting to’ method [35]. For concentrations above 40wt%, the contact angle dropped dramatically to 10° for a concentration of 65wt%, which is characteristic of a highly hydrophilic surface, suggesting a good degree of surface coverage. Thus, all subsequent studies were performed on PDMS surfaces treated with a 65wt% monomer solution after 50 UV runs (Table 1).

Dynamic water contact angle measurements were also performed on the optimal surface (Table 1). The advancing angle (AA) is characteristic of the wettability of the hydrophobic part of the surface whereas the receding angle (RA) is ascribed to the hydrophilic part. One can observe that AA, RA and the hysteresis (AA-RA) decreased dramatically, after the polymer was grafted onto the surface, from 116, 58 and 57° (control 1) to 36, 12 and 23° (PDMS-

PVBAC), respectively, suggesting once again a good surface coverage. Changes in hysteresis values are commonly ascribed to changes in chemical and/or physical surface heterogeneities.

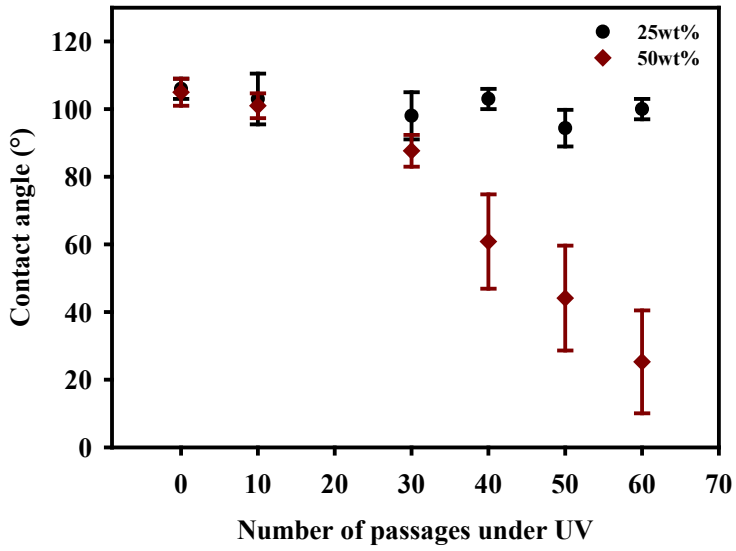

Figure 1. Static water contact angle values of PDMS modified with 25 and 50 wt% monomer solution with different number of passages under UV.

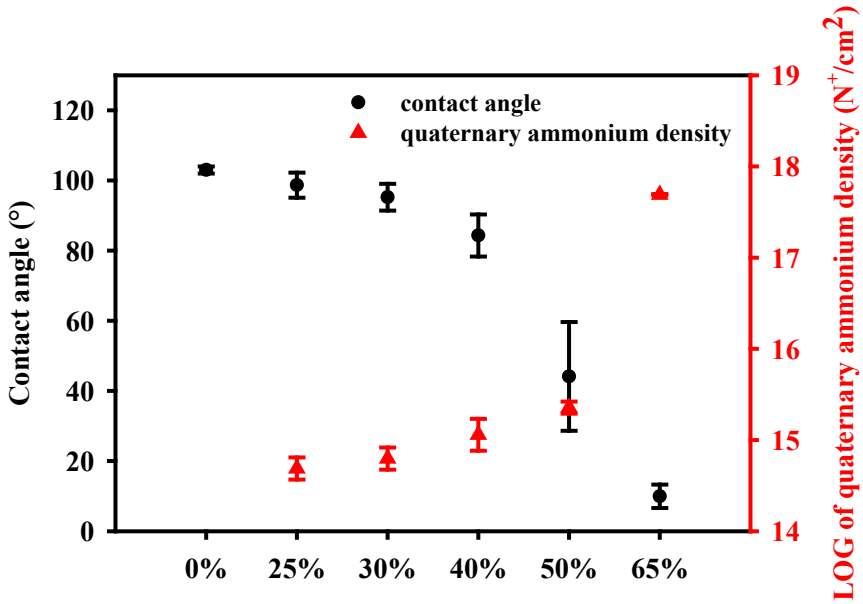

Figure 2. Static water contact angle values and log of quaternary ammonium density of modified PDMS with 25, 30, 40, 50 and 65wt% monomer solution, under 50 UV runs.

Table 1. Data of water contact angle measurements and surface charge densities on the optimal treated PDMS surface (65wt% monomer solution under 50 UV runs) and its controls.

Samples	Static θ_{water} (°)[a]	Dynamic θ_{water} (°)[a]			QA density $N^+.cm^{-2}$	Roughness by AFM[b] (nm)	
		AA	RA	Hyst (°)		Ra	RMS
PDMS (control 1)	108±2	116±3	58±4	57±2	ND[c]	0.9±0.1	1.2±0.2
PDMS-MeOH (control 2)	99±7	121±8	45±10	77±2	ND[c]	/	/
PDMS-VBAC without UV (control 3)	105±2	118±2	54±1	65±2	ND[c]	/	/
PDMS-PVBAC	10±3	36±2	12±5	23±4	$(4.8\pm0.1)\times10^{17}$	5.5±0.6	6.7±0.6

[a] θ_{water}: contact angle with water; **AA**: Advancing Angle; **RA:** Receding Angle; **Hyst**: Hysteresis.

[b] Ra: arithmetic roughness, RMS: Mean Square roughness.

[c] ND: means not determined, because of the absence of a UV/visible signal.

Assessment of surface charge density is very useful to predict the contact killing efficiency of quaternary ammonium surfaces [50-57]. It has been shown that the surface must exhibit a charge density above 10^{14} $N^+.cm^{-2}$ to kill efficiently *E. coli* and *S. epidermidis* [57].

The values of charge density of cationic PDMS surfaces prepared with different monomer concentrations at 50 UV passages are depicted in Figure 2 and Table 1. One can observe that all the values were above 10^{14} $N^+.cm^{-2}$, suggesting a high potential for bacterial killing. Furthermore, these values increased with the hydrophilicity of the surface, i.e. with decreasing values of the contact angle with water, reaching a very high value of 4.8×10^{17} $N^+.cm^{-2}$ for the optimal surface. On the other hand, cationic PDMS surfaces with water contact angle above 80° exhibited charge densities ranging from 5×10^{14} to 5×10^{15} $N^+.cm^{-2}$, i.e. close to those of analogous surfaces prepared by the “grafting to” approach [35].

Moreover, the proposed "grafting from" photo process has many advantages over the "grafting to" hydrosilylation process [35]:

- The synthesis of the QA monomer (grafting from) is faster and easier than the synthesis of the corresponding copolymer (grafting to).
- The photografting process is very fast than the hydosilylation process.
- The photografting process provides an effective surface modification after full crosslinking of PDMS compared to the hydosilylation process, with respectively: Charge density values around 10^{17} N^+/cm^2 vs. 10^{14} N^+/cm^2 and WCA of 10° vs. 102°. In addition, the enhancement of the surface grafting by hydrosilylation, using partially cured PDMS or by changing the A/B ration of the Sylgard 184 components, led to maximal values of charge densities of about 10^{15} N^+/cm^2 and WCA of about 88°, which was still lower than the 'grafting from' values.

Surface characterization by AFM

AFM analyses revealed the structural and topographical changes on the PDMS surfaces after photochemical grafting and polymerization of the cationic monomer (Figure 3 and supplementary data). The roughness values of these PDMS surfaces are depicted in Table 1. The native PDMS surface was very smooth with an arithmetic roughness of about 0.9±0.1 nm and a mean square roughness of about 1.2±0.2 nm (Figure 3-A). The quaternary ammonium PDMS surface exhibited an increased roughness values of about 5.5±0.6 nm and 6.7±0.6 nm, respectively (Figure 3-B). One can observe also that the surface coverage increased with the concentration of the starting monomer solution, which led to the increase of the surface hydrophilicity and the decrease of the average roughness values and/or their standard deviations (supplementary data). In addition, AFM images suggest an island-like growth of polymer chains in all three spatial directions. In fact, the polymerization reactions are initiated only from the surface sites where BP is present. Moreover, the start times of the initiation and propagation steps of the free radical polymerization can vary from site to site, depending on the accessibility of the BP, causing a gradient of grafted polymer leading to chemical (coverage) and physical (roughness) surface heterogeneities. The white spots in the AFM images can be ascribed to polymer aggerates on the surface. The spots in the untreated surface are rarely present, which can be ascribed to slight surface contamination by dust or other particles in the atmosphere or during manipulation with the clamp.

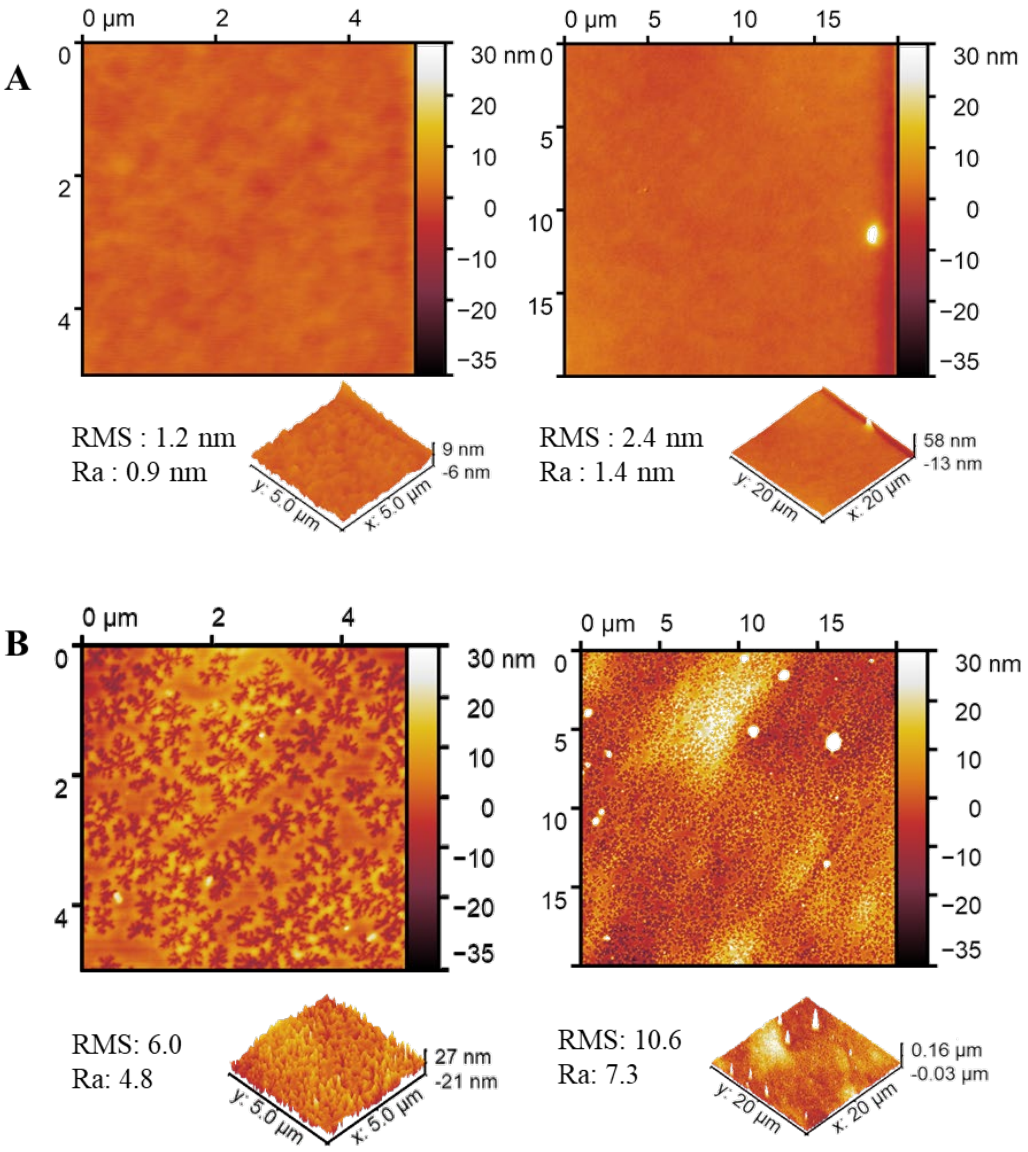

Figure 3. AFM images of (A) PDMS surface (control 1) and (B) PDMS-PVBAC surface.

Spectroscopic surface characterizations

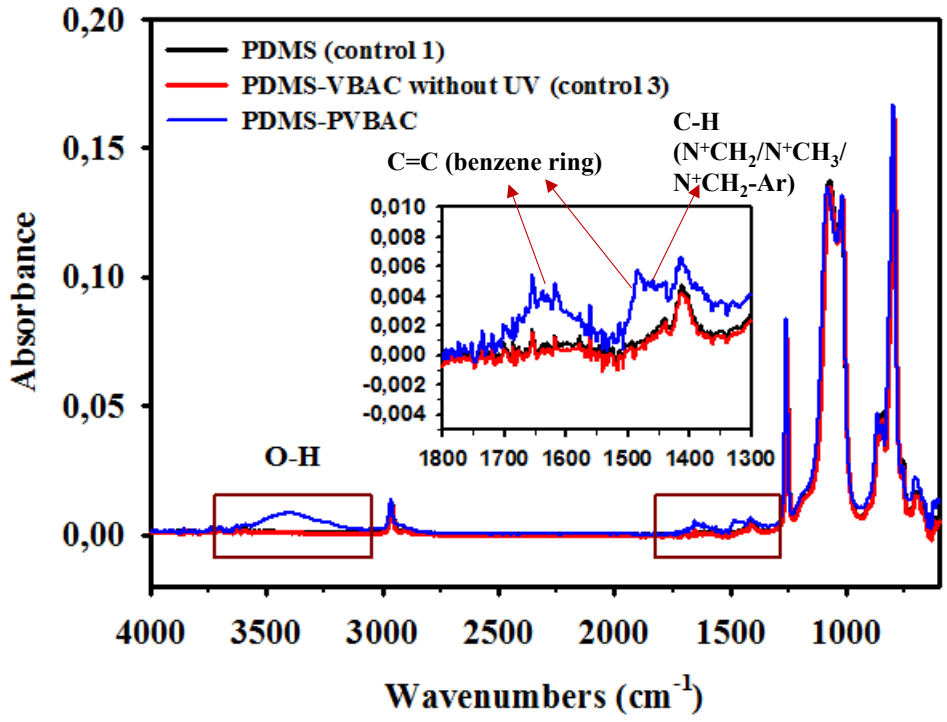

Figure 4. FTIR- ATR spectra of (from the top to bottom): PDMS (control 1), PDMS-VBAC without UV (control 3) and PDMS-PVBAC.

FTIR-ATR analysis (Figure 4) of the prepared cationic surface, compared to its controls, showed supplementary bands between 1440 and 1700 cm^{-1} ascribed to the benzyl ring of the grafted cationic polymer and also to the C-H bending vibration in N^+-CH_2-Ar, N^+-CH_2 and N^+-CH_3 (1440 and 1498 cm^{-1}). A slight contribution of the butyl chain was also observed in the region of 2800 - 3100 cm^{-1} (supplementary information). One can observe also a band at 3300 cm^{-1} arising from moisture, due to the hygroscopic character of the cationic surface. The FTIR spectra of controls 1 and 3 were identical, suggesting that UV treatment was indispensable for the grafting reaction to occur and that the washing with methanol to remove the monomer was effective.

The atomic compositions of PDMS and PDMS-PVBAC surfaces were obtained by XPS and the results are presented in the Table 2. XPS analysis of the PDMS surface showed clearly the presence of carbon, oxygen and silicon with a composition close to that expected. The slight enrichment observed for O and Si could be explained by the fact that Sylgard 184 does not have a pure PDMS chemical structure, it contains hydro-siloxane (Si-H) groups in residual amount after curing, which may contribute to the observed decrease in carbon content.

The presence of residual SiO_2 precursor is also a likely reason. PDMS-PVBAC surface also revealed the presence of N (1.2%) and Cl (1.2%) at a ratio of 1, associated with a strong enrichment of carbon, suggesting that the photo-grafting reaction was successful. It is noteworthy that the C/N and C/Cl ratios are equal to 15 in the VBAC and PVBAC, which explain the low values of the N and Cl percentages.

Table 2. XPS elemental analysis of the optimal modified PDMS surface and its unmodified PDMS control.

	C1s	O1s	Si2p	N1s	Cl2p	C/O	C/Si	O/Si	N/Cl	O/Cl
PDMS	43.4	30.2	26.4	--	--	1.4	1.6	1.1	--	--
PDMS-PVBAC	71.7	14.7	11.2	1.2	1.2	4.9	6.4	1.3	1.0	12.3

A way to represent the grafting density is to calculate an average thickness of the organic layer formed at the surface of the PDMS substrate. Thus, using a model including the coverage rate of the grafter layer on the PDMS surface, it is possible to use the following set of equations to determine an average thickness of island [58]:

$$I_{Cl} = \gamma K n_{Cl}^{layer} \sigma_{Cl} \lambda_{Cl}^{layer} T_{Cl} (1 - exp \frac{-d}{\lambda_{Cl}^{layer}}) \qquad (1)$$

$$I_{Si} = \gamma K n_{Si}^{PDMS} \sigma_{Si} \lambda_{Si}^{PDMS} T_{Si} \left(exp \frac{-d}{\lambda_{Si}^{layer}} \right) + (1 - \gamma) K n_{Si}^{PDMS} \sigma_{Si} \lambda_{Si}^{PDMS} T_{Si} (2)$$

With γ is the coverage rate, I is the intensity of photoelectrons emitted by the element X, K a constant characteristic of the spectrometer, σ the photoionization cross section of the core level of the considered element, λ the inelastic mean free path of the photoelectrons emitted by the core level of the considered element, n is the bulk concentration, T the transmission function for the electrons emitted by the core level of the element and d the thickness of the organic layer (values are given in the supplementary data).

Thus, assuming that the coverage rate is between 50 and 60%, as suggested by the AFM images, solving these equations resulted in an equivalent average grafted layer thickness of about 1.2-1.35nm.

Assessment of the surface bactericidal properties

The bactericidal properties of the PDMS cationic surfaces against *E. coli* (Gram-), *S. aureus* (Gram+) and *S. epidermidis* (Gram+) were studied by confocal fluorescent microscopy through the Live and Dead assay. Figure 5 displays examples of Live and Dead fluorescent images performed on modified and unmodified PDMS surfaces. Bacteria were spread onto the surfaces and then stained with a mixture of fluorescent probes that stain bacteria with damaged membrane red and those with intact membrane green. For the cationic PDMS surfaces, only red bacteria were observed confirming their contact killing property.

Moreover, the adhesion of *E. coli* (Figure 5A) and *S. epidermidis* (Figure 5B) seems to be principally governed by electrostatic forces since the bacteria have an overall negative charge and their attachment onto cationic surfaces is very dense (around 10^6 cell/cm^2) and very fast comparing to the unmodified PDMS surface (control), which did not display any significative bacteria attachment after 1h of contact. This result is consistent with the literature data in terms of the dependence of the surface bacterial density and the bactericidal efficiency on the surface charge density. Similar surfaces prepared by the "grafting to" method exhibited 98 to 100% killing efficiency after 1h of contact with *E. coli* and *S. epidermidis* suspensions. They also displayed a density of surface attached bacteria between 10^5 and 10^6 cell/cm^2, while the charge densities varied from 2×10^{14} to 1.2×10^{15} $N^+.cm^{-2}$ [35]. In contrast, *S. aureus* exhibited surprisingly high affinity and attachment on the unmodified PDMS surface (around 10^6 cell/cm^2), where they keep their viability, suggesting that this attachment is independent on the electrostatic phenomenon. On the other hand, after 1h of contact with the cationic PDMS surface, the integrity of the bacterial membrane was also perturbed and quasi-only red bacteria were observed (Figure 5C).

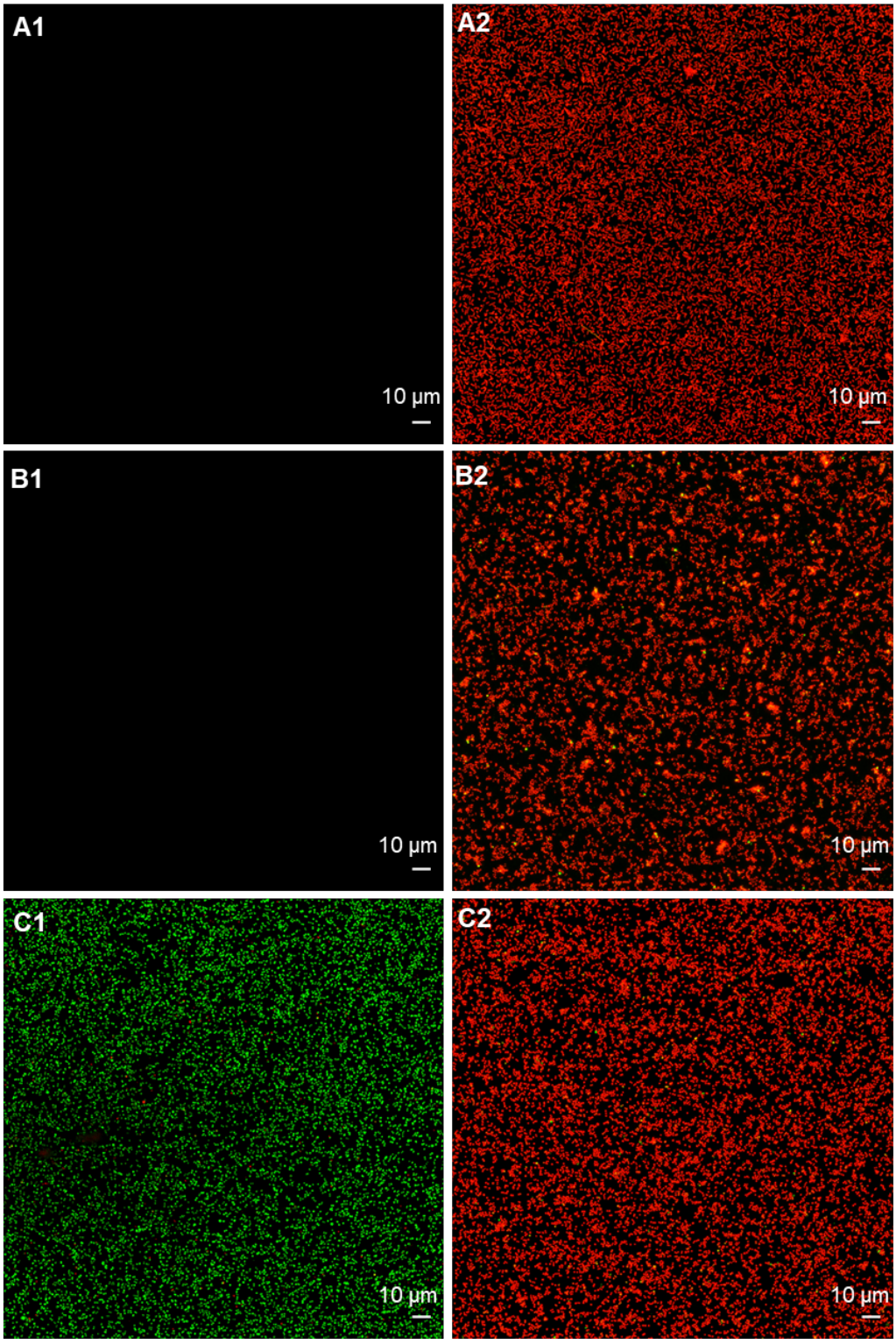

Figure 5. Fluorescence microscopy images of sessile bacteria cells stained with a marker of viability and deposited on surfaces of modified and unmodified PDMS surfaces: **(A1)** *E. coli* on unmodified PDMS surface (control), **(A2)** *E. coli* on cationic PDMS-PVBAC surface, **(B1)** *S. epidermidis* on unmodified PDMS surface (control), **(B2)** *S. epidermidis* on cationic PDMS-PVBAC surface, **(C1)** *S. aureus* on unmodified PDMS surface (control), **(C2)** *S. aureus* on cationic PDMS-PVBAC surface. Bacteria become non-viable after less than 1h of contact with the charged surface.

The bacterial killing capacity of the optimal cationic surface against *E. coli* and *S. aureus* in suspension was also studied using a modified ASTM standard: E2149-01. The long-term bactericidal activity of a cationic surface depends on the concentration of bacteria exposed to it. To study this parameter, the surface was challenged with different bacterial concentrations in suspension during 1h of contact, then the number of viable cells in suspension was counted by bacterial enumeration on BHI agar plates (Figure 6). The cationic surfaces exhibited a high bactericidal activity with a quantitative eradication of bacteria in suspension. One can observe that a drop off in the percentage of bacterial killing occurs at around 10^8 cells/cm^2, which corresponds to the limit of coverage of the surface by bacteria. Indeed, it has been shown that the bactericidal power of the cationic surface increases with its charge density. Above 5×10^{15} charges/cm^2 the surface becomes capable of killing at least one monolayer of *E. coli* cells, before passing through fouling and losing its bioactivity. Since the bacteria cell covers about 1 µm^2 of the surface, 1 cm^2 should be completely covered with around 10^8 cells if they are perfectly arrayed [49]. Furthermore, under the shaking conditions of this test, all suspended bacteria must be in contact with the surface during the hour of testing. Bacteria will attach firmly to the surface but can potentially be driven off by surface shear forces. When the number of bacteria reaches or exceeds the number of bacteria saturating the surface, the unoccupied spaces on the surface are reduced and some bacteria escape death [49]. Thus, the bactericidal effect of the QA surface in bacterial suspension is its ability to bind bacteria, to kill them and keep them on it.

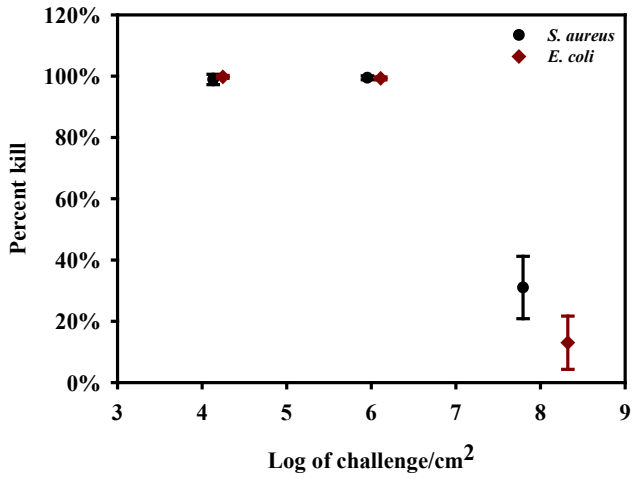

Figure 6. Determination of the bacterial killing capacity for the optimal cationic PDMS surface (PDMS-PVBAC) with a charge density of (4.8±0.1) $\times10^{17}$ $N^+.cm^{-2}$. Samples were incubated with increasing challenges of *E. coli*. The survivors were counted and compared with a control.

One can observe also is that QA-PDMS surfaces prepared by the photografting process showed higher capacity in terms of bacterial killing capacity compared to analogues prepared by the hydrosilylation process. Indeed, when hydrosilylation was performed after PDMS curing, 96% of killing efficiency was obtained on the surface. The enhancement of the surface grafting by hydrosilylation, using partially cured PDMS or by changing the A/B ration of the Sylgard 184 components led to about 100% of bacterial killing capacity on the surface, which was not, however, measured in suspension [35]. On the other hand, on the base of these results and the reported dependance of killing capacity on charge density [49], we can suggest that the longevity of the QA-PDMS surfaces prepared by the photografting process is higher, since it will take more time to these surfaces to be exposed to bacterial concentration that passivate it.

Some studies have evidenced that, in solution, quaternary ammonium may be cytotoxic, depending on concentration, time exposure and chemical structure [59-61]. However, the biocompatibility of cationic surfaces needs further investigations to determine whether we would use them for medical device applications [62]. In a previous work [35], we have demonstrated that plasmatic proteins, because they are electrically charged, are adsorbed on QA surfaces, which quantitatively lost their bactericidal efficiency after 24 hours of contact with them. Consequently, this result suggested to avoid their use in blood contact applications. On the other hand, currently, we can suggest to use this kind of surface in all silicone devices that are not in contact with blood, such as the external surfaces of catheter chambers and extracorporeal equipment.

Conclusion

Bactericidal cationic PDMS surfaces were successfully prepared by photo-induced polymerization of a styrene ammonium monomer from the surface in the presence of benzophenone. The reaction was optimized in terms of duration and monomer concentration. By varying these two parameters, surface charge densities and contact angle with water (hydrophilicity) can be fine-tuned from about 10^{14} to 10^{17} $N^{+}.cm^{-2}$ and from about 100 to 10°, respectively. The Live and Dead test by fluorescence microscopy revealed an efficient contact killing of the optimal surface against *E. coli*, *S. aureus* and *S. epidermidis*. Bacterial enumeration showed that this surface is capable of killing bacteria in suspension up to a concentration greater than 10^{6} CFU/mL. Finally, the prepared QA-PDMS surfaces revealed higher performances comparing to the analogues prepared by the hydrosilylation process.

Acknowledgments

Authors thanks the INSA ROUEN NORMANDIE and the China Scholarship Council (CSC) for the financial supports. ***This manuscript is a tribute to the 50-year anniversary of the French Polymer Group (Groupe Français des Polymères - GFP).***

Data availability statement

The raw/processed data required to reproduce these findings cannot be shared at this time due to technical or time limitations.

References

[1] H. Gu, S. W. Lee, J. Carnicelli, T. Zhang, and D. Ren, “Magnetically driven active topography for long-term biofilm control,” Nat. Commun., vol. 11, no. 1, pp. 1–11, 2020.

[2] M. Salwiczek et al., “Emerging rules for effective antimicrobial coatings,” Trends Biotechnol., vol. 32, no. 2, pp. 82–90, 2014.

[3] Y. Lou, P. Thebault, F. Burel, and N. Kebir, “Antibacterial properties of metal and PDMS surfaces under weak electric fields,” Surf. Coatings Technol., p. 125912, 2020.

[4] J. Hasan and K. Chatterjee, “Recent advances in engineering topography mediated antibacterial surfaces,” Nanoscale, vol. 7, no. 38, pp. 15568–15575, 2015.

[5] D. Alves and M. Olívia Pereira, “Mini-review: Antimicrobial peptides and enzymes as promising candidates to functionalize biomaterial surfaces,” Biofouling, vol. 30, no. 4, pp. 483–499, Apr. 2014.

[6] Z. Li, S. Wang, X. Yang, H. Liu, Y. Shan, X. Xu, S. Shang, Z. Song, “Antimicrobial and antifouling coating constructed using rosin acid-based quaternary ammonium salt and N-vinylpyrrolidone via RAFT polymerization,” Appl. Surf. Sci., vol. 530, pp. 147193, 2020.

[7] B.-L Wang, J.-L Wang, D.-D Li, K.-F Ren, J. Ji, “Chitosan/poly (vinyl pyrollidone) coatings improve the antibacterial properties of poly(ethylene terephthalate),” Appl. Surf. Sci., vol. 258, no. 20, pp. 7801-7808C, 2012.

[8] M. Lu, S. Yu, Z. Wang, Q. Xin, T. Sun, X. Chen, Z. Liu, X. Chen, J. Weng, J. Li, “Zwitterionic choline phosphate functionalized chitosan with antibacterial property and superior water solubility,” Eur. Polym. J., vol. 134, pp. 109821, 2020

[9] P. Ayaz, B. Xu, X. Zhang, J. Wang, D. Yu, J. Wu, “A pH and hyaluronidase dual-responsive multilayer-based drug delivery system for resisting bacterial infection,” Appl. Surf. Sci., vol. 527, pp. 146806, 2020.

[10] J. Muller, A. C. Quesada, C. González-Martínez, A. Chiralt, “Antimicrobial properties and release of cinnamaldehyde in bilayer films based on polylactic acid (PLA) and starch,” Eur. Polym. J., vol. 96, pp. 316-325, 2017.

[11] M. Akia, C. Rodriguez, L. Materon, R. Gilkerson, K. Lozano, “Antibacterial activity of polymeric nanofiber membranes impregnated with Texas sour orange juice,” Eur. Polym. J., vol. 115, pp. 1-5, 2019.

[12] R. Kaur and S. Liu, “Antibacterial surface design – Contact kill,” Prog. Surf. Sci., vol. 91, no. 3, pp. 136–153, 2016.

[13] J. Foksowicz-Flaczyk, J. Walentowska, M. Przybylak, and H. Maciejewski, “Multifunctional durable properties of textile materials modified by biocidal agents in the sol-gel process,” Surf. Coatings Technol., vol. 304, pp. 160–166, 2016.

[14] A. C. Rios et al., “Alternatives to overcoming bacterial resistances: state-of-the-art,” Microbiol. Res., vol. 191, pp. 51–80, 2016.

[15] S. Farah, “Antimicrobial Quaternary Ammonium Polymers for Biomedical Applications,” Antimicrob. Mater. Biomed. Appl., vol. 5, p. 277, 2019.

[16] J. Yan, L. Zheng, K. Hu, L. Li, C. Li, L. Zhu, H. Wang, Y. Xiao, S. Wu, J. Liu, B. Zhang, F. Zhang, "Cationic polyesters with antibacterial properties: Facile and controllable synthesis and antibacterial study," Eur. Polym. J., vol. 110, pp. 41-48, 2019.

[17] J. Velazco-de-la-Garza, L. Avérous, G. de Jesús Sosa-Santillán, E. Pollet, A. Zugasti-Cruz, C. A. Sierra-Rivera, N. V. Pérez-Aguilar, E. Oyervides-Muñoz, “Biological properties of novel polysuccinimide derivatives synthesized via quaternary ammonium grafting,” Eur. Polym. J., vol. 131, pp. 109705, 2020.

[18] A. Palantoken, M. S. Yilmaz, N. A. Unubol, E. Yenigul, S. Pişkin, T. Eren, "Synthesis and characterization of a ROMP-based polycationic antimicrobial hydrogel," Eur. Polym. J., vol. 112, pp. 365-375, 2019.

[19] B. Dizman, M. O. Elasri, and L. J. Mathias, "Synthesis and antimicrobial activities of new water-soluble bis-quaternary ammonium methacrylate polymers," J. Appl. Polym. Sci., vol. 94, no. 2, pp. 635–642, 2004.

[20] T. Ikeda, H. Hirayama, H. Yamaguchi, S. Tazuke, M. Watanabe, "Polycationic biocides with pendant active groups: molecular weight dependence of antibacterial activity," Antimicrob Agents Chemother., vol. 30, pp. 132-136, 1986.

[21] J. Guo et al., "Antibacterial activity of cationic polymers: side-chain or main-chain type?," Polym. Chem., vol. 9, no. 37, pp. 4611–4616, 2018.

[22] T. Ikeda, H. Hirayama, K. Suzuki, H. Yamaguchi, and S. Tazuke, "Biologically active polycations, 6. Polymeric pyridinium salts with well-defined main chain structure," Die Makromol. Chemie, vol. 187, no. 2, pp. 333–340, 1986.

[23] A. B. Swanson, "Silicone Rubber Implants for Replacement of Arthritic or Destroyed Joints in the Hand," Surg. Clin. North Am., vol. 48, no. 5, pp. 1113–1127, 1968.

[24] M. Bračič, O. Sauperl, S. Strnad, I. Kosalec, O. Plohl, L. F. Zemljič, "Surface modification of silicone with colloidal polysaccharides formulations for the development of antimicrobial urethral catheters," Appl. Surf. Sci., vol. 463, no. 1 , pp. 889-899, 2019.

[25] A. Colas and J. Curtis, "Silicone biomaterials: history and chemistry," Biomater. Sci. an Introd. to Mater. Med., vol. 2, pp. 80–85, 2004.

[26] A. U. Daniels, "Silicone breast implant materials," Swiss Med. Wkly., vol. 142, no. JULY, 2012.

[27] K. W. Dunn, P. N. Hall, and C. T. K. Khoo, "Breast implant materials: sense and safety," Br. J. Plast. Surg., vol. 45, no. 4, pp. 315–321, 1992.

[28] A. Colas, "Silicones: preparation, properties and performance," Dow Corning, Life Sci., 2005.

[29] J. R. Henstock, L. T. Canham, and S. I. Anderson, "Silicon: the evolution of its use in biomaterials," Acta Biomater., vol. 11, pp. 17–26, 2015.

[30] J. Winiecka-Krusnell and E. Linder, "Bacterial infections of free-living amoebae," Res. Microbiol., vol. 152, no. 7, pp. 613–619, 2001.

[31] Q. Gao et al., "Rationally designed dual functional block copolymers for bottlebrush-like coatings: In vitro and in vivo antimicrobial, antibiofilm, and antifouling properties," Acta Biomater., vol. 51, pp. 112–124, 2017.

[32] A. I. Doulgeraki, P. Di Ciccio, A. Ianieri, and G. J. E. Nychas, "Methicillin-resistant food-related Staphylococcus aureus: a review of current knowledge and biofilm formation for future studies and applications," Res. Microbiol., vol. 168, no. 1, pp. 1–15, 2017.

[33] C. Donzel et al., "Hydrophilic poly (dimethylsiloxane) stamps for microcontact printing," Adv. Mater., vol. 13, no. 15, pp. 1164–1167, 2001.

[34] A. Oláh, H. Hillborg, and G. J. Vancso, "Hydrophobic recovery of UV/ozone treated poly (dimethylsiloxane): adhesion studies by contact mechanics and mechanism of surface modification" Appl. Surf. Sci., vol. 239, no. 3–4, pp. 410–423, 2005.

[35] N. Kébir, I. Kriegel, M. Estève, and V. Semetey, "Preparation of bactericidal cationic PDMS surfaces using a facile and efficient approach," Appl. Surf. Sci., vol. 360, pp. 866–874, 2016.

[36] W. Mussard, N. Kebir, I. Kriegel, M. Estève, and V. Semetey, "Facile and efficient control of bioadhesion on poly(dimethylsiloxane) by using a biomimetic approach," Angew. Chemie, vol. 123, no. 46, pp. 11063–11066, 2011.

[37] D.-J. Guo, H.-M. Han, S.-J. Xiao, and Z.-D. Dai, "Surface-hydrophilic and protein-resistant

silicone elastomers prepared by hydrosilylation of vinyl poly(ethylene glycol) on hydrosilanes-poly (dimethylsiloxane) surfaces," Colloids Surfaces A Physicochem. Eng. Asp., vol. 308, no. 1–3, pp. 129–135, 2007.

[38] Y. Wu, Y. Huang, and H. Ma, "A facile method for permanent and functional surface modification of poly(dimethylsiloxane)," J. Am. Chem. Soc., vol. 129, no. 23, pp. 7226–7227, 2007.

[39] H. Chen, Y. Chen, H. Sheardown, and M. A. Brook, "Immobilization of heparin on a silicone surface through a heterobifunctional PEG spacer," Biomaterials, vol. 26, no. 35, pp. 7418–7424, 2005.

[40] H. Chen, Z. Zhang, Y. Chen, M. A. Brook, and H. Sheardown, "Protein repellant silicone surfaces by covalent immobilization of poly(ethylene oxide)," Biomaterials, vol. 26, no. 15, pp. 2391–2399, 2005.

[41] Y. Wang, H.-H. Lai, M. Bachman, C. E. Sims, G. P. Li, and N. L. Allbritton, "Covalent micropatterning of poly(dimethylsiloxane) by photografting through a mask," Anal. Chem., vol. 77, no. 23, pp. 7539–7546, 2005.

[42] S. Sugiura, J. Edahiro, K. Sumaru, and T. Kanamori, "Surface modification of polydimethylsiloxane with photo-grafted poly (ethylene glycol) for micropatterned protein adsorption and cell adhesion," Colloids Surfaces B Biointerfaces, vol. 63, no. 2, pp. 301–305, 2008.

[43] B. L. Leigh, E. Cheng, L. Xu, A. Derk, M. R. Hansen, and C. A. Guymon, "Antifouling photograftable zwitterionic coatings on PDMS substrates," Langmuir, vol. 35, no. 5, pp. 1100–1110, 2018.

[44] Y. Jiao, L. Niu, S. Ma, J. Li, F. R. Tay, and J. Chen, "Quaternary ammonium-based biomedical materials: State-of-the-art, toxicological aspects and antimicrobial resistance," Prog. Polym. Sci., vol. 71, pp. 53–90, 2017.

[45] T. Zhou et al., "Surface functionalization of biomaterials by radical polymerization," Prog. Mater. Sci., vol. 83, pp. 191–235, 2016.

[46] Q. Xu, Z. Zheng, B. Wang, H. Mao, and F. Yan, "Zinc Ion Coordinated Poly(Ionic Liquid) Antimicrobial Membranes for Wound Healing," ACS Appl. Mater. Interfaces, vol. 9, no. 17, pp. 14656–14664, 2017.

[47] T. Ikeda and S. Tazuke, "Synthesis and antimicrobial activity of poly (trialkylvinylbenzylammonium chloride) s," Makromol. Chemie Macromol. Chem. physicis, vol. 185(5), pp. 869–876, 1984.

[48] J.C. Tiller, C.J. Liao, K. Lewis, A.M. Klibanov, "Designing surface that kill bacteria on contact," Proc. Natl. Acad. Sci. USA., vol. 98, pp. 5981-5985, 2001.

[49] H. Murata, R. R. Koepsel, K. Matyjaszewski, and A. J. Russell, "Permanent, non-leaching antibacterial surfaces-2: How high density cationic surfaces kill bacterial cells," Biomaterials, vol. 28, no. 32, pp. 4870–4879, 2007.

[50] J. C. Tiller, C.-J. Liao, K. Lewis, and A. M. Klibanov, "Designing surfaces that kill bacteria on contact," Proc. Natl. Acad. Sci., vol. 98, no. 11, pp. 5981–5985, 2001.

[51] N. M. Milović, J. Wang, K. Lewis, and A. M. Klibanov, "Immobilized N-alkylated polyethylenimine avidly kills bacteria by rupturing cell membranes with no resistance developed," Biotechnol. Bioeng., vol. 90, no. 6, pp. 715–722, 2005.

[52] S. B. Lee, R. R. Koepsel, S. W. Morley, K. Matyjaszewski, Y. Sun, and A. J. Russell, "Permanent, nonleaching antibacterial surfaces. 1. Synthesis by atom transfer radical polymerization," Biomacromolecules, vol. 5, no. 3, pp. 877–882, 2004.

[53] J. C. Tiller, S. B. Lee, K. Lewis, and A. M. Klibanov, "Polymer surfaces derivatized with poly

(vinyl-N-hexylpyridinium) kill airborne and waterborne bacteria," Biotechnol. Bioeng., vol. 79, no. 4, pp. 465–471, 2002.

[54] J. Lin, J. C. Tiller, S. B. Lee, K. Lewis, and A. M. Klibanov, "Insights into bactericidal action of surface-attached poly (vinyl-N-hexylpyridinium) chains," Biotechnol. Lett., vol. 24, no. 10, pp. 801–805, 2002.

[55] J. Lafarge, N. Kebir, D. Schapman, and F. Burel, "Design of self-disinfecting PVC surfaces using the click chemistry," React. Funct. Polym., vol. 73, no. 11, pp. 1464–1472, 2013.

[56] J. Lin, S. Qiu, K. Lewis, and A. M. Klibanov, "Mechanism of bactericidal and fungicidal activities of textiles covalently modified with alkylated polyethylenimine," Biotechnol. Bioeng., vol. 83, no. 2, pp. 168–172, 2003.

[57] R. Kügler, O. Bouloussa, and F. Rondelez, "Evidence of a charge-density threshold for optimum efficiency of biocidal cationic surfaces," Microbiology, vol. 151, no. 5, pp. 1341–1348, 2005.

[58] E. Gardin, S. Zanna, A. Seyeux, D. Mercier, A. Allion-Maurer, P. Marcus, "Early stage of marine biofilm formation on duplex stainless steel," Biointerphases, vol. 15, pp. 041014, 2020.

[59] C. Debbasch, M.D. St Jean, P.J. Pisella, P. Rat, J.M. Warnet, C. Baudouin, "Quaternary ammonium cytotoxicity in a human conjunctival cell line," J Fr Ophtalmol., vol 22, no. 9, pp. 950-958, 1999.

[60] D. Fischer, Y. Li, B. Ahlemeyer, J. Krieglstein, T. Kissel, "In vitro cytotoxicity testing of polycations: influence of polymer structure on cell viability and hemolysis," Biomaterials, vol 24, no. 7, pp. 1121-1131, 2003.

[61] T. Eren, A. Som, J. R. Rennie, C. F. Nelson,Y. Urgina, K. Nüsslein, E. B. Coughlin, G. N. Tew, "Antibacterial and Hemolytic Activities of Quaternary Pyridinium Functionalized Polynorbornenes," Macromol. Chem. Phys., vol 209, pp. 516–524, 2008.

[62] H. Bouloussa, A.Saleh-mghir, C. Valotteau, C. Cherifi, N. Hafsia, et al., "A Graftable Quaternary Ammonium Biocidal Polymer Reduces Biofilm Formation and Ensures Biocompatibility of Medical Devices," Advanced Materials Interfaces, Wiley, 2021, pp.2001516.

Supporting information

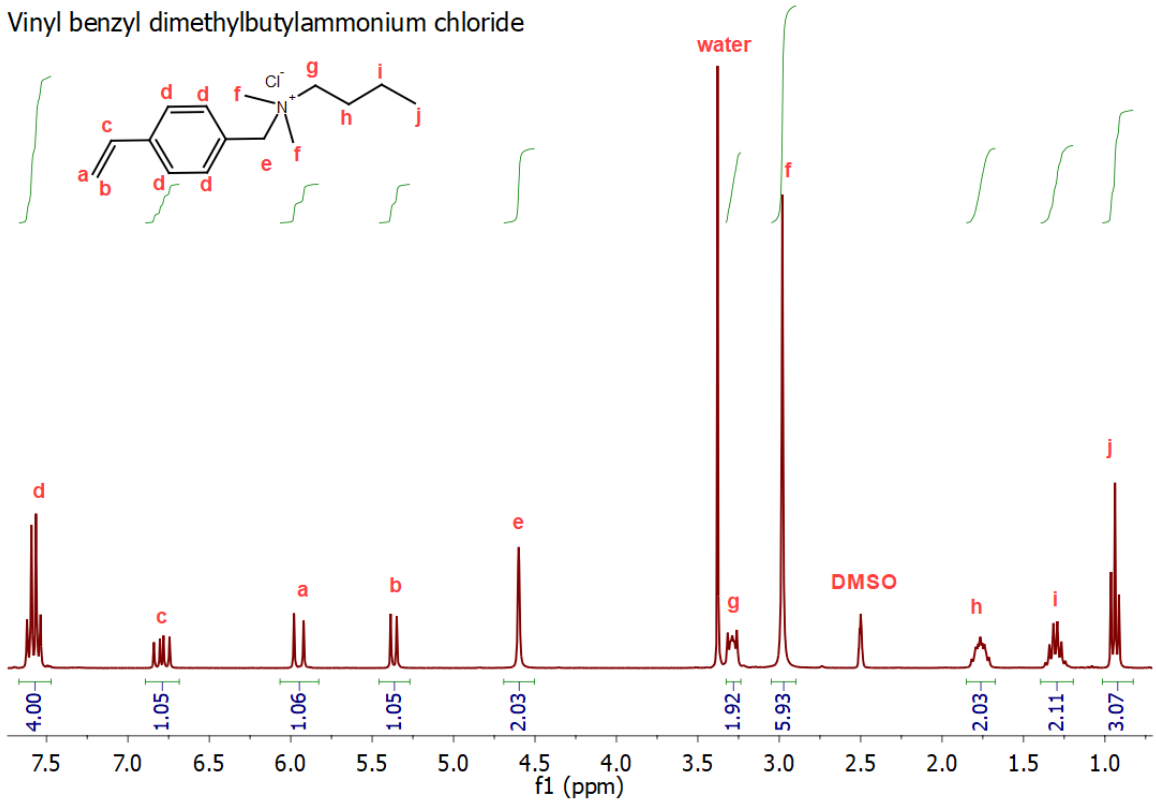

Figure S1. 1H NMR spectrum in DMSO-d6 of VBAC.

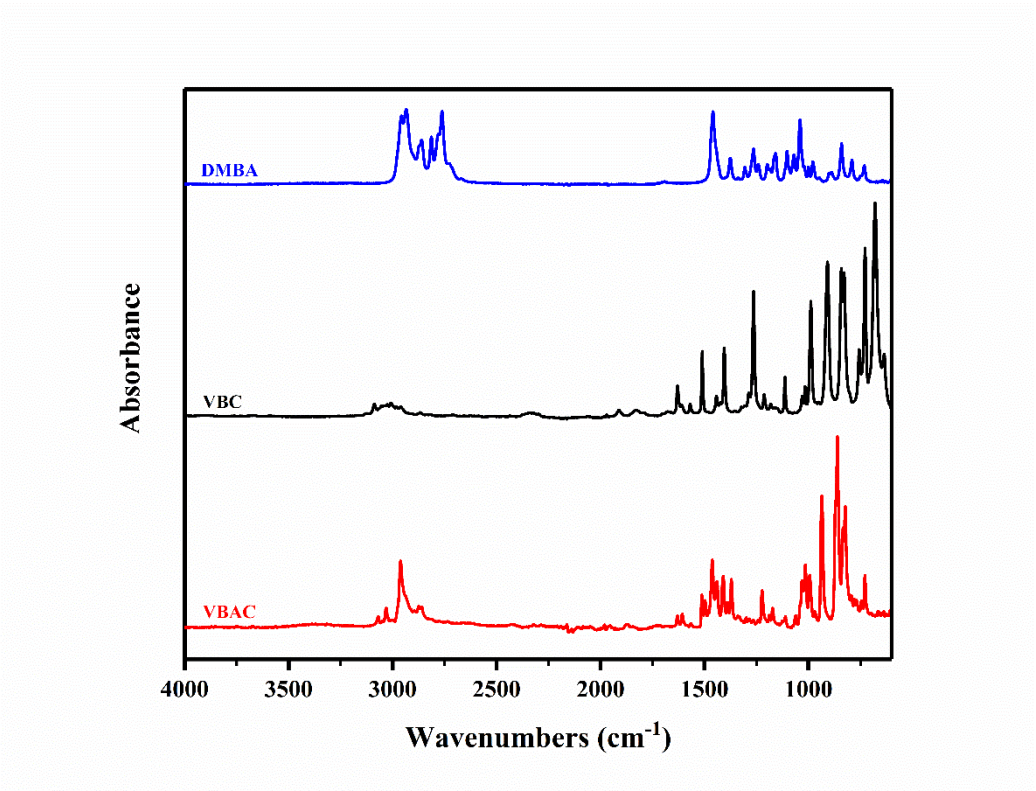

Figure S2. Global FTIR-ATR spectrum from 4000 to 600 cm^{-1} of DMBA, VBC and VBAC.

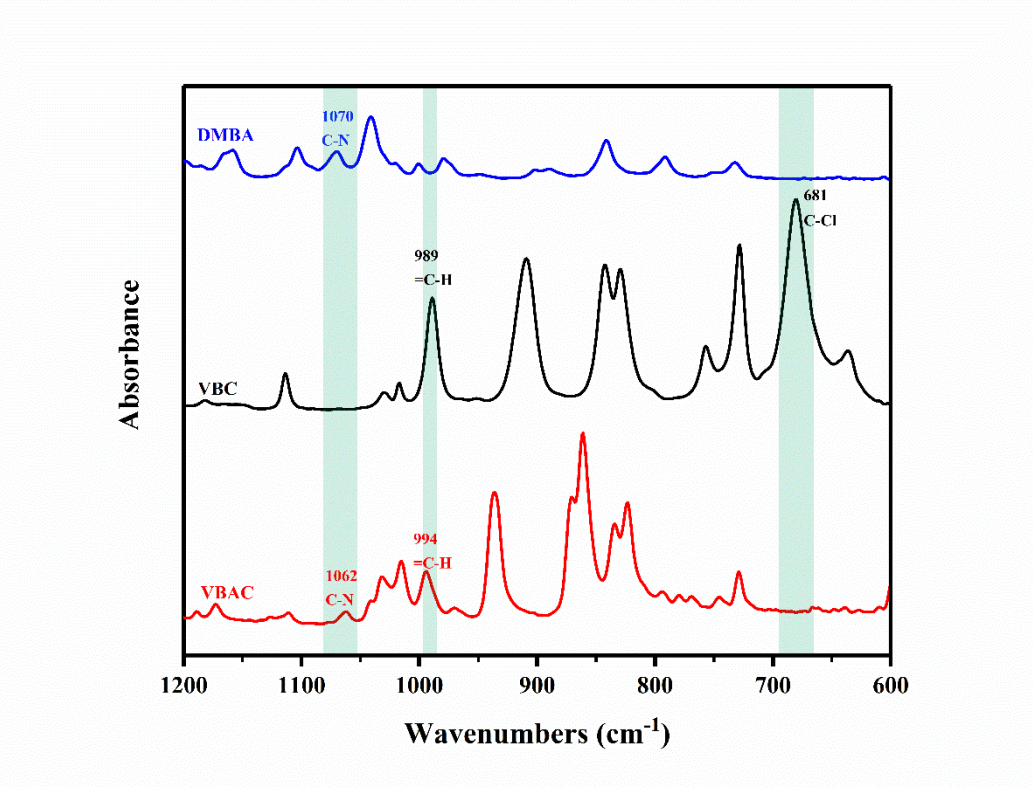

Figure S3. FTIR-ATR spectrum zooms from 1200 to 600 cm^{-1} of DMBA, VBC and VBAC.

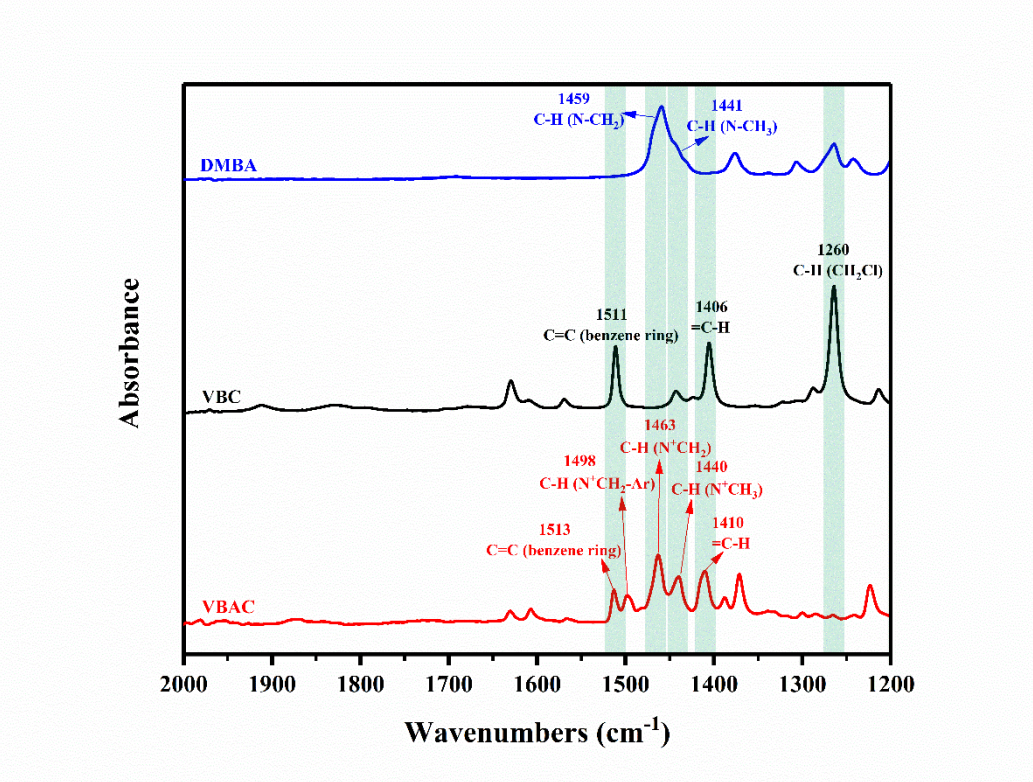

Figure S4. FTIR-ATR spectrum zooms from 2000 to 1200 cm^{-1} of DMBA, VBC and VBAC.

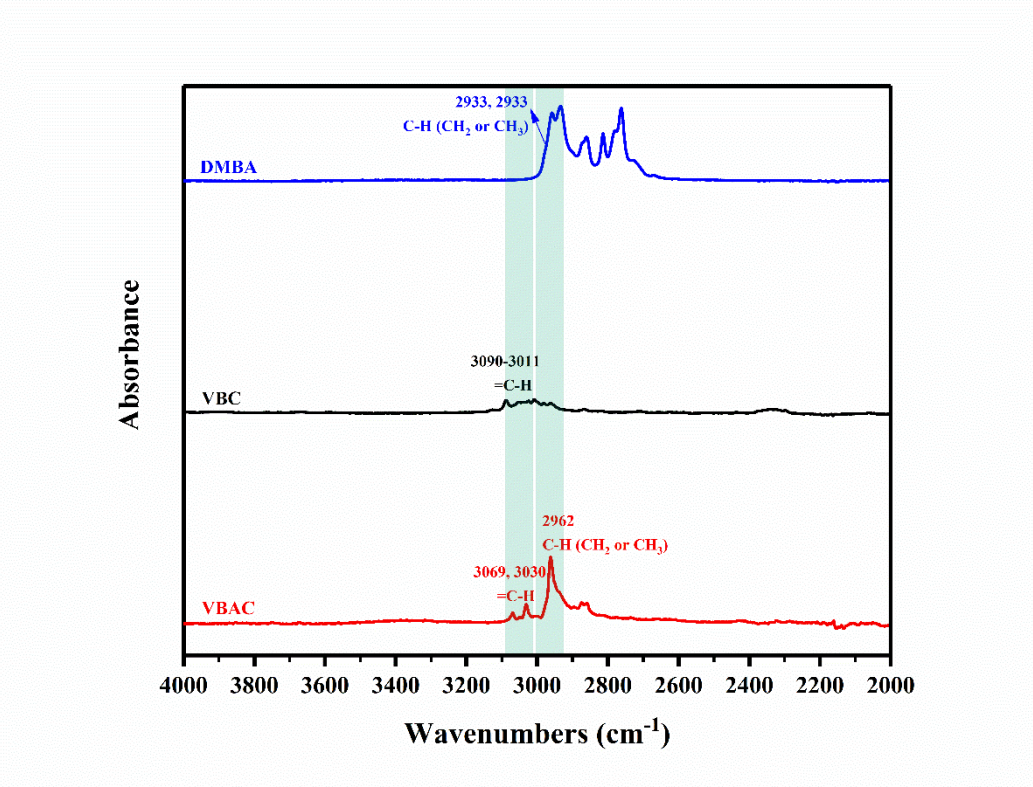

Figure S5. FTIR-ATR spectrum zooms from 4000 to 2000 cm^{-1} of DMBA, VBC and VBAC.

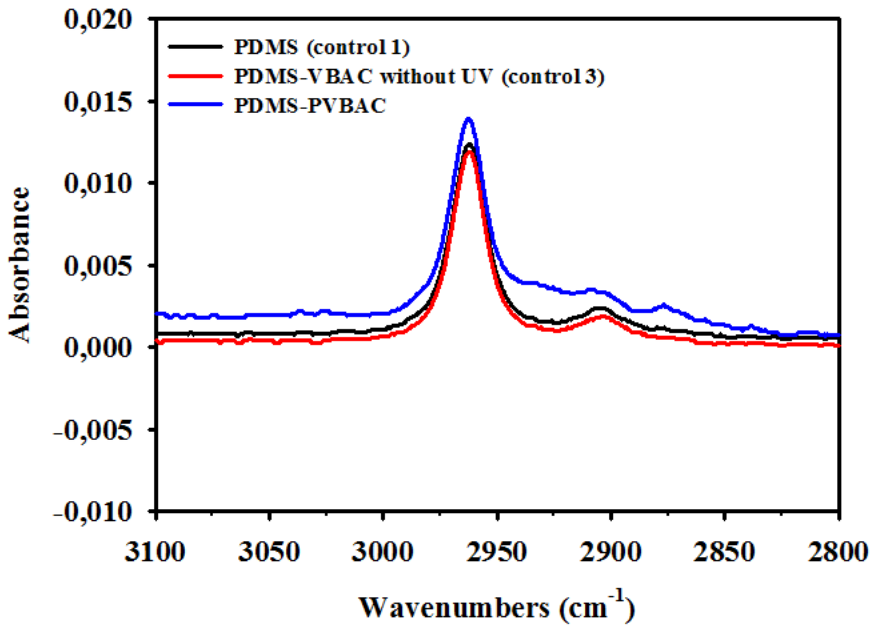

Figure S6. FTIR-ATR spectrum zooms (from 3100 to 2800 cm^{-1}) of (from top to bottom): PDMS (control 1), PDMS-VBAC without UV (control 3) and PDMS-PVBAC.

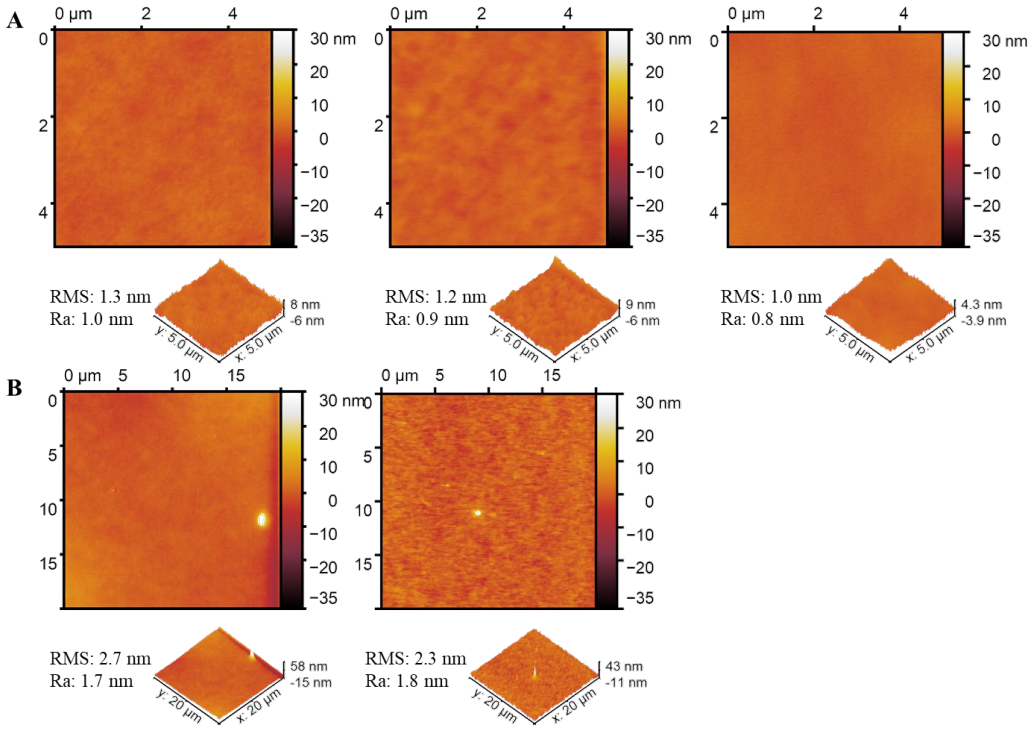

Figure S7. AFM images of PDMS surfaces at different size: A) 5×5 µm^2 with RMS and Ra of 1.2 ± 0.2 nm and 0.9 ± 0.1 nm respectively, B) 20×20 µm^2 with RMS and Ra of 2.3 ± 0.0 and 1.6 ± 0.3.

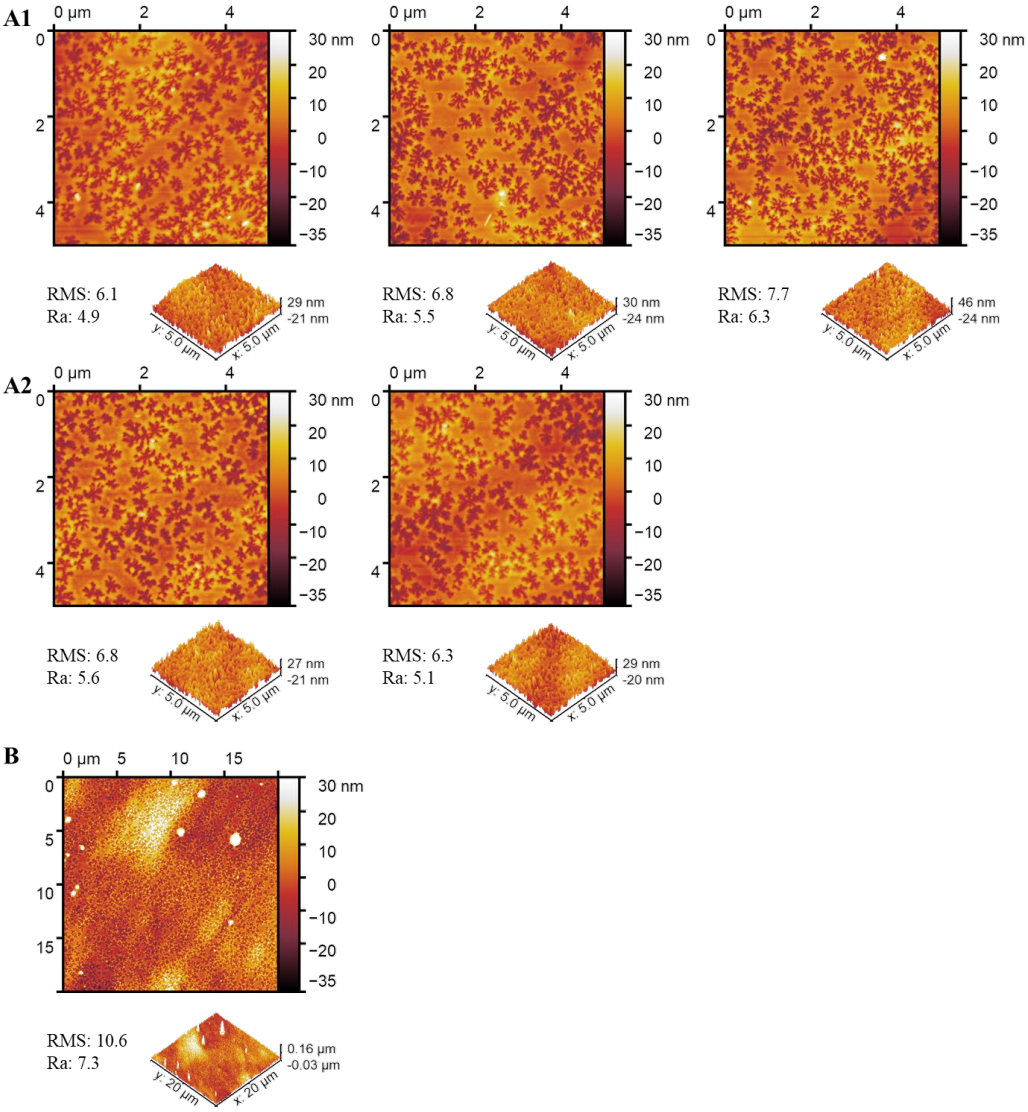

Figure S8. AFM images of PDMS surfaces prepared with monomer solution at 65wt% with 50 passages under UV (with water contact angle around 10°) at different size: A1-2) 5×5 µm^2 with RMS and Ra of 6.7 ± 0.6 nm and 5.5 ± 0.6 nm respectively, B) 20×20 µm^2.

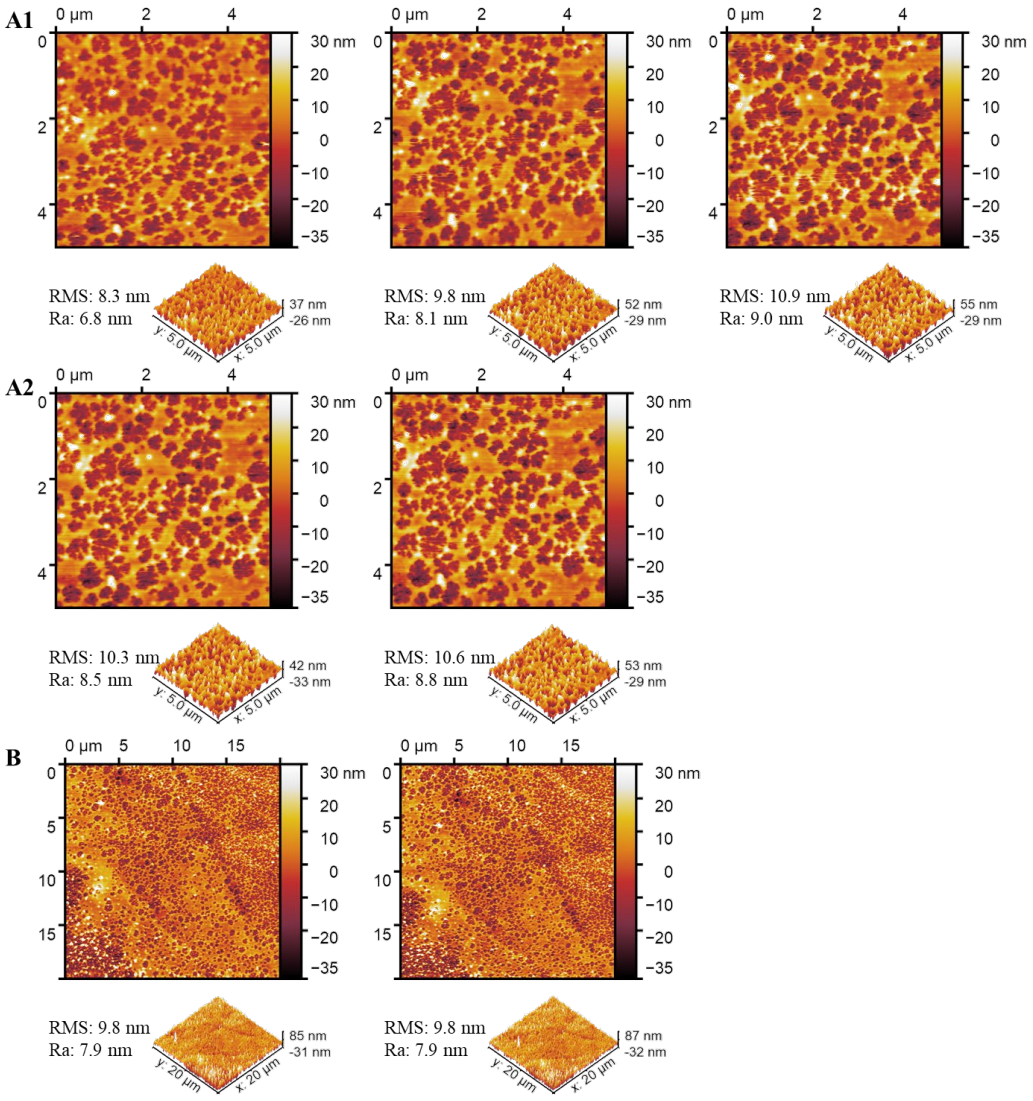

Figure S9. AFM images of PDMS surfaces prepared with monomer solution at 50wt% with 50 passages under UV (with water contact angle around 50°) at different size: A1-2) 5×5 µm^2 with RMS and Ra of 10.0 ± 1.0 nm and 8.3 ± 0.9 nm respectively, B) 20×20 µm^2 with RMS and Ra of 9.8 ± 0.0 nm and 7.9 ± 0.0 nm respectively.

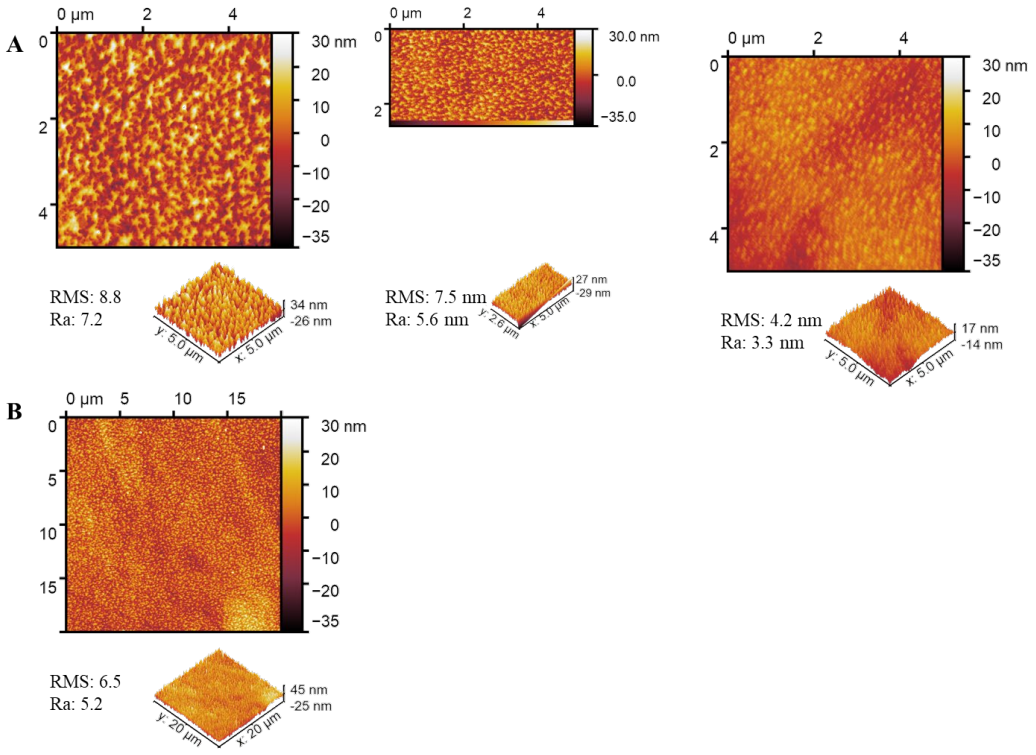

Figure S10. AFM images of PDMS surfaces prepared with monomer solution at 40wt% with 50 passages under UV (with water contact angle around 77°) at different size: A) 5×5 µm^2 with RMS and Ra of 6.8 ± 2.4 nm and 5.5 ± 2.0 nm respectively, B) 20×20 µm^2.

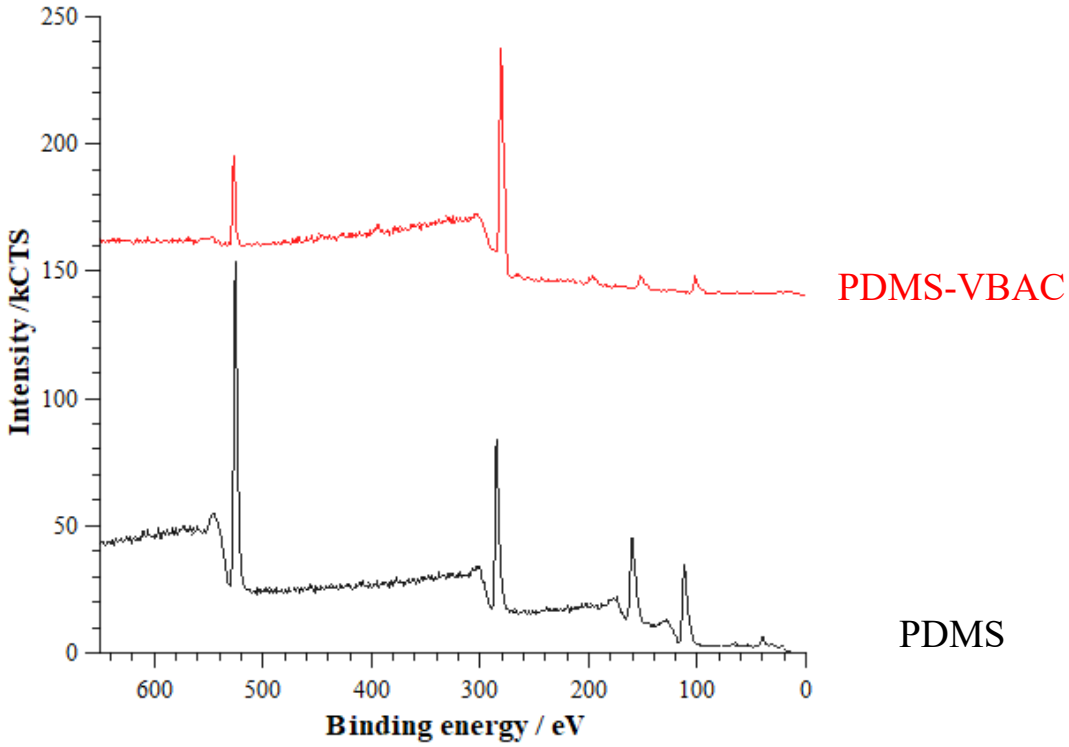

Figure S11. Survey XPS spectrum of PDMS-PVBAC surface and its unmodified PDMS control.

Table S1: Characteristic values used for the estimation of the organic layer thickness.

Elements	**Si2p**		**Cl2p**
Intensity (cts.s^{-1})	5841		1650
σ	0.817		2.28
T	2864		2975
Bulk concentration (mol.cm^{-3})	$n_{Si}^{PDMS} = 0.013$		$n_{Cl}^{layer} = 0.004$
Mean free path (nm)	$\lambda_{Si}^{PDMS} = 3.6$	$\lambda_{Si}^{layer} = 3.6$	$\lambda_{Cl}^{layer} = 3.4$

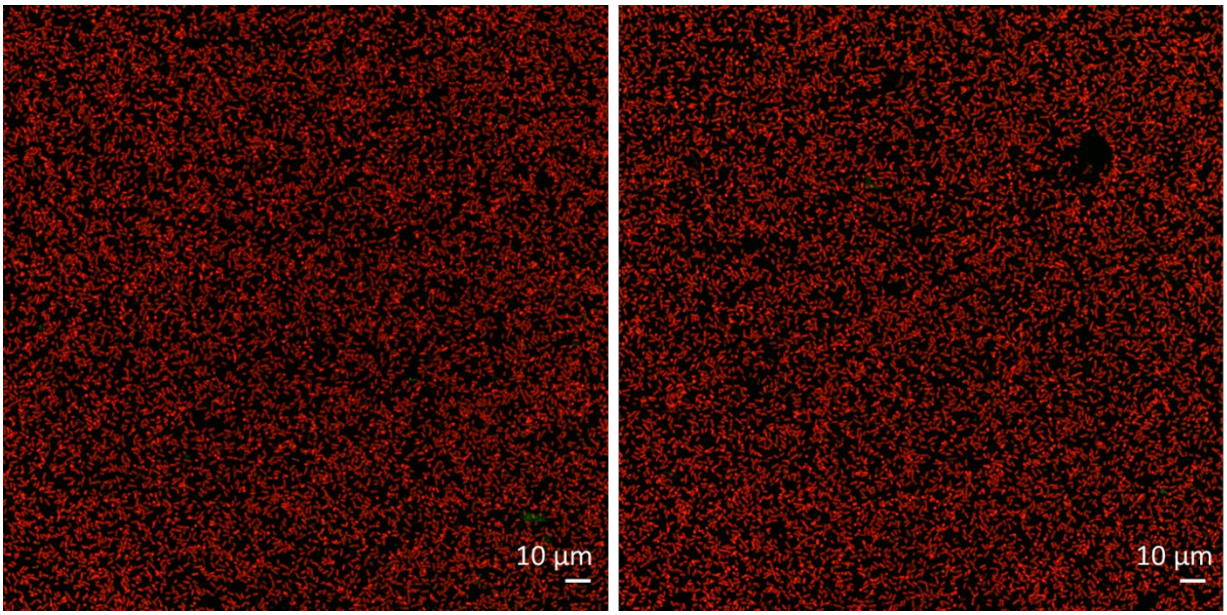

Figure S12. Supplemental fluorescence microscopy images of sessile *E. coli* cells stained with a marker of viability and deposited on surfaces of PDMS-PVBAC surfaces.

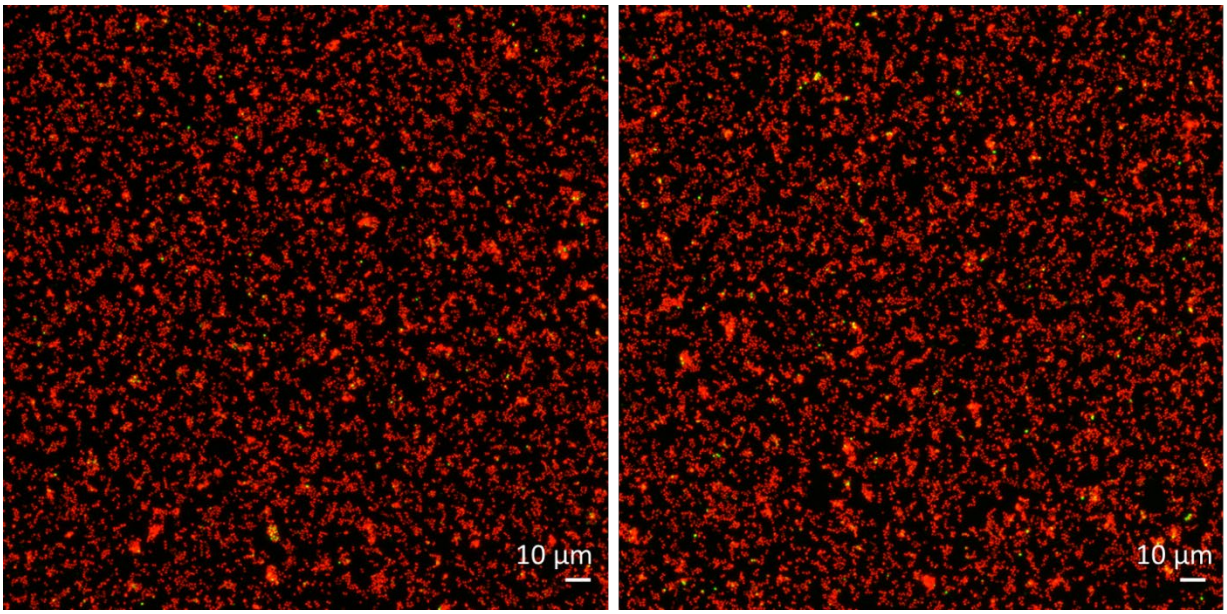

Figure S13. Supplemental fluorescence microscopy images of sessile *S. epidermidis* cells stained with a marker of viability and deposited on surfaces of PDMS-PVBAC surfaces.

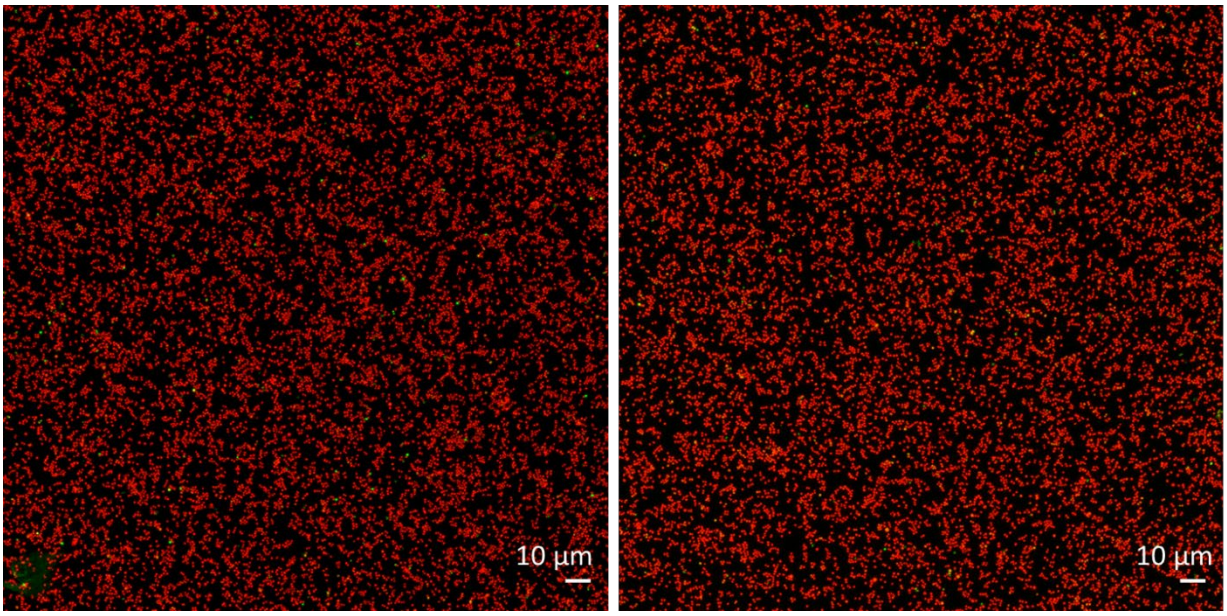

Figure S14. Supplemental fluorescence microscopy images of sessile *S. aureus* cells stained with a marker of viability and deposited on surfaces of PDMS-PVBAC surfaces.

IV.2 Article 4: Preparation of bactericidal surfaces with high quaternary ammonium content through photo-initiated polymerization of *N*-[2-(acryloyloxy)ethyl]-*N,N*-dimethyl-*N*-butylammonium iodide from native and thiolated PDMS surfaces

Yuzhen Lou[1], Damien Schapman[2], Dimitri Mercier[3], Stéphane Alexandre[4], Fabrice Burel[1], Pascal Thebault[4], Nasreddine Kébir[1]

[1] Normandie Université, INSA Rouen Normandie, Laboratoire PBS, UMR CNRS 6270 & FR 3038, Avenue de l'Université, 76801 Saint Etienne du Rouvray, France

[2] Normandie Université, UNIROUEN, IFR MP 23, PRIMACEN, 76821 Mont-Saint-Aignan, France

[3] PSL Research University, Chimie ParisTech – CNRS, Institut de Recherche de Chimie Paris, 11 rue Pierre et Marie Curie, 75005 Paris, France

[4] Normandie Université, UNIROUEN, laboratoire PBS, UMR CNRS 6270 & FR 3038, 76821 Mont-Saint-Aigan, France

Correspondence to:

Nasreddine KEBIR (E-mail: *nasreddine.kebir@insa-rouen.fr*)

Pascal THEBAULT (E-mail: *pascal.thebault@univ-rouen.fr*)

Abstract

N-[2-(acryloyloxy)ethyl]-*N,N*-dimethyl-*N*-butylammonium iodide was successfully photo-polymerized from native and thiolated PDMS surface, in the presence of benzophenone. The directly and indirectly grafted surfaces exhibited quaternary ammonium densities of about 10^{15} and 10^{17} charge/cm^2, respectively, and very high hydrophilicity compared to non-grafted surfaces. The live and dead tests performed by fluorescence microscopy revealed an effective contact bactericidal effect of this surface against *Escherichia coli* and *Staphylococcus epidermidis*.

Keywords: Quaternary ammonium; photo; grafting from; PDMS; bactericidal; thiol.

Introduction

Silicones, especially PDMS, is a very important family of polymer materials combining flexibility, hydrophobicity, chemical and thermal stability as well as biocompatibility. Silicone materials are widely used in the medical field, such as joint implants, catheters, kidney dialysis machines and breast prostheses [1-7]. However, like any organic material, it is subject to biofouling and bacterial contamination phenomena leading to serious health and economic problems [8]. Consequently, many approaches have been developed to overcome this problem [9-21].

The chemical tethering of antibacterial polymers onto the PDMS surface is one of the most serious routes to avoid its contamination and/or biofouling. Due to its chemical stability, PDMS often undergoes physical pretreatment, such as plasma, to generate functional anchoring sites, as for example hydroxyl groups, leading to very hydrophilic surfaces [11]. However, due to the fast diffusion of these groups within the bulk regenerating hydrophobicity, the post-chemical grafting must be performed rapidly (i.e., few minutes after) [12].

During the two last decades, two direct chemical routes for PDMS surface derivatization were described in the literature [13-21]. Hydrosilylation coupling reaction was used to graft bioactive polymers or molecules bearing carbon-carbon double bonds onto PDMS surface presenting Si-H groups [13-18]. The extent of Si-H groups can be varied by tuning the ratio between the PDMS components and/or their curing time [13-16]. Si-H groups can also be inserted on the surface by an acid-catalyzed reaction with poly(methylhydroxysiloxane) [17-18]. The use of the hydrosilylation process to prepare bactericidal PDMS surface bearing quaternary ammonium (QA) groups has been described in the work of Kebir *et al.* [13]. The authors synthesized a Poly(*N*,*N*-dimethylbutyl vinylbenzyl ammonium chloride) copolymer bearing carbon-carbon double bounds and grafted it by hydrosilylation onto PDMS surfaces. The extent of polymer grafting was tuned by varying the Si-H content through variations performed on the curing time or the relative composition in the silicone components. The charge densities of the obtained cationic PDMS surfaces ranged from 1.8×10^{14} to 2.8×10^{15} $N^{+}.cm^{-2}$ and the contact angle with water (WCA) varied from 102 and 88°, respectively. However, the direct grafting on fully cured PDMS offered the lowest surface coverage and wettability. Nevertheless, high killing efficiency (96-100%, respectively) against *E. coli* and *S. epidermidis* after 1h of contact was obtained in all cases.

Photo-induced grafting, in presence of benzophenone, have also been used in few studies for the direct chemical modification of PDMS surfaces. Thus, acrylic acid, [19] polyethylene glycol monoacrylate and polyethylene glycol diacrylate [20] have been photo-grafted through a mask to prepare micropatterned PDMS surfaces. Recently, antifouling PDMS surfaces were designed through simultaneous photo-grafting/photo-crosslinking reactions of zwitterionic polymers, i.e. poly(sulfobetaine methacrylate) or poly(carboxybetaine methacrylate), using poly(ethylene) glycol diacrylate as crosslinker [21].

Thus, in this work, we describe the use of this straightforward photochemical process to prepare highly QA-functionalized bactericidal cationic PDMS surfaces through surface photo-initiated radical polymerization of *N*-[2-(acryloyloxy)ethyl]-*N,N*-dimethyl-*N*-butylammonium iodide, in the presence of benzophenone as photo-initiator. The main objective of this work is to prepare new QA-PDMS surfaces with high bactericidal longevity and hydrophilicity comparing to analogues prepared by the hydrosilylation process. In addition, cationic PDMS surface with grafted acrylate ammonium chains have never been prepared neither by the hydrosilylation 'grafting to' nor by the photochemical 'grafting from' processes. It is to note that each chemical structure of the grafted polymer brings to the surface original physico-chemcial properties and biological activity spectra. We will start by describing the optimization of this process on the native and fully cured PDMS surface. Then, in order to increase the reactivity of this surface, thiol groups will be introduced (PDMS-T), using the same photochemical process. The polymer grafting on the native and thiolated PDMS surfaces will be studied by FTIR-ATR and XPS spectroscopies as well as by contact angle and charge density measurements. The antimicrobial properties of the cationic surfaces will be investigated by the live and dead fluorescent test.

Experimental section

Materials

Sylgard® 184 was purchased from DOW chemical company (USA). 2-(dimethylamino)ethyl acrylate (98%) (DMAEA) and 1-iodobutane (99%) were purchased from Alfa Aesar. Dry methanol (99,8%), acetone and extra dry acetonitrile were purchased from Acros Organics. Pure hydroquinone was purchased from Prolabo. Dry diethyl ether and glass coverslip (18 mm×18 mm, Fisherbrand™) were purchased from Thermo Fisher Scientific. Pentaerythritol tetrakis (3-mercaptopropionate) (PTTMP) was purchased from Aldrich.

Benzophenone (BP) (≥99%) was purchased from Merck. Ultrapure water was obtained from a Milli-Q system (Siemens, France). All the chemicals were used without further purification.

S. epidermidis (ATCC 35984) and *E. coli* (K12 MG1655) strains were stored as frozen aliquots in brain heart infusion (BHI, Bacto, France) broth and 30 % of glycerol at -20 °C. The LIVE/DEAD Bacterial Viability Kit, L7007 (SYTO®9 dye, 1.67 mM / Propidium iodide, 18.3 mM) was purchased form Thermo Fisher Scientific. All solutions used for the antibacterial assay were sterilized by autoclave (121°C, 15 min).

Preparation of N-[2-(acryloyloxy)ethyl]-N,N-dimethyl-N-butylammonium iodide (AONAI)

N-[2-(acryloyloxy)ethyl]-*N*,*N*-dimethyl-*N*-butylammonium iodide (AONAI) was synthesized according to a procedure described in the literature, [22-24]with some modifications. Briefly, in a three-neck round-bottom flask equipped with magnetic stirring and a condenser, 1-iodobutane (0.0703 mol) and 2-(dimethylamino)ethyl acrylate (DMAEA) (0.06586 mol) were added dropwise to a vigorously stirred solution of dry acetonitrile (30 ml) containing a small amount of hydroquinone (0.03 g) at 40 °C under inert atmosphere. The mixture was left to react 48h under stirring. Then, the mixture was concentrated and added dropwise into a large excess (10 folds in volume) of dry diethyl ether. After 30 min, the recrystallized product was collected by filtration and dried under vacuum (yield: 91 %).

^{1}H NMR (300 MHz, DMSO) δ: 6.39 (dd, J = 17.3 and 1.7 Hz, 1H), 6.21 (dd, J = 17.1 and 10.3 Hz, 1H), 6.05 (dd, J = 13.7 and 1.5 Hz, 1H), 4.55 (s, 2H), 3.79 – 3.61 (m, 2H), 3.41 – 3.35 (m, 2H), 3.11 (s, 6H), 1.81 – 1.56 (m, 2H), 1.37 – 1.15 (m, 2H), 0.94 (t, J = 7.5 Hz, 3H). FTIR-ATR (cm^{-1}): 3031 (=C-H stretching vibration); 3000-2800 (C-H stretching vibration in CH, CH_2 and CH_3 groups); 1730 (C=O stretching vibration of the ester group); 1634(C=C stretching vibration of the vinyl group); 1491 (C-H bending vibration in N^+-CH_2 (ester side)); 1464 (C-H bending vibration in N^+-CH_2 (butyl chain side)); 1448 (C-H bending vibration in N^+-CH_3); 1406 (=C-H bending vibration); 1063 (C-N stretching vibration).

Preparation of PDMS film

15 g of a mixture of the two parts of Sylgard® 184, i.e. base and curing agent, at a ratio of 10:1 (w/w), were casted into a low-density polyethylene petri dish square (120×120×17 mm^3). The mixture was then degassed under vacuum, until the air bubbles were completely removed. The PDMS film was formed after two days at room temperature and was cut into 18

× 18 mm^2 squares with a thickness less than 1 mm. The curing time can be considerably reduced by increasing the temperature (few hours at 70°C and about 1h at 120°C) [13].

Preparation of PDMS-PAONAI and PDMS-TPAONAI surfaces

PDMS films were first immersed in an acetone solution containing 20 wt% of BP for 30 min to absorb enough BP for the photo-grafting. The samples were quickly washed with methanol and then placed on a plate to dry in the dark. Then 50 to 80 µl of an acetone solution containing PTTMP was applied to the dry samples and covered with a glass slide so that the PTTMP solution was spread evenly over the surface of the PDMS by capillary force. The PDMS assembly was placed in a UV conveyor (UV Fusion Light Hammer 6), and irradiated with the UV light emitted from a small diameter electrodeless bulb combined with the elliptical reflector, microwave-powered lamp (500 watts/inch) at a lamp-PDMS distance of 53 mm. Then, the BP-initiated photo grafting and photopolymerization of the PTTMP took place from the PDMS surface. After grafting, substrates were collected and washed in acetone overnight with slight shaking and washed again with acetone the next day before drying to remove all unreacted BP or PTTMP. The substrates were noted PDMS-T. Then, photopolymerization were realized by using the methanol solution containing AONAI in the same way on substrate of PDMS or PDMS-T and they were noted PDMS-PAONAI and PDMS-TPAONAI, respectively.

After modification, the samples were collected by immersion in water to detach from the glass slide and then washed with methanol three times. Then, the samples were washed in methanol overnight with slight shaking and washed again with methanol the next day before vacuum drying to ensure that all unreacted monomer and ungrafted BP or AONAI compounds were removed.

Characterizations

^{1}H NMR spectra were recorded on a Bruker 300 MHz spectrometer. The ATR-FTIR spectra were recorded on a Nicolet IS-50 FTIR (Thermo, USA) spectrometer using the VariGATR accessory (Harrick Scientific, Pleasantville, NY) and the DTGS detector on three independent samples for each experimental condition, with a wave-number range between 600 and 4000 cm^{-1}. The data was obtained with a spectral resolution of 4 cm^{-1} by 250 scans.

Static and dynamic water contact angles measurements were performed using a contact angle goniometer “digidrop” (United Kingdom) in air at room temperature on at least three independent samples.

X-Ray Photoelectron spectroscopy (XPS) analysis was performed using a Thermo Electron Escalab 250 spectrometer, with a monochromatic Al Kα X-ray source (hν = 1486.6eV) operating at a pressure around 10^{-9} mbar. The spectrometer was calibrated using Au4f7/2 at 84.1eV. The take-off angle was 90° and the analyzed surface was a 500µm diameter disk. Survey spectra were recorded with a pass energy of 100eV and a step of 1eV and C1s, O1s, Si2p high level resolution spectra were recorded with a pass energy of 20eV and a step of 0.1eV. The charge effect was evaluated using the main component of the C1s peak, associated with C-C/C-H hydrocarbons with a binding enery of 285eV. Spectra were recorded using the Thermo Avantage software and analyzed using CasaXPS software.

The topography of PDMS surfaces before and after modification were analyzed by using a Nanoscope 8 Multimode microscope (Bruker Nano Surfaces, Santa Barbara, CA, USA). Imaging was achieved in the air using the PeakForce®-QNM mode with a 100µm piezoelectric scanner. A silicon (RTESPA-300, Bruker) cantilever with a spring constant of about 40 N/m and a silicon tip was used. Images were obtained with a PeakForce tapping frequency of 1 kHz and the auto-amplitude on. The AFM imaging was performed in multiple locations on at least two independent samples at two scan sizes: 5 x 5 and 20 x 20 μm^2. All images are presented in the height mode and are top view images. Flatten & three points levelling operations were usually done using the Gwyddion AFM software.

Determination of the surface accessible quaternary ammonium density

Modified and unmodified PDMS surfaces (1.8 × 1.8 cm^2) were immersed in a solution of fluorescein sodium salt (1% in distilled water) for 10 min. Afterwards, the unreacted fluorescein molecules were removed by washing with distilled water. The samples were then placed in 3 mL of a 0.5% solution of hexadecyltrimethyl ammonium bromide to exchange with the bounded fluorescein molecules under ultrasound for 15min. 0.45 mL of saturated $NaHCO_3$ solution was added after sonication. Then the absorbance of solution was recorded at 501 nm. The fluorescein concentration was then calculated using a calibration curve.

Antibacterial activity assay (Live/Dead test)

A 130 µl droplet of *E. coli* or *S. epidermidis* suspension in distilled water (5.8×10^8 cells/ml) was spread on the modified surfaces (1.8 cm×1.8 cm) using a glass slide with the same surface size for 1 h. Then the glass slide was taken away and the studied surface was washed by distilled water flow to remove the non-attached bacteria. After that, a 130 µl mixture of two fluorescent markers: the SYTO® and the propidium iodide, was deposed and spread on the

surface for 15 min. The mixture was diluted prior to use (20 µmol/l of SYTO®9). Images (1024x1024 pixels) of surfaces were acquired using an upright fixed-stage Leica TCS SP8 CFS confocal microscope (Leica Microsystems, Nanterre, France) equipped with diodes laser (Coherent, Les Ulis, France) at 488 nm to excite the SYTO®9 and at 552 nm to excite Propidium Iodide and a conventional scanner at 400 Hz. Using a 63x (1.40, oil immersion) objective, fluorescence emission was sequentially detected through hybrid detector (Leica Microsystems, Nanterre, France) in photon counting mode with a specific band from 500 to 540 nm for SYTO®9 and 580 to 630 nm for Propidium Iodide. Z-Stack's images were acquired using an adapted step-size from Nyquist Criteria. ImageJ (Rasband W.S., U.S. National Institutes of Health, Bethesda, Maryland, USA, http://imagej.nih.gov/ij/, 1997-2020) was used to adjust brightness and contrast and to perform z projections of 3D images (xyz) [25].

Results and discussion

Cationic polymers bearing quaternary ammonium (QA) groups exhibit high biocidal activity against bacteria, fungi, parasites and viruses. Moreover, this activity is dramatically dependent on the chemical structure of the polymer involving the hydrophilic-hydrophobic balance, the molecular weight and the length or nature of the alkyl chains of the QA groups [26-34]. For instance, Lu *et al*. [33] have prepared by quaternization poly(dimethylaminoethyl methacrylate (poly(DMAEMA)) with benzyl chloride (BC), butyl bromide (BB), dodecyl bromide (DB) or hexadecyl bromide (HB) and have found that polymers quaternarized with BC and BB exhibited the highest bactericidal activity in solution. Lafarge *et al*. [34] have prepared a copolymer based on poly(DMAEMA), quaternarized with butyl iodide and bearing propargyl groups, and have grafted it onto azidated PVC surface by the click HDC cycloaddition. The obtained cationic PVC surfaces exhibited a high bactericidal effect against *E. coli* and *S. epidermidis*.

In this work, we study the photo-initiated surface radical polymerization of *N*-[2-(acryloyloxy)ethyl]-*N*,*N*-dimethyl-*N*-butylammonium iodide) (AONAI) from native and thiolated PDMS surfaces, in order to design high QA-functionalized bactericidal surface. we anticipated that this process will offer a grafted polymer with an appropriate molecular weight and/or surface charge density that promotes high and long-term bactericidal effect on the PDMS surface.

Study of the direct photo-initiated polymerization of AONAI from native and thiolated PDMS surfaces (preparation of PDMS-PAONAI and PDMS-T-PAONAI)

N-[2-(acryloyloxy)ethyl]-*N*,*N*-dimethyl-*N*-butylammonium iodide (AONAI) monomer was synthesized by the reaction of 1-Iodobutane with 2-(dimethylamino)ethyl acrylate (DMAEA) in acetonitrile at 40°C for 48h, in the presence of hydroquinone as a stabilizer avoiding the self-polymerization of the acrylate monomer. The pure monomer was obtained by recrystallization and was soluble in water and alcohol solvents.

The ^{1}H NMR spectrum (Figure S1) of the obtained monomer mainly revealed the signals of protons of the carbon-carbon double bonds at 6.02 to 6.38 ppm and the protons of methyl and methylene groups in the α position to the ammonium group from 3.1 to 3.7 ppm, respectively. In addition, the FTIR analysis showed the complete conversion of the amine group into an ammonium group, through mainly the appearance of new bands at around 1491 and 900-950 cm^{-1} (Figures S2, S3, S4 and S5).

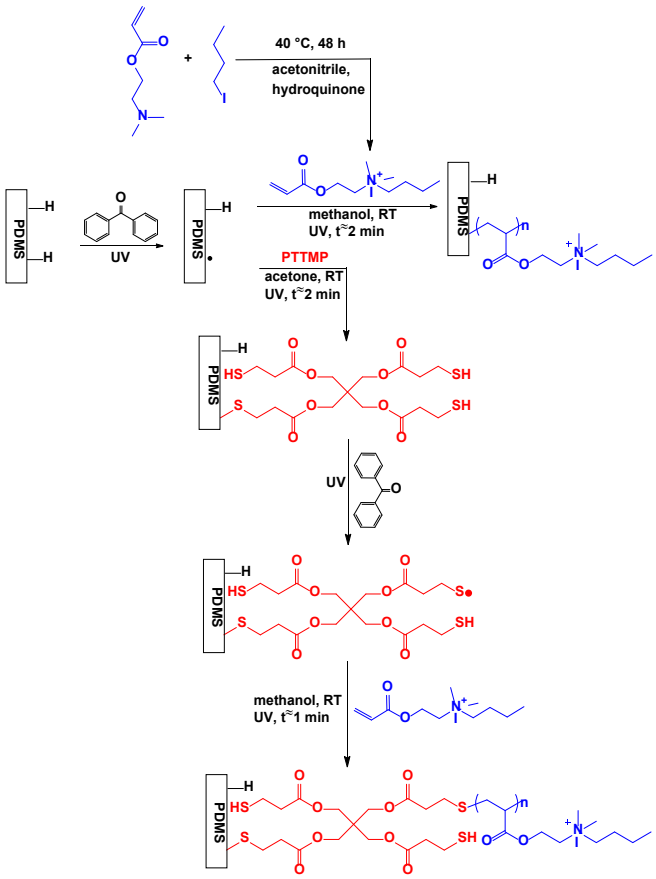

Scheme 1. Synthesis of N-[2-(acryloyloxy)ethyl]-N, N-dimethyl-N-butylammonium iodide (AONAI) and its photo-polymerization from the PDMS surface with or without Pentaerythritol tetrakis (3-mercaptopropionate) (PTTMP) pretreatment.

The radical photo-polymerization of the acrylate ammonium monomer from the native PDMS surface was initiated by benzophenone (Scheme 1) and was monitored at several reaction times (number of passages under UV) and concentrations of the started monomer solution. The studied PDMS film was a totally cured Sylgard®184 prepared at the conventional ratio of PartA/PartB = 1/10. A drop of the acrylate ammonium monomer solution was spread on the PDMS surface by deposing a thin glass plate on it. The sample was then placed in the UV conveyor for 1.55 s of UV exposure by passage. 50 to 90 passages were used, depending on the grafting efficiency. Three PDMS surface controls were also prepared, i.e. untreated PDMS (control 1), PDMS treated with methanol and UV (80 passages) (control 2) and PDMS treated with a monomer solution (76wt%) during 80 passages in the conveyer without UV exposure (control 3).

The extent of polymer grafting onto silicone surfaces was evaluated by water contact angle measurements (Figures 1, Tables 1). PDMS controls (1, 2 and 3, Table 1) displayed water contact angle values around 108±2, 99±7 and 105±3°, respectively, which are consistent with the high hydrophobicity of PDMS and suggesting no modification of the PDMS surface properties without UV.

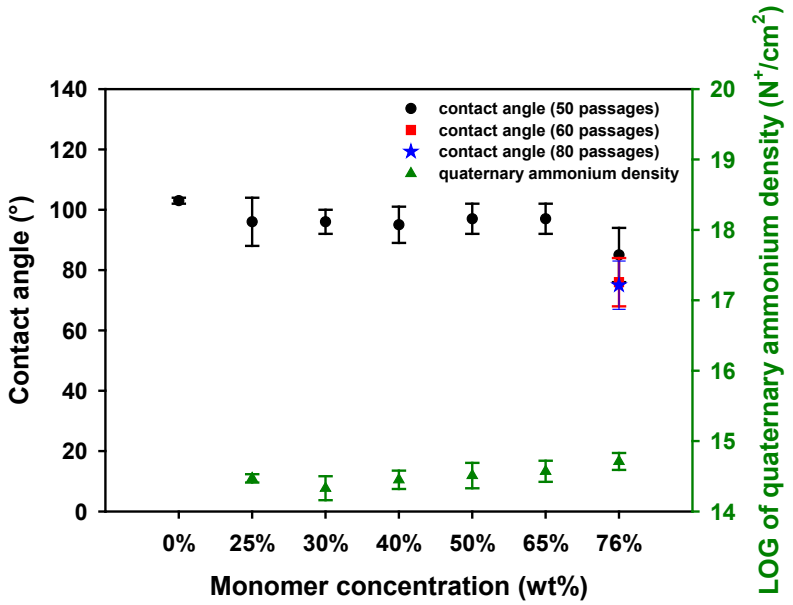

Figure 1. Water static contact angle of directly modified PDMS with a series of monomer concentration solution: 25wt%, 30wt%, 40wt%, 50wt%, 65wt% and 76%, using 50, 60 and 80 passages under UV. Values of Log of quaternary ammonium density were recorded for 50 passages.

The influence of the monomer concentration on the extent of polymer grafting onto the surface after 50 to 80 passages under UV was first studied (Figure 1). One can observe that for a monomer concentration ranging from 25 to 65 wt% and a number of passages under UV of

50, the water contact angle slightly decreased from 108° to around 95°, which suggests a weak surface grafting efficiency. For a monomer concentration at 76 wt%, the average water contact angle value decreased to around 85°. At this concentration, when the number of passages was increased to 60 or 80, the average water contact angle fell to a steady value around 75°, which was considered as the optimal value.

Measurement of the dynamic water contact angles were achieved on the optimal surface (Table 1). It is noteworthy that the advancing angle (AA) is corelated to the wettability of the hydrophobic part of the surface while the receding angle (RA) arise from the hydrophilic part. For the direct surface modification, the values of AA, RA and the hysteresis (AA-RA) changed dramatically after the polymer grafting. The PDMS surface treated only with methanol (control 2) or with AONAI without UV (control 3) did not exhibit any significant change on the surface comparing to the native one (control 1). AA dropped from 116 to 83°, RA dropped from 58 to 9° and hysteresis increased from 57° to 74° (Table 1, control 1 and PDMS-AONAI, respectively). However, the increase of the hysteresis is usually ascribed either to a physical (roughness) and/or chemical (gradient of grafting density) heterogeneities of the prepared surface.

The contact killing capacity of quaternary ammonium surfaces is directly linked to their surface charge density. Indeed, it has been shown in many studies that the surface must display a minimal charge density value of 10^{14} $N^+.cm^{-2}$ to kill effectively *E. coli* and *S. epidermidis* [13, 34-37]. The charge density values of the cationic PDMS surfaces prepared at different monomer concentrations and passages are presented in Figure 1 and Table 1. One can observe charge density values ranging from around 10^{14} to 10^{15} $N^+.cm^{-2}$. The optimal surface, obtained with a monomer solution at 76 wt% and 60 passages under UV, exhibited a charge density value of $(2.5\pm0.6) \times 10^{15}$ $N^+.cm^{-2}$ suggesting, anyway, a high potential of bacterial killing.

Table 1. Data of contact angles measurements and surface charge densities on the optimal treated PDMS surfaces and their controls.

Samples	Static θ_{water} (°)[a]	Dynamic θ_{water} (°)[a]			QA density ($N^+.cm^{-2}$)	Roughness by AFM[b] (nm)	
		AA	RA	Hyst		Ra	RMS
PDMS (control 1)	108±2	116±3	58±4	57±2	ND	1.4	2.4
PDMS-MeOH (control 2)	99±7	121±8	45±10	77±2	ND	/	/
PDMS-AONAI without UV (control 3)	106±3	116±1	40±4	76±5	ND	/	/
PDMS-PAONAI	75±8	83±2	9±1	74±1	(2.5±0.6) $\times 10^{15}$	11.2	18.2
PDMS-T (control 4)	97±8	121±2	68±1	53±2	ND	2.8	3.8
PDMS-T-AONAI without UV (control 5)	103±3	116±1	39±5	77±5	ND	/	/
PDMS-T-PAONAI	28±8	44±4	15±4	29±0	(9.6±0.3) $\times 10^{16}$	7.6	10.2

[a] **θ_{water}**: contact angle with water; **AA**: Advancing Angle; **RA:** Receding Angle; **Hyst**: Hysteresis (AA-RA).

[b] Ra: arithmetic roughness, RMS: Mean Square roughness.

Overall, the direct photo-grafting process provided an effective surface modification after full crosslinking of the PDMS compared to the hydosilylation process performed on similar surfaces [13], with respectively, charge density values around 10^{15} N^+/cm^2 vs. 10^{14} N^+/cm^2 and WCA of 76° vs. 102°. However, these values were very close to those obtained after the enhancement of the surface grafting by hydrosilylation, using partially cured PDMS or by changing the A/B ration of the Sylgard 184 components.

Thus, the direct photo-initiated polymerization of the acrylate ammonium monomer from the native PDMS surface was not sufficient to get highly functionalized quaternary ammonium surfaces, as expected for a grafting from process.

As mentioned before, to enhance quaternary ammonium density, a thiolation pretreatment of the PDMS surface was performed. Indeed, by radical-initiation process, forming radical polymerization sites from thiol groups is clearly easier than from methyl groups. Thus, a drop of pentaerythritol tetrakis (3-mercaptopropionate) (PTTMP) in methanol solution was spread on the PDMS surface by mean of a glass plate. The PTTMP concentration was varied from 25 to 75 wt% with a number of passages under UV of 50 and the number of passages was varied from 30 to 100 for a PTTMP concentration at 50 wt% (Figure 2). One can observe that, regardless the thiolation conditions, the obtained water contact angle was around 100° (against 108° for the native PDMS) suggesting a degree of modification of the PDMS surface with PTTMP. However, since PTTMP is hydrophobic, the impact of the PDMS surface modification on its wettability was not significant.

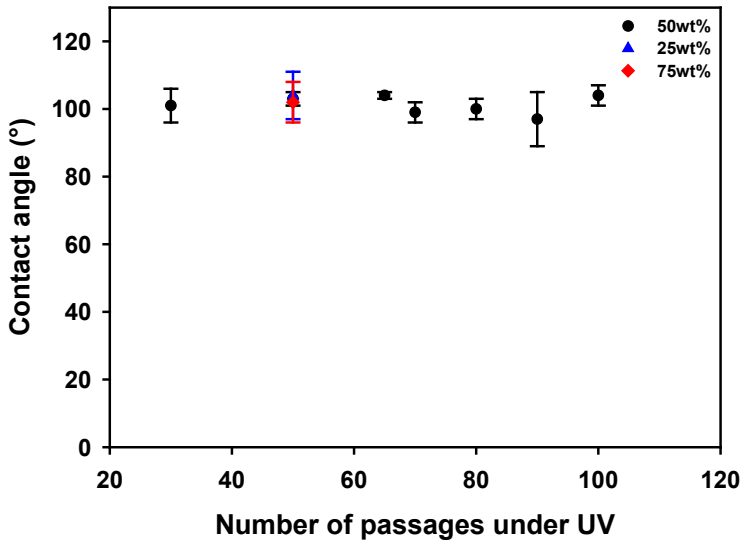

Figure 2. Water static contact angle of modified PDMS with PTTMP solution at different concentration and under several number of passages under UV.

The photo-initiated polymerization of AONAI from the thiolated surface was performed by varying the monomer concentration from 25 to 76 wt% and the number of passages from 50 to 60 with also different conditions of the thiolation step (Table 2). A monomer concentration of 76 wt% and 50 passages under UV were found to be the optimal conditions leading to the most hydrophilic and functionalized surface, with a contact angle with water around 28°.

Indeed, because of solubility and viscosity concerns, the concentration cannot be increased above 76wt%. In addition, when we increased the number of passages under UV both for thiolation and photopolymerization the value of the contact angle with water remained around 28° (Table 2).

The thiolated PDMS surface (Table 1, control 4) revealed AA, RA and hysteresis values of 121, 68 and 53°, respectively. After treatment with the monomer solution in the absence of UV (control 5), a slight decrease of the RA was observed under room conditions suggesting a low degree of grafting, which attest the high reactivity of thiol groups. After the polymer grafting under UV, the optimal modified surface showed a dramatical decrease of these three parameters to 44, 15 and 29°, respectively, suggesting a very high surface coverage.

The intermediate cationic surfaces exhibited charge density values slightly above 10^{15} $N^{+}.cm^{-2}$, whereas the optimal surface displayed a value close to 10^{17} $N^{+}.cm^{-2}$ suggesting a very high potential of bacterial killing. These results demonstrated the importance of the pretreatment by thiolation to have the highest surface coverage and grafting density.

Thus, the optimal grafted surface exhibited higher charge density and hydrophilicity values comparing to the best QA-PDMS surface prepared by hydrosilylation. i.e 10^{17} N^{+}/cm^{2}, vs 10^{15} N^{+}/cm and WCA of 28° vs. 88°.

In summary, for all the next studies, the direct modification of the native PDMS surfaces was performed with a monomer solution at 76 wt% with 60 passages under UV and the indirect modification was performed on thiolated PDMS surfaces treated with a monomer solution at 76 wt% with 50 passages under UV (Table 1). For the thiolation step, a solution of PTTMP at 50 wt% with 90 passages under UV was used (Table 2).

Table 2. Water static contact angle and surface charge densities of modified PDMS with monomer solution by using PDMS pretreated with PTTMP (PDMS-T) under different conditions.

P(T)[a]	P(AONAI)[b]	$C_{(AONAI)}$ (wt%)[c]	θ_{water} (°)[d]	QA density ($N^+.cm^{-2}$)
50	50	25	57±26	$(4.3\pm0.7)\times10^{15}$
50	50	30	54±25	$(3.4\pm0.6)\times10^{15}$
50	50	40	63±24	$(3.6\pm0.04)\times10^{15}$
50	50	50	50±28	$(1.9\pm0.1)\times10^{15}$
50	50	65	52±20	$(1.8\pm0.5)\times10^{15}$
70	50	65	56±21	/
80	50	65	51±21	/
90	50	65	45±20	/
90	50	76	28±8	$(9.6\pm0.3)\times10^{16}$
100	60	76	27±11	/

[a] Number of passages under UV of PDMS with 50wt% PTTMP solution.

[b] Number of passages under UV of PDMS-T with monomer solution.

[c] The concentration of monomer.

[d] θ_{water}: contact angle with water.

Surface characterization by AFM

AFM analyses revealed the structural and topographical changes on the PDMS surfaces after thiolation as well as after direct and indirect photo-chemical polymerizations of the cationic monomer (Figure 3). The roughness values of the prepared PDMS surfaces compared to their controls are presented in Table 2. The native PDMS exhibited a very smooth surface with an arithmetic roughness of around 1.4 nm (Figure 3-A).

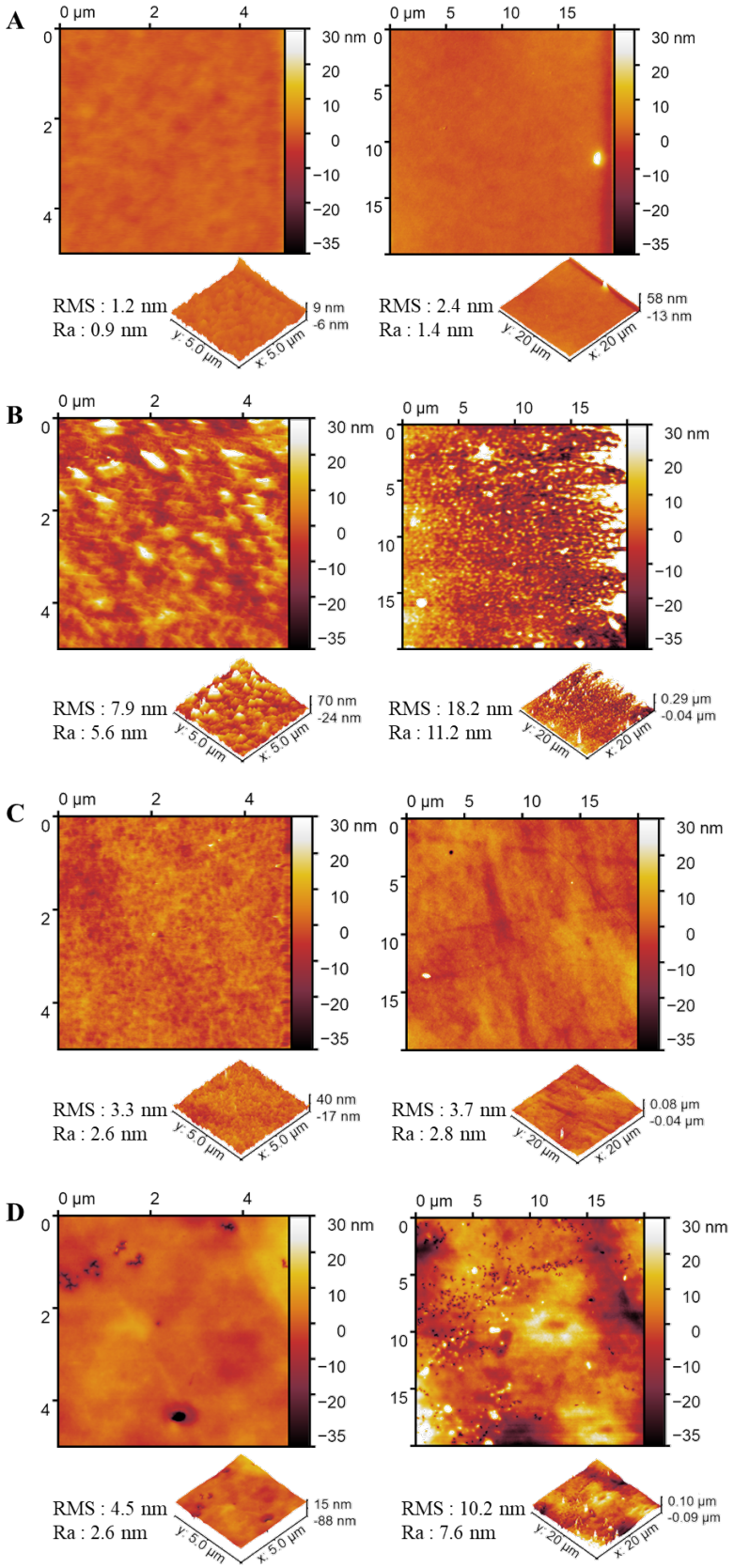

Figure 3. AFM images of (A) PDMS surface (control 1), (B) PDMS-PAONAI surface, (C) PDMS-T surface (control 4) and (D) PDMS-T-PAONAI surface.

The directly functionalized quaternary ammonium PDMS surface (PDMS-PAONAI) displayed an increased roughness around 11.2 nm with a lot of island suggesting an heterogenous grafting of the polymer (Figure 3-B). The roughness of the thiolated PDMS surface (PDMS-T) was around 2.8 nm without any aggregates (Figure 3-C), and increased to 7.6 nm after polymer grafting (PDMS-T-PAONAI) (Figure 3-D). However, a homogeneous grafting of the polymer was observed on the surface except for some areas where holes can be observed. AFM analysis confirmed contact angle and quaternary ammonium density values, i.e., that the thiolated cationic PDMS surface exhibited a higher surface coverage than the non thiolated one.

Spectroscopic surface characterizations

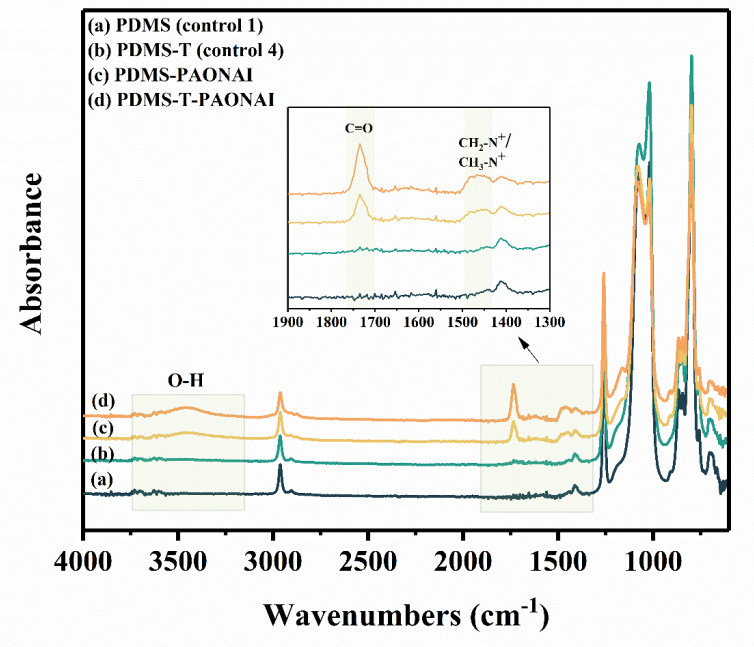

Figure 4. ATR-FTIR spectra of (a) PDMS (control 1), (b) PDMS-T (control 4), (c) PDMS-PAONAI and (d) PDMS-T-PAONAI.

The FTIR-ATR analysis (Figures 4, S6, S7 and S8) of the prepared cationic surfaces, compared to their controls, showed the appearance of a new band at around 1730 cm^{-1} arising from the carbonyl group of the grafted cationic polymer. The C-H bending vibration in N^+-CH_2 and N^+-CH_3 were observed between 1440 and 1498 cm^{-1}. A slight contribution of the butyl chain was also observed in the region of 2800 - 3100 cm^{-1} (Figure S6). Due to the hygroscopic character of the cationic surface, one can observe also a new band at 3300 cm^{-1} arising from the moisture. The FTIR spectra of controls 1 to 5 were identical, suggesting that: 1- The grafted PTTMP formed a very thin monomolecular layer, which was not detected by this technique; 2-

UV treatment was indispensable for the grafting reaction to occur; 3- the washing of the surface with methanol to remove the unreacted monomer was effective.

XPS analysis (Figure S9) afforded the atomic compositions of the different modified and unmodified PDMS surfaces. The results are depicted in Table 3. As expected, XPS analysis of the PDMS reference surface shows the presence of carbon, oxygen and silicon (survey spectra in the supporting information). The atomic composition is close to the expected one for PDMS. A weak enrichment in silicon and oxygen, could be ascribed to residual SiO_2 coming from the synthesis process of the PDMS and also to residual Si-H groups after curing. After grafting, new characteristic elements of the grafted organic layers were observed by XPS. Thus, for the PDMS-PAONAI surface, nitrogen (1.4 at. %) and iodine (1.1 at. %) were detected in a close concentration, as expected. PDMS-T surface exhibited a sulfur composition of 1.7 at.%. For the PDMS-T-PAONAI surface, nitrogen (4.9 at. %), iodine (3.9 at. %) and sulfur (1 at %) were observed. Combined to the increase of the C at. %, these results suggested a successful grafting for each step.

Actually, it is possible to determine an average thickness for each grafted layer. Fort the PDMS-PAONAI and PDMS-T, the thickness can be estimated using a simplified model considering a homogeneous and continuous organic layer on the top of the PDMS. For the PDMS-T-PAONAI which is composed of 2 distinct organic layers, a bilayer model has been used. Thus, the average thickness values have been calculated by solving the following set of three equations.

$$I_N = Kn_N^{PAONAI}\sigma_N\lambda_N^{PAONAI}T_N(1 - exp\frac{-d_{PAONAI}}{\lambda_N^{PAONAI}}) \quad (1)$$

$$I_S = Kn_S^{T}\sigma_S\lambda_S^{T}T_S(1 - exp\frac{-d_T}{\lambda_S^{T}})\exp(\frac{-d_{PAONAI}}{\lambda_S^{PAONAI}}) \quad (2)$$

$$I_{Si} = Kn_{Si}^{PDMS}\sigma_{Si}\lambda_{Si}^{PDMS}T_{Si}\exp(\frac{-d_T}{\lambda_{Si}^{T}})(\exp(\frac{-d_{PAONAI}}{\lambda_{Si}^{PAONAI}}) \quad (3)$$

With:

I: intensity of photoelectrons emitted by the element X; K: a spectrometer constant; σ: the photoionization cross section of the core level of the considered element; λ: the inelastic mean free path of the photoelectrons emitted by the core level of the considered element; n: the bulk concentration; T: the transmission function for the electrons emitted by the core level of the element and d the thickness of the organic layer (values are given in Table S1).

The average thicknesses of the organic layer in PDMS-PAONAI and PDMS-T have been estimated to be 0.7 and 0.2 nm, respectively. For the PDMS-T-PAONAI, a similar average thickness (0.2 nm) was obtained for the intermediate Pentaerythritol tetrakis layer (T layer), whereas the PAONAI layer exhibited and average thickness of 2.6 nm. However, this method has some limitations: (i) The density of the grafted polymer is assimilated to the density of its monomer, i.e. around 1g/cm^3, which is a rough approximation since the polymer is grafted as spaced brushes on the PDMS surface. The brushes could also contain ramifications due to chain transfer during the radical polymerization; (ii) The mathematical model doesn't take into account the surface roughness and the surface coverage by the grafted polymer. It considers that the polymer chains were perfectly arranged on the surface, which is also hypothetic and not actual; (iii) Since XPS detects only 10 nm of the extreme surface, the grafted density can be under estimated if the real thickness exceeds 10 nm, particularly in the case of the presence of islands. Usually, thicknesses obtained by this method are lower than 5 nm.

Thus, this method gives a way to express the polymer grafting density as an average thickness of a hypothetic homogeneous and compact polymer layer and not as an actual thickness. Indeed, if we take a look on AFM images, we can see that the difference in height between dark and light zones is around 60 nm. In addition, in many areas of the surface, the real thickness exceeded 10 nm, suggesting an under estimation of the grafting density and the average thicknesses determined by XPS.

Table 3. XPS elemental analysis of the optimal PDMS modified surface and its unmodified PDMS control

	C1s	O1s	Si2p	N1s	I3d	S2p
PDMS	43.4	26.4	30.2	--	--	--
PDMS-PAONAI	46.5	27.2	23.6	1.4	1.1	--
PDMS-T	47.1	28.3	22.9	--	--	1.7
PDMS-T-PAONAI	56.7	19.0	13.3	4.9	3.9	1.0

Assessment of the surface bactericidal properties

The bactericidal properties of the prepared cationic PDMS surfaces were studied by confocal fluorescent microscopy through the Live and Dead test, against *E. coli* (Gram-) and *S. epidermidis* (Gram+), two of the pathogens mostly involved in bacterial contaminations.

Actually, in the literature there are two suggested mechanisms for the bactericidal action of QA surfaces [38]. The most popular one suggests that long cationic polymer chains penetrate cells and thereby damage the membrane, like a needle that bursts a balloon. The second one suggests an ion exchange between the positive charges on the surface and the structurally critical mobile divalent cations within the membrane, which diffuse out of the membrane. The loss of these cations causes membrane destruction.

Bacteria were put in contact with the cationic surfaces as well as their controls during 1h, and then adhered bacteria were stained with a mixture of fluorescent probes that stained bacteria with damaged membrane in red and bacteria with intact membrane in green. The Live and Dead fluorescent images are presented in Figures 5, S10, S11, S12 and S13. One can observe that both thiolated (PDMS-T-PANONAI) and non-thiolated (PDMS-PANONAI) cationic PDMS surfaces exhibited a high bactericidal effect, i.e. quasi-only red bacteria were observed on contact with them (Figure 5-A2, B2, A4 and B4). Some residual green bacteria were observed in a few areas, often on other bacteria but not in contact with the cationic surface. Furthermore, the density of *E. coli* (Figure 5-A2 and A4) and *S. epidermidis* (Figure 5-B2 and B4) on the cationic surfaces was very high (around 10^6 cell/cm^2) and their attachment was very fast comparing to the non-cationic PDMS surfaces (controls 1 (PDMS) and 4 (PDMS-T)), for which no bacteria attachment was observed after 1h of contact. This suggests that the bacterial adhesion in this case is mainly governed by the electrostatic forces, since bacteria have an overall negative charge. This dependence of the bactericidal efficiency against *E. coli* and *S. epidermidis* as well as the bacterial adhesion on the charge density of cationic surfaces is in good agreement with the literature. For instance, the previously-mentioned azidated cationic PVC surface, grafted with an acrylate quaternary ammonium copolymer by the HDC click addition, exhibited a surface charge density around 6×10^{14} charge.cm^{-2}, bacterial densities around 5×10^5 cell/cm^2 with a killing efficiency around 99 % after 1h of contact [34]. Moreover, the prepared QA-PDMS surfaces displayed higher capacity in terms of bacterial killing capacity (around 100%) compared to analogues prepared by the hydrosilylation process after full PDMS curing (around 96%) [13]. On the other hand, the analogue surfaces prepared before curing or

with higher Si-H content in the component mixture led to similar short-term bactericidal effect [13].

Moreover, the long-term biocidal functionality of QA coatings depends on the surface charge density and also on the concentration of the bacteria exposed to the surface (the challenge). Murata *et al*. [38] have shown that cationic surfaces with charge densities above 5.10^{15} charges/cm^2, are able to kill at least a monolayer of *E. coli* cells (10^8 CFU/cm^2), before going through fouling and loss of bioactivity. Under real-world conditions, extreme infection or contamination occurs when the bacterial concentration is about 10^3 CFU/cm^2, which is far from the concentration that passivates the prepared cationic surface with around 10^{17} charges/cm^2. Therefore, the passivating bacterial concentration, can take a very long time to be reached, depending on the number of bacteria to which this surface is exposed.

Finally, quaternary ammonium may exhibit cytotoxicity in solution, depending on concentration, time exposure and chemical structure [39-41]. However, the biocompatibility of QA surfaces needs further investigations to define clearly their potential of application in the medical field [42]. Elsewhere [13], we have established that plasmatic proteins, owing to their electrical charges, adsorbed on QA surfaces, which caused their fouling after only 24 hours of contact. Therefore, at this time, we can suggest to employ this kind of surface in non-blood contact silicone devices, such as the external surfaces of catheter chambers and extracorporeal equipment.

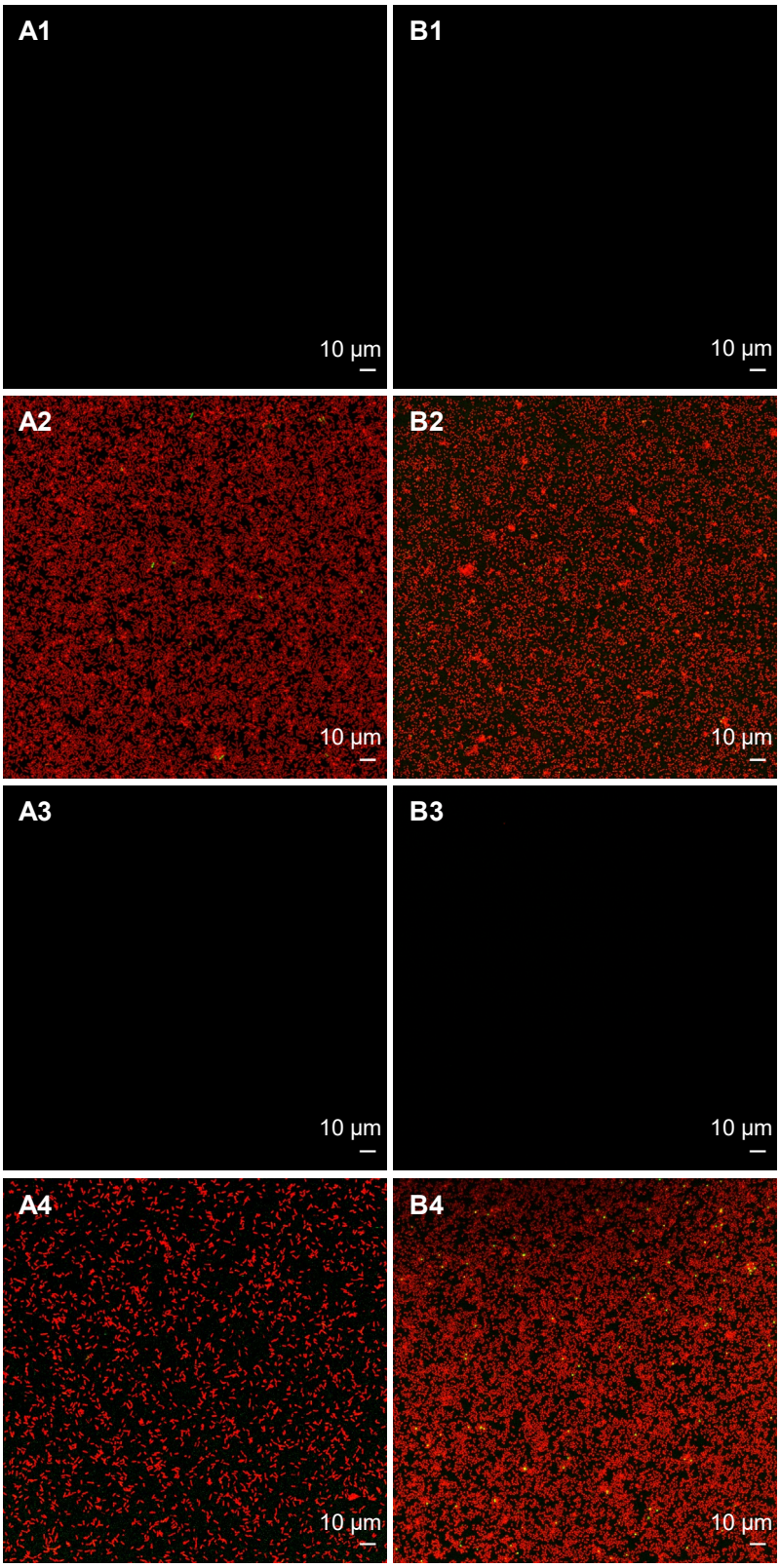

Figure 5. Fluorescence microscopy images of sessile bacteria cells stained with a marker of viability and deposited on surfaces of modified and unmodified PDMS surfaces: (A1) *E. coli* on unmodified PDMS surface (control 1), (A2) *E. coli* on cationic PDMS-PAONAI surface, (A3) *E. coli* on PDMS-T surface (control 5), (A4) *E. coli* on cationic PDMS-T-PANONAI surface, (B1) *S. epidermidis* on unmodified PDMS surface (control 1), (B2) *S. epidermidis* on cationic PDMS-PAONAI surface, (B3) *S. epidermidis* on PDMS-T surface (control 5), (B4) *S. epidermidis* on cationic PDMS-T-PANONAI surface.

Conclusion

In this work, we have evidenced the possibility of designing bactericidal cationic PDMS surfaces, with tunable quaternary ammonium content and hydrophilicity, by a benzophenone photo-induced polymerization of an acrylate ammonium monomer from native and thiolated PDMS surfaces. The direct photopolymerization led to an optimal PDMS surface with a water contact angle around 75° and a charge density around 10^{15} $N^{+}.cm^{-2}$, i.e. like a 'grafting to' method. Pretreatment of the PDMS surface by thiolation led to cationic PDMS surfaces with increased surface hydrophilicity (contact angle around 28°) and increased charge density to around 10^{17} $N^{+}.cm^{-2}$. The Live and Dead test by fluorescence microscopy revealed an efficient contact killing of all the prepared cationic surfaces against *E. coli* and *S. epidermidis*. By increasing the surface charge density, the longevity of the cationic PDMS surface was implicitly enhanced. The prepared surfaces can be intended for application as biomaterials or medical devices without contact with blood.

Acknowledgments

Authors thanks the INSA ROUEN NORMANDIE and the China Scholarship Council (CSC) for the financial supports.

Data availability statement

The raw/processed data required to reproduce these findings cannot be shared at this time due to technical or time limitations.

References

[1] A. B. Swanson, "Silicone Rubber Implants for Replacement of Arthritic or Destroyed Joints in the Hand," *Surg. Clin. North Am.*, vol. 48, no. 5, pp. 1113–1127, 1968.

[2] M. Bračič, O. Sauperl, S. Strnad, I. Kosalec, O. Plohl, L. F. Zemljič. "Surface modification of silicone with colloidal polysaccharides formulations for the development of antimicrobial urethral catheters," *Appl. Surf. Sci.*, vol. 463, no. 1 , pp. 889-899, 2019.

[3] A. Colas and J. Curtis, "Silicone biomaterials: history and chemistry," *Biomater. Sci. an Introd. to Mater. Med.*, vol. 2, pp. 80–85, 2004.

[4] A. U. Daniels, "Silicone breast implant materials," *Swiss Med. Wkly.*, vol. 142, no. JULY, 2012.

[5] K. W. Dunn, P. N. Hall, and C. T. K. Khoo, "Breast implant materials: sense and safety," *Br. J. Plast. Surg.*, vol. 45, no. 4, pp. 315–321, 1992.

[6] A. Colas, "Silicones: preparation, properties and performance," *Dow Corning, Life Sci.*, 2005.

[7] J. R. Henstock, L. T. Canham, and S. I. Anderson, "Silicon: the evolution of its use in biomaterials," *Acta Biomater.*, vol. 11, pp. 17–26, 2015.

[8] A. I. Doulgeraki, P. Di Ciccio, A. Ianieri, and G. J. E. Nychas, "Methicillin-resistant food-related Staphylococcus aureus: a review of current knowledge and biofilm formation for future studies and applications," *Res. Microbiol.*, vol. 168, no. 1, pp. 1–15, 2017.

[9] A. Tripathy, A. Kumar, S. Sreedharan, G.Muralidharan, A. Pramanik, D. Nandi, and P. Sen, "Fabrication of Low-Cost Flexible Superhydrophobic Antibacterial Surface with Dual-Scale Roughness," *ACS Biomaterials Science and Engineering*, vol. 4, no. 6, pp. 2213-2223, 2018.

[10] A. Tripathy, A. Kumar, A. R. Chowdhury, K. Karmakar, S. Purighalla, V. K. Sambandamurthy, D. Chakravortty and P. Sen, "A Nanowire-Based Flexible Antibacterial Surface Reduces the Viability of Drug-Resistant Nosocomial Pathogens," *ACS Applied Nano Materials*, vol. 1, no. 6, pp. 2678-2688, 2018.

[11] C. Donzel *et al.*, "Hydrophilic poly (dimethylsiloxane) stamps for microcontact printing," *Adv. Mater.*, vol. 13, no. 15, pp. 1164–1167, 2001.

[12] A. Oláh, H. Hillborg, and G. J. Vancso, "Hydrophobic recovery of UV/ozone treated poly (dimethylsiloxane): adhesion studies by contact mechanics and mechanism of surface modification" *Appl. Surf. Sci.*, vol. 239, no. 3–4, pp. 410–423, 2005.

[13] N. Kébir, I. Kriegel, M. Estève, and V. Semetey, "Preparation of bactericidal cationic PDMS surfaces using a facile and efficient approach," *Appl. Surf. Sci.*, vol. 360, pp. 866–874, 2016.

[14] W. Mussard, N. Kebir, I. Kriegel, M. Estève, and V. Semetey, "Facile and efficient control of bioadhesion on poly(dimethylsiloxane) by using a biomimetic approach," *Angew. Chemie*, vol. 123, no. 46, pp. 11063–11066, 2011.

[15] D.-J. Guo, H.-M. Han, S.-J. Xiao, and Z.-D. Dai, "Surface-hydrophilic and protein-resistant silicone elastomers prepared by hydrosilylation of vinyl poly(ethylene glycol) on hydrosilanes-poly (dimethylsiloxane) surfaces," *Colloids Surfaces A Physicochem. Eng. Asp.*, vol. 308, no. 1–3, pp. 129–135, 2007.

[16] Y. Wu, Y. Huang, and H. Ma, "A facile method for permanent and functional surface modification of poly(dimethylsiloxane)," *J. Am. Chem. Soc.*, vol. 129, no. 23, pp. 7226–7227, 2007.

[17] H. Chen, Y. Chen, H. Sheardown, and M. A. Brook, "Immobilization of heparin on a silicone surface through a heterobifunctional PEG spacer," *Biomaterials*, vol. 26, no. 35, pp. 7418–7424, 2005.

[18] H. Chen, Z. Zhang, Y. Chen, M. A. Brook, and H. Sheardown, "Protein repellant silicone surfaces by covalent immobilization of poly(ethylene oxide)," *Biomaterials*, vol. 26, no. 15, pp.

2391–2399, 2005.

[19] Y. Wang, H.-H. Lai, M. Bachman, C. E. Sims, G. P. Li, and N. L. Allbritton, "Covalent micropatterning of poly(dimethylsiloxane) by photografting through a mask," *Anal. Chem.*, vol. 77, no. 23, pp. 7539–7546, 2005.

[20] S. Sugiura, J. Edahiro, K. Sumaru, and T. Kanamori, "Surface modification of polydimethylsiloxane with photo-grafted poly (ethylene glycol) for micropatterned protein adsorption and cell adhesion," *Colloids Surfaces B Biointerfaces*, vol. 63, no. 2, pp. 301–305, 2008.

[21] B. L. Leigh, E. Cheng, L. Xu, A. Derk, M. R. Hansen, and C. A. Guymon, "Antifouling photograftable zwitterionic coatings on PDMS substrates," *Langmuir*, vol. 35, no. 5, pp. 1100–1110, 2018.

[22] A. I. Khalaf, Y. Assem, A. A. Yehia, A. M. Rabia, and T. A. Zidan, "Optical, dielectric, and mechanical properties of exfoliated poly (N, N-dimethylaminoethyl methacrylate)/Clay nanocomposites prepared via In-situ bulk polymerization," *Polym. Compos*., vol. 39, no. 8, pp. 2603–2610, 2018.

[23] C. Zhou, M. D. Weir, K. Zhang, D. Deng, L. Cheng, and H. H. K. Xu, "Synthesis of new antibacterial quaternary ammonium monomer for incorporation into CaP nanocomposite," *Dent. Mater.*, vol. 29, no. 8, pp. 859–870, 2013.

[24] D. C. Grothe, W. Meyer, and S. Janietz, "Acrylate functionalized tetraalkylammonium salts with ionic liquid properties," *Molecules*, vol. 17, no. 6, pp. 6593–6604, 2012.

[25] Schneider, C.A., Rasband, W.S., Eliceiri, K.W. "NIH Image to ImageJ: 25 years of image analysis," *Nature Methods* vol. 9, no. 7 pp. 671-675, 2012.

[26] W. Zhong, C. Dong, R. Liuyang, Q. Guo, H. Zeng, Y. Lin, A. Zhang, "Controllable synthesis and antimicrobial activities of acrylate polymers containing quaternary ammonium salts," *React. Funct. Polym*., vol. 121, pp. 110-118, 2017.

[27] J. G. Lundin, P. N. Coneski, P. A. Fulmer, J. H. Wynne, "Relationship between surface concentration of amphiphilic quaternary ammonium biocides in electrospun polymer fibers and biocidal activity," *React. Funct. Polym.*, vol. 77, pp. 39-46, 2014.

[28] Z. Huang, R. Liuyang, C. Dong, Y. Lei, A. Zhang, Y. Lin, "Polymeric quaternary ammonium salt activity against Fusarium oxysporum f. sp. cubense race 4: Synthesis, structure-activity relationship and mode of action," *React. Funct. Polym.*, vol. 114, pp. 13-22, 2017.

[29] A. Palantoken, M. S. Yilmaz, N. A. Unubol, E. Yenigul, S. Pişkin, T. Eren, "Synthesis and characterization of a ROMP-based polycationic antimicrobial hydrogel," *Eur. Polym. J*., vol. 112, pp. 365-375, 2019.

[30] B. Dizman, M. O. Elasri, and L. J. Mathias, "Synthesis and antimicrobial activities of new water-soluble bis-quaternary ammonium methacrylate polymers," *J. Appl. Polym. Sci.*, vol. 94, no. 2, pp. 635–642, 2004.

[31] D. Sha, J. Xu, X. Yang, Y. Xue, X. Liu, C. Li, M. Wei, Z. Liang, K. Shi, B. Wang, Y. Tang, X. Ji, "Synthesis and antibacterial activities of quaternary ammonium salts with different alkyl chain lengths grafted on polyvinyl alcohol-formaldehyde sponges," *React. Funct. Polym*., vol. 158, pp. 104797, 2021.

[32] J. Guo et al., "Antibacterial activity of cationic polymers: side-chain or main-chain type?," *Polym. Chem*., vol. 9, no. 37, pp. 4611–4616, 2018.

[33] G. Lu, D. Wu, R. Fu, "Studies on the synthesis and antibacterial activities of polymeric quaternary ammonium salts from dimethylaminoethyl methacrylate," *React. Funct. Polym.*, vol. 67, no. 4, pp. 355-366, 2007.

[34] J. Lafarge, N. Kebir, D. Schapman, and F. Burel, "Design of self-disinfecting PVC surfaces using the click chemistry," *React. Funct. Polym*., vol. 73, no. 11, pp. 1464–1472, 2013.

[35] Y. Jiao, L. Niu, S. Ma, J. Li, F. R. Tay, and J. Chen, "Quaternary ammonium-based biomedical materials: State-of-the-art, toxicological aspects and antimicrobial resistance," *Prog. Polym. Sci*., vol. 71, pp. 53–90, 2017.

[36] T. Zhou et al., "Surface functionalization of biomaterials by radical polymerization," *Prog. Mater. Sci.*, vol. 83, pp. 191–235, 2016.

[37] J. C. Tiller, C.-J. Liao, K. Lewis, and A. M. Klibanov, "Designing surfaces that kill bacteria on contact," *Proc. Natl. Acad. Sci*., vol. 98, no. 11, pp. 5981–5985, 2001.

[38] H. Murata, R. R. Koepsel, K. Matyjaszewski, and A. J. Russell, "Permanent, non-leaching antibacterial surfaces-2: How high density cationic surfaces kill bacterial cells," *Biomaterials*, vol. 28, no. 32, pp. 4870–4879, 2007.

[39] C. Debbasch, M.D. St Jean, P.J. Pisella, P. Rat, J.M. Warnet, C. Baudouin. "Quaternary ammonium cytotoxicity in a human conjunctival cell line," *J Fr Ophtalmol*., vol. 22, no. 9, pp. 950-958, 1999.

[40] D. Fischer, Y. Li, B. Ahlemeyer, J. Krieglstein, T. Kissel, "In vitro cytotoxicity testing of polycations: influence of polymer structure on cell viability and hemolysis," *Biomaterials*, vol. 24, no. 7, pp. 1121-1131, 2003.

[41] T. Eren, A. Som, J. R. Rennie, C. F. Nelson,Y. Urgina, K. Nüsslein, E. B. Coughlin, G. N. "Tew. Antibacterial and Hemolytic Activities of Quaternary Pyridinium Functionalized Polynorbornenes," *Macromol. Chem. Phys.*, vol. 209, pp. 516–524, 2008.

[42] H. Bouloussa, A.Saleh-mghir, C. Valotteau, C. Cherifi, N. Hafsia, et al.. "A Graftable Quaternary Ammonium Biocidal Polymer Reduces Biofilm Formation and Ensures Biocompatibility of Medical Devices," *Advanced Materials Interfaces,* vol. 8, no. 5, pp.2001516, 2021.

Supporting information

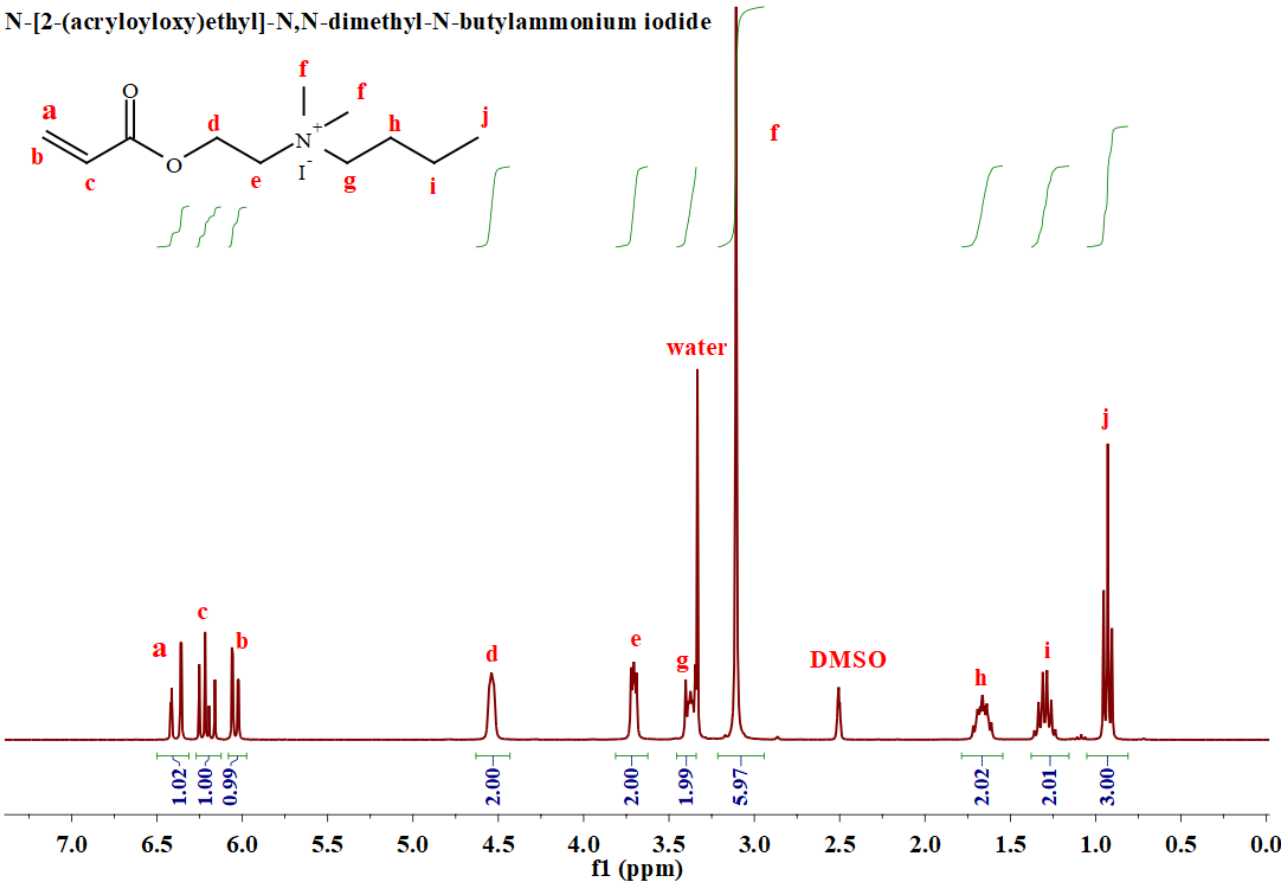

Figure S1. 1H NMR spectrum in DMSO-d_6 of AONAI.

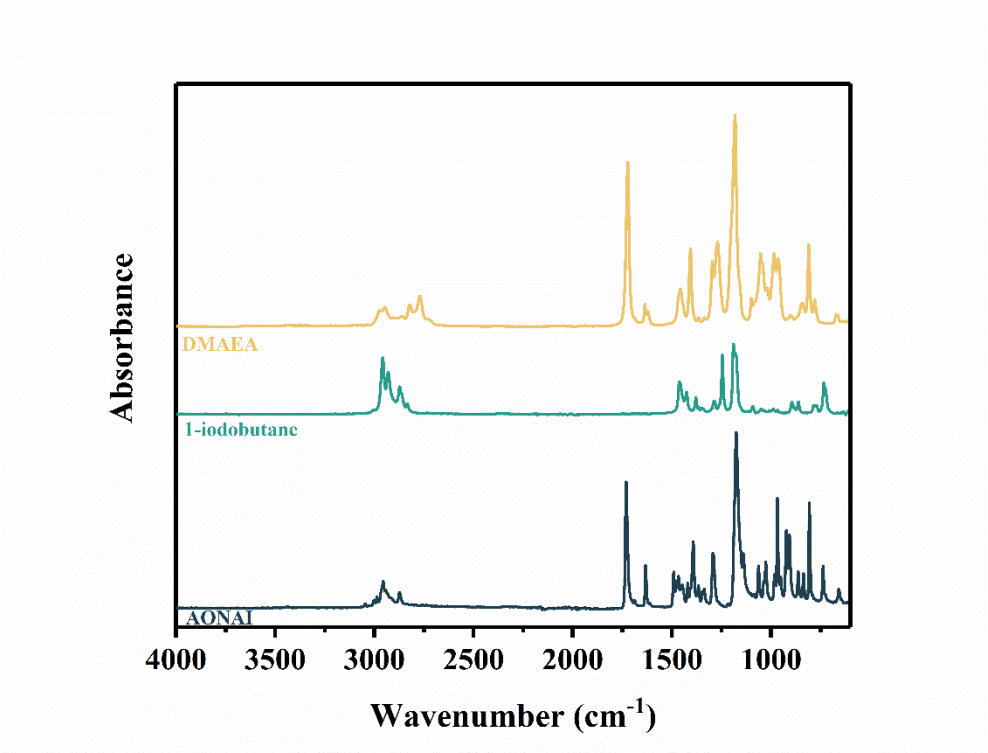

Figure S2. Global FTIR-ATR spectrum from 4000 to 600 cm^{-1} of DMAMA, 1-iodobutane and AONAI.

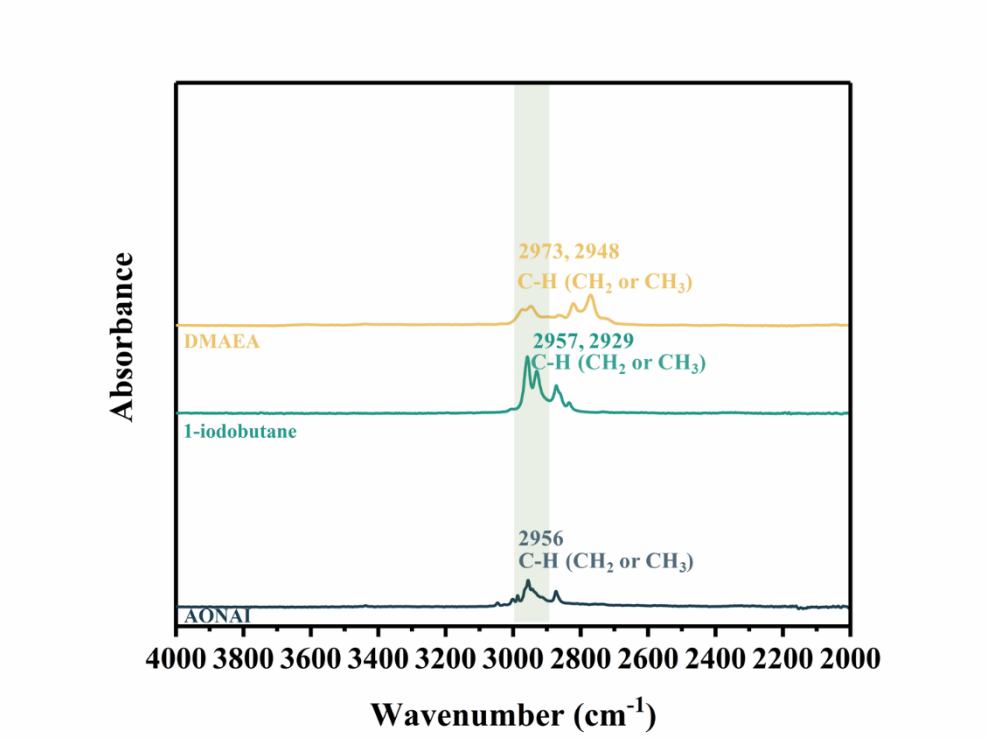

Figure S3. FTIR-ATR spectrum zooms from 4000 to 2000 cm^{-1} of of DMAMA, 1-iodobutane and AONAI.

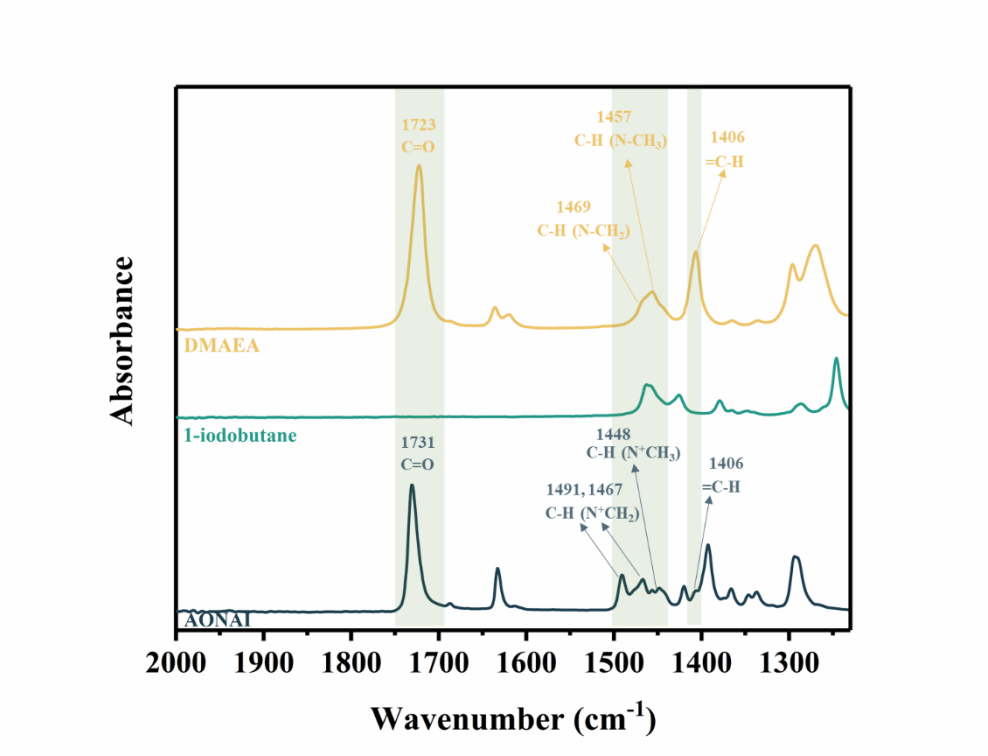

Figure S4. FTIR-ATR spectrum zooms from 2000 to 1230 cm^{-1} of of DMAMA, 1-iodobutane and AONAI.

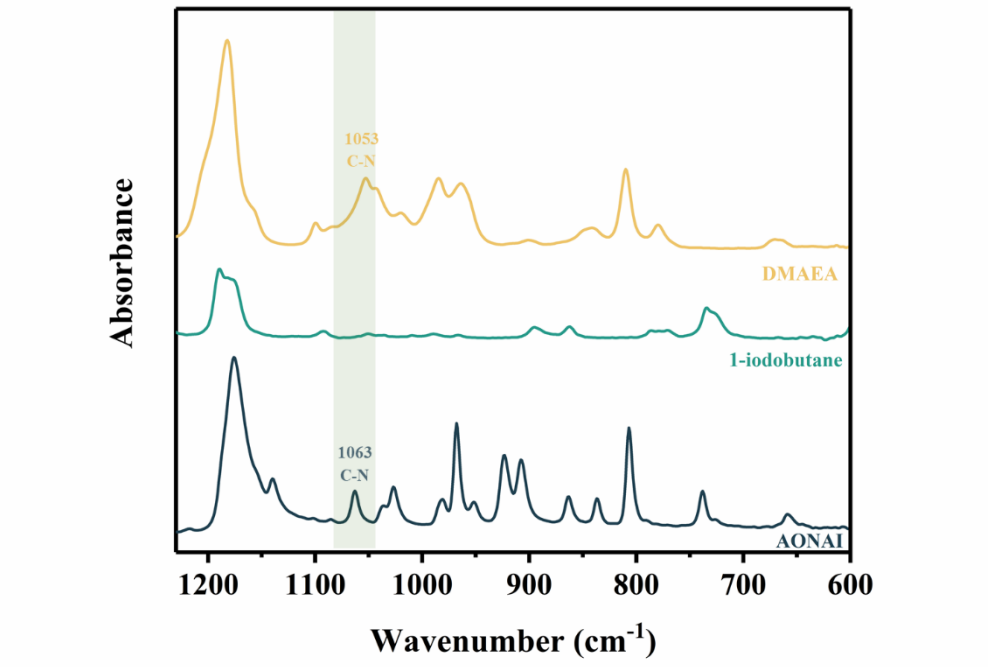

Figure S5. FTIR-ATR spectrum zooms from 1230 to 600 cm^{-1} of of DMAMA, 1-iodobutane and AONAI.

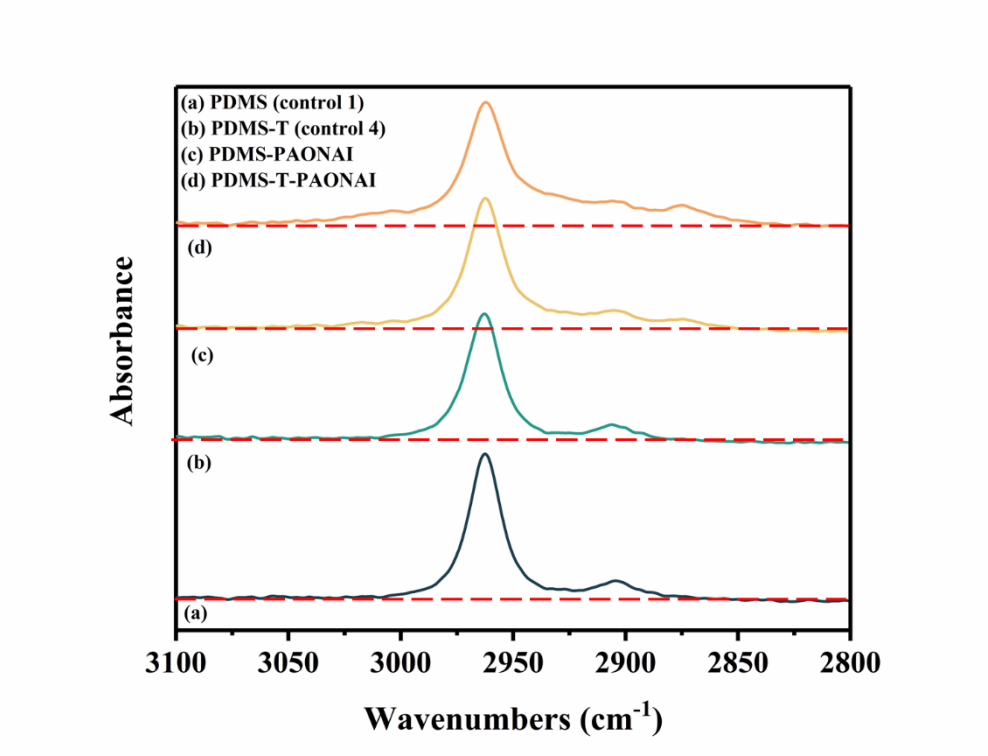

Figure S6. FTIR-ATR spectrum zooms (from 3100 to 2800 cm^{-1}) of (a) PDMS (control 1), (b) PDMS-T (control 4), (c) PDMS-PAONAI and (d) PDMS-T-PAONAI.

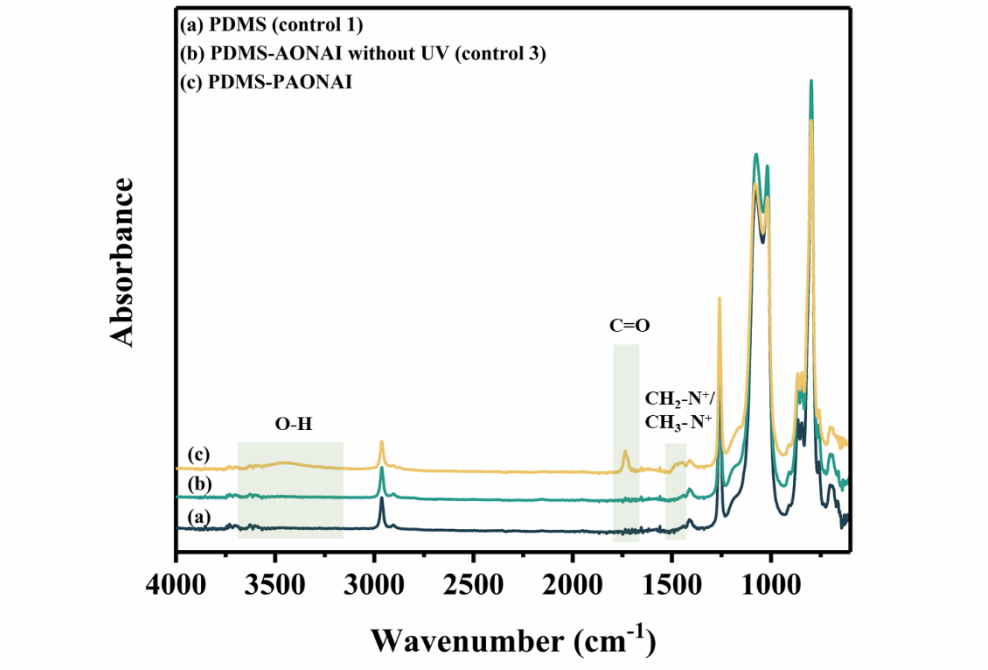

Figure S7. ATR-FTIR spectra of (a) PDMS (control 1), (b) PDMS-AONAI without UV (control 3) and (c) PDMS-PAONAI.

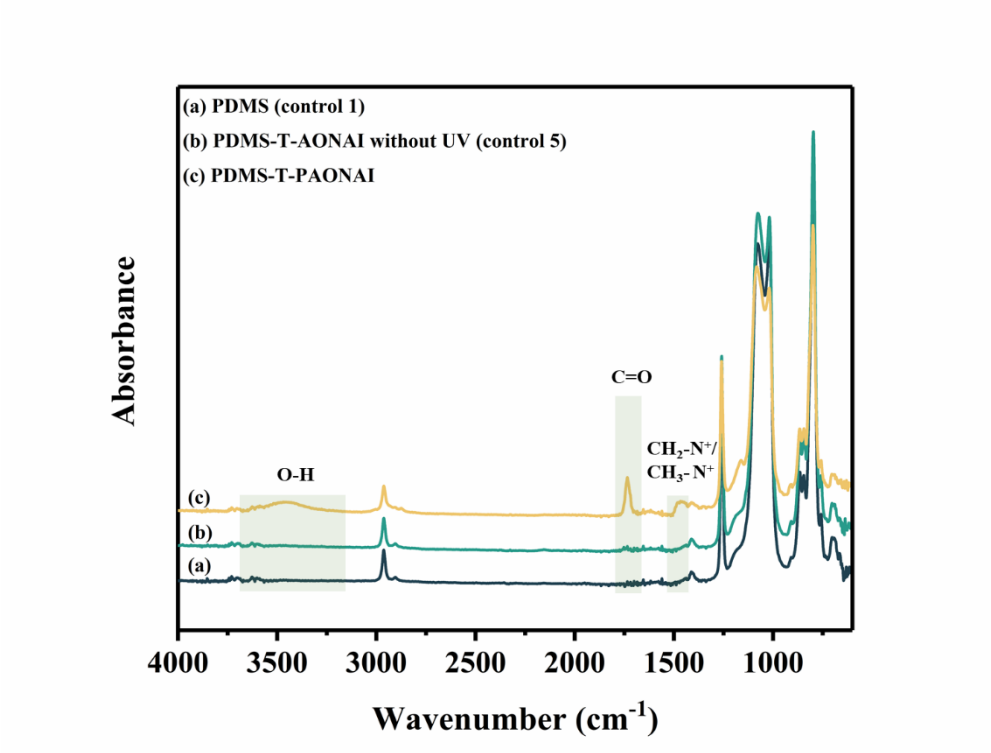

Figure S8. ATR-FTIR spectra of (a) PDMS (control 1), (b) PDMS-T-AONAI without UV (control 6) and (c) PDMS-T-PAONAI.

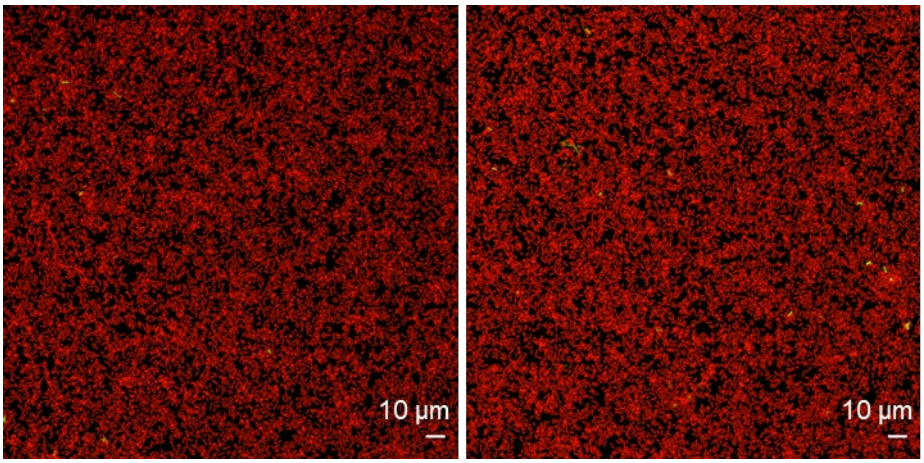

Figure S9. Supplemental fluorescence microscopy images of sessile *E. coli* cells stained with a marker of viability and deposited on surfaces of PDMS-PAONAI surfaces.

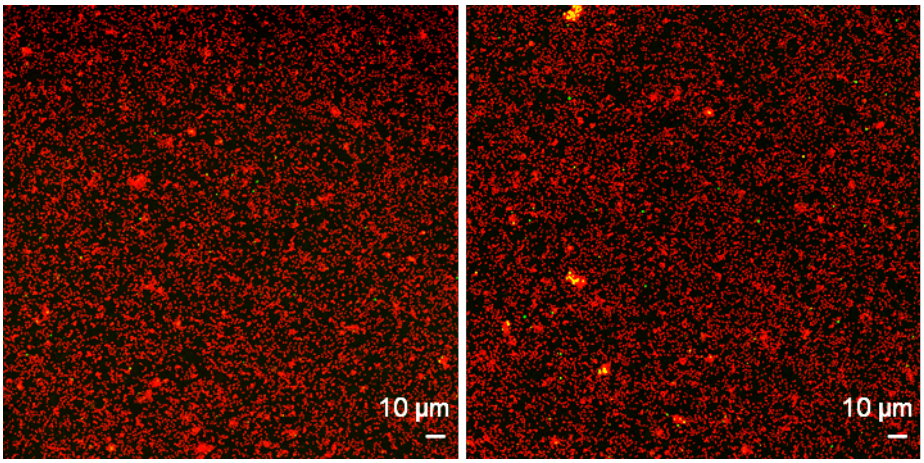

Figure S10. Supplemental fluorescence microscopy images of sessile *S. epidermidis* cells stained with a marker of viability and deposited on surfaces of PDMS-PAONAI surfaces.

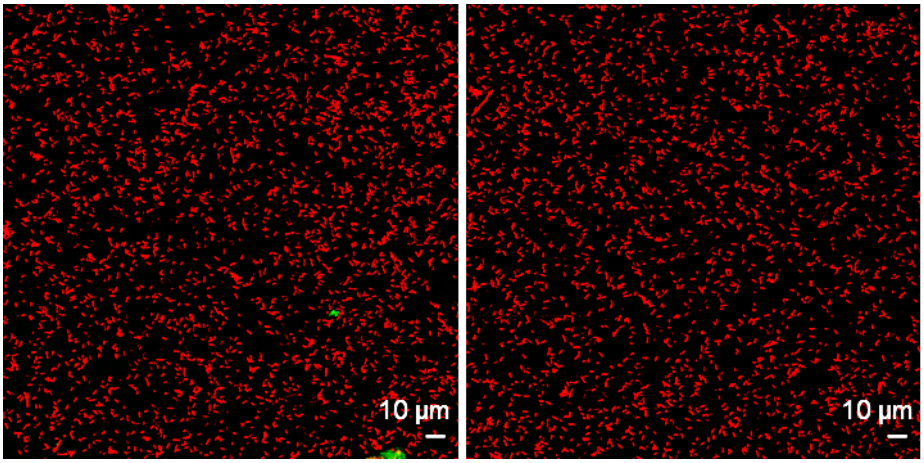

Figure S11. Supplemental fluorescence microscopy images of sessile *E. coli* cells stained with a marker of viability and deposited on surfaces of PDMS-T-PAONAI surfaces.

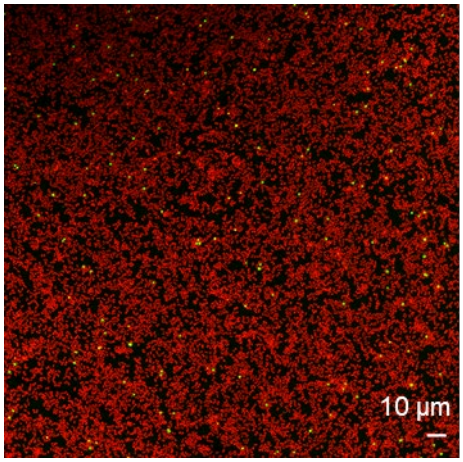

Figure S12. Supplemental fluorescence microscopy images of sessile *S. epidermidis* cells stained with a marker of viability and deposited on surfaces of PDMS-T-PAONAI surfaces.

Table S1: Characteristic values used for the estimation of the organic layer thickness.

Elements	Si2p	N1s	S2s
σ	0.817	1.67	1.8
T	2864	3233	2940
Bulk concentration (mol.cm^{-3})	$n_{Si}^{PDMS} = 0.013$	$n_{N}^{PAONAI} = 0.003$	$n_{S}^{T} = 0.010$
Mean free path (nm)	$\lambda_{Si}^{PDMS} = 3.6$	$\lambda_{Si}^{PAONAI} = 3.5$ $\lambda_{N}^{PAONAI} = 2.9$ $\lambda_{S}^{PAONAI} = 3.2$	$\lambda_{Si}^{T} = 3.5$ $\lambda_{S}^{T} = 3.2$

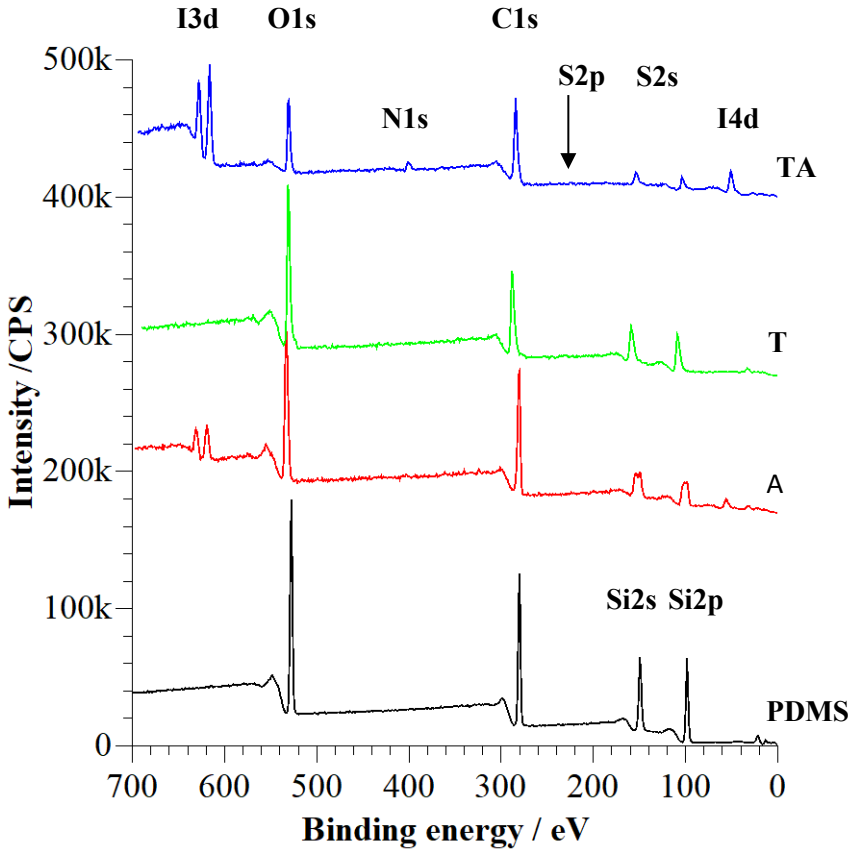

Figure S13. Survey XPS spectra of PDMS, PDMS-PAONAI, PDMS-T and PDMS-T-PAONAI surfaces.

IV.3 Article 5: Preparation of bactericidal PDMS surfaces by benzophenone photo-initiated grafting of polynorbornenes functionalized with quaternary phosphonium or pyridinium groups

Yuzhen Lou[1], Damien Schapman[2], Dimitri Mercier[3], N. Ceren Süer[4], Tarik Eren[4], Pascal Thebault[5], Nasreddine Kébir[1]

[1] Normandie Université, INSA Rouen Normandie, Laboratoire PBS, UMR CNRS 6270 & FR 3038, Avenue de l'Université, 76801 Saint Etienne du Rouvray, France

[2] Normandie Université, UNIROUEN, IFR MP 23, PRIMACEN, 76821 Mont-Saint-Aignan, France

[3] PSL Research University, Chimie ParisTech – CNRS, Institut de Recherche de Chimie Paris, 11 rue Pierre et Marie Curie, 75005 Paris, France

[4] Department of Chemistry, Yildiz Technical University, Davutpasa Campus, 34220, Esenler, Istanbul, Turkey

[5] Normandie Université, UNIROUEN, laboratoire PBS, UMR CNRS 6270 & FR 3038, 76821 Mont-Saint-Aigan, France

Correspondence to:

Nasreddine KEBIR (E-mail: *nasreddine.kebir@insa-rouen.fr*)

Pascal THEBAULT (E-mail: *pascal.thebault@univ-rouen.fr*)

Abstract

Cationic ROMP-polymers bearing ammonium or phosphonium groups were photo-grafted onto a PDMS surface via the thiol-ene click reaction, in the presence of benzophenone. The PDMS surface was first thiolated using pentaerythritol tetrakis (3-mercaptopropionate) (PTTMP) under UV, in the presence of benzophenone. The obtained cationic surfaces exhibited charge densities above 10^{14} charge/cm^2 and a higher degree of hydrophilicity compared to non-grafted surfaces. The live and dead tests performed by fluorescence microscopy revealed an effective contact bactericidal effect of these surfaces against *Escherichia coli* and *Staphylococcus epidermidis*.

Keywords: Quaternary ammonium; ROMP; photo; grafting to; PDMS; bactericidal; thiol-ene.

Introduction

The increase of antibiotic-resistant microorganisms in recent years has become a crucial issue, which has spurred significant research efforts to develop more effective antimicrobial treatments that use different bactericidal mechanisms to neutralize infectious diseases [1]. While around 2.8 million cases of antibiotic-resistant infections occur each year in the United States. More than 35,000 of these cases result in death [2]. Cationic antimicrobial polymers represent a growing and evolving class of biocides as an alternative to existing biocides and antibiotics [3].

Since man-made materials are completely vulnerable to microbial growth, they can easily survive in a humid environment by attaching microbial cells to their surface. As the number of cells increases at the surface, they often begin to form a biofilm from a polysaccharide matrix with embedded cells. This formed biofilm allows microbial cells to survive under harsh conditions [4]. Unfortunately, embedded cells are up to 1,000 times less sensitive to most antibiotics and other biocides [5]. Moreover, many toxins expelled from biofilms make them pathogenic, and resistant infections spread [6]. Furthermore, there may be an exchange of antibiotic genes between bacteria within the biofilm, resulting in multiple resistant bacteria being combined [7].

Antimicrobial polymers show some advantages over existing biocides and are therefore becoming increasingly important in the surface area [8]. Cationic antimicrobial polymers generally show high activity, a broad-spectrum activity and have low resistance to build potential and reduced toxicity. These biocidal polymers can be physically affiliated onto some surfaces, especially glass, which exhibit affinity with them. Since antimicrobial polymers have high molecular weights and low diffusion coefficients, their leakage from these surfaces is restricted [9]. In addition, antimicrobial polymers can also be covalently bonded to surfaces, without losing their biological activity [10].

Polydimethylsiloxane (PDMS) is one of the most important polymer-based biomaterials. It is very flexible, chemically and thermally stable and biocompatible. It can be used in many different forms such as joint implants, catheters, kidney dialysis machines and breast prostheses [11]–[17]. Nevertheless, PDMS is a very hydrophobic material undergoing biofouling and bacterial contamination, which imply an important health and economic impacts [18]–[20].

One of the promising strategies to resolve these problems is the chemical anchoring of cationic antibacterial polymers onto the PDMS surface. However, because of its chemical stability, the PDMS surface often needs a physical pretreatment to introduce coupling sites. For

instance, oxygen plasma has been applied to create hydroxyl groups on the PDMS surface rendering it very hydrophilic [21]. Actually, in few minutes of contact with air, the surface hydroxyl groups diffuse in the polymer matrix bulk, which lead to hydrophobic recovery and the loss of surface functionalization. Therefore, the post-chemical grafting must be achieved just after the physical treatment [22].

Nowadays there is only two chemical pathways for the direct chemical modification of the PDMS surface [23]–[31]. The first one is the hydrosilylation reaction between Si-H groups present in the PDMS surface and carbon-carbon double bonds incorporated in bioactive polymers [23]–[28]. By varying the ratio between the PDMS components and/or their curing time or by insertion of poly(methylhydroxysiloxane), the concentration of Si-H groups can be fine-tuned [23]–[28]. The second one is the photo-induced 'grafting from' process of monomers or macromonomers, namely acrylic acid [29], polyethylene glycol monoacrylate, polyethylene glycol diacrylate [30], sulfobetaine methacrylate and carboxybetaine methacrylate [31], and vinylbenzyldimethylbutylammonium chloride [32] from the PDMS surfaces, in the presence of benzophenone as photo-initiator.

In this work, we describe a straightforward photo-grafting of ROMP-synthesized bactericidal polynorbornenes bearing quaternary phosphonium (p(OPPh)) or pyridinium (p(OPyHex)) groups onto native and thiolated PDMS surfaces, in the presence of benzophenone. The physico-chemical and antimicrobial properties of the cationic surfaces are assessed and discussed with the literature data.

Experimental section

Materials

Sylgard® 184 was purchased from DOW chemical company (USA). Dry methanol (99,8%), acetone was purchased from Acros Organics. Glass coverslip (18 mm×18 mm, Fisherbrand™) were purchased from Thermo Fisher Scientific. Pentaerythritol tetrakis (3-mercaptopropionate) (PTTMP) was purchased from Aldrich. Benzophenone (BP) (≥99%) was purchased from Merck. Ultrapure water was obtained from a Milli-Q system (Siemens, France). All the chemicals were used without further purification.

S. epidermidis (ATCC 35984) and *E. coli* (K12 MG1655) strains were stored as frozen aliquots in brain heart infusion (BHI, Bacto, France) broth and 30 % of glycerol at -20 °C. The LIVE/DEAD Bacterial Viability Kit, L7007 (SYTO®9 dye, 1.67 mM / Propidium iodide, 18.3 mM) was purchased from Thermo Fisher Scientific. Phosphate buffered saline (PBS), prepared from the PBS tablets (Gibro, Swiss) and ultrapure water, was autoclaved before use.

Preparation of p(OPPh) and p(OPyHex)

The monomers and polymers with molecular weight of 10 000 g/mol used in the study were synthesized as described in the literature [33], [34].

Phosphonium based monomer synthesis started with a Diels-Alder reaction between maleic anhydride and furan to obtain the starting compound of exo-7-oxabicyclo[2.2.1]hept-5-ene-2,3-dicarboxylic anhydride [35]. After that, imide transformation was conducted with 3-bromopropyl amine hydrobromide, according to the literature [36]. Bromo oxanorbornene product (0.5 g, 1.75 mmol) was dissolved in 11 mL of ethyl acetate. Excess amount of triphenylphosphine (1.376 g, 5.25mmol) was added to reaction medium. The reaction was stirred under nitrogen in a sealed vessel at 50 °C for 24 h. The precipitate of the reaction was washed with ethyl acetate and THF and dried under nitrogen.

Pyridinium based monomer was synthesized by the reaction of 3-(Aminomethyl)pyridine (2.4 mL, 22 mmol) and exo-7-oxabicyclo[2.2.1]hept-5-ene-2,3-dicarboxylic anhydride (1.92 g, 11 mmol) in the presence of 6 mL *N,N*-dimethylacetamide at 60 °C and stirred for 20 min. After addition of a catalytic amount of sodium acetate (0.5 g, 5 mmol) in 2 mL acetic anhydride to the solution, the reaction mixture was stirred for 2 h at 90 °C. The mixture was diluted with ethyl acetate, washed with brine and concentrated using a rotary evaporator connected to a vacuum pump. Product was purified by column chromatography using ethyl acetate:hexane (4:1, v/v). Quaternization of pyridine bearing oxanorbornene (0.13 g, 0.47 mmol) was obtained by using the bromohexane (0.67 g, 4.7 mmol) in the presence of acetonitrile solution stirred for 48 h at 60 °C, quaternized monomer was obtained by precipitation from diethyl ether.

For polymerization of p(OPPh), freshly prepared Grubbs third generation catalyst in 0.5 mL of dry dichloromethane was added in one shot to the forcibly stirring monomer solution in 2 mL dry chloroform and stirred for 24 h at room temperature. Afterwards the polymerization was stopped by addition of 0.5 mL 30 % ethylvinyl ether (in dichloromethane). Polymer, p(OPPh), was precipitated and washed with diethyl ether and dried under nitrogen.

For polymerization of OPyHex, the monomer was dissolved in dry methanol and after addition of Grubbs third generation catalyst dissolved in dichloromethane stirred for 2 hours. All polymers were confirmed by thin layer chromatography (TLC) before the polymerization was terminated.

Preparation of PDMS film

15 g of a mixture of the two parts of Sylgard® 184, i.e. base and curing agent, at a ratio of 10:1 (w/w), were casted into a low-density polyethylene petri dish square (120×120×17 mm^3). The mixture was then degassed under vacuum, until the air bubbles were completely removed. The PDMS film was formed after two days at room temperature and was cut into 18 × 18 mm^2 squares with a thickness less than 1 mm. The curing time can be considerably reduced by increasing the temperature (few hours at 70°C and about 1h at 120°C) [23].

Preparation of PDMS-T-p(OPPh) and PDMS-T-p(OPyHex) surfaces

To prepare PDMS-T, the PDMS films were first immersed in an acetone solution containing 20 wt% of BP for 30 min to absorb enough BP for the photo-grafting. The samples were quickly washed with methanol and then placed on a plate to dry in the dark. Then 50 to 80 µl of an acetone solution containing PTTMP (25 to 75wt%) was applied to the dry samples and covered with a glass slide so that the PTTMP solution was spread evenly over the surface of the PDMS by capillary force. The PDMS assembly was placed in a UV conveyor (UV Fusion Light Hammer 6), and irradiated with the UV light emitted from a small diameter electrodeless bulb combined with the elliptical reflector, microwave-powered lamp (500 watts/inch) at a lamp-PDMS distance of 53 mm. Then, the BP-initiated photo grafting and photopolymerization of the PTTMP took place from the PDMS surface. After grafting, PDMS-T were collected and washed in acetone overnight with slight shaking and washed again with acetone the next day before drying to remove all unreacted BP or PTTMP.

Then, PDMS-T-p(OPPh) or PDMS-T-p(OPyHex) were prepared by using the methanol solution containing p(OPPh) or p(OPyHex) in the same way on substrate of PDMS-T. After grating, the samples were collected by immersion in water to detach from the glass slide and then washed with methanol three times. The samples were washed in methanol overnight with slight shaking and washed again with methanol the next day before vacuum drying to ensure that all unreacted monomer, ungrafted BP, p(OPPh) or p(OPyHex) compounds were removed.

Measurements

The ATR-FTIR spectra were recorded on a Nicolet IS-50 FTIR (Thermo, USA) spectrometer using the VariGATR accessory (Harrick Scientific, Pleasantville, NY) and the DTGS detector on three independent samples for each experimental condition, with a wave-number range between 600 and 4000 cm^{-1}. The data was obtained with a spectral resolution of 4 cm^{-1} by 250 scans.

^{1}H NMR (500 MHz) and ^{13}C NMR (125 MHz) spectra were recorded on a Bruker Avance III 500 MHz spectrometer. ^{31}P NMR spectra were obtained using a Varian Mercury VX 400 MHz BB spectrometer.

Static and dynamic water contact angles measurements were measured using a contact angle goniometer "digidrop" (United Kingdom) in air at room temperature on at least three independent samples and at least three droplets by sample.

X-Ray Photoelectron spectroscopy (XPS) analysis was performed using a Thermo Electron Escalab 250 spectrometer, with a monochromatic Al Kα X-ray source (hν = 1486.6eV) operating at a pressure around 10^{-9} mbar. The spectrometer was calibrated using Au4f7/2 at 84.1eV. The take-off angle was 90° and the analyzed surface was a 500 µm diameter disk. Survey spectra were recorded with a pass energy of 100eV and a step of 1eV and C1s, O1s, Si2p high level resolution spectra were recorded with a pass energy of 20eV and a step of 0.1eV. The charge effect was evaluated using the main component of the C1s peak, associated with C-C/C-H hydrocarbons with a binding energy of 285eV. Spectra were recorded using the Thermo Avantage software and analyzed using CasaXPS software.

The topography of PDMS surfaces before and after modification were analyzed by using a Nanoscope 8 Multimode microscope (Bruker Nano Surfaces, Santa Barbara, CA, USA). Imaging was achieved in the air using the PeakForce®-QNM mode with a 100µm piezoelectric scanner. A silicon (RTESPA-300, Bruker) cantilever with a spring constant of about 40 N/m and a silicon tip was used. Images were obtained with a PeakForce tapping frequency of 1 kHz and the auto-amplitude on. The AFM imaging was performed in multiple locations on at least two independent samples at two scan sizes: 5 × 5 and 20 × 20 μm^2. All images are presented in the height mode and are top view images.

Determination of the surface accessible quaternary ammonium and phosphonium densities

Modified and unmodified PDMS surfaces (1.8 × 1.8 cm^2) were immersed in a solution of fluorescein sodium salt (1% in distilled water) for 10 min. Afterwards, the unreacted fluorescein molecules were removed by washing with distilled water. The samples were then placed in 3 mL of a 0.5% solution of hexadecyltrimethyl ammonium bromide to exchange with the bounded fluorescein molecules under ultrasound for 15min. 0.45 mL of saturated $NaHCO_3$

solution was added after sonication. Then the absorbance of solution was recorded at 501 nm. The fluorescein concentration was then calculated using a calibration curve.

Antimicrobial activity assay (Live/Dead test)

A 130 µl droplet of *E. coli* or *S. epidermidis* suspension in distilled water (about 5×10^8 CFU/ml) was spread on the modified surfaces (1.8×1.8 cm^2) using a glass slide with the same surface size for 1 h. Then the glass slide was taken away and the PDMS surfaces were washed by distilled water flow to remove the non-attached bacteria. After that, a 130 µl mixture of two fluorescent markers: the SYTO® and the propidium iodide, were deposed and spread on the surfaces for 15 min. The mixture was diluted prior to use (20 µmol/l of SYTO®9). Images (1024 × 1024 pixels) of surfaces were acquired using an upright fixed-stage Leica TCS SP8 CFS confocal microscope (Leica Microsystems, Nanterre, France) equipped with diodes laser (Coherent, Les Ulis, France) at 488 nm to excite the SYTO®9 and at 552 nm to excite Propidium Iodide and a conventional scanner at 400 Hz. Using a 63× oil immersion objective (1.40), fluorescence emission was sequentially detected through hybrid detector (Leica Microsystems, Nanterre, France) in photon counting mode with a specific band from 500 to 540 nm for SYTO®9 and 580 to 630 nm for Propidium Iodide. Z-Stack's images were acquired using an adapted step-size from Nyquist Criteria. ImageJ (Rasband W.S., U.S. National Institutes of Health, Bethesda, Maryland, USA, http://imagej.nih.gov/ij/, 1997-2020) was used to adjust brightness and contrast and to perform z projections of 3D images (xyz). The Live and Dead test was performed on at least three independent samples, and two/three representative pictures by sample were recorded.

Results and discussion

Phosphonium monomer was synthesized in three steps. First, a Diels-Alder adduct (exo-7-oxabicyclo[2.2.1]hept-5-ene-2,3-dicarboxylic anhydride) was obtained from maleic anhydride and furan. Then, imide transformation, in the presence of sodium acetate/acetic anhydride mixture, was performed with 3-bromopropylamine hydrobromide. This bromo oxanorbornene derivative was further reacted with triphenyl phosphine by nucleophilic addition route to afford a phosphonium bearing oxanorbornene monomer [33]. Similarly, pyridinium based monomer was prepared by reacting the previous Diels Alder adduct with pyridin-3-ylmethanamine, in the presence of catalytic amount of sodium acetate Then, the pyridine ring was reacted with hexyl bromide to afford a quaternary pyridinium salt [34].

The prepared cationic monomers were then used in the ROMP type polymerization to procure well-defined polymers with controlled molecular weight and dispersity (Đ) close to 1. Polymers with a targeted number of average molecular weight of 10 000 g/mol were obtained by adjusting the catalyst concentration.

Chemical structures of monomers and polymers were confirmed by NMR techniques. Complete conversion from monomer to polymer was inspected by the whole disappearance of the monomer olefin proton peaks at 6.0–6.3 ppm and the appearance of polymer backbone olefinic broad proton signals at 5.1–5.6 ppm. Binding aryl carbon to phosphonium cation was detected at δ 118 ppm in the ^{13}C NMR spectrum. Phosphonium peak of the p(OPPh) was observed at 24.5 ppm in the spectra of ^{31}P NMR. Pyridinium based polymers showed the characteristic peak of the protons in alpha position to the ammonium group at 2.1 ppm in the ^{1}H NMR spectrum, while ^{13}C NMR analysis showed the corresponding methylene carbons at 39 ppm. The molecular weights of the homopolymers were calculated by ^{1}H NMR end group analysis [33, 34] which was close to the targeting theoretical M_n values of the polymers.

The photo-grafting initiated by benzophenone of the cationic polymers onto the PDMS surface was first tested without pretreatment. The PDMS films (Sylgard®184) prepared at the conventional ratio of PartA (curing agent)/PartB (base) = 1/10 and were totally cured. A drop of the cationic polymer solution (10 to 50wt% in methanol) was spread on the PDMS surface by covering it with a thin glass plate. The sample was then introduced in the UV conveyor for 1.55 s of UV exposure by passage. Despite varying the concentration of the polymer solution and the number of passages under UV (50 to 90) the direct polymer grafting on the PDMS surface was not efficient as suggested by the water contact angle (WCA), which was very close to the value of the untreated PDMS (Table 1, control 1), i.e. 108°.

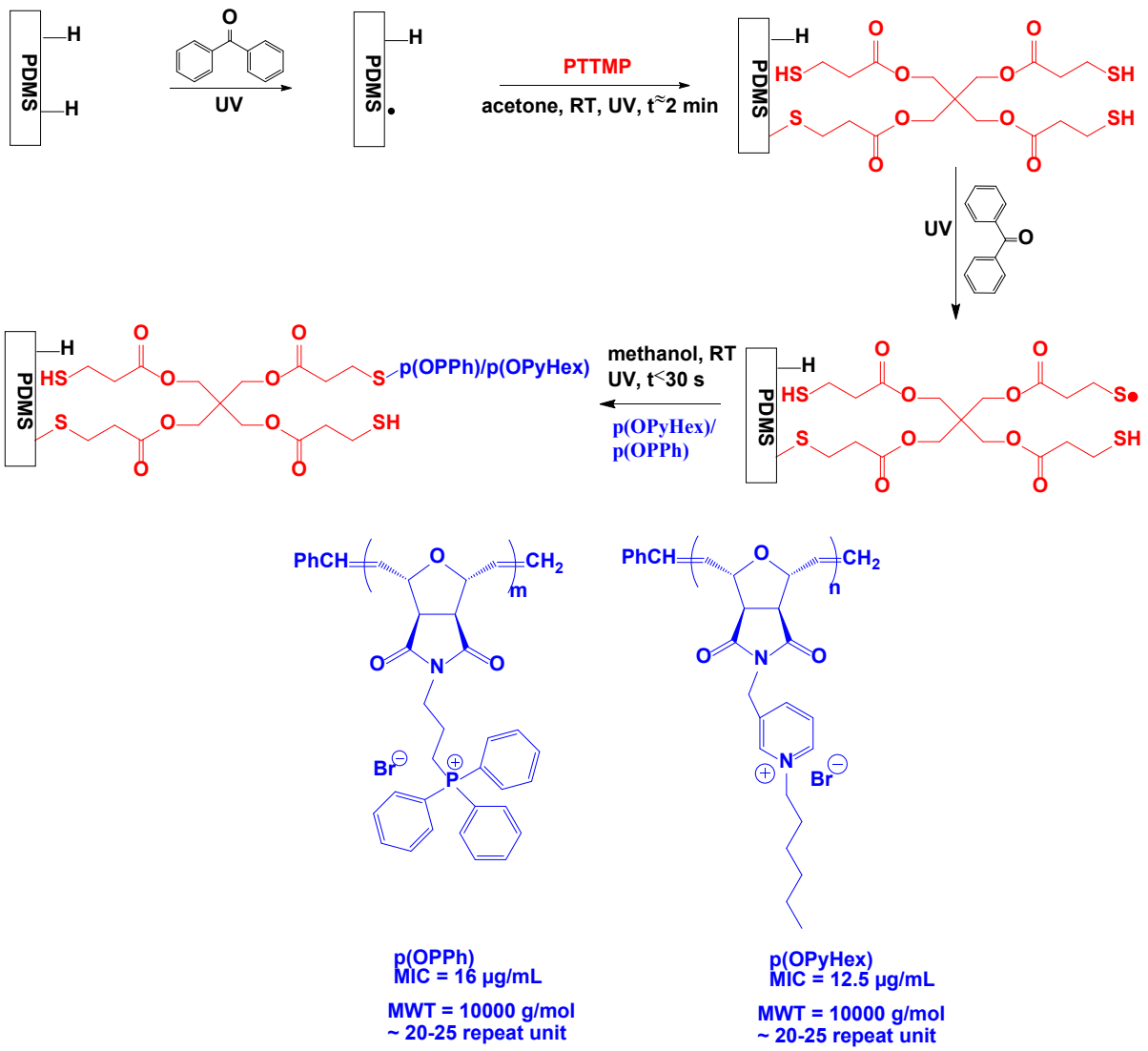

Figure 1. Photografting of p(OPPh) or p(OPyHex) onto PDMS surface with Pentaerythritol tetrakis (3-mercaptopropionate) (PTTMP) pretreatment.

Therefore, we have achieved a thiolation pretreatment of the PDMS surface to increase its reactivity (Figure 1). Indeed, radical sites can easily be formed from thiol groups under UV to achieve thiol-ene coupling reaction with the carbon-carbon double bonds of the polymers. Thus, a drop of solution of pentaerythritol tetrakis (3-mercaptopropionate) (PTTMP) in methanol was spread on the PDMS surface using a glass plate. The sample was disposed in the UV conveyor for several passages under UV. Various PTTMP concentration, ranged from 25 to 75wt%, and number of passages, ranged from 30 to 100, were tested. A constant value of the water contact angle of around 100° was obtained regardless the thiolation conditions (Table 1, control 3). For the next step, the thiolation was achieved with a solution of PTTMP at 50 wt% with 90 passages under UV, leading to the lowest standard deviation of the WCA value.

Then, the cationic polymers were grafted on the thiolated PDMS surfaces under UV at several exposure times and polymer concentrations. The optimal conditions were obtained for a polymer concentration of 10 wt% and a number of passages under UV of 15 leading to the most hydrophilic and functionalized surfaces, with WCA values of 78 and 98° for PDMS-T-p(OPyHex) and PDMS-T-p(OPPh) surfaces, respectively (Table 1). The difference in WCA values between the two surfaces can be ascribed to the higher hydrophobic character of the p(OPPh) compared to p(OPyHex), which is due to the number of carbons on theses polymers (three phenyl groups versus one hexyl chain, respectively). This difference can also be partially ascribed to the overall surface coating efficiencies. Indeed, since the cationic polymers are hydrophilic and water soluble, increasing their grafting density would lead to an increase in surface hydrophilicity and a decrease of WCA.

Table 1. Data of contact angles measurements and surface charge densities on the optimal treated PDMS surface (10 wt% of polymer solution under UV, under 15 passages under UV) and their controls.

	Static mode	**Dynamic mode**			**Charge density**	**Roughness by AFM[b] (nm)**	
Samples	**θ_{water} (°)[a]**	**AA (°)[a]**	**RA (°)[a]**	**Hyst (°)[a]**	**charge.cm^{-2}**	**Ra**	**RMS**
PDMS (control 1)	108±2	116±3	58±4	57±2	ND	1.4	2.4
PDMS-T (control 2)	97±8	121±2	68±1	53±2	ND	2.8	3.7
PDMS-T-p(OPPh)	98±4	106±11	34±16	73±25	(4.8±1.1) ×10^{14}	6.1	8.5
PDMS-T-p(OPyHex)	78±9	93±10	27±23	67±21	(3.2±0.5) ×10^{14}	8.1	12.9

[a] **θ_{water}**: contact angle with water; **AA**: Advancing Angle; **RA**: Receding Angle; **Hyst**: Hysteresis.

[b] Ra: Arithmetic Average Roughness and RMS: Root Mean Square Roughness, from the 20×20 µm^2 images.

Measurements of the dynamic water contact angles were achieved on the optimal surfaces (Table 1). The advancing angle (AA) is correlated to the wettability of the hydrophobic parts of the surface while the receding angle (RA) is ascribed to the hydrophilic parts. Unmodified PDMS surfaces (control 1) exhibited values of AA, RA and the hysteresis (AA-RA) of 116°, 58° and 57°, respectively. The thiolated PDMS surface (control 2) showed AA, RA and hysteresis values of 121°, 68° and 53°, respectively, confirming the success of the

thiolation reaction. After treatment with the polymer solutions under UV, the modified surface showed a decrease of AA and RA to 106° and 34° for PDMS-T-p(OPPh) and to 93° and 27° for PDMS-T-p(OPyHex), respectively, suggesting a significant degree of surface grafting. However, the hysteresis increased to 73° and 63°, respectively, suggesting either a physical (roughness) and/or chemical (gradient of grafting density) gradients of the grafted surfaces.

The surface charge density is an important parameter that has been thoroughly used in the literature to predict the contact killing capacity of quaternary ammonium and quaternary phosphonium surfaces. Indeed, it has been established that the surface must own a minimal charge density value of 10^{14} charge.cm^{-2} to kill quantitatively *E. coli* and *S. epidermidis* [23], [37]-[40]. The charge density values of the optimal cationic PDMS surfaces are displayed in Table 1. PDMS-T-p(OPPh) surface exhibited a charge density of $(4.8\pm1.1)\times10^{14}$ P^+.cm^{-2} whereas PDMS-T-p(OPyHex) showed a value of $(3.2\pm0.5)\times10^{14}$ N^+.cm^{-2} suggesting a high potential of bacterial killing of these prepared surfaces.

Surface characterization by AFM

AFM images of the prepared cationic surfaces and their controls are shown in Figure 2 and the supplementary information. One can observe structural and topographical variations on the PDMS surfaces after thiolation as well as after photo-grafting of the cationic polymers. The roughness values, from the 20×20 μm^2 images, of these modified and unmodified PDMS surfaces are presented in Table 1. The unmodified PDMS surface was very smooth with an arithmetic average roughness value of about 1.4 nm and a mean square roughness of about 2.4 nm (Figure 2-A, Table 1). White spots on this surface were rarely observed, which can be attributed to slight surface contamination by dust or particles from atmosphere or through manipulation with the clamp. The thiolated PDMS surface (PDMS-T) exhibited an increased roughness value around 2.8 nm and 3.7 nm, respectively (Figure 2-B, Table 1). PDMS-T-p(OPPh) surface (Figure 2-C, Table 1) exhibited roughness values around 6.1 nm and 8.5 nm whereas the roughness values of PDMS-T-p(OPyHex) (Figure 2-D, Table 1) were of 8.1 and 12.9 nm, respectively. However, both the two cationic surfaces showed the presence of polymer aggregates (white spots), which is often observed with the ‘grafting to’ method. Moreover, some big aggregates, of around 5 nm diameter, were observed on the PDMS-T-p(OPyHex) surface. However, some zones of this surface were quasi-empty of aggregates and displayed roughness values of 0.6 and 1 nm, respectively, i.e. lower than those of PDMS-T. This result suggests that the p(OPyHex) was homogenously grafted on these zones.

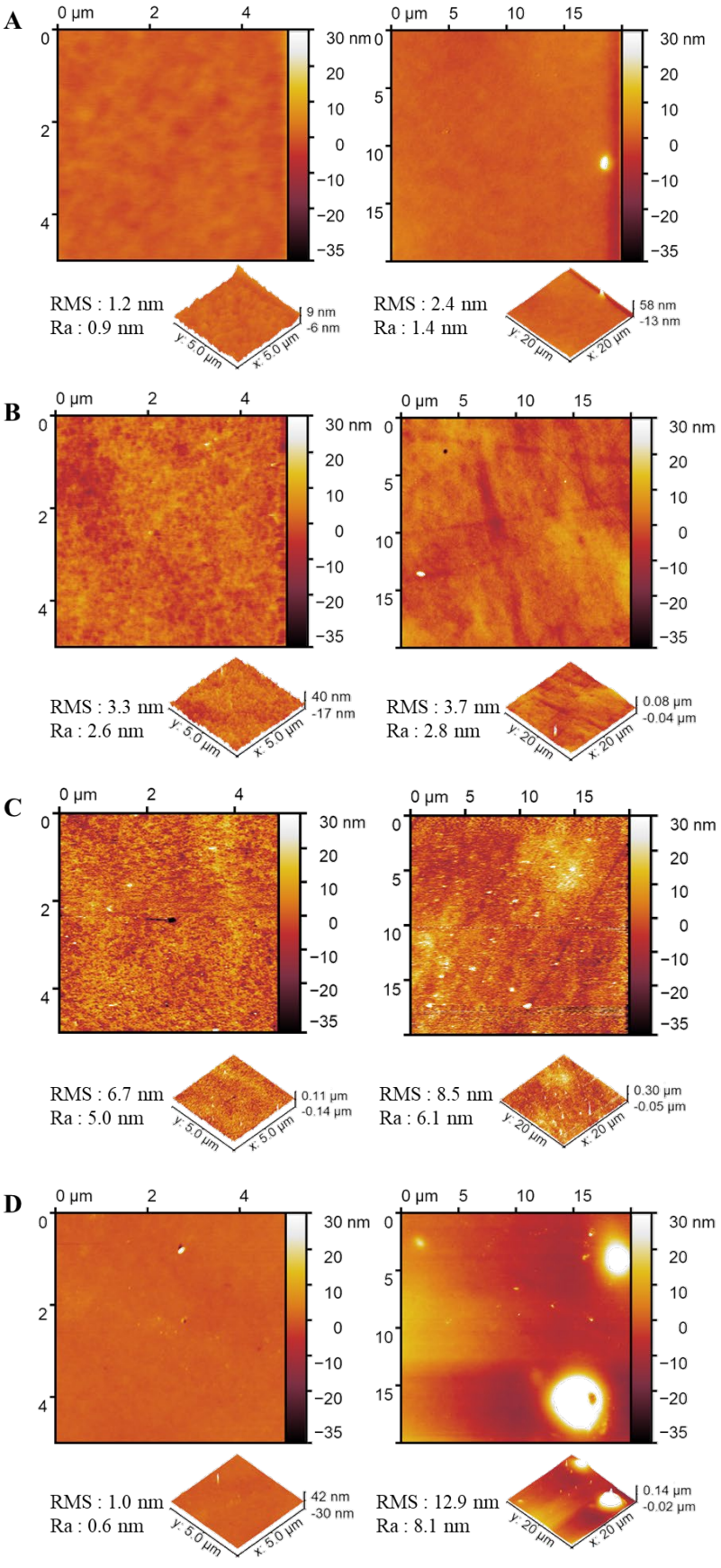

Figure 2. AFM images of (A) PDMS surface (control 1), (B) PDMS-T surface (control 3), (C) PDMS-T-p(OPPh) surface and (D) PDMS-T-p(OPyHex) surface.

The FTIR-ATR spectra of the prepared cationic surfaces, compared to their controls are shown in Figure 3. Zooms of the region between 1150 and 1900 cm^{-1} are given in the supporting information. The grafted PTTMP, which should form a very thin monomolecular layer, was not detected by this technique due to their weak amount on the surface. The PDMS-T-p(OPyHex) showed the appearance of a new band at around 1700 cm^{-1} arising from the stretching vibration of the carbonyl group of the imide function present in the grafted cationic polymer. One can observe also the stretching vibration band related to the polymer's carbon-carbon double bonds at 1636 cm^{-1}. A small band at 1503 cm^{-1} arising from the bending vibration of C-H in CH_2-N^+ groups was also observed. However, the characteristic bands corresponding to the imide function was not observed within the PDMS-T-p(OPPh) surface. This can be explained by the lower concentration of this function (~2 folds) within the p(OPPh). Moreover, the presence of big aggregates on the PDMS-T-p(OPyHex) surface may also be the reason of an increased signal intensity of the imide group in its FTIR spectrum. Anyway, these results suggest that the grafting density of p(OPyHex) on the surface was higher than the one of p(OPPh).

On the other hand, according to water contact angle results, PDMS-T-p(OPyHex) was more hydrophilic (78°) and more hygroscopic than the PDMS-T-p(OPPh) surface, which explain the appearance of a small band at 3300 cm^{-1} arising from the moisture in its FTIR spectrum.

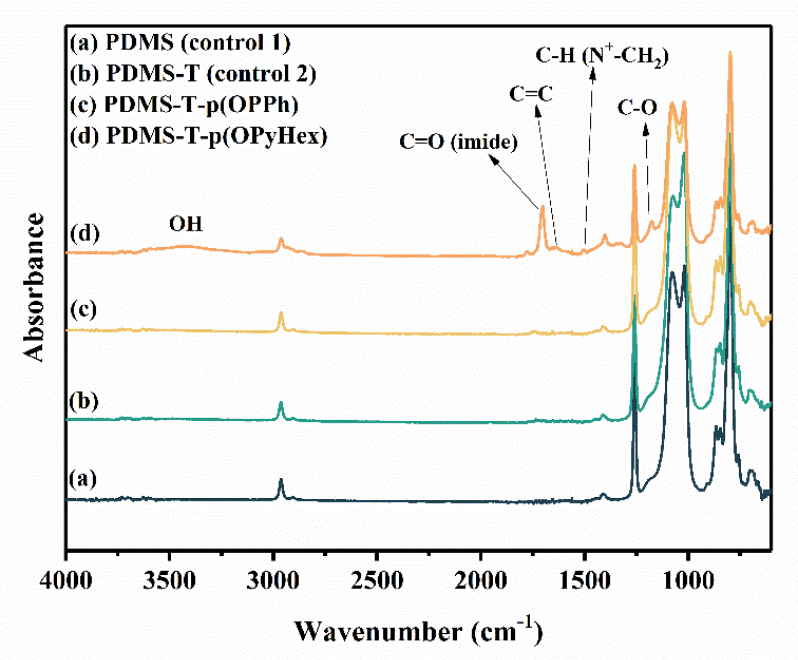

Figure 3. ATR-FTIR spectra of (a) PDMS (control 1), (b) PDMS-T (control 2), (c) PDMS-T-p(OPPh) and (d) PDMS-T-p(OPyHex).

The elemental analysis of the modified and unmodified PDMS surfaces was performed by XPS analysis. The results are presented in Table 2. The XPS analysis of the PDMS surface shows the presence of carbon, oxygen and silicon. A small enrichment of O and Si was observed for the native PDMS and could be explained by a residual SiO_2 coming from the synthesis process of the PDMS and also by the presence of residual Si-H groups after curing. After grafting of the PTTMP, peaks assigned to the sulfur element appear and an increase of the carbon amount was observed, confirming the presence of the grafted molecule on the surface.

Table 2. XPS elemental analysis of the optimal PDMS modified surface and its unmodified PDMS control.

	C1s	**O1s**	**Si2p**	**N1s**	P2p	Br3d	S2p	**C/O**	**C/Si**	**O/Si**	**N/Br**
PDMS	38.2	32.4	29.3	--	--	--	--	1.2	1.3	1.1	--
PDMS-T	47.1	28.3	22.9	--	--	--	1.7	1.7	2.1	1.2	--
PDMS-T-p(OPPh)	49.3	24	24.8	<0.3	<0.3	0.3	1.4	2.1	2.0	1.0	--
PDMS-T-p(OPyHex)	57.6	21.6	14.6	3.5	--	1.7	1	2.7	4.0	1.5	2

After grafting of p(OPPh) on the PDMS surfaces, a weak amount of Br was detected (0.3 at. %) with a decrease of sulfur amount, suggesting that the p(OPPh) was grafted on the surface. Unfortunately, the very weak amount of N and P (<0.3 at%) do not allow a fine quantification. This result can likely be explained by the ratios C/N and C/P equal to 21 in this polymer, conjugated to a partial coverage of the surface. Another aspect to consider is the π-π stacking between phenyl groups that may impact the relative accessibilities of P and Br atoms to the X-ray beam. Concerning the p(OPyHex), the ratio C/N and C/Br being equal to 10 and 20, respectively, N and Br elements of this polymer were detected with weak values (3.5 and 1.7%) and were in the expected stoichiometry (2/1). Thus, with regards to the surface elemental composition, the average grafting density is likely higher in the case of p(OPyHex) than in the case of p(OPPh). This can be explained by a lower concentration and accessibility of the carbon-carbon double bonds, due to the steric hindrance of triphenyl unit, as well as a lower solubility in methanol in the case of p(OPPh), leading to the decrease of its reactivity towards the surface's thiol groups and the decrease of its grafting yield. The presence of big aggregates on the PDMS-T-p(OPyHex) surface may also explain this result.

Assessment of the surface bactericidal properties

Previously, we have demonstrated that phosphonium containing polynorbornenes (p(OPPh)) [41] and quaternary pyridinium functionalized polynorbornenes (p(OPyHex)) [42] have strong biocidal activities in solution against *Staphylococcus aureus* and *E. coli* respectively, with Minimal Inhibitory Concentrations (MIC) around 15 µg/mL. The bactericidal properties of p(OPPh) have also been evidenced in the solid state as a non-grafted coating on a glass surface [41]. The ROMP based cationic pyridinium polymer with a hexyl unit exhibited the highest bactericidal efficiency in the solid state against E. coli, killing 99% of the bacteria in 5 min [42]. In addition, the introduction of phosphonium species at the polymer backbone would also increase its thermal stability. This would provide biocidal surface properties at high temperatures.

The most common mechanisms for the bactericidal action of cationic surfaces suggest that the long cationic polymer chains infiltrate the cells and thus destroy the membrane, like a needle bursting a balloon. Since cationic surfaces with short polymer and alkyl chains have shown bactericidal effects, a second mechanism has been highlighted in the literature, suggesting an ion exchange between the positive charges of the surface and the divalent cations of the membrane, which are released from the cell. The loss of these structurally critical mobile cations leads to the destruction of the membrane [43].

The bactericidal properties of p(OPPh) and p(OPyHex) grafted onto PDMS surfaces were studied by the Live and Dead test, using confocal fluorescent microscopy, against *E. coli* (Gram-) and *S. epidermidis* (Gram+). Bacteria were dispersed on modified and unmodified PDMS surfaces during 1h. Then, they were stained with a mixture of SYTO 9 and propidium iodide as fluorescent probes that stained bacteria with damaged membrane in red and bacteria with intact membrane in green. Examples of the Live and Dead fluorescent images are shown in Figure 4. One can observe that both PDMS-T-p(OPyHex) and PDMS-T-p(OPPh) surfaces displayed a high bactericidal effect. Indeed, after 1h of contact with the cationic surfaces the quasi-totality (>98%) of adhered bacteria was red (Figure 4-A3, B3, A4 and B4). Moreover, the density of *E. coli* (Figure 4-A3 and A4) and *S. epidermidis* (Figure 4-B3 and B4) on the cationic surfaces was relatively high (around 10^5 cells/cm^2). Oppositely, unmodifed PDMS surfaces (controls 1 (PDMS) and 4 (PDMS-T)), didn't display any bacteria attachment after 1h of contact. This behavior has already been observed in our previous works [23, 37]. For instance, PDMS surfaces grafted with poly(vinylbenzyl dimethylbutylammonium chloride) via the "grafting to" method exhibited 98 to 100% killing efficiency after 1h of contact with *E. coli*

and *S. epidermidis*. The surface bacterial density ranged from 10^5 to 10^6 cell/cm^2 when the charge densities varied from 2×10^{14} to 1.2×10^{15} charge.cm^{-2} [23]. Actually, when bacteria have affinity with the surface, the increase of roughness would increase the bacterial adhesion because of the increase of the surface contact. However, in our case the difference of roughness between the cationic and non-cationic surfaces (controls: PDMS and PDMS-T) is not significant and *E. coli* and *S. epidermidis* have not affinity with the controls. Bacteria are allowed to sediment on the surfaces, after washing with water, they are totally removed from the hydrophobic control but are strongly adhered to the cationic surface owing to high attractive electrostatic interaction.

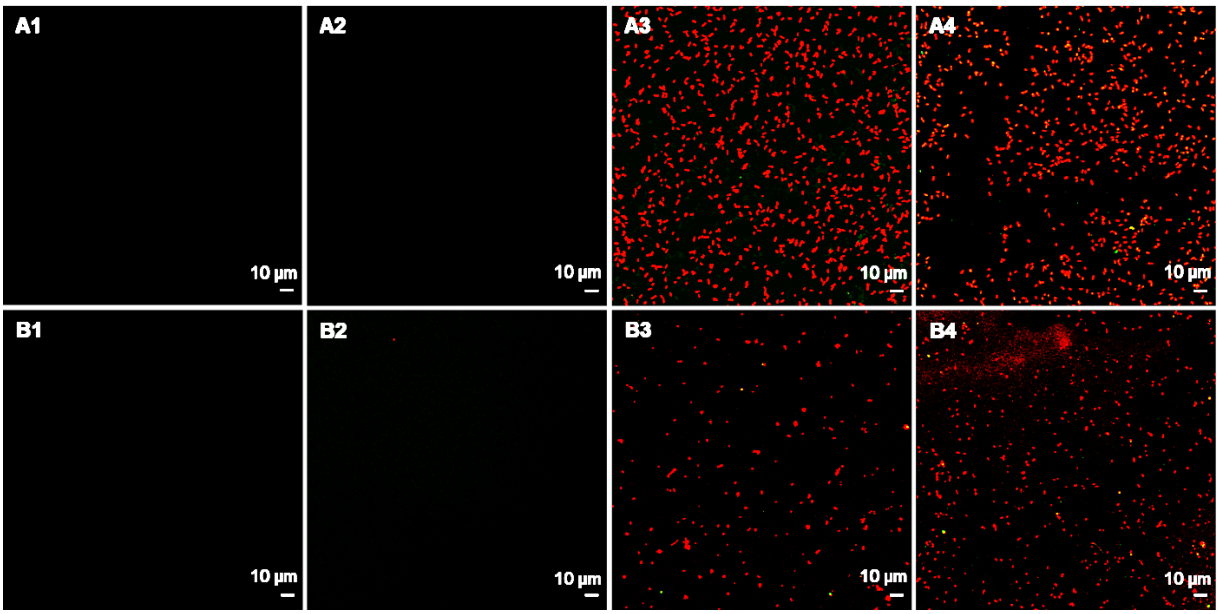

Figure 4. Fluorescence microscopy images of sessile bacteria cells stained with a marker of viability and deposited on surfaces of modified and unmodified PDMS surfaces: (A1) *E. coli* on unmodified PDMS surface (control 1), (A2) *E. coli* on PDMS-T surface (control 3), (A3) *E. coli* on PDMS-T-p(OPPh) surface, (A4) *E. coli* on PDMS-T-p(OPyHex) surface, (B1) *S. epidermidis* on unmodified PDMS surface (control 1), (B2) *S. epidermidis* on PDMS-T surface (control 3), (B3) *S. epidermidis* on PDMS-T-p(OPPh) surface, (B4) *S. epidermidis* on PDMS-T-p(OPyHex) surface.

In addition, a zone inhibition experiment was performed with *E. coli* and *S. epidermidis* on treated and untreated surfaces. Controls, consisting of PDMS-T surfaces on which the cationic polymers were deposited without UV exposure or subsequent washing, were also prepared. These controls showed a zone of inhibition with *S. epidermis* but not with *E. coli*, which is usually less sensitive in this test. The grafted cationic surfaces did not show a zone of inhibition, suggesting that they are non-leaching.

The long-term biocidal activity of a cationic surface is essentially related to its charge density and also to the concentration of the bacteria exposed to it (the challenge). It has been demonstrated [43] that a cationic surface with a charge density greater than 5.10^{15} charges/cm^2, is capable of killing at least a monolayer of *E. coli* cells (10^8 CFU/cm^2), before undergoing

fouling and losing its bioactivity. The live and dead test was performed with an extreme challenge of 1.5×10^8 CFU/cm^2 to achieve maximum bacterial adhesion on the surface leading to its saturation and passivation. Excess bacteria were washed away and the adherent bacteria (around 10^5 cells/cm^2), thanks to the electrostatic forces promoted by the cationic charges, died. Under real conditions, extreme infection or contamination is reached when the bacterial concentration is about 10^3 CFU/cm^2. Therefore, the passivating bacterial concentration for our cationic surfaces (around 10^5 cells/cm^2), can take a long time to be reached, depending on the number of bacteria to which these surfaces are exposed.

In previous studies, both p(OPPh) and p(OPyHex) have shown relatively high hemolytic activities in solution toward red blood mammalian cells [33,34]. In addition, we have also shown that cationic surfaces lost their bactericidal efficiency after 24 hours of contact with plasmatic proteins, which adsorbed easily on the surface by electrostatic attraction forces [23]. Therefore, at this time, we suggest to avoid the use of these surfaces in blood contact applications. On the other hand, they could be used for instance as external surface of catheter chambers and extracorporeal equipment.

Conclusion

Bactericidal cationic PDMS surfaces were successfully designed by a benzophenone photo-grafting process of ROMP-prepared cationic polymers. The grafting reaction was optimized in terms of duration and polymer concentration. The prepared surfaces exhibited surface charge densities above 10^{14} charge.cm^{-2} and contact angle with water around 98° and 78° related to quaternary phosphonium and quaternary ammonium groups, respectively. The Live and Dead test by fluorescence microscopy revealed an efficient contact killing of these surfaces against *E. coli* and *S. epidermidis*. In the future studies, we intend to prepare analogue surfaces by developing a photo-initiated ROMP ‘grafting from’ method, which would result in higher surface grafting density and coverage as well as higher hydrophilicity. Recharge ability as well as biofilm formation on the passivated cationic surfaces will be investigated.

Acknowledgments

Authors thanks the INSA ROUEN NORMANDIE, Yildiz Technical University (Pr. Tarik EREN, project ID: FBA-2021-4120) and the China Scholarship Council (CSC) for the financial supports.

This manuscript is a tribute to the 50-year anniversary of the French Polymer Group (Groupe Français des Polymères - GFP).

Data availability statement

The raw/processed data required to reproduce these findings cannot be shared at this time due to technical or time limitations.

References

[1] R. Yañez-Macías *et al.*, "Combinations of antimicrobial polymers with nanomaterials and bioactives to improve biocidal therapies," *Polymers (Basel).*, vol. 11, no. 11, p. 1789, 2019.

[2] U. S. D. of H. and H. Services, "CDC. Antibiotic Resistance Threats in the United States, 2019," *Atlanta, GA, USA US Dep. Heal. Hum. Serv. CDC*, 2019.

[3] N. M. Milović, J. Wang, K. Lewis, and A. M. Klibanov, "Immobilized N-alkylated polyethylenimine avidly kills bacteria by rupturing cell membranes with no resistance developed," *Biotechnol. Bioeng.*, vol. 90, no. 6, pp. 715–722, 2005.

[4] F. Siedenbiedel and J. C. Tiller, "Antimicrobial polymers in solution and on surfaces: overview and functional principles," *Polymers (Basel).*, vol. 4, no. 1, pp. 46–71, 2012.

[5] T.-F. Mah, B. Pitts, B. Pellock, G. C. Walker, P. S. Stewart, and G. A. O'Toole, "A genetic basis for Pseudomonas aeruginosa biofilm antibiotic resistance," *Nature*, vol. 426, no. 6964, pp. 306–310, 2003.

[6] G. J. Gabriel, A. Som, A. E. Madkour, T. Eren, and G. N. Tew, "Infectious disease: Connecting innate immunity to biocidal polymers," *Mater. Sci. Eng. R Reports*, vol. 57, no. 1–6, pp. 28–64, 2007.

[7] E. Klein, D. L. Smith, and R. Laxminarayan, "Hospitalizations and deaths caused by methicillin-resistant Staphylococcus aureus, United States, 1999–2005," *Emerg. Infect. Dis.*, vol. 13, no. 12, p. 1840, 2007.

[8] J. Yan *et al.*, "Cationic polyesters with antibacterial properties: facile and controllable synthesis and antibacterial study," *Eur. Polym. J.*, vol. 110, pp. 41–48, 2019.

[9] M. Alvarez-Paino *et al.*, "Antimicrobial surfaces obtained from blends of block copolymers synthesized by simultaneous atrp and click chemistry reactions," *Eur. Polym. J.*, vol. 93, pp. 53–62, 2017.

[10] J. Velazco-De-La-Garza *et al.*, "Biological properties of novel polysuccinimide derivatives synthesized via quaternary ammonium grafting," *Eur. Polym. J.*, vol. 131, p. 109705, 2020.

[11] A. B. Swanson and L. F. Peltier, "Silicone Rubber Implants for Replacement of Arthritic or Destroyed Joints in the Hand.," *Clin. Orthop. Relat. Res.*, vol. 342, pp. 4–10, 1997.

[12] M. Bračič, O. Šauperl, S. Strnad, I. Kosalec, O. Plohl, and L. F. Zemljič, "Surface modification of silicone with colloidal polysaccharides formulations for the development of antimicrobial urethral catheters," *Appl. Surf. Sci.*, vol. 463, pp. 889–899, 2019.

[13] A. Colas and J. Curtis, "Silicone biomaterials: history and chemistry," *Biomater. Sci. an Introd. to Mater. Med.*, vol. 2, pp. 80–85, 2004.

[14] A. U. Daniels, "Silicone breast implant materials," *Swiss Med. Wkly.*, vol. 142, no. JULY, 2012.

[15] K. W. Dunn, P. N. Hall, and C. T. K. Khoo, "Breast implant materials: sense and safety," *Br. J. Plast. Surg.*, vol. 45, no. 4, pp. 315–321, 1992.

[16] A. Colas, "Silicones: preparation, properties and performance," *Dow Corning, Life Sci.*, 2005.

[17] J. R. Henstock, L. T. Canham, and S. I. Anderson, "Silicon: the evolution of its use in biomaterials," *Acta Biomater.*, vol. 11, pp. 17–26, 2015.

[18] J. Winiecka-Krusnell and E. Linder, "Bacterial infections of free-living amoebae," *Res. Microbiol.*, vol. 152, no. 7, pp. 613–619, 2001.

[19] Q. Gao *et al.*, "Rationally designed dual functional block copolymers for bottlebrush-like coatings: In vitro and in vivo antimicrobial, antibiofilm, and antifouling properties," *Acta Biomater.*, vol. 51, pp. 112–124, 2017.

[20] A. I. Doulgeraki, P. Di Ciccio, A. Ianieri, and G.-J. E. Nychas, "Methicillin-resistant food-related Staphylococcus aureus: a review of current knowledge and biofilm formation for future studies and applications," *Res. Microbiol.*, vol. 168, no. 1, pp. 1–15, 2017.

[21] C. Donzel *et al.*, "Hydrophilic poly (dimethylsiloxane) stamps for microcontact printing," *Adv. Mater.*, vol. 13, no. 15, pp. 1164–1167, 2001.

[22] A. Oláh, H. Hillborg, and G. J. Vancso, "Hydrophobic recovery of UV/ozone treated poly (dimethylsiloxane): adhesion studies by contact mechanics and mechanism of surface modification," *Appl. Surf. Sci.*, vol. 239, no. 3–4, pp. 410–423, 2005.

[23] N. Kebir, I. Kriegel, M. Estève, and V. Semetey, "Preparation of bactericidal cationic PDMS surfaces using a facile and efficient approach," *Appl. Surf. Sci.*, vol. 360, pp. 866–874, 2016.

[24] W. Mussard, N. Kebir, I. Kriegel, M. Estève, and V. Semetey, "Facile and efficient control of bioadhesion on poly (dimethylsiloxane) by using a biomimetic approach," *Angew. Chemie*, vol. 123, no. 46, pp. 11063–11066, 2011.

[25] D.-J. Guo, H.-M. Han, S.-J. Xiao, and Z.-D. Dai, "Surface-hydrophilic and protein-resistant silicone elastomers prepared by hydrosilylation of vinyl poly (ethylene glycol) on hydrosilanes-poly (dimethylsiloxane) surfaces," *Colloids Surfaces A Physicochem. Eng. Asp.*, vol. 308, no. 1–3, pp. 129–135, 2007.

[26] Y. Wu, Y. Huang, and H. Ma, "A facile method for permanent and functional surface modification of poly (dimethylsiloxane)," *J. Am. Chem. Soc.*, vol. 129, no. 23, pp. 7226–7227, 2007.

[27] H. Chen, Y. Chen, H. Sheardown, and M. A. Brook, "Immobilization of heparin on a silicone surface through a heterobifunctional PEG spacer," *Biomaterials*, vol. 26, no. 35, pp. 7418–7424, 2005.

[28] H. Chen, Z. Zhang, Y. Chen, M. A. Brook, and H. Sheardown, "Protein repellant silicone surfaces by covalent immobilization of poly (ethylene oxide)," *Biomaterials*, vol. 26, no. 15, pp. 2391–2399, 2005.

[29] Y. Wang, H.-H. Lai, M. Bachman, C. E. Sims, G. P. Li, and N. L. Allbritton, "Covalent micropatterning of poly (dimethylsiloxane) by photografting through a mask," *Anal. Chem.*, vol. 77, no. 23, pp. 7539–7546, 2005.

[30] S. Sugiura, J. Edahiro, K. Sumaru, and T. Kanamori, "Surface modification of polydimethylsiloxane with photo-grafted poly (ethylene glycol) for micropatterned protein adsorption and cell adhesion," *Colloids Surfaces B Biointerfaces*, vol. 63, no. 2, pp. 301–305, 2008.

[31] B. L. Leigh, E. Cheng, L. Xu, A. Derk, M. R. Hansen, and C. A. Guymon, "Antifouling photograftable zwitterionic coatings on PDMS substrates," *Langmuir*, vol. 35, no. 5, pp. 1100–1110, 2018.

[32] Y. Lou, D. Schapman, D. Mercier, S. Alexandre, F. Burel, P. Thebault, N. Kébir. "Self-disinfecting PDMS surfaces with high quaternary ammonium functionality by direct surface photoinitiated polymerization of vinylbenzyldimethylbutylammonium chloride," *Eur. Polym. J.*, vol. 152, pp. 110473, 2021.

[33] N. C. Süer, C. Demir, N. A. Ünübol, Ö. Yalçın, T. Kocagöz, and T. Eren, "Antimicrobial activities of phosphonium containing polynorbornenes," *RSC Adv.*, vol. 6, no. 89, pp. 86151–86157, 2016.

[34] T. Eren *et al.*, "Antibacterial and hemolytic activities of quaternary pyridinium functionalized polynorbornenes," *Macromol. Chem. Phys.*, vol. 209, no. 5, pp. 516–524, 2008.

[35] A. Palantoken, M. S. Yilmaz, N. A. Unubol, E. Yenigul, S. Pişkin, and T. Eren, "Synthesis and characterization of a ROMP-based polycationic antimicrobial hydrogel," *Eur. Polym. J.*, vol. 112, pp. 365–375, 2019.

[36] H. S. Bazzi and H. F. Sleiman, “Adenine-containing block copolymers via ring-opening metathesis polymerization: synthesis and self-assembly into rod morphologies,” *Macromolecules*, vol. 35, no. 26, pp. 9617–9620, 2002.

[37] J. Lafarge, N. Kebir, D. Schapman, and F. Burel, “Design of self-disinfecting PVC surfaces using the click chemistry,” *React. Funct. Polym.*, vol. 73, no. 11, pp. 1464–1472, 2013.

[38] Y. Jiao, L. Niu, S. Ma, J. Li, F. R. Tay, and J. Chen, “Quaternary ammonium-based biomedical materials: State-of-the-art, toxicological aspects and antimicrobial resistance,” *Prog. Polym. Sci.*, vol. 71, pp. 53–90, 2017.

[39] T. Zhou *et al.*, “Surface functionalization of biomaterials by radical polymerization,” *Prog. Mater. Sci.*, vol. 83, pp. 191–235, 2016.

[40] J. C. Tiller, C.-J. Liao, K. Lewis, and A. M. Klibanov, “Designing surfaces that kill bacteria on contact,” *Proc. Natl. Acad. Sci.*, vol. 98, no. 11, pp. 5981–5985, 2001.

[41] C. Demir *et al.*, “Biocidal activity of ROMP-polymer coatings containing quaternary phosphonium groups,” *Prog. Org. Coatings*, vol. 135, pp. 299–305, 2019.

[42] E. Altay, M. A. Yapaöz, B. Keskin, G. Yucesan, and T. Eren, “Influence of alkyl chain length on the surface activity of antibacterial polymers derived from ROMP,” Colloids Surfaces B Biointerfaces, vol. 127, pp. 73–78, 2015.

[43] H. Murata, R. R. Koepsel, K. Matyjaszewski, and A. J. Russell, “Permanent, non-leaching antibacterial surfaces-2: How high density cationic surfaces kill bacterial cells,” *Biomaterials*, vol. 28, no. 32, pp. 4870–4879, 2007.

Supporting information

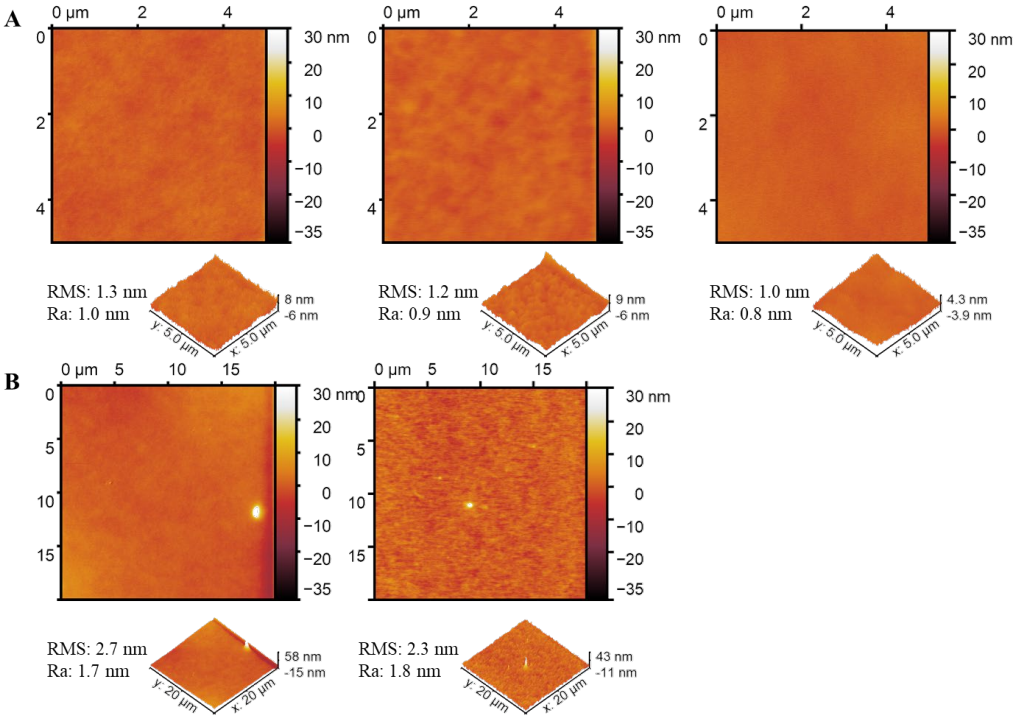

Figure S1. AFM images of PDMS surfaces at different size: A) 5×5 µm^2 with RMS and Ra of 1.2 ± 0.2 nm and 0.9 ± 0.1 nm respectively, B) 20×20 µm^2 with RMS and Ra of 2.5 ± 0.2 and 1.8 ± 0.1.

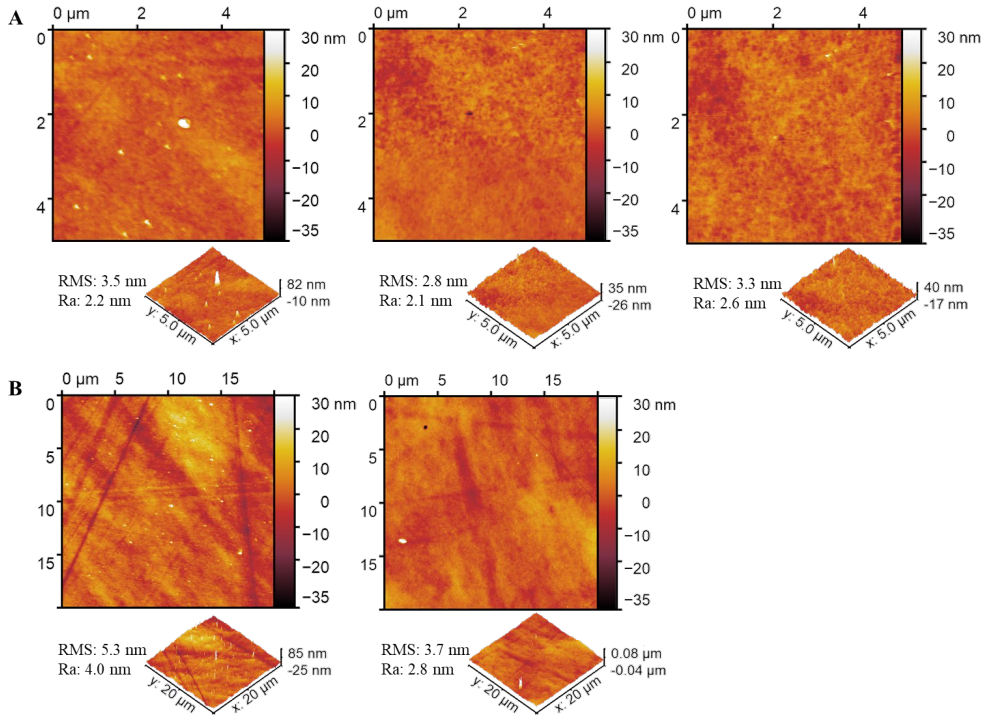

Figure S2. AFM images of PDMS-T surfaces at different size: A) 5×5 µm^2 with RMS and Ra of 3.2 ± 0.4 nm and 2.3 ± 0.3 nm respectively, B) 20×20 µm^2 with RMS and Ra of 4.5 ± 0.8 and 3.4 ± 0.6.

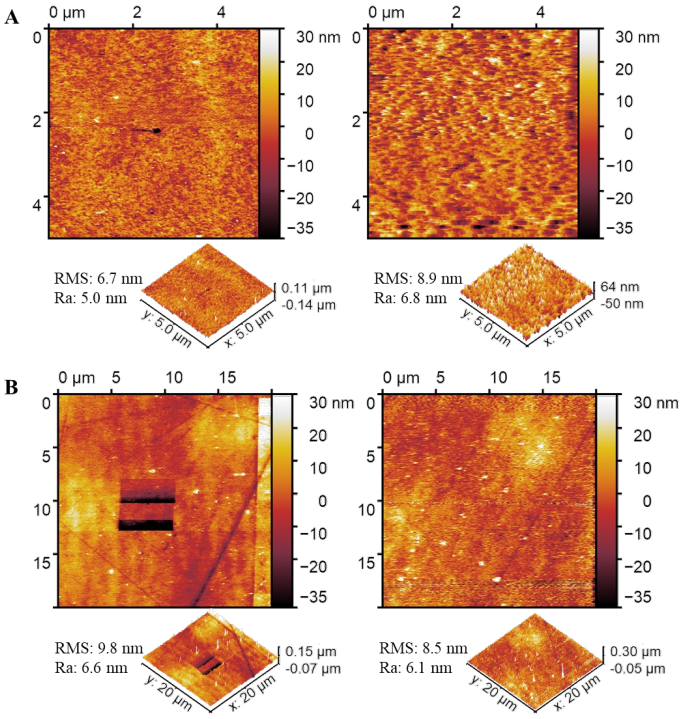

Figure S3. AFM images of PDMS-p(OPPh) surfaces at different size: A) 5×5 µm^2 with RMS and Ra of 7.8 ± 1.1 nm and 5.9 ± 0.9 nm respectively, B) 20×20 µm^2 with RMS and Ra of 9.2 ± 0.7 and 6.4 ± 0.3.

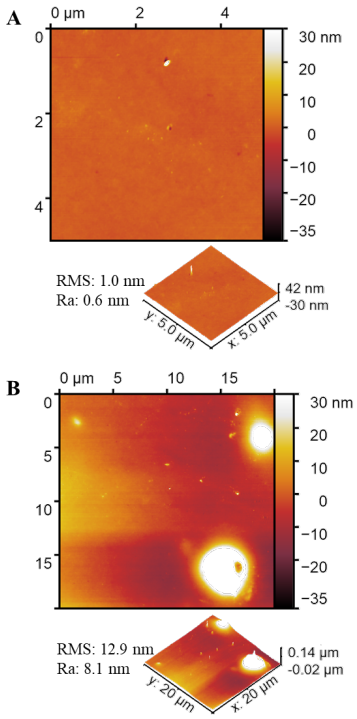

Figure S4. AFM images of PDMS-p(OPyHex) surfaces at different size: A) 5×5 µm^2, B) 20×20 µm^2.

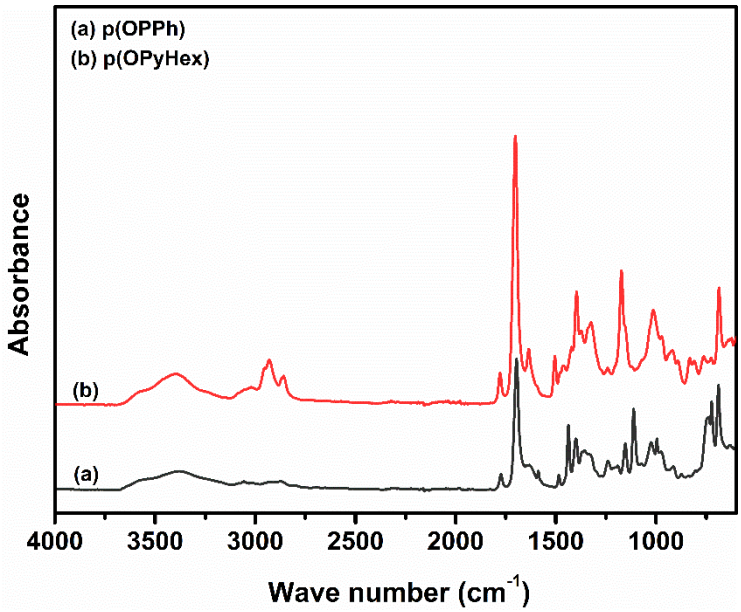

Figure S5. FTIR-ATR spectrum of (a) p(OPPh) and (b) p(OPyHex).

FTIR-ATR (cm^{-1}) of p(OPPh): 1697 (C=O); 1587 (C=C); 1356 (C-N) 1153 (C-O-C).

FTIR-ATR (cm^{-1}) of p(OPyHex): 1702 (C=O); 1325 (C-N); 1173 (C-O-C).

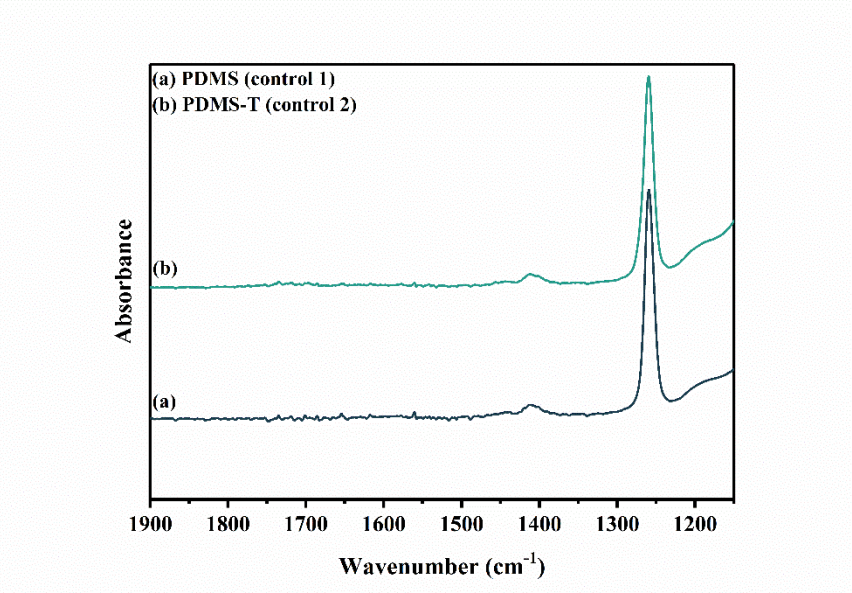

Figure S6. FTIR-ATR spectrum of (a) PDMS and (b) PDMS-T in the region of 1150 to 1900 cm^{-1}.

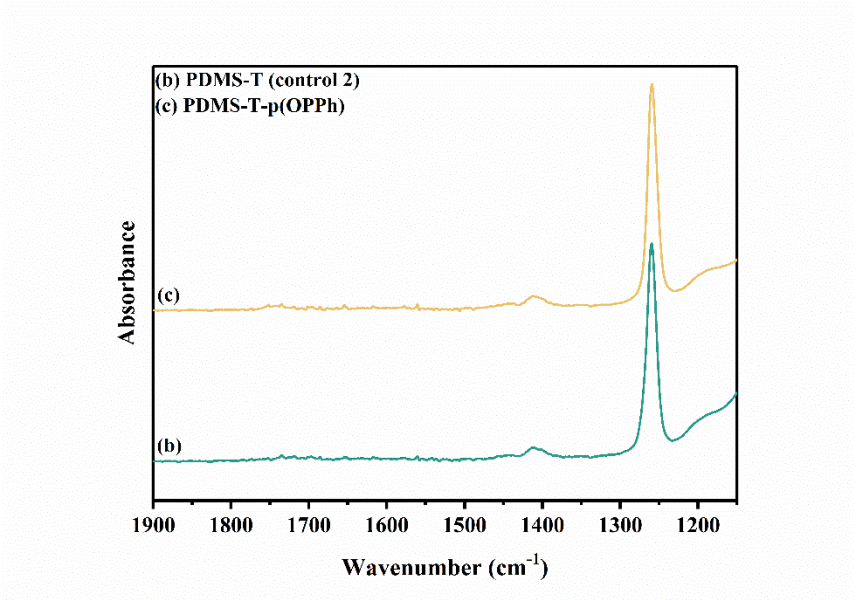

Figure S7. FTIR-ATR spectrum of (c) PDMS-T-p(OPPh) and (b) PDMS-T in the region of 1150 to 1900 cm^{-1}.

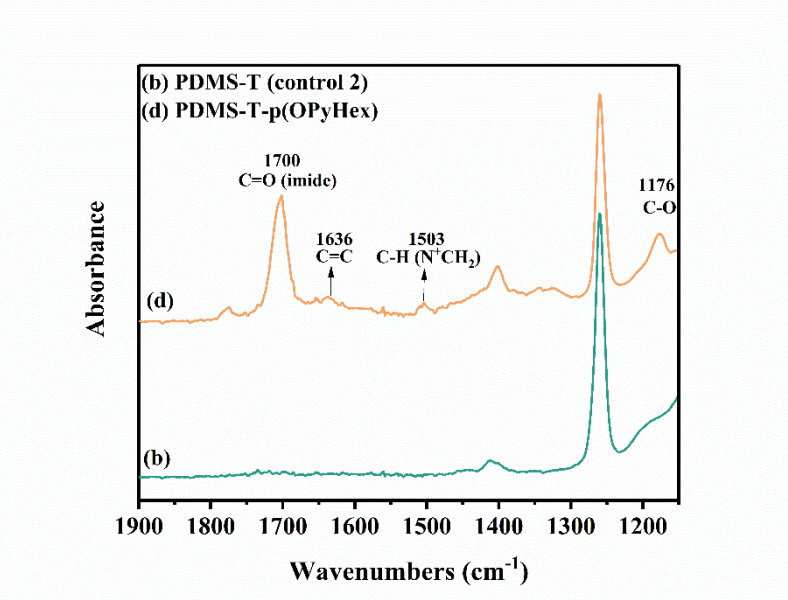

Figure S8. FTIR-ATR spectrum of (d) PDMS-T-p(OPyHex) and (b) PDMS-T in the region of 1150 to 1900 cm^{-1}.

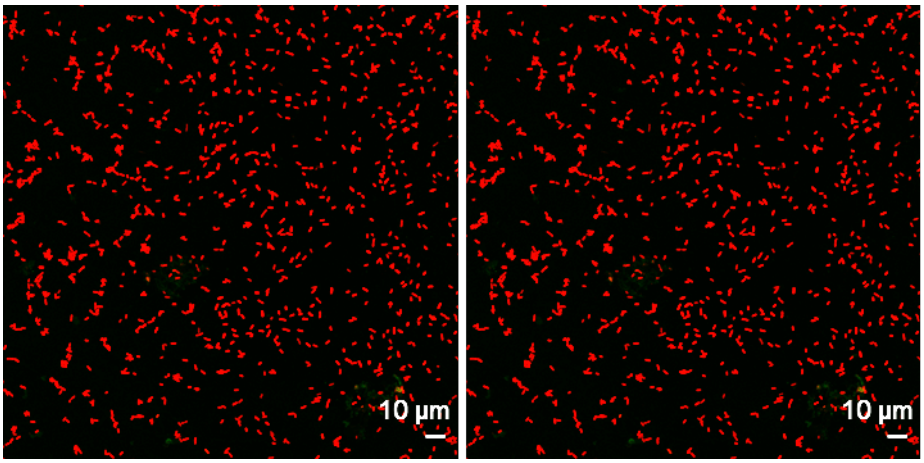

Figure S9. Supplemental fluorescence microscopy images of sessile *E. coli* cells stained with a marker of viability and deposited on surfaces of PDMS-T-p(OPPh) surfaces.

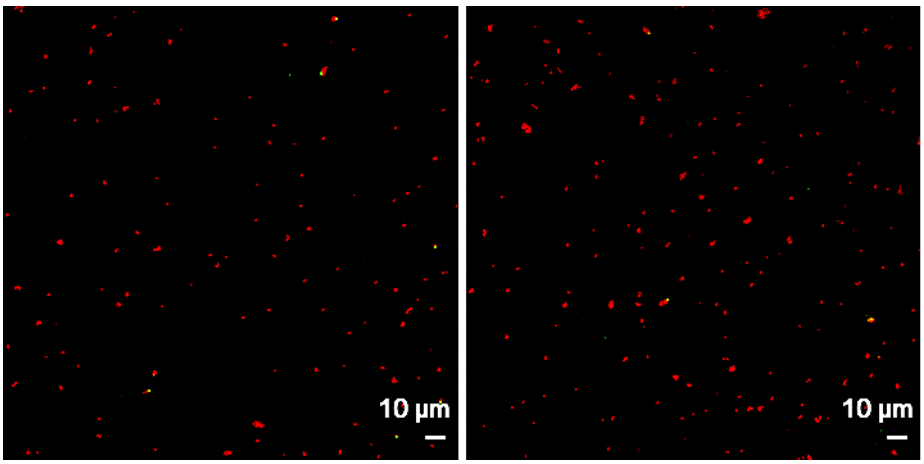

Figure S10. Supplemental fluorescence microscopy images of sessile *S. epidermidis* cells stained with a marker of viability and deposited on surfaces of PDMS-T-p(OPPh) surfaces.

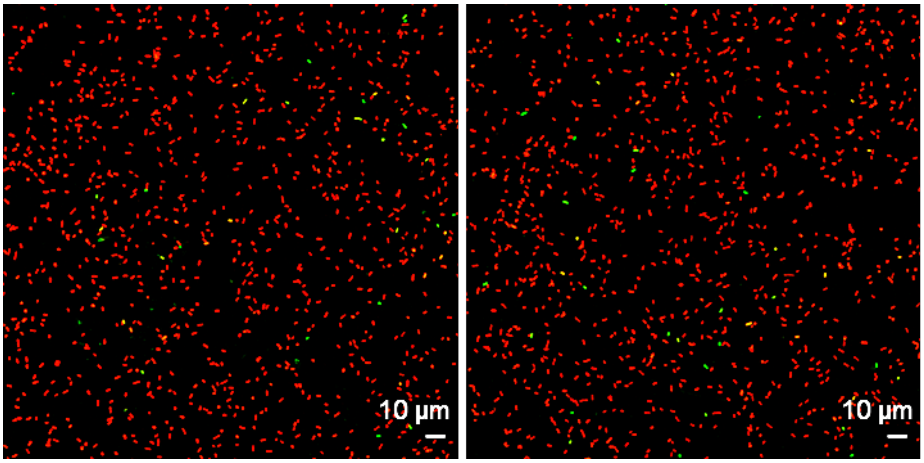

Figure S11. Supplemental fluorescence microscopy images of sessile *E. coli* cells stained with a marker of viability and deposited on surfaces of PDMS-T-p(OPyHex) surfaces.

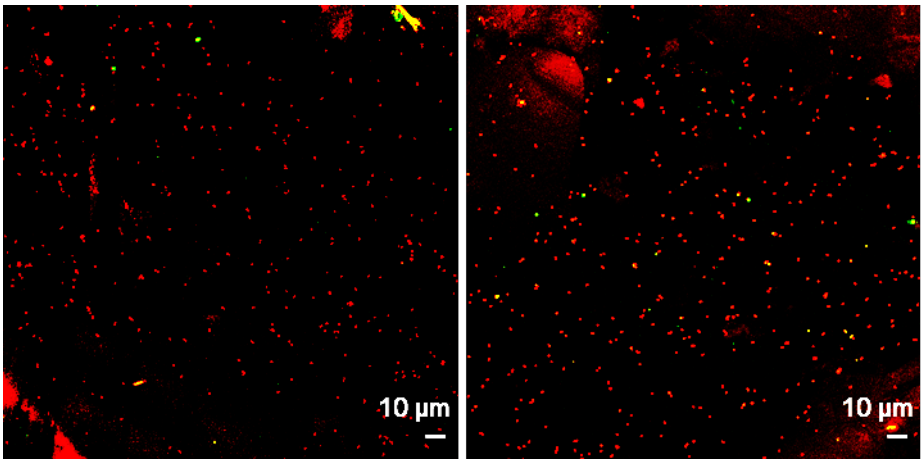

Figure S12. Supplemental fluorescence microscopy images of sessile *S. epidermidis* cells stained with a marker of viability and deposited on surfaces of PDMS-T-p(OPyHex) surfaces.

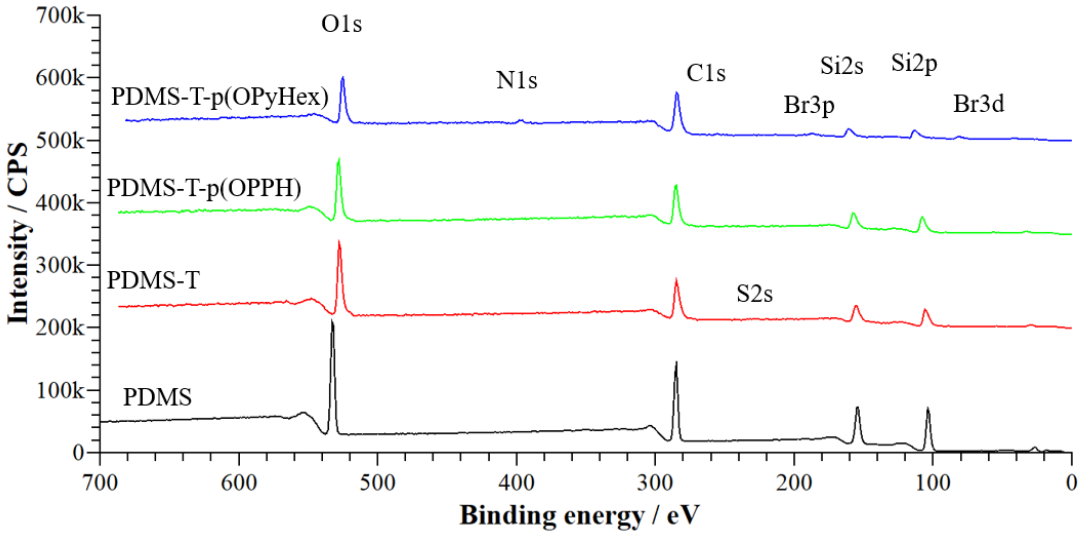

Figure S13. XPS analysis of PDMS, PDMS-T, PDMS-T-p(OPPh) and PDMS-T-p(OPyHex).

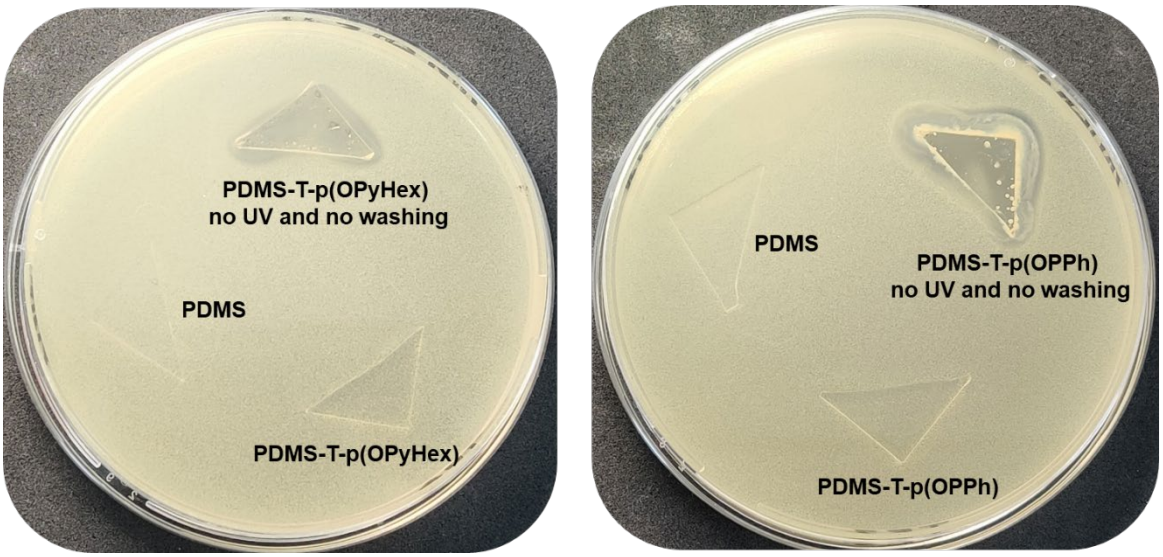

Figure S14. Inhibition Zone experiment with *S. epidermidis* performed on PDMS, PDMS-T-p(OPPh) and PDMS-T-p(OPyHex), with and without UV treatment and washing.

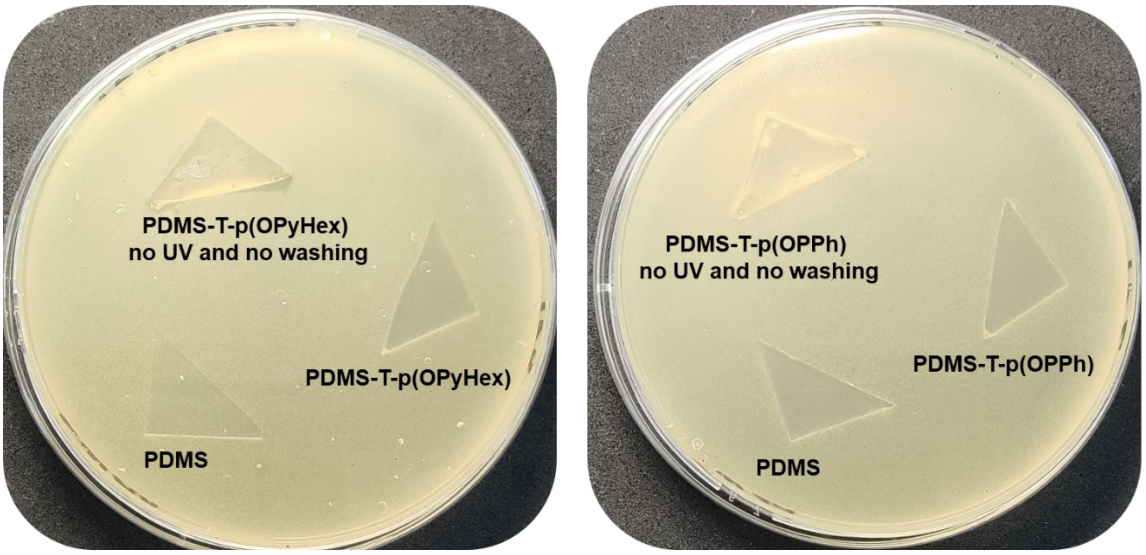

Figure S15. Inhibition Zone experiment with *E. coli* performed on PDMS, PDMS-T-p(OPPh) and PDMS-T-p(OPyHex), with and without UV treatment and washing.

IV.4 Informations supplémentaires

Nous avons également évalué, comme dans la partie IV.1, la capacité des surfaces optimales (PDMS-PAONAI et PDMS-T-PAONAI) à éradiquer des bactéries en suspension contre *E. coli* et *S. aureus* en utilisant la norme ASTM modifiée, E2149-01. Les surfaces ont été exposées à une suspension bactérienne d'une concentration d'environ 10^3 UFC/ml pendant 1h, puis le nombre de cellules viables en suspension a été estimé sur gélose BHI. Les résultats sont représentés sur la Figure IV-1.

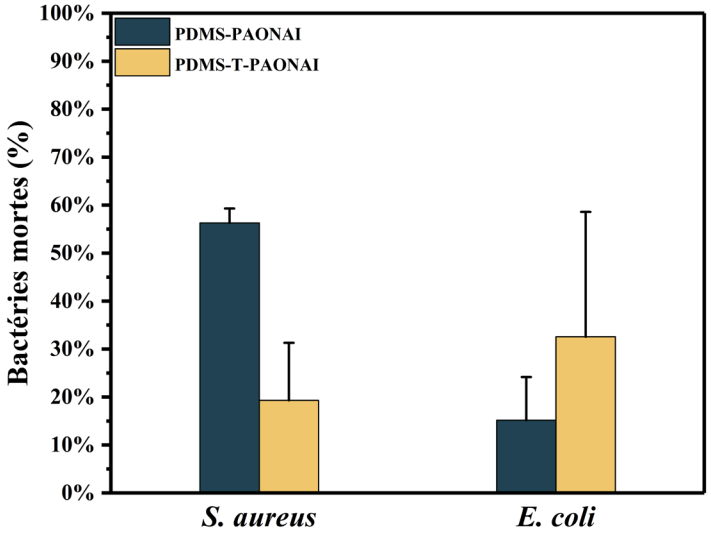

Figure IV-1. Détermination de la capacité d'éradication de *S. aureus* et *E. coli* par la surface PDMS cationique optimale en pourcentage de bactéries mortes par rapport à une surface de PDMS non modifiée.

D'après les résultats, on peut observer que même en partant d'une faible concentration bactérienne, les surfaces PDMS-PAONAI et PDMS-T-PAONAI ne présentent pas une capacité bactéricide importante contre les bactéries en suspension. Cependant, comme décrit dans l'article, ces surfaces ont démontré un effet bactéricide élevé lors des analyses par microscopie à fluorescence (présence uniquement de bactéries rouges), où les bactéries sont mises en contact avec la surface cationique par sédimentation. Vu que l'étape clé dans le mécanisme d'action en suspension est l'attraction/l'adhésion des bactéries sur la surface par les ammoniums quaternaires, il semblerait qu'il y ait une défaillance à ce niveau avec les surfaces à chaînes acrylates (contrairement aux surfaces préparées à partir du styrène ammonium décrit dans l'article IV.1). En effet, sous l'effet de l'agitation mécanique, les forces de cisaillements sont importantes au niveau de la surface, et vu la souplesse des chaînes acrylates par rapport aux chaînes de polystyrène, les bactéries pourraient avoir du mal à s'y accrocher et la partie non accrochée se retrouverait donc toujours en « vie » en suspension.

Conclusion générale et perspectives

Dans ce travail, nous avons étudié l'élaboration de surfaces de PDMS antibactériennes selon trois approches différentes.

La première, qui a fait l'objet du chapitre II, a consisté en l'étude de l'adhésion de bactéries à Gram positif (*S. aureus, S. epidermidis et E. faecalis*) et à Gram négatif (*E. coli et P. aeruginosa*) sur des surfaces d'électrodes métalliques revêtues ou non de PDMS, sous un champ électrique d'intensités variables. Trois métaux ont été testés à savoir Zn, Al et Cu. Après 2h de contact avec les suspensions bactériennes, les électrodes en Zn ont montré une différence de 1,5-2 log d'UFC/cm^2 entre la cathode et l'anode pour des tensions de 0,2 et 0,4 V, sans éradication significative des bactéries en suspension. Dans les mêmes conditions, les électrodes en Al se sont révélées inactives pour limiter et diriger l'adhésion bactérienne, probablement en raison de l'oxydation de la surface provoquant sa passivation. Cependant, à 1V, les électrodes de Zn et de Al sont devenues bactéricides en tuant les bactéries en suspension. D'autre part, l'effet bactéricide des électrodes de Cu a été très élevé à 0 V et semble être renforcé par la présence d'un champ électrique (effet synergique). A cause de cette activité bactéricide, l'adhésion bactérienne sur sa surface a été trop faible pour voir une différence d'adhésion entre la cathode et l'anode. Une fois recouverte de PDMS, l'effet bactéricide du Cu a disparu et une différence de 1 log d'UFC/cm^2, spécifique au genre staphylocoque, a été observée entre les deux électrodes au-dessus de 10 V. Enfin, cette étude a démontré que la force électrostatique est le facteur prédominant régissant l'adhésion bactérienne pour les surfaces de Zn mais pas pour celles de Al et de PDMS. Pour les travaux futurs, une tension élevée pourrait être utilisée afin d'augmenter l'effet électrostatique répulsif des bactéries sur les surfaces de PDMS. De plus, les électrodes métalliques pourraient être utilisées comme agents de désinfection physique à 1V sans courant électrique.

Dans la deuxième approche (chapitre III) un nouveau dérivé de claramine a été synthétisé et greffé avec succès sur la surface de PDMS par une réaction de chimie click chimio-sélective de type CuAAC. L'analyse XPS de la région N1s a confirmé le greffage covalent du dérivé de claramine par la formation d'un cycle triazole. Les résultats préliminaires par microscopie à fluorescence ont montré que la membrane de *E. coli* et *S. epidermidis* a été déstabilisée probablement par une forte attraction électrostatique via la chaîne aminée cationique du dérivé de la claramine greffée. Ces résultats ont confirmé l'importance de l'orientation des molécules actives une fois immobilisées et l'utilité de la réaction CuAAC. Cependant, des analyses complémentaires pour quantifier la densité du dérivé de claramine seront à réaliser (dosage des fonctions amines, analyses approfondies par XPS, marquage

fluorescent de la claramine, …). De plus, une immobilisation covalente de la claramine par différents sites pourrait être envisagée pour confirmer l'importance de l'orientation sur l'activité antibactérienne du composé immobilisé. Cette approche utilisant un dérivé de claramine peut être potentiellement appliqué dans des dispositifs médicaux pour prévenir les infections bactériennes et surmonter le problème de la résistance bactérienne. Pour une application future, la biocompatibilité et les propriétés antibactériennes de ces surfaces *in vivo* devront être étudiées de manière plus approfondie.

Dans la troisième approche, qui a fait l'objet du chapitre IV, des surfaces de PDMS cationiques ont été préparées avec succès via des procédés de 'grafting from' et 'grafting to' photo-induits, en présence de benzophénone comme photo-amorceur. Ainsi, dans une première partie, les surfaces cationiques ont été préparées par photo-polymérisation d'un monomère de styrène ammonium à partir de la surface. La réaction a été optimisée en termes de durée et de concentration en monomère. En faisant varier ces deux paramètres, les densités de charge de surface et les valeurs d'angle de contact avec l'eau (hydrophilie) ont pu être ajustés finement entre environ 10^{14} à 10^{17} $N^{+}.cm^{-2}$ et environ 100 à 10°, respectivement. Le test Live and Dead par microscopie à fluorescence a révélé une déstabilisation des membranes de *E. coli, S. aureus* et *S. epidermidis* après 1h de contact avec la surface optimale. Un test de numération bactérienne normé, applicable à des surfaces présentant des densités de charge supérieures à 5.10^{15} $N^{+}.cm^{-2}$, a montré que ces surfaces sont capables d'attirer, fixer et tuer les bactéries à partir d'une suspension jusqu'à une concentration supérieure à 10^{6} UFC/mL. Enfin, les surfaces QA-PDMS préparées ont révélé des performances plus élevées par rapport aux analogues préparés, dans des travaux précédents, par le processus d'hydrosilylation. Dans une seconde partie, des surfaces cationiques ont été conçues par photo-polymérisation d'un monomère d'acrylate ammonium à partir de surfaces de PDMS natives et thiolées. La photopolymérisation directe a conduit à une surface de PDMS optimale ayant une valeur d'angle de contact avec l'eau d'environ 75° et une densité de charge d'environ 10^{15} $N^{+}.cm^{-2}$, qui sont des valeurs proches de celles obtenues via un procédé " grafting to ". Le prétraitement de la surface de PDMS par thiolation a conduit à des surfaces de PDMS cationiques avec une hydrophilie de surface accrue (angle de contact autour de 28°) et une densité de charge d'environ 10^{17} $N^{+}.cm^{-2}$. Le test Live and Dead par microscopie à fluorescence a révélé un effet antibactérien par contact élevée de toutes les surfaces cationiques préparées contre *E. coli* et *S. epidermidis*. Cependant, dans les conditions du test normée de numération bactérienne, contrairement aux surfaces styrène ammonium, ces surfaces à densité de charge très élevées n'ont pas été efficace pour attirer et

fixer les bactéries en suspension puis les tuer, ce qui révèle une limitation de ce test en raison de sa dépendance à la structure chimique de surface. Dans une troisième et dernière partie, des surfaces de PDMS cationiques ont été préparées avec succès par un procédé de photo-greffage (grafting to) de polymères cationiques, porteurs de groupements phosphonium quaternaire et ammonium quaternaire, synthétisés par ROMP par un partenaire turc (équipe du Pr. T. EREN). La réaction de greffage a été optimisée en termes de durée et de concentration de polymère. Les surfaces préparées ont présenté des densités de charge de surface supérieures à 10^{14} charge.cm^{-2} et une valeur de l'angle de contact avec l'eau d'environ 98° et 78° liés aux groupes phosphonium quaternaire et ammonium quaternaire, respectivement. Le test Live and Dead par microscopie à fluorescence a révélé une activité antibactérienne par contact efficace de ces surfaces contre *E. coli* et *S. epidermidis*.

La biocompatibilité des surfaces cationiques doit faire l'objet d'études supplémentaires pour déterminer si elles peuvent être utilisées pour des applications en tant que dispositifs médicaux. Dans un travail précédent, nous avions démontré que les protéines plasmatiques, parce qu'elles sont chargées électriquement, sont adsorbées sur les surfaces cationiques, qui perdent quantitativement leur efficacité bactéricide après 24 heures de contact avec elles. Par conséquent, il serait à priori préférable d'utiliser ce type de surface dans tous les dispositifs en silicone qui ne sont pas en contact avec le sang, comme les surfaces externes des chambres de cathéter et les équipements extracorporels.